

# Phlebot: The Robotic Phlebotomist

by

Paulo Carvalho, Anurag Kesari and Sean Weaver

Submitted to the Robotics Engineering Program and the Department of  
Biomedical Engineering

in partial fulfillment of the requirements for the degree of

Bachelor of Science

at

WORCESTER POLYTECHNIC INSTITUTE

May 2015

© Paulo Carvalho, Anurag Kesari and Sean Weaver, MMXV. All rights reserved.

The authors hereby grant to WPI permission to reproduce and to distribute publicly paper and electronic copies of this thesis document in whole or in part in any medium now known or hereafter created.

Certified by.....

Patrick Flaherty

Assistant Professor, Biomedical Engineering Department

Certified by.....

Gregory Fischer

Associate Professor, Robotics Engineering Program

This report represents the work of WPI undergraduate students submitted to the faculty as evidence of completion of a degree requirement. WPI routinely publishes these reports on its website without editorial or peer review. For more information about the projects program at WPI, please see

<http://www.wpi.edu/academics/ugradstudies/project-learning.html>



# Phlebot: The Robotic Phlebotomist

by

Paulo Carvalho, Anurag Kesari and Sean Weaver

Submitted to the Robotics Engineering Program and the Department of Biomedical  
Engineering

on April 30, 2015, in partial fulfillment of the  
requirements for the degree of  
Bachelor of Science

## Abstract

The robotic phlebotomist MQP, Phlebot, was undertaken as an effort to address the burdens associated with the collection of blood specimen, known as phlebotomy, on both patients and the medical practitioners responsible for the procedure. The device is intended to reduce potentially fatal needlestick injuries, reduce patient stress through accurate vein cannulation, improve blood specimen quality through process efficiency, and alleviate understaffed medical facilities by automating a routine task. Published work in this field is limited; however, there are at least three other devices performing a similar function: the Bloodbot, VeeBot, and Vasculogic. The aforementioned devices while able to perform venipuncture are limited by their size, cost, and complexity. In this report we present the design methodology and verification for the Phlebot. We have succeeded in developing a modular system architecture spanning both hardware and software allowing for parallel development and testing of each subsystem by using a combination of classical and model-based design approaches. Full system validation has demonstrated preliminary indicators of successful vein isolation, puncture site selection, and needle insertion. Our next steps for this project include the addition of subsystems pertaining to point of care diagnosis, pain distraction, and needle disposal.

MQP Supervisor: Patrick Flaherty  
Title: Assistant Professor  
Department: Biomedical Engineering Department

MQP Supervisor: Gregory Fischer  
Title: Associate Professor  
Department: Robotics Engineering Program

# Executive Summary

## Introduction

Phlebotomy, though ubiquitous, is notorious for frequently causing patient distress due to failed blood draw attempts that require multiple needle sticks. This is especially prevalent in patients such as small children, the elderly and those with deep veins or higher fat content that occludes the veins. These problems can be addressed by a robotic device that can employ sensory systems which are more sensitive than those of a human and a needle positioning system that is extremely precise and practically tremor-free.

The design of the Phlebot is highly modular and evolved through a model-based design approach. Three primary subsystems comprise the robot – a cartesian positioning stage, the imaging system and the needle insertion mechanism (NIM). The development and testing of these subsystems are discussed in the following sections.

## Cartesian Stage

The enclosure with the integrated cartesian stage shown in figure 0-1 is the primary structural element of the device that houses the custom-designed electronics control board, a Raspberry Pi computer and the NIM. The stage employs 3 stepper motors coupled with lead screws to achieve highly precise positioning (50 microns) of the NIM at a chosen venipuncture site. The patient's arm is inserted into the device through an aperture lined by an inflatable cuff. The cuff is meant to stabilize the arm during the procedure and act as a tourniquet for better visibility of the vasculature of the ante-cubital fossa (ACF).

## Imaging System

The imaging system of the Phlebot consists of an infrared camera and an array of NIR multi-wavelength LED light sources. Previous attempts at vein imaging using NIR for clinical use were primarily augmented reality approaches. The raw images from

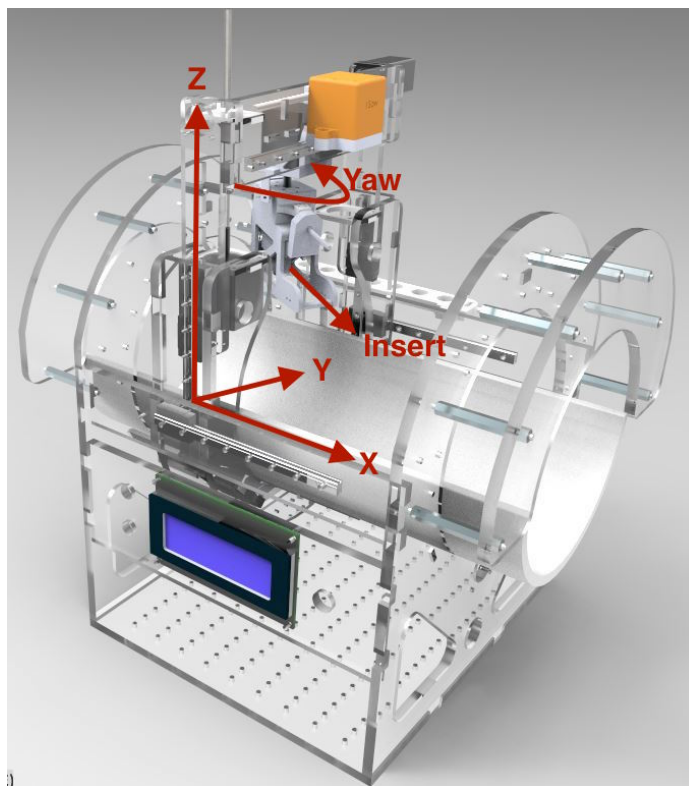


Figure 0-1: Phlebot - The Portable Robotic Phlebotomist with 5 Degrees of Freedom

the Phlebot's camera under various illumination conditions are combined and the resulting image is processed in OpenCV to enhance the veins. The image processing algorithm operates on a grayscale image and includes the following steps:

1. A median filter with 3px radius to denoise the image
2. An FFT bandpass filter with a 3-40px pass band
3. Binarization by thresholding
4. Erosion and dilation repeated until a threshold number of structures is reached
5. Outlier elimination based on distance from local centroid
6. Edge smoothing
7. Skeletonization to obtain vein centre lines instead of boundaries

In addition to the above steps, a linear Hough transform was used to fit veins to possible needle trajectories. The parameters of the imaging system such as the shutter speed, field of view and wavelength were experimentally determined through an IRB-approved small-scale study which examined the correlation between the parameters and the resulting image quality.

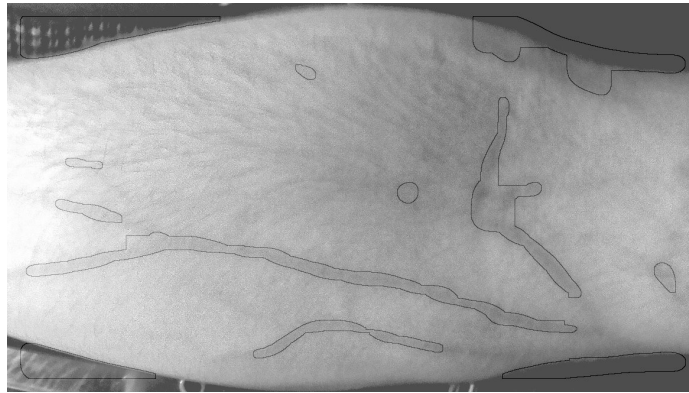


Figure 0-2: Result of the Vein Detection Algorithm in the ACF Region

Figure 0-2 shows an image with veins identified using the algorithm described above.

## Needle Insertion Mechanism

The needle insertion mechanism, shown in figure 0-3, is a 3D printed end effector that rides on the cartesian stage. It contains a magnetic quick-release needle holder for safety and ease of needle change between procedures. A geared brushless DC motor is used to actuate the insertion axis with an 86 micron resolution, comfortably within the average vein diameter. A very high-resolution force sensor is mounted aft of the mechanism to register the subtle changes in force as the needle punctures through the skin and the vein wall. This force data is observed by an insertion controller running at 800Hz that detects barrier penetration and stops insertion at a safe depth. Several rounds of data collection and analysis were used to characterize the dynamics of barrier penetration. A set of 11 phantoms designed to mimic dynamical properties of different veins and surrounding tissue combinations (viscoelastic moduli) was used

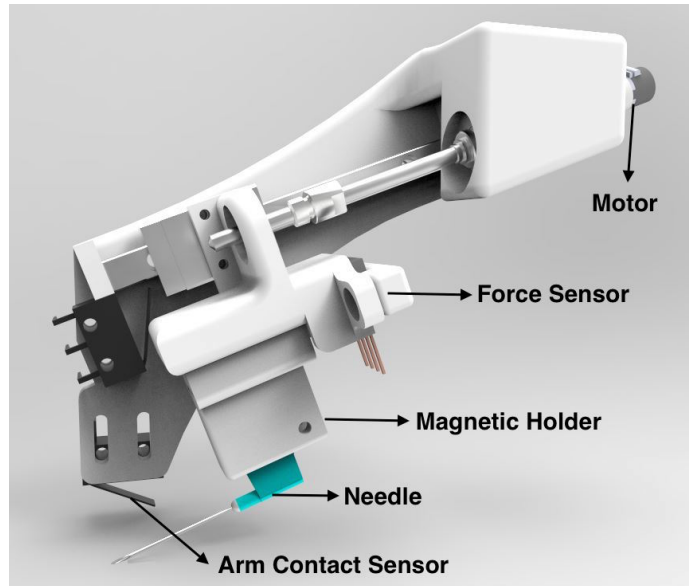


Figure 0-3: Needle Insertion Mechanism (NIM)

for validation. Figure 0-4 shows the force profile for an insertion procedure. The inflection points, which represent punctures, are prominent.

## Conclusion

The project demonstrated the feasibility of a portable robotic device capable of autonomous venipuncture. The NIR imaging system is able to identify veins in the forearm not easily visible to the naked eye. The needle insertion mechanism is able to reliably insert the needle into a phantom to a safe depth under computer control with force feedback from the needle tip. With a modular system architecture, subsystems can be individually tested and validated. The various subsystems that comprise the Phlebot are the result of combining novel approaches to robotic needle-insertion with improvements to existing technology.

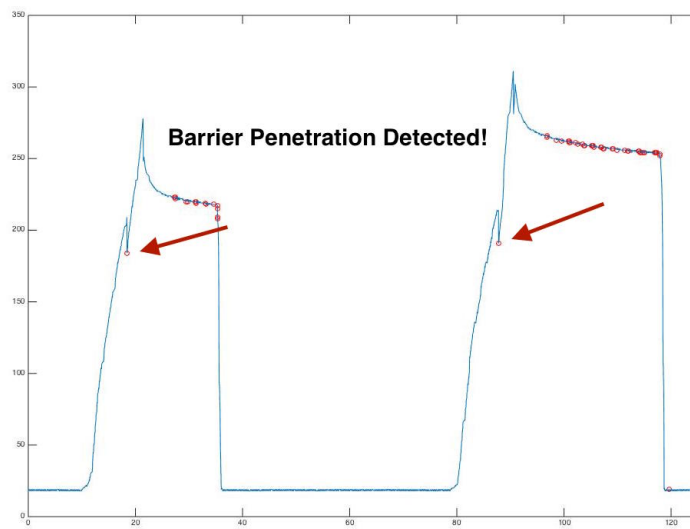


Figure 0-4: Force Profile During 2 Insertions into Phantoms for Validation of Barrier Penetration Detection Technique



## Authorship

The project both in realization and writing was divided into multiple parts spear-headed by different team members. The major contributor to several of the projects parts are outlined in table 1. Notice that said contributors refer to their actual development of that portion of the project and not necessarily the writing.

<b>Project Division</b>	<b>Main Contributor</b>
Background	Anurag, Sean
Vein Detection: Main Study	Sean
Vein Detection: Algorithm	Anurag
Mechanics: Stage	Paulo
Mechanics: NIM	All
Mechanics: Attachment	All
Software: Low-Level	Paulo
Software: High-Level	Anurag
Electronics	Paulo
Needle Insertion Controller	Sean

Table 1: Main contribution for each project division



## Acknowledgments

We dedicate this paper to our friends and families for their positive support, and to our advisers for their inertial guidance. We would like to give special thanks to Susan Milkman and Tom Goodrich, staff at the WPI Healthcare Delivery Institute, whose hard work kept the lab running. Finally, we would like to thank WPI for giving us the opportunity to work on such a rigorous and challenging project.



# Contents

<b>1</b>	<b>Introduction</b>	<b>23</b>
1.1	Chapter Summary . . . . .	23
1.2	Practice of Phlebotomy - An Overview and History . . . . .	23
1.3	Blood Samples - Requirements and Uses . . . . .	24
1.4	Complications in Phlebotomy . . . . .	25
1.5	Prior Art . . . . .	27
1.5.1	Related Technology . . . . .	27
1.5.2	Robotic Technology . . . . .	29
<b>2</b>	<b>Design Overview</b>	<b>33</b>
2.1	Chapter Summary . . . . .	33
2.2	Overall Project Goals and Requirements . . . . .	33
2.3	Timeline - Project Progression . . . . .	34
2.4	Research and Development Cost . . . . .	35
<b>3</b>	<b>Vein Detection</b>	<b>37</b>
3.1	Summary . . . . .	37
3.2	Problem Formulation . . . . .	37
3.3	System Development . . . . .	38
3.3.1	Small-Scale Imaging Study: Design . . . . .	38
3.3.2	Small-Scale Imaging Study: Materials . . . . .	47
3.4	Vein Detection Algorithm . . . . .	53
3.5	Future Direction . . . . .	57

<b>4</b>	<b>Mechanical Design</b>	<b>59</b>
4.1	Chapter Summary . . . . .	59
4.2	Cartesian Stage . . . . .	59
4.2.1	Summary . . . . .	59
4.2.2	System Background . . . . .	59
4.2.3	System Requirements . . . . .	60
4.2.4	System Development . . . . .	61
4.2.5	Future Direction . . . . .	65
4.3	Needle Insertion Mechanism (NIM) . . . . .	66
4.3.1	Summary . . . . .	66
4.3.2	System Requirements . . . . .	66
4.3.3	System Development . . . . .	68
4.3.4	NIM – Version 6 . . . . .	72
4.3.5	Future Direction . . . . .	72
4.4	Attachment Mechanism . . . . .	73
4.4.1	Summary . . . . .	73
4.4.2	System Background . . . . .	73
4.4.3	System Requirements . . . . .	73
4.4.4	System Development . . . . .	73
4.4.5	Future Direction . . . . .	77
<b>5</b>	<b>Electronics Design</b>	<b>79</b>
5.1	Chapter Summary . . . . .	79
5.2	Background . . . . .	79
5.3	Main Board . . . . .	80
5.3.1	System Requirements . . . . .	80
5.3.2	System Development . . . . .	81
5.3.3	Future Direction . . . . .	85
5.4	Infrared Lighting Rig . . . . .	86
5.4.1	System Requirements . . . . .	86

5.4.2	System Development . . . . .	87
5.4.3	Future Direction . . . . .	87
<b>6</b>	<b>Software Design</b>	<b>91</b>
6.1	Chapter Summary . . . . .	91
6.2	Embedded Software . . . . .	91
6.2.1	Software Background . . . . .	91
6.2.2	Software Requirements . . . . .	92
6.2.3	Software Development . . . . .	92
6.2.4	Future Direction . . . . .	98
6.3	High-Level Software . . . . .	98
6.3.1	Chapter Summary . . . . .	98
6.3.2	Software Background . . . . .	99
6.3.3	System Requirements . . . . .	99
6.3.4	System Development . . . . .	99
6.3.5	Future Direction . . . . .	101
<b>7</b>	<b>Needle Insertion Controller</b>	<b>105</b>
7.1	Summary . . . . .	105
7.2	Problem Formulation . . . . .	105
7.3	Background . . . . .	105
7.4	System Development . . . . .	107
7.5	Future Direction . . . . .	111
<b>8</b>	<b>Conclusion</b>	<b>113</b>
<b>A</b>	<b>Cuff Study: Materials and Glue</b>	<b>119</b>
<b>B</b>	<b>Financial Summary</b>	<b>129</b>
<b>C</b>	<b>Interface Document: IRRigV2</b>	<b>133</b>
<b>D</b>	<b>Interface Document: Main Board V1</b>	<b>145</b>

<b>E</b>	<b>Interface Document: Main Board V2</b>	<b>173</b>
<b>F</b>	<b>Low-Level Communication Protocol</b>	<b>205</b>
<b>G</b>	<b>Phantom Testing on Instron</b>	<b>215</b>
<b>H</b>	<b>Notes on Failure Conditions</b>	<b>221</b>
<b>I</b>	<b>JIRA Log</b>	<b>225</b>



# List of Figures

0-1	Phlebot - The Portable Robotic Phlebotomist with 5 Degrees of Freedom	5
0-2	Result of the Vein Detection Algorithm in the ACF Region . . . . .	6
0-3	Needle Insertion Mechanism (NIM) . . . . .	7
0-4	Force Profile During 2 Insertions into Phantoms . . . . .	8
1-1	VeinViewer device. . . . .	28
1-2	AccuVein device. . . . .	28
1-3	Bloodbot . . . . .	29
1-4	Veebot . . . . .	30
1-5	VascuLogic's VenousPro . . . . .	31
2-1	Project Issues Tracking in Jira . . . . .	36
3-1	Representation of parameter interaction for small scale study. . . . .	40
3-2	Flow chart depicting the four phases of the experiment . . . . .	43
3-3	Experimental and Nuisance Variables . . . . .	44
3-4	Small scale image study tester. . . . .	49
3-5	Version 2 of the tester with investigator's arm being imaged . . . . .	50
3-6	Agreement between investigators on significance of ANOVA columns	52
3-7	Agreement between investigators on significance of interaction . . . . .	53
3-8	Forearm . . . . .	54
3-9	Preliminary Image Processing Routine . . . . .	55
3-10	Raw Colour Image of the Ante-Cubital Fossa . . . . .	56
3-11	Raw IR Image of the Ante-Cubital Fossa . . . . .	56

3-12	Processed IR Image of the Ante-Cubital Fossa . . . . .	57
3-13	Candidate needle trajectories and venipuncture sites . . . . .	57
4-1	Overall mechanical design. . . . .	60
4-2	Stage V1 render and real. . . . .	62
4-3	Stage V2 render and real. . . . .	62
4-4	Stage V3 render and real. . . . .	63
4-5	Stage V4 render and real. . . . .	64
4-6	Stage V5 render and real. . . . .	65
4-7	Depiction of probable future direction stage V6. . . . .	67
4-8	NIM – Version 1 . . . . .	68
4-9	NIM Version 2 . . . . .	69
4-10	NIM Version 3 . . . . .	70
4-11	NIM Version 4 . . . . .	71
4-12	NIM Version 5 . . . . .	71
4-13	NIM Version 6 . . . . .	72
4-14	N-linkage attachment mechanism. . . . .	74
4-15	Motorised tensioning band attachment mechanism . . . . .	75
4-16	Active belt attachment mechanism. . . . .	76
4-17	Passive velcro attachment mechanism. . . . .	77
4-18	Inflatable cuff development. . . . .	78
5-1	Power regulation schematic for Main Board V1 . . . . .	84
5-2	Power-up sequence for Main Board V1. . . . .	85
5-3	Pictures of Main Board V1 and Main Board V2 . . . . .	88
5-4	Pictures of Infrared Rig version 1 and 2 . . . . .	89
6-1	UML class diagram for Main Code V1. . . . .	94
6-2	UML class diagram for Main Code V2. . . . .	96
6-3	UML class diagram for UI Code V1. . . . .	97
6-4	UML class diagram for NIM Code V1. . . . .	102

6-5	Typical Workflow for the Phlebot . . . . .	103
6-6	Phlebot Control Center V1 . . . . .	103
6-7	Phlebot Control Center V2 . . . . .	104
6-8	Phlebot Control Center V3 . . . . .	104
7-1	Discovering Elastic Moduli of Phantoms . . . . .	108
7-2	Stress vs strain of phantom sample 3 with regression line . . . . .	109
7-3	Insertion and puncture detection on silicon tube. . . . .	110



# List of Tables

1	Main contribution for each project division . . . . .	9
2.1	Pair wise comparison chart of project requirements. . . . .	34
2.2	Project Timeline: Expected vs. Actual . . . . .	35
2.3	Budget estimate from early stages of project planning. . . . .	36
3.1	Main study fractional factorial experiment (Part 1). . . . .	47
3.2	Main study fractional factorial experiment (Part 2). . . . .	47
3.3	Experimental variable level. . . . .	52
4.1	Decision matrix for stage motor selection. . . . .	61
4.2	Decision matrix for selection of attachment mechanism. . . . .	74
5.1	Summary of Main Board requirements . . . . .	80
5.2	Comparison of features between Main Board V1 and Main Board V2. . . . .	81
5.3	Feature list of ATMEGA family microcontrollers . . . . .	82
5.4	Comparison of inertial measurement units of Main Board V1 and V2. . . . .	83
5.5	Comparison of power regulation in Main Board V1 and V2. . . . .	85
5.6	Comparison of requirements between IRRig versions. . . . .	86
5.7	Feature comparison between IRRig versions. . . . .	87
6.1	Summary of embedded software requirements. . . . .	92
7.1	Relative Concentrations of PVC and Plasticizer for each test phantom . . . . .	107
7.2	Elastic modulus for each phantom . . . . .	109



# Chapter 1

## Introduction

### 1.1 Chapter Summary

This chapter introduces the history of phlebotomy, its evolution and current medical practices. The various diagnostic tests dependent on accurate blood sample collection are explained in connection with their clinical needs. Possible complications emerging from improper procedures and the The chapter concludes with a survey of the state of the art in robotic approaches to phlebotomy.

### 1.2 Practice of Phlebotomy - An Overview and History

Phlebotomy, in its modern form, is a relatively young practice in the two-thousand-year-old history of western medicine. Until as recently as the 1860s, bloodletting was very commonly prescribed by European physicians for treating many common diseases and ailments such as pneumonia, fevers, migraines etc [25, 16]. The procedure itself was carried out by barbers with their crude implements in their surgeries. A vein on the forearm of the patient was punctured with a scalpel and blood allowed to drip into a graduated container placed underneath. Sometimes, leeches were used for this purpose, making the procedure only slightly less painful. Tens of millions

of leeches were imported for this purpose during the 1830s in France and England. Although ancient Indian and Greek physicians used bloodletting for a wide range of specific conditions, its prescription spread rampantly in medieval Europe until it became the go-to method to cure any and all ailments [17]. One of the first people to scientifically challenge this seemingly crude and ubiquitous procedure was English physician William Harvey. It was Harvey who first presented a rigorous anatomical study of systemic circulation in living beings complete with detailed pictures in his *de Motu Cordis*. Drawing from his findings, he disproved the efficacy of bloodletting as a cure for many ailments. The Dutch scientist Leeuwenhoek, with his handcrafted microscopes, was able to validate Harveys theoretical assertions and confirm the experimental findings through closer observation of blood vessels. By the end of the nineteenth century, a more scientific approach to medicine was favored as scientists such as Joseph Lister, Louis Pasteur and Robert Koch showed that germs and not humors were responsible for diseases. By the beginning of the twentieth century, bloodletting had almost completely died out and replaced with scientific medicine. Today, phlebotomy refers to the specific medical procedure of gaining access to venous blood either for sampling, therapy or injections. It is performed by inserting a needle into a vein on the forearm and extracting the blood by means of a low-pressure suction through a syringe or a vacutainer.

### 1.3 Blood Samples - Requirements and Uses

As the body's method for transporting waste, nutrients, and chemical signals, blood is crucial for understanding a patient's physiological state. Taken both in routine physicals and when trying to investigate the cause of illness, the NIH lists 17 main categories for blood tests [28]:

- Complete Blood Count
- Red Blood Cells
- White Blood Cells



- Platelets
- Hemoglobin
- Hematocrit
- Mean Corpuscular Volume
- Blood Chemistry Tests/Basic Metabolic Panel
- Blood Glucose
- Calcium
- Electrolytes
- Kidneys
- Blood Enzyme Tests
- Troponin
- Creatine Kinase
- Blood Tests To Assess Heart Disease Risk
- Blood Clotting Tests

Within each of these categories there are many tests each focusing investigating a specific disease or condition. The result is hundreds of tests requiring high quality blood samples, making venipuncture the most common invasive medical procedure [15].

## 1.4 Complications in Phlebotomy

Typically, a blood sample will be taken by either a trained phlebotomist or a nurse and the tests performed by hematologist. Critical to this process is proper labeling of the specimen; however, it is thought that labeling errors occur between 0.1 to 5 percent

of the time depending on the clinic [36]. While this may seem like a small percentage, since the procedure is performed at least 1 billion times annually in the United States the effects are not insignificant [8]. In cases where frequent testing is required to determine whether a treatment is effective, such as for cancer patients, multiple blood draws are required within a short timeframe. Repeated draws can cause severe trauma in children, many of whom are intolerant to consistent venipuncture, and immense pain for the elderly, whose veins are prone to collapse [citation needed]. Even when dealing with healthy adults, proper cannulation can be difficult, and while infrequent the injuries associated with improper phlebotomy, such as nerve pain, can be long lasting [8]. While a relatively simple procedure, the issues surrounding phlebotomy are not insignificant and measures need to be taken for their reduction.

In addition to the systemic issues inherent to phlebotomy, i.e. the difficulty in proper cannulation and the errors which arise in proper tracking of blood specimen, further problems arise in ensuring the specimen collected is suitable for analysis. Factors which render a sample unusable before analysis are part of what is referred to as the preanalytic phase [36]. While the causes of errors in the preanalytic phase are not solely associated with blood collection, it is estimated that inappropriate collection procedures account for 60 of the total [22]. In those cases where a sample is unusable due to errors in the preanalytic phase, a second round of collection is necessary causing not only greater patient discomfort but also causing delayed treatment for other patients particularly in emergency rooms where improper specimen collection can cause delays of up to 2 hours [23]. A significant amount of research has been done to assess the aspects of the venipuncture procedure leading to inadequate specimen collection [27] [22] [21]. Perhaps the greatest culprit is the choice of blood collection devices. These devices include the type and gauge of the needle, tourniquet use, intravenous (IV) catheter versus straight needle, and vacutainers versus syringes. While it has been found that the use of straight needles and vacutainers result in a reduction of hemolysis, IV catheters are often preferred in emergency departments [12]. Additionally, it has been found that hemolysis rates are higher when blood is drawn from the right arm versus the left [12]. While the use of a tourniquet may lead to increased

rates of hemolysis, this is typically due to improper tensioning and release on the part of the clinician. While not all blood tests are affected by hemolysis, this does not reduce the importance of collecting non-hemolyzed blood specimen [39]. Other causes of unsuitable specimen are less common but include the transfer of analyte from one collection container to another, temperature of the specimen, and the delay between sample collection and sample analysis [36]. In addition to technologies and reforms aimed at reducing the error in the preanalytic phase, the advancement of point-of-care analysis devices will reduce the chances of failed clinical tests.

In addition to complications with the analysis of blood specimen, multiple attempts at cannulation are frequently undertaken by phlebotomists. This is the case because first attempts have only a limited success rate of approximately 75% as phlebotomists are trained to rely on tactile feedback more than visual feedback of veins. This causes severe patient distress and commonly leads to trypanophobia, the fear of needles, usually in children. Patients are not the only ones at risk of incurring complications during phlebotomy. Every year, 385,000 needlestick injuries to clinicians are reported in the United States alone. As much as 55% of these injuries occur during needle use and disposal when the needles are being resheathed. [30] A larger number of needlestick injuries go unreported each year.

## **1.5 Prior Art**

### **1.5.1 Related Technology**

Currently there are no commercially available systems for image-guided autonomous or semi-autonomous robotic phlebotomy. However, there are devices on the market which enable better visualization of the veins such as AccuVein and VeinViewer.[26] These devices, shown in figures 1-2 and 1-1, use an imaging system to image the region under observation, enhance the contrast of vasculature and project the enhanced image onto the patient. [37, 29] This augmented reality approach is currently the most popular approach to improving success of phlebotomy and venous access in

general.

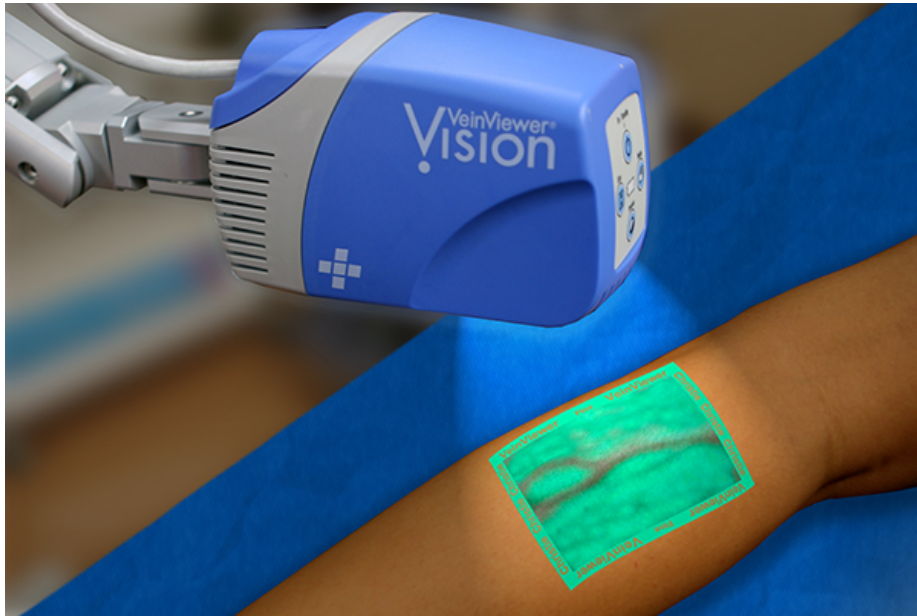


Figure 1-1: VeinViewer device projecting image of veins over patient's arm.



Figure 1-2: AccuVein projecting image of veins over patient's arm.

NoNeedles Venipuncture Inc. is a startup from Florida that is exploring a radical alternative to traditional needle-based venipuncture. Their system, currently under development, employs a high-precision laser beam to create a microchannel through

the skin into the vein for blood draw. The laser beam is positioned using an ultrasound probe. After the blood draw is complete, the laser is used to cauterize the wound and seal it.

## 1.5.2 Robotic Technology

Robot-assisted techniques for phlebotomy have been gaining much traction in recent years. The Phlebot is on par with other systems currently under development. Here, we will look at 3 systems in detail and compare their technical approaches to the problem of robotic phlebotomy.

### Bloodbot

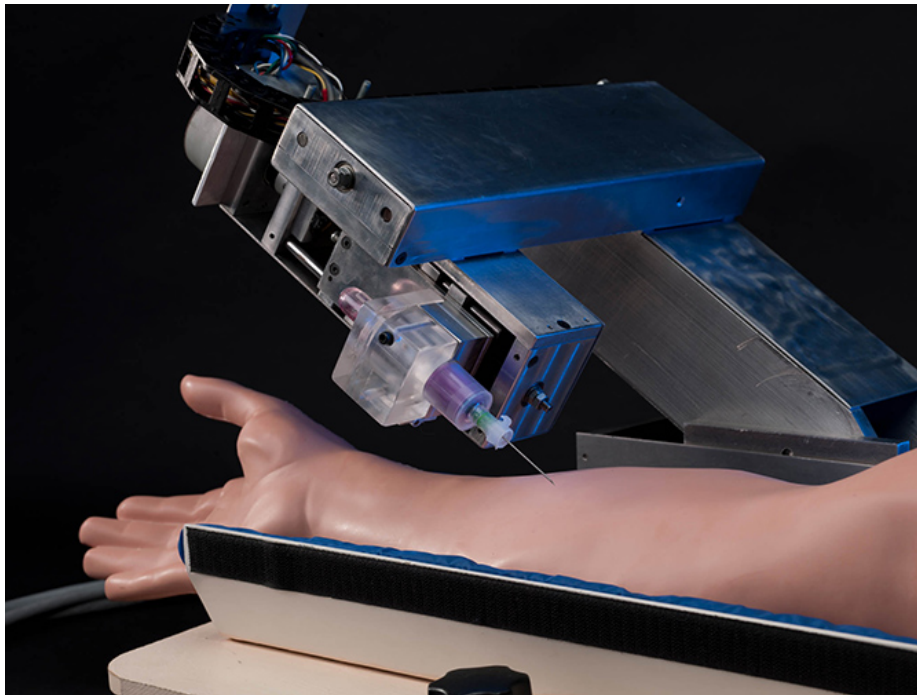


Figure 1-3: Bloodbot

Bloodbot was designed at the Mechatronics in Medicine Laboratory at the Imperial College London in 2001 (see figure 1-3). It used three linear motion axes driven by stepper motors to position a sensing probe or needle in 3D space and a fourth rotary axis that allowed the entire mechanism to tilt in order to vary the angle of

needle insertion. A piezo-resistive force sensor was used to measure the force from the probe or the needle during insertion. By measuring the difference in the forces encountered when the probe is over a vein versus surrounding tissue, the team was able to characterize the elastic properties of the vein and use that model to distinguish between veins and the surrounding tissue. During venipuncture, the force sensor is used to detect the needle's entry into the vein as there is an inflection point in the force profile during the needles motion. Bloodbot was the first robot to prove that an autonomous venipuncture solution was feasible but research on the device appears to have been discontinued for over a decade.

## Veebot

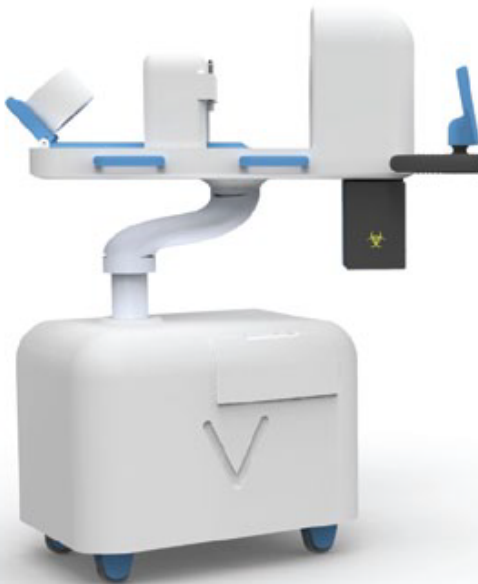


Figure 1-4: Veebot

Veebot is a robotic phlebotomist envisioned by Stanford graduate students and is currently under development for commercialisation. It features a near-IR imaging system to locate veins and an ultrasound probe for measuring blood flow in the veins. The device itself is bulky and not very portable (see figure 1-4). A list of recent

additions to the device include automatic needle disposal and tourniquet.

## VenousPro

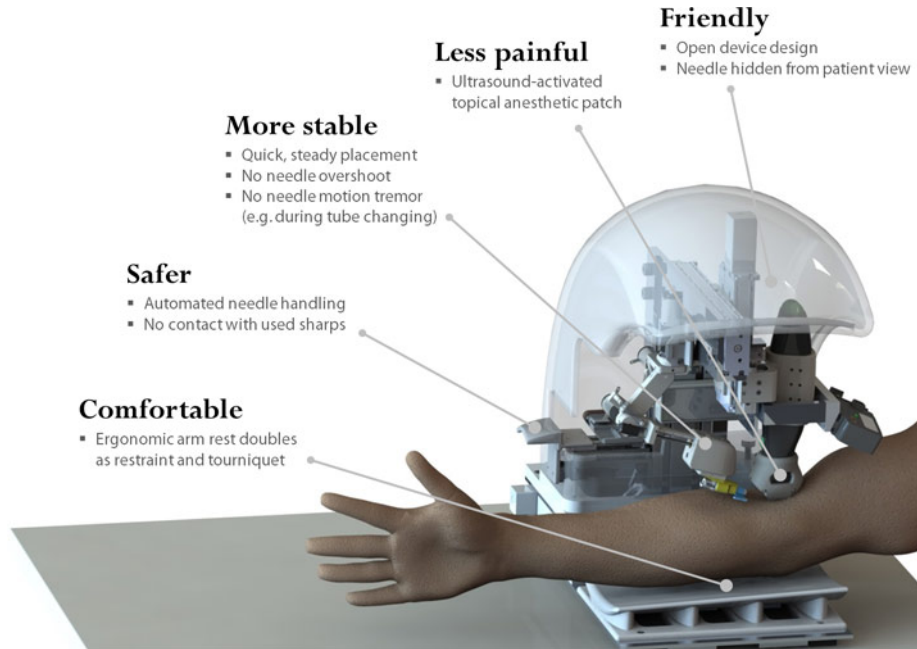


Figure 1-5: Vasculogic's VenousPro

Vasculogic's VenousPro is a robotic phlebotomist that comes closest to the Phlebot in terms of functionality. It has an open design, appears to be portable and like the Veebot, employs ultrasound in addition to infrared imaging.[24] (see figure 1-5). A 3D model of the vein is constructed from these 2 sensors and the vein is tracked in real-time for needle guidance. [9]





# Chapter 2

## Design Overview

### 2.1 Chapter Summary

This chapter gives an overview of the design process of the Phlebot, including the project planning and budget. To be an improvement on current health-care practices, the Phlebot needed to be designed to fit tight specifications; however the prototype presented is still far from the final realization envisioned by the investigators. The timeline for the project shows that the ambition and zeal of the team when the project began did not match with the true complexity of developing a surgical robot. Even so, on a shoestring budget the team was able to create a fully functional prototype which begins to meet the design requirements put forth by the team.

### 2.2 Overall Project Goals and Requirements

The Phlebot's relevance and utility can only be realized if it is able to fulfill the deficiencies currently faced in phlebotomy. Further, the device must be easily integrated into a clinician's routine in a way they find acceptable. After long discussion and two interviews with phlebotomists, the following pairwise comparison chart, figure 2.1, was used to rank the areas of greatest importance in the design of the Phlebot.

Our goal in this project was to complete a prototype ready to perform clinical tests covering the entire phlebotomy procedure. Additionally, we had hoped to have

Goals	Inexpensive	Robust	Safe	Easily Used	Autonomous	Accurate	Portable	Universal	Expedient	Score
<b>Inexpensive</b>	x	0	0	0	0.5	0.5	0	0.5	1	<b>2.5</b>
<b>Robust</b>	1	x	0	0.5	1	0.5	0	1	1	<b>5</b>
<b>Safe</b>	1	1	x	1	1	1	0.5	1	1	<b>7.5</b>
<b>Easily Used</b>	1	0.5	0	x	1	0	0	1	1	<b>4.5</b>
<b>Autonomous</b>	0.5	0	0	0	x	1	0.5	1	1	<b>4</b>
<b>Accurate</b>	0.5	0.5	0	1	0	x	0	1	1	<b>4</b>
<b>Portable</b>	1	1	0.5	1	0.5	1	x	1	1	<b>7</b>
<b>Universal</b>	0.5	0	0	0	0	0	0	x	0.5	<b>1</b>
<b>Expedient</b>	0	0	0	0	0	0	0	0.5	x	<b>0.5</b>

Table 2.1: Pair wise comparison chart of project requirements.

plans already drafted for introducing additional features, such as pain distraction, to the completed Phlebot to improve the functionality and relevance of the device. Unfortunately, the Phlebot was not developed to the team’s desired state due to a greater complexity and expense originally anticipated by the team. Regardless, the final constructed prototype is only one or two revisions away from meeting the lofty goals set forth by the team all those months ago.

## 2.3 Timeline - Project Progression

As with many projects, the schedule initially made for the development of the Phlebot was more optimistic than realistic. Table 2.3 shows our initial projections versus our actual progress. Project progress was tracked through Jira (see appendix I). Figure 2-1 shows issues created and resolved over a 300-day period. Initially, we did not take into consideration the extent we should verify and validate our design choices; however, when the time came we were vehement in our analysis of the current prototype. This allowed us to quickly progress from one design to another and called for splitting the project into separate modules to facilitate parallel development of the critical subsystems. As we were finding new requirements and constraints from one design iteration to the next, it became difficult to narrow down a timeline to accurately reflect the direction we were taking. As such we borrowed the idea of sprints from agile software development and would plan our advancement from one sprint to another. It is only at the current stage of the Phlebot, in which there is a working prototype, that accurate long term planning can take place.

Month	Initial Projection	Actual Implementation
January '14	Project Justification List of Design Requirements Project Timeline	Met
February '14	Budget Speak to clinicians	Met
March '14	Define project scope Experiment with vein imaging	Met
April '14	Proof of concept	Met
May '14	Hardware Development	Hardware Development
June '14	" "	Rapid Prototyping
July '14	" "	Prototype Validation
August '14	" "	Vision R&D
September '14	Fully Functional Hardware Prototype (Mechanical & Electrical)	" "
October '14	Software Development Hardware Testing	" "
November '14	" "	Low Level Software
December '14	Software Complete	Fully Functional Hardware Prototype
January '15	System Validation	Debugging System Integration
February '15	" "	Vein Selection Algorithm Needle Insertion Control
March '15	Begin clinical trials	Preliminary System Testing Documentation
April '15	" "	" "

Table 2.2: Project Timeline: Expected vs. Actual

## 2.4 Research and Development Cost

The team was asked for a budget estimation in the early stages of project design and consideration. Table 2.3 illustrates said budget. In it a factor of 3 was estimated between the development cost and that of the actual prototype cost. Interestingly, excluding set-up costs, the team was able to keep within the expected budget with the total development cost of approximately 5200 dollars (excluding equipment cost) and an actual prototype cost of approximately 2000 dollars. For more information on the budget appendix B shows an exhaustive list of all purchases in the MQP.

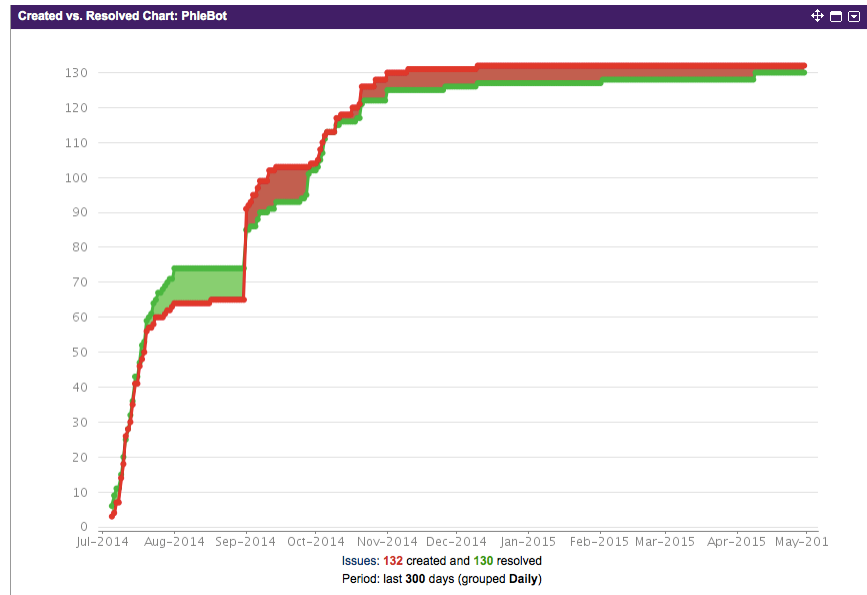


Figure 2-1: Project Issues Tracking in Jira

Category	Description	Development Cost (\$)	Actual Cost (\$)
Vein Detection	Imaging, Tonography, etc.	1345	320
Mechanics	Motors, 3D Printing, Machining	2359	1378
Electronics	Motor Driver, Processing Unit	1354	600
Auxilliary Sensors	Temperature, Pressure, Light, Inertial	500	80
Phantom	Buy,Make,Steal?	600	0
Passive Hardware	Case, Straps, Cuffs, Tubes etc.	965	200
Accessories	Needles, Laser	200	0
Books	Knowledge	300	Priceless. But 0.
		<b>Total (\$)</b>	<b>Total (\$)</b>
		7623	2578

Table 2.3: Budget estimate from early stages of project planning.

# Chapter 3

## Vein Detection

### 3.1 Summary

A major issue in automated phlebotomy is vein selection and detection. Previous solutions have tackled the problem by using ultrasonography, stereoscopic NIR imaging, or tactile feedback.[19, 26] Our approach relies on a 2D NIR imaging combined with a vein extraction algorithm to determine suitable insertion sites. To determine the factors of greatest importance in the imaging system a preliminary fractional factorial study was conducted on 9 subjects which showed the two factors of consistent significance were the wavelength and the shutter speed. The test was carried out by an automatic test robot which varied the image system parameters under test. Finally, a vein extraction algorithm was developed to locate potential insertion sites from an image.

### 3.2 Problem Formulation

There are three main tasks which must be accomplished by the Phlebot in order to successfully collect a blood sample. First, the robot must have a way to detect the veins of the patient and select the one which is most likely to result in successful puncture of the vein on the first try. Next, the robot must properly align and insert the needle at the correct depth into the patients arm. Finally, the blood sample vial

must be filled and the needle removed and disposed of. The focus of the experiment outlined in this document deals with ensuring the proper detection and selection of the veins. The method currently being used for vein detection is a NIR imaging system consisting of an IR light source, a camera lens with a band-pass filter to isolate the wavelength of light detected, and the camera itself. Once the image has been captured, a computer vision system will be used to select the appropriate vein candidate for drawing blood. To ensure the vein detection algorithm would work across the entire population we studied the effect of varying the parameters of the imaging system and its effect on the image captured.

## **3.3 System Development**

### **3.3.1 Small-Scale Imaging Study: Design**

#### **Optics Background**

To understand the design of the experiment, it is helpful to have a basic understanding of optics and how varying parameters of the imaging system will affect the photo taken. The three components required for an imaging system are the camera, lens, and light source. The camera is responsible for two main parameters which relate directly to the optics; the sensor size and the number of pixels. The effect of the other camera parameters cannot be influenced by the choice of lens. The lens is the device responsible for adapting a given sensor to an application, but it is important to have already chosen a camera able to meet the requirements of the imaging system. The parameters inherent to the choice of lens are the focal length, the aperture/iris setting (f-number), and the angular field of view. Often the use of monochromatic light improves the ability of imaging system by avoiding chromatic aberration, as such an optical filter can be added to the lens to allow only a narrow band of wavelengths to reach the camera. The final piece of the imaging system, other than the object under study, is the lighting system which has three parameters that can be varied directly: the location, intensity, and wavelength of light. The dependent variables

of the imaging system of greatest interest for this application are the resolution, contrast, and field of view. It is these three variables on which the image processing algorithm depends; however, there is another parameter, the depth of field, important to the design of the Phlebot. The depth of field measures how well the resolution is maintained as the lens is moved out of best focus. While equations 1 - 8 govern the imaging system, they are not enough to fully characterize the output. For instance, it is well known that the intensity of the light source is critical to providing the proper illumination in turn improving the contrast, yet this is not shown in the equations. Advanced topics in optics, such as distortion and vignetting, have been not been included in this paper. While both are important aspects of the imaging system, their explanation is beyond the background required for understanding the experiment. The parameters are shown in figure 3-1. For an in depth explanation of distortion see [5], for vignetting see [6].

Below are the equations governing the output of the imaging system based on the parameters of the camera, lens, and light source. Each equation is accompanied by a brief description of how it affects the output. Further, figure 1 shows the interaction between all the experimental variables and the output of the imaging system.

The angular field of view  $\theta$  is governed by the lens, the image field of view (FOV), and the working distance (WD) as shown in equation 3.1. The image field of view measures how large an area is captured in the image.

$$\tan\left(\frac{\theta}{2}\right) = \frac{FOV}{2 * WD} \quad (3.1)$$

Resolution can be measured in two ways, either in  $\mu m$  or line pairs (lp) per millimeter, both representing the smallest resolvable area. The resolution of the image in lp is given by equation 3.2. It should be noted that this is the maximum resolution of the camera, not of the imaging system as a whole.

$$\frac{ImageSpaceResolution}{lp/mm} = \frac{1000\mu m/mm}{2 * PixelSize(\mu m)} \quad (3.2)$$

The primary magnification (PMAG), given by equation 3.3, measures how much

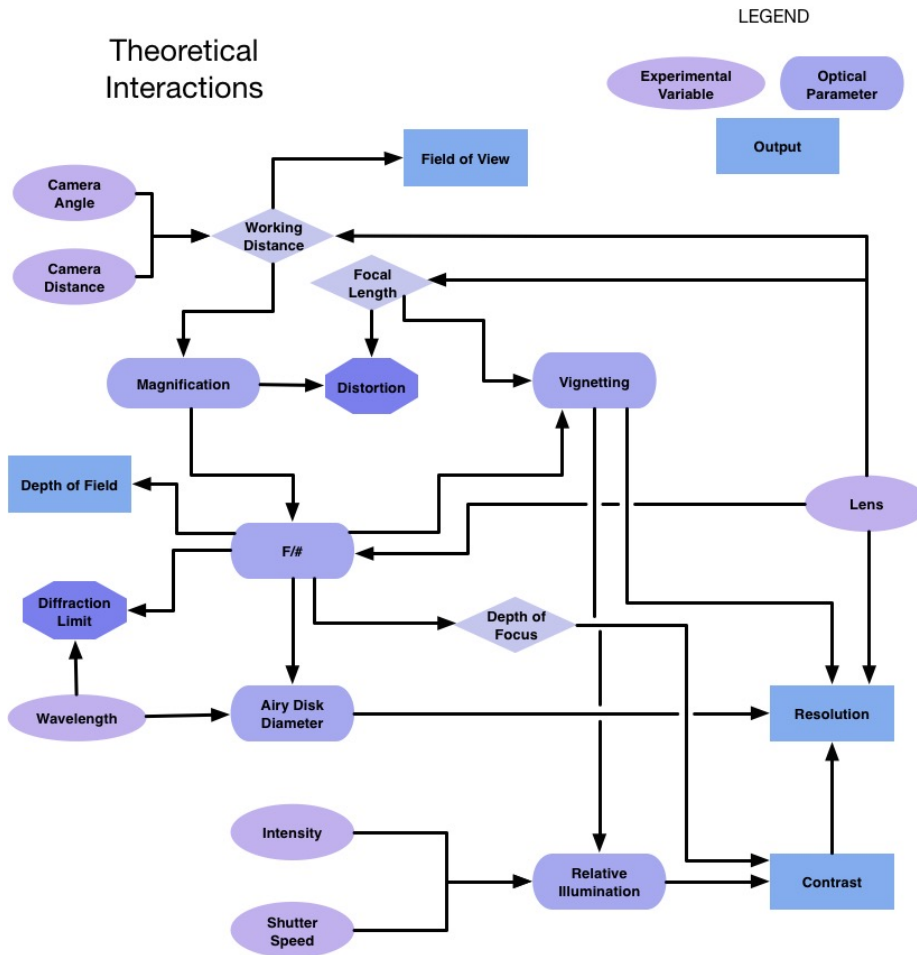


Figure 3-1: Representation of parameter interaction for small scale study.



the image is magnified when the lens is a given distance away from the object being photographed.

$$PMAG = \frac{SensorSize}{FieldofView} \quad (3.3)$$

Contrast can be calculated from the difference in intensity between pixels as given by equation 3.4. The amount of contrast seen by the camera depends primarily on the f-number of the lens and the illumination. Using monochromatic light will result in greater contrast.

$$\%Contrast = \frac{l_{max} - l_{min}}{l_{max} + l_{min}} * 100 \quad (3.4)$$

The theoretical f-number is given by equation 3.5 and remains constant for fixed lenses. The effect of the f-number can be seen in 1. DEP is the effective aperture diameter.

$$f/\# = \frac{EFL}{D_{EP}} \quad (3.5)$$

The theoretical f-number assumes the lens to be an infinite distance away from the object under study. When this assumption does not hold true, equation 3.6 is used to determine the working f-number.

$$(f/\#)W = (1 + |PMAG|) * f/\# \quad (3.6)$$

The smallest spot which can be resolved by the optics is given by equation 3.7 where  $\lambda$  is the wavelength of the light in  $\hat{\text{ijm}}$ . This is due to the diffraction of the light as it enters the sensor. This equation is known also known as the Rayleigh Criterion.,

$$MinimumSpotSize = 2.44 \times \lambda \times f/\# \quad (3.7)$$

The diffraction limit is the maximum resolution which can be achieved by the imaging system at a given wavelength and aperture setting. This limit is given by

the equation 3.8.

$$DiffractionLimit = \frac{1000\mu m/mm}{f/\# \times \lambda} \quad (3.8)$$

## Experiment Background

While the theoretical interaction between these variables are known, the importance of each for this application is not. Due to the differences in absorption of given wavelengths of light between the veins and the surrounding tissue, the output of the imaging system is subject to variation based on the physical properties of the arm. This variation is not easily or accurately represented by a mathematical model. Further, there are parameters of the imaging system that do not have a simple mathematical representation yet still need to be accounted for in the design. To obviate the uncertainty caused by the physical properties of the arm and the unmodeled optical properties, the experiment outlined herein will consist of the following four phases: characterization of the most significant variables, the interaction between the most significant variables, the optimal values for the most significant variables, and how robust the output is to slight changes in the camera distance, camera angle, and light intensity. For the first three phases, the results of the previous phase will be used to determine the parameters of the next. The fourth phase, the measurement of robustness, is independent of the previous phases. A flowchart showing the experimental flow is shown in figure 3-2 and the variables shown in figure 3-3.

## Experiment Setup

a) Experimental and Nuisance Variables: Before explaining the experimental procedure an introduction to both the experimental and nuisance variables will be given. The experimental variables, those whose effect are being studied in this experiment, are shown in figure 3-3. Further, this flowchart shows all the possible levels which are being considered for the experimental values; however, this does not mean that all levels will be included. The experimental variables were chosen based on the governing principles of the optics as explained previously. In addition to the six experimental

**Experiment  
Flow**

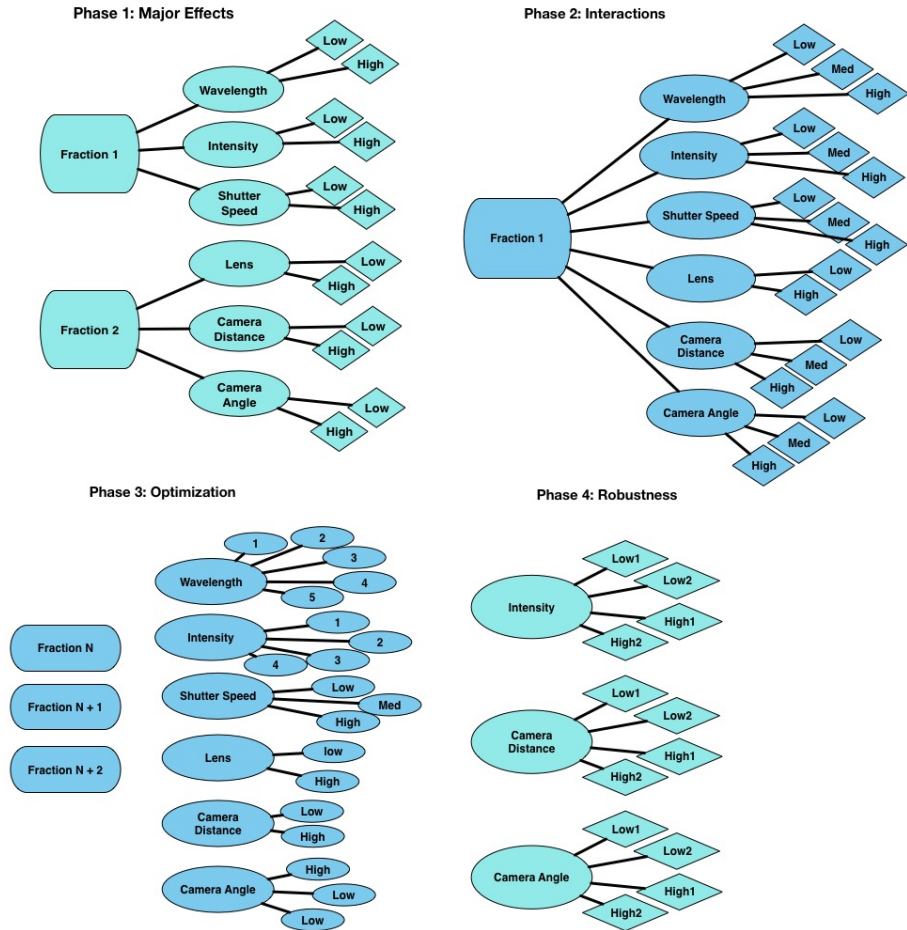


Figure 3-2: Flow chart depicting the four phases of the experiment

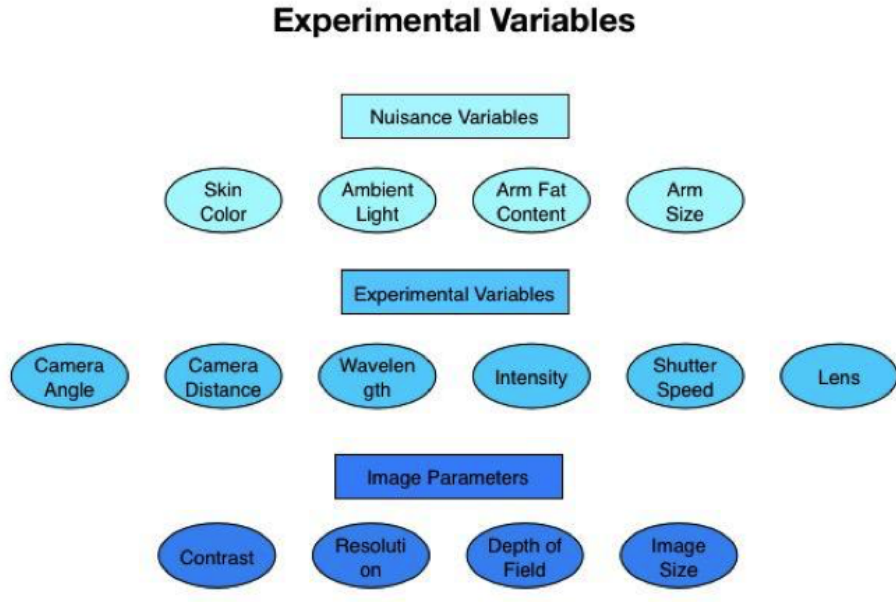


Figure 3-3: Experimental and Nuisance Variables

variables, there are also seven nuisance variables being considered in this experiment. The nuisance variables, as shown in figure 4, are split between controllable and measured. The controllable nuisance factors are ones which can be directly controlled by the investigators through the test fixture for the arm position and the use of an optical filter for the ambient light. The measured nuisance variables are parameters which deal directly with the choice of subject and cannot be controlled, as such they will be measured and recorded. For the measured nuisance variables, only two levels will be considered. The two levels will be chosen such that they are opposites. In addition to covering both extremes of the nuisance variable, recording only two levels will help maintain the anonymity of the participants. This is not an exhaustive list of all possible nuisance variables but were determined to be the ones which are most likely to have an affect on the output.

b) Subject Selection: The subjects to be considered for this experiment are the students, staff, and faculty of Worcester Polytechnic Institute. Since the absorption of NIR wavelengths by tattoo ink is unknown and not directly related to the parameters under investigation, individuals with tattoos around the Cubital Fossa will not be considered for this experiment. To reduce the variation in the output due to dif-

ferences in potential subjects, the same group of subjects will be used for each phase of the experiment. A minimum of four subjects will be chosen and at most eight subjects will be chosen. The intent for this choice is to have a single replicate associated with each level of the measured nuisance variables (i.e. two males and two females); however, subjects will not be chosen specifically to meet this intent. Instead, it is assumed that the variation in the population being sampled from is great enough that this will not be an issue. A sample size based on the nuisance variables was chosen to get an estimate the worst case variance which can be expected due to uncontrollable factors. The upper limit of eight subjects was chosen because it doubles the chance of having a single replicate for each level of the measured nuisance variables while also limiting the total number of subjects for an initial experiment to a number which is manageable by the investigators.

c) Tester: To standardize the data collection and reduce test time, the investigators will design and build a robotic tester. The tester will be responsible for varying the experimental parameters, except for the choice of lens, during each test. The lens will be changed by the operators during the test. Further, the tester will include a fixture responsible for immobilizing the subjects arm while the test is being performed. The camera chosen for the tester will remain constant through this experiment. The variance introduced by the tester will be characterized by performing gauge repeatability and reproducibility (GR&R). The GR&R will be performed on the three student investigators cycling through a full factorial experiment with three repeats. The ANOVA method will be used to generate the GR&R scores. d) Test Procedure: Each test, no matter which phase, will begin with the investigators describing the test to be performed and once again asking the subject if they consent to being a part of this study. Should the patient consent, they will have their right arm, unless blemished by an identifying mark in which case the left arm will be used, placed into the fixture which will hold the arm in place. Next, the tester will begin running through the experimental parameters which have been included for the current experiment phase. An image will be taken at each level and stored on the on-board computer of the tester. When the time comes to change the lens, the tester

will stop and an operator will replace the lens. The amount of time taken for a given run will depend on the speed of the tester, currently unknown, and the phase of the experiment.

#### B. Phase 1

The first phase of the study is meant to determine which of the experimental variables are of the most significance. This phase consists of two  $2^6/3$  fractional factorial experiments with each factor being represented at two levels. This results in 16 runs per subject corresponding to 16 images of the Cubital Fossa being taken. Tables 3.1 and 3.2 show value of the levels for each experimental variable. The + means the highest level for the experiment will be used and the - means the lowest level will be used.

#### C. Phase 2

Phase two takes the most significant factors found from the first phase and does a full factorial experiment with three levels for all factors except the lens for which only two factors will be used. The intent of this phase is to characterize the interactions between the factors. Since a fractional factorial study was used in the first phase, many of the runs needed for this phase will have already been run. This will greatly reduce the test time required.

#### D. Phase 3

The third phase of the study will consist of a combination of fractional factorial studies where the number of fractions is chosen based on the strength of interactions between factors determined in the previous phase. In this experiment, all possible levels for each of the factors will be used. The purpose of this phase is to obtain an estimate of the optimal value for each of the factors.

#### E. Phase 4

Phase 4 is independent of the three preceding phases, and will not use the use the values for the experimental variables shown in figure 3. Since this phase is meant to characterize the robustness of the imaging system to slight perturbations which cannot be controlled during the operation of the robot, four levels will be used for the camera distance, camera angle, and shutter speed. The four levels will consist

of two which are considered high that differ by no more than 10% and another two considered low differing by a similar amount.

Experimental Variables					
Wavelength	Intensity	Shutter Speed	Camera Angle	Camera Distance	Lens
A	B	C	D	E	F

LEGEND						
Basic Design						
Run	A	B	C	D = AB	E = AC	F = BC
1	-	-	-	+	+	+
2	+	-	-	-	-	+
3	-	+	-	-	+	+
4	+	+	-	+	-	-
5	-	-	+	+	-	-
6	+	-	+	-	+	-
7	-	+	+	-	-	+
8	+	+	+	+	+	+

Table 3.1: Table representing the  $2^{6-3}$  fractional factorial experiment in which the full factors are the shutter speed, the wavelength, and the intensity of the light.

Basic Design						
Run	D	E	F	A = DE	B = DF	C = EF
1	-	-	-	+	+	+
2	+	-	-	-	-	+
3	-	+	-	-	+	+
4	+	+	-	+	-	-
5	-	-	+	+	-	-
6	+	-	+	-	+	-
7	-	+	+	-	-	+
8	+	+	+	+	+	+

Table 3.2: Table representing the  $2^{6-3}$  fractional factorial experiment in which the full factors are the lens, the camera angle, and the camera distance.

### 3.3.2 Small-Scale Imaging Study: Materials

Before starting the study, we first took the following measures:

1. Obtained IRB approval to perform the study (HHS IRB # 00007374).

2. Designed, built, and tested a robot to automatically change the experimental variables
3. Collected and Scheduled Study participants

The study obtained IRB approval through the WPI IRB by following the procedure listed on their website. All student investigators completed the National Institute of Health web based training course on Protecting Human Research Participants prior to seeking IRB approval. The primary contact for matters regarding the study is Sean Weaver. The calibrations needed to develop the experiment were performed on the student investigators.

### **Automatic Test Robot**

We built an automated tester that would repeatably vary the imaging parameters for the study. The automated tester had three design revisions before deemed operational. The tester has two main components: the camera system and the illumination. It was necessary for the design to provide both consistent illumination and the ability to quickly step between different wavelengths of illumination. A further restriction on the tester was the ability of the camera to interface with a raspberry pi computer limiting the available choices of camera to be used. This restriction was due both to cost, ease of use, and the design of the PhleBot which would be using a raspberry pi for image acquisition and processing. By extending this decision to the tester, the results obtained are closer to what would be expected when implemented on the final device. The initial design is shown in the figure 4-3.

This version of the tester was meant to work in the following manner:

- Position of the tester is changed in relation to the current subject.
- Vertical position of the camera would be set by the rack and pinion mechanism on the back of the robot.
- A second motor would rotate the turntable so the camera would be at a different angle with respect to the region of interest (ROI)



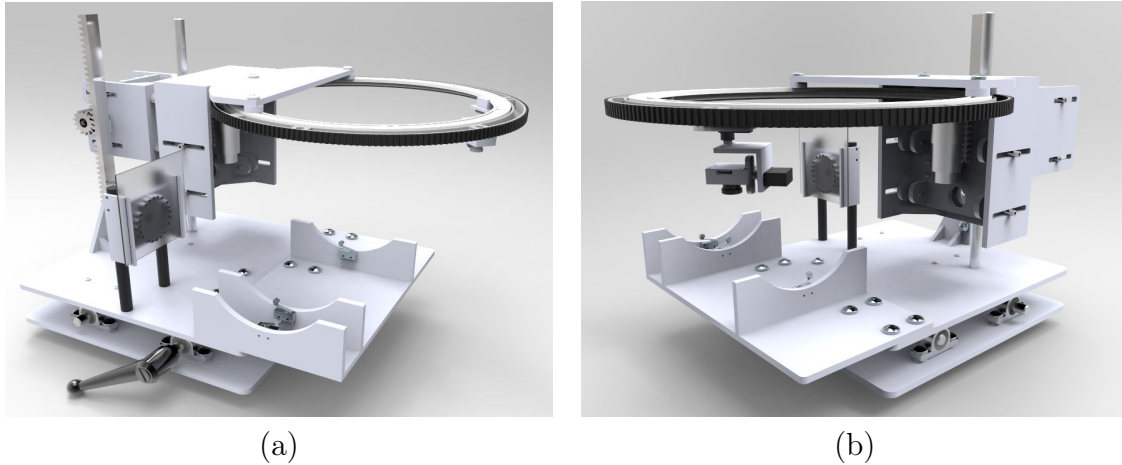


Figure 3-4: Small scale image study tester. (a) view 1 (b) view 2

- Two servos would change the pose of the camera to maintain line of sight with ROI

Unfortunately, the tester had a fatal design flaw in the rack and pinion mechanism where the pinion would not maintain contact with pinion. This issue was meant to be addressed by tension springs pulling the pinion onto the rack, but this was not the case when built. A major design overhaul was undertaken rather than an attempt to fix the flaw in the first version.

TesterV2 used the same general design as TesterV1 with the turntable mechanism now responsible for motion in the z direction and the rack and pinion mechanism now responsible for horizontal motion. Further, the arm fixture and light source were decoupled from the rest of the device. The location of each component of the tester was marked in the final setup of the TesterV2.

The position of the camera on the end effector was controlled through a simple PD loop. Camera angle was controlled by small DC servomotors. Since the location of the subjects antecubital fossa would vary slightly due anatomical differences, the specifications for the positioning of the end effector had wide tolerances,  $\pm 1$  cm, which the tester was able to meet. Figure 3-5 shows an TesterV2 with one of the investigator's arms being imaged.

The third and final version of the tester was a slight modification to version 2 in which the light source was changed from PWM'd LEDs to an incandescent light and

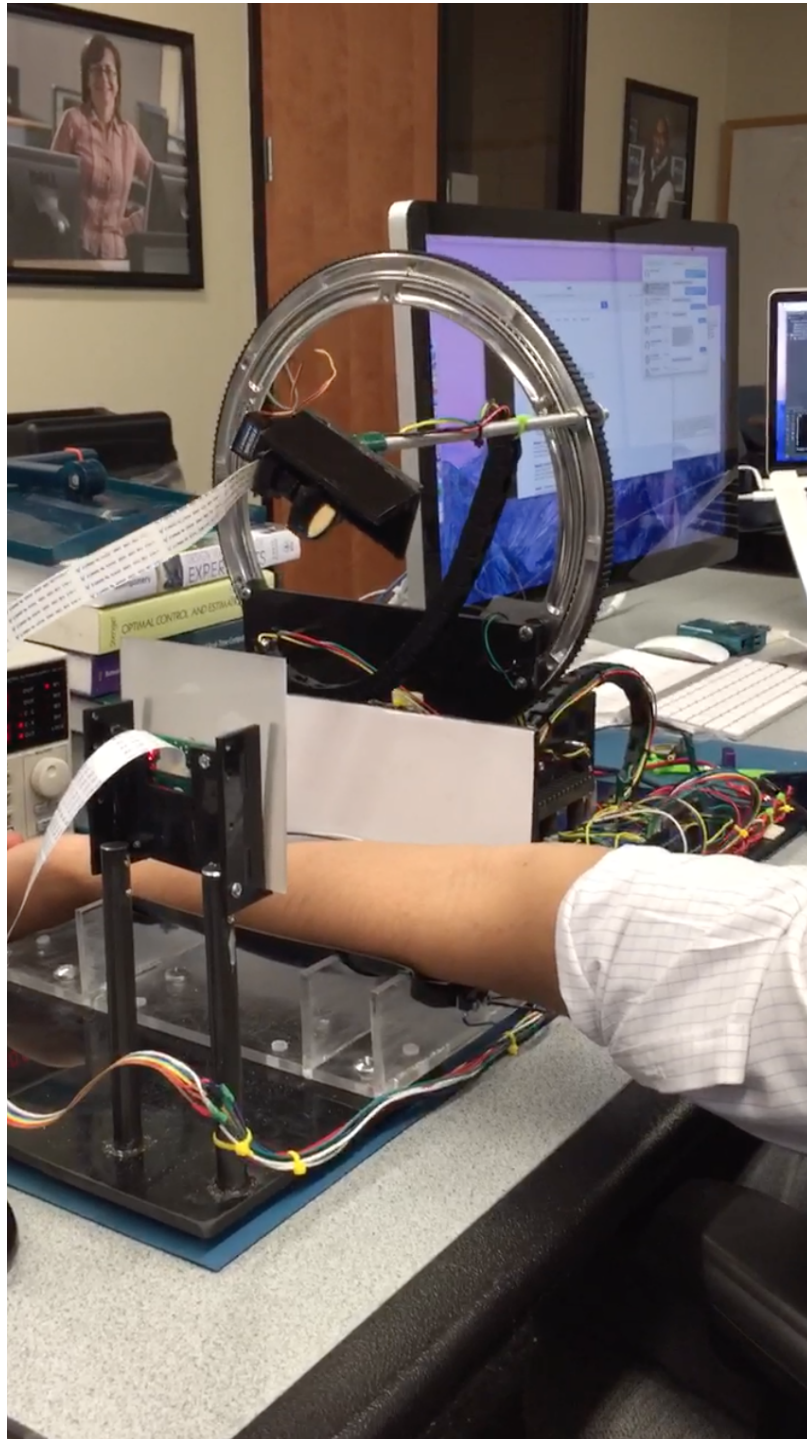


Figure 3-5: Version 2 of the tester with investigator's arm being imaged

minor modifications made to the camera/filter housing to make it more robust. While there is some change in intensity versus wavelength from the incandescent bulb, in the small range under investigation (700nm-900nm) there was only a slight increase in intensity at longer wavelengths which would not effect the result of the experiment given that intensity was one of the variables being investigated. The modification to the camera housing prevented external light from reaching the sensor.

## **Calibration**

Before beginning the experiment, the investigators calibrated the tester and camera. Calibration of the tester was done by determining adequate camera positions and orientations at which the study would be conducted. This calibration was done by manually assigning encoder positions to the motors and taking an image. Nine different positions were chosen at three heights. Since camera's come with automatic adjustments to pertinent parameters to provide a better image, it was necessary to set each parameter not under investigation to a specific value otherwise there would have been unknown bias in the results. To determine the values to be used during the experiment, all values of each parameter were cycled through and the resulting image examined by the investigators.

## **Results and Discussion**

Of the phases listed in the experimental setup, only phase one was implemented. Nine subjects, 5 female & 4 male, were participants in the study. All of the experimental variables except for the camera lens were varied. The lens was not changed given the amount of time required to swap from one lens to another. Three images were taken for each combination of experimental variables. Table 3.3 shows the values for each experimental variable included in the investigation.

To assess the impact varying the experimental variables had on the image, the investigators rated each image from one to 4 on how visible the veins were, where a one indicated the veins were not visible and a four meant they clearly stood out. Analysis of the ratings was done both for each individual investigator and across investigators

Wavelength	Shutter Speed	Position	Intensity	ISO
700	10,000	1a, 1b, 1c	0	100
733	40,000	2a, 2b, 2c	1	200
766	150,000	3a, 3b, 3c	X	X
855	X	X	X	X
880	X	X	X	X

Table 3.3: Levels of each experimental variable included in small scale study. Each numbered position corresponds to a height and the letters correspond to a different horizontal position and angle.

Agreement on Statistical Significance by ANOVA Columns

Subject	1	2	3	5	6	7	8	9
Intensity/ISO	All	2,3	None	None	None	None	1,2	None
Intensity/Shutt	All	2,3	None	None	None	None	All	None
Intensity/Wave	All	2,3	None	None	None	None	1,2	None
Intensity/Pos	All	2,3	None	None	None	None	1,2	None
ISO/Shutt	2	3	2,3	None	None	None	All	1
ISO/Wave	2	3	None	None	None	None	All	1
ISO/Pos	2	3	None	None	None	None	All	1
Shutt/ISO	All	All	All	All	All	All	All	1,2
Shutt/Wave	All	All	All	All	All	1	All	All
Shutt/Pos	All	All	All	All	All	All	All	1,2
Wave/ISO	All	2,3	None	All	1,3	All	1,3	1
Wave/Shutt	All	All	All	All	1,3	All	1,3	1,3
Wave/Pos	All	2,3	None	All	1,3	X	1,3	1,3

Figure 3-6: Agreement between investigators on significance of ANOVA columns

by performing 2-way ANOVA across each experimental variable. Figure 3-6 shows the agreement between investigators on statistical significance for the columns of the ANOVA table by subject. The columns of the ANOVA table correspond to the first variable listed in each row. Figure 3-7 shows the agreement between investigators on interaction of two experimental variables by subject. The investigators concluded the wavelength and the shutter speed were the two experimental parameters of significance which should be investigated in further studies, i.e. the implementation of phases 2-4 explained in experimental design. Further, the results indicate that the shutter speed and the wavelength are tied and this interaction merits further investigation. It should be noted that the shutter speed is also tied to the intensity of the light reaching the camera's sensor.

Agreement on Statistical Significance on ANOVA Interaction

Subject	1	2	3	5	6	7	8	9
Intensity/ISO	All	None	None	None	None	2	None	3
Intensity/Shutt	All	1	1	None	2,3	None	None	None
Intensity/Wave	All	1,3	All	2,3	2,3	None	None	None
Intensity/Pos	2	None	None	None	None	None	3	None
ISO/Shutt	1,2	2	3	None	2,3	None	2,3	None
ISO/Wave	All	All	All	All	2,3	None	2,3	None
ISO/Pos	None	None	None	None	None	None	None	None
Shutt/ISO	1,2	2	3	None	2,3	None	2,3	None
Shutt/Wave	All	All	All	All	All	All	All	All
Shutt/Pos	None	1,3	1	1	2	None	1	1
Wave/ISO	All	All	All	All	2,3	None	2,3	None
Wave/Shutt	All	All	All	All	All	All	All	All
Wave/Pos	None	All	1,2	None	1	X	1,2	1

Figure 3-7: Agreement between investigators on significance of interaction

While the method for analyzing the pictures is qualitative, the investigators thought it would provide the best preliminary results. Another method of analyzing the results would have been to have the investigators highlight each of the visible veins in a picture and manually calculate the contrast between the veins and the surrounding tissue. Since there were thousands of images this would have taken more time than the investigators had available to spend on the data. Automation of this processing could only be accomplished by having a properly validated vein extraction algorithm.

We believe the results presented herein to be sufficient proof that the wavelength and intensity (via shutter speed) are the two variables which merit further investigation. In the course of the study, the investigators also learned that a proper field of illumination is required for proper imaging, typically requiring multiple sources.

### 3.4 Vein Detection Algorithm

Using the parameters obtained from the small-scale imaging study, the contrast enhancement was worked into a more concrete image processing routine with several intermediate steps. The goal of the vein detection algorithm was to identify veins and provide a starting point for the selection of candidate needle insertion sites.

The steps from the image processing routine were independently tested to study

their contribution to vein contrast enhancement. The very first images taken were of the forearm with a LinkSprite TTL JPEG Infrared Camera. These images were then filtered in the fourier domain to remove low frequency components and enhance the higher frequency components with a specified directional tolerance. The results of this step are shown in figure 3-8.

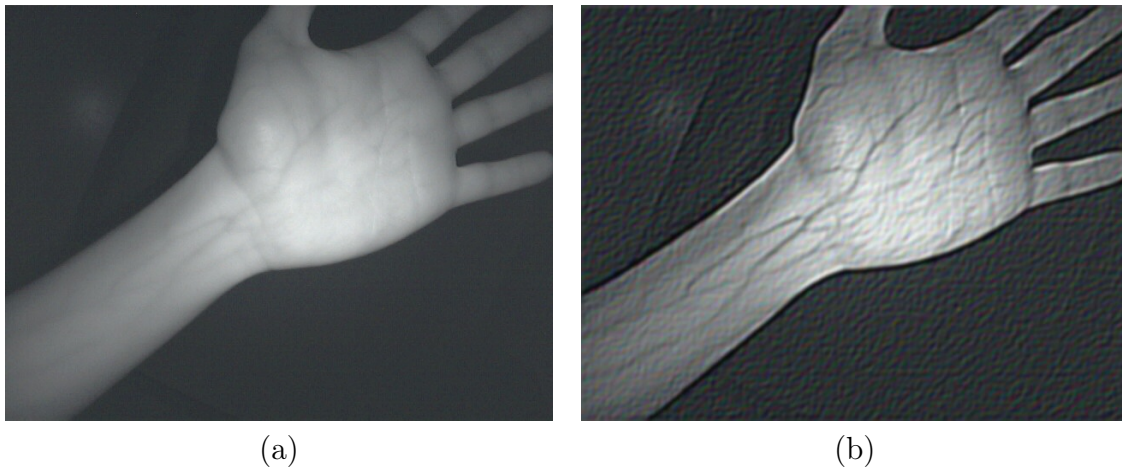


Figure 3-8: Infrared Image of Forearm at 880nm. (a) Raw Image from Camera. (b) After Fourier Domain Filtering.

The filtering showed promising results by making the veins much more prominent. With this in place, a complete image-processing routine, shown in figure 3-9, was developed to segment out veins reliably from the image and output a geometric description of the veins which can then be used by a computer vision algorithm to choose an appropriate venipuncture site.

The frequency bandpass filter, applied after standard image pre-processing steps, is a gaussian filter in the frequency domain that filters out small structures (camera scanline artifacts for example) and enhances the contrast of the veins. Since the veins mostly run along the length of the forearm (within some angular tolerance) and not laterally, the filter can be biased to suppress artifacts in directions that favor better results of the veins. This directional tolerance of the filter was set to 10% with acceptable results but the possibility of an ideal value for this parameter remains to be explored. Erosion and dilation (Opening) are then performed with small thresholds to eliminate structures less than 5 px across. Repeating this process too many times

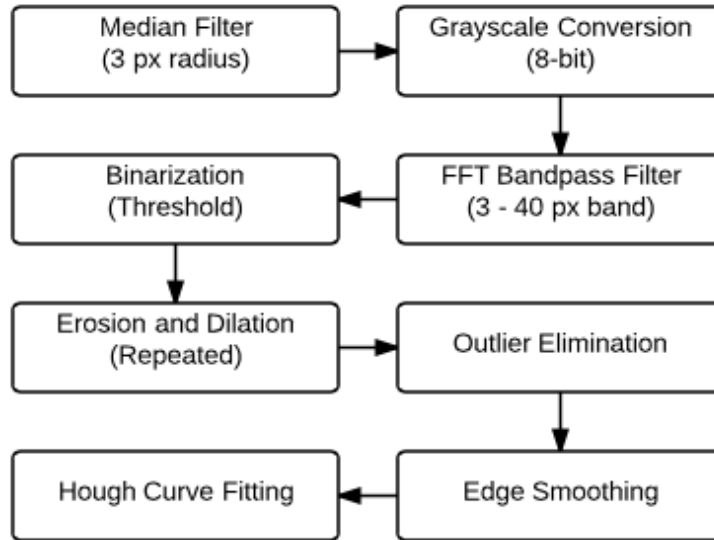


Figure 3-9: Preliminary Image Processing Routine

could potentially erode some of the veins thus damaging the useful information in the image. Instead, a final step in the elimination of outlying blobs which involves weighting them based on not just on their size but also on their distance from the centroid of a fixed neighbourhood of potential veins. A small stray vein that is closer to the edge of the region of interest (RoI) is a poorer candidate for insertion than a larger one closer to the RoI center. The blobs with the  $n$  (set to a conservative value of 3 in our tests) lowest weights were then discarded. After this step, non-maximal suppression is applied to better define the vein boundaries followed by smoothing to help the Hough line transform better fit a curve to the veins. The results of this procedure applied to an image of the ante-cubital fossa (ACF, or elbow region) of the arm, omitting the last curve fitting step for clarity, are shown in figures 3-10, 3-11 and 3-12.

The algorithm for finding venipuncture sites works as follows:

1. Skeletonize the processed image to find vein centre curves.
2. A Probabilistic Hough line transform is used to find lines in the image.
3. Linearly spaced points on each line are then classified as lying either inside (interior points) or outside the vein blob (exterior points).



Figure 3-10: Raw Colour Image of the Ante-Cubital Fossa

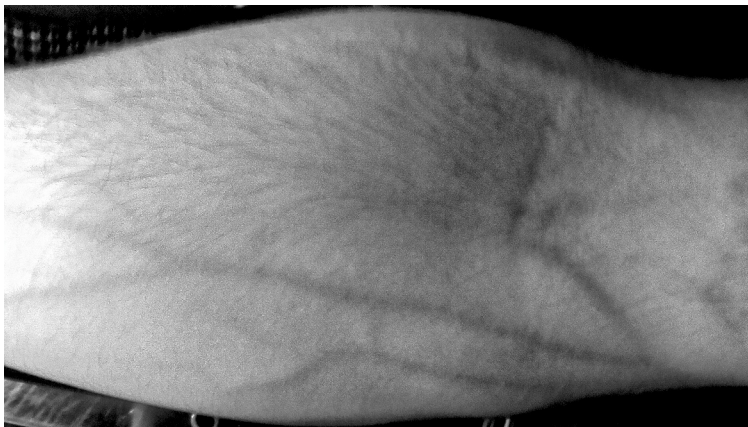


Figure 3-11: Raw IR Image of the Ante-Cubital Fossa

4. The exterior points are eliminated as they are potentially less safe than points that are detected on the vein.
5. The longest consecutive run of interior points is then chosen as the candidate insertion trajectory for the needle.
6. The best candidate vein and entry point are identified and a user is allowed to confirm the selection or make an adjustment before proceeding.

This algorithm was tested on images from 9 test subjects and one of the results is shown in figure 3-13. The red lines lying between the ‘+’ marks are the candidate needle trajectories. In each case, the black ‘+’ represents the venipuncture points closest to the needle insertion mechanism. As is evident, the technique is able to fit



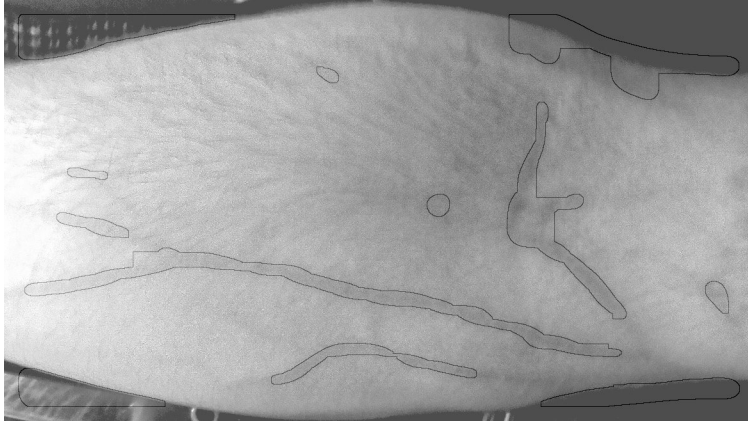


Figure 3-12: Processed IR Image of the Ante-Cubital Fossa

straight lines to veins and classify the interior and exterior points reasonably well. However the chosen insertion points may not be optimal as some of them lie too close to the edge of the arm and pose a potential safety concern.

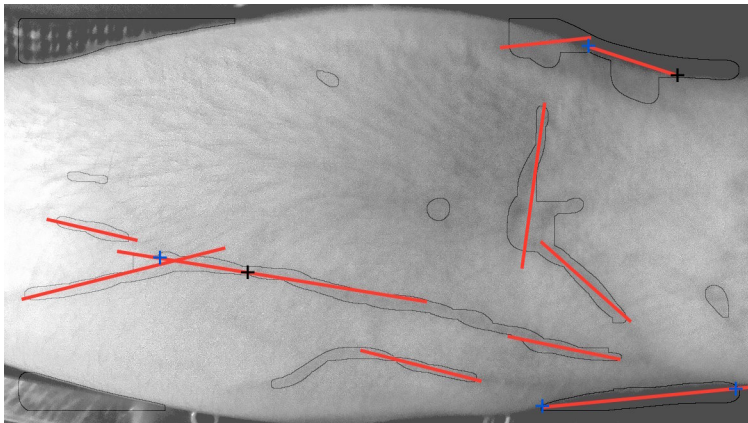


Figure 3-13: Candidate needle trajectories and venipuncture sites from computer vision algorithm.

### 3.5 Future Direction

There are clearly certain limitations to the algorithm presented above: Firstly, it models veins as straight lines. This is a tight assumption overall since veins demonstrate branching and other complex patterns [38]. This can be addressed through a generalized Hough transform to fit arbitrary analytic curves to the veins [6]. The straight

line model may be valid only along a small segment of a vein but may be acceptable on such a scale since the needles used are straight. Secondly, the results were effective for a pilot study as part of the initial development effort, but before scale-up it will be necessary to perform a larger study to ensure generalizability of the approach. We believe that the understanding of the expected difference between patients garnered from a larger study will allow us to develop more robust imaging techniques, such as combining images taken under intentionally varied conditions, which will improve the ability of the detection algorithm to provide reliable results. Further improvements to the algorithm potentially include online model selection based on machine-learned vein models with training images provided by experienced phlebotomists.

# Chapter 4

## Mechanical Design

### 4.1 Chapter Summary

The mechanical design of the Phlebot consists of three main subsystems shown in figure 4-1. First, the cartesian stage which contains all other mechanical entities and is responsible for moving the insertion mechanism into position. Second, the needle insertion mechanism (NIM) which is responsible for performing the insertion into the patient arm once placed at the insertion site. Finally, an attachment mechanism that secures the device onto the patient's limb during the procedure. This section will detail each of the aforementioned systems and its multiple iterations.

### 4.2 Cartesian Stage

#### 4.2.1 Summary

This section will present the development and realization of several iterations of the Phlebot stage. The final design will then be introduced.

#### 4.2.2 System Background

The stage is the largest mechanical entity of the prototype. It performs two major functions: Houses all of the device parts and moves the needle insertion mechanism

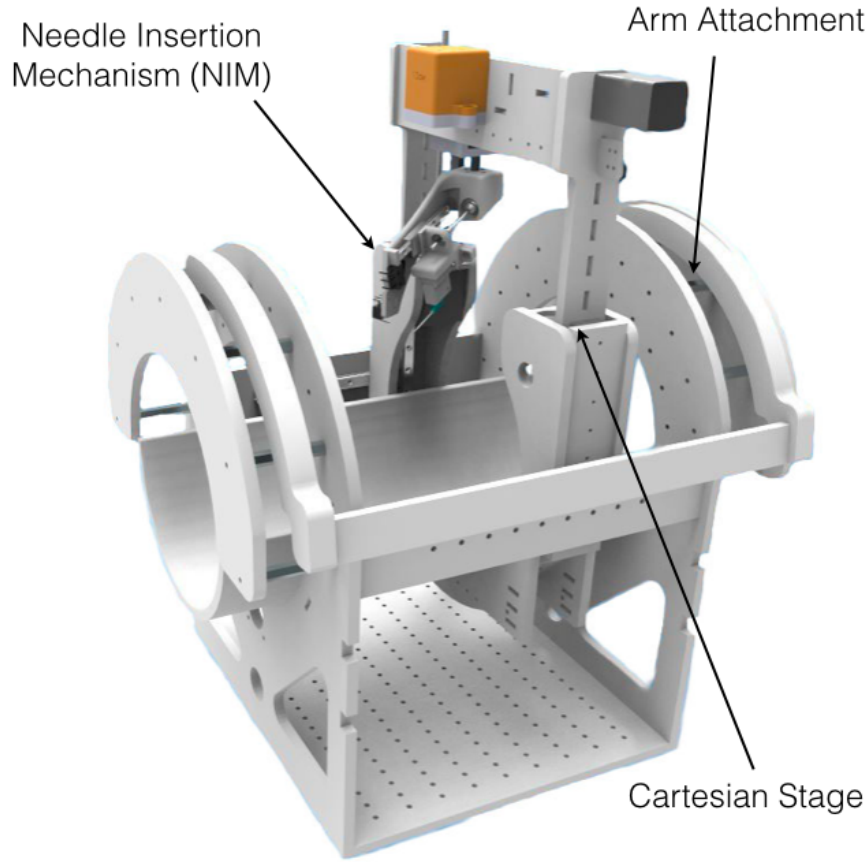


Figure 4-1: Overall mechanical design of the Phlebot. Cartesian stage, needle insertion mechanism and attachment mechanism are labeled for easier identification.

into insertion position. In housing all the parts, the stage must be large enough to contain the attachment mechanism, the patients arm and the vision system while still allowing for an unobstructed workspace for the needle insertion mechanism to move inside.

### 4.2.3 System Requirements

Keeping in line with the criteria of safety, robustness, ease of use and portability to which the prototype is being designed to, the stage attempts to meet the following set of derivatives from said criteria: Repeatability and precision which are required for safety; robustness; ease of use; and, overall size and workspace size which are derived from portability. Notice that portability is, in this case, gauged to be better for smaller overall sizes and larger internal workspace.

## 4.2.4 System Development

The stage was the single most iterated system in the device going through 5 major modifications and several revisions. In the following sections each of the versions will be presented showing a clear progress between iterations as needed features were added, bugs eliminated and unnecessary features removed. However, before diving into the evolution of the stage it is important to discuss the selection of one its principal components: The actuation scheme.

Table 4.1 summarizes the motors and actuation schemes tested for driving the stage. The SPG motor by Nanotec received the highest rating and for this reason was used in the prototypes version 1 through 3. However, a 2 month delay in the delivery of the components due to a disorganized supplier, high cost and low speed due to a high gear reduction ratio, caused the team to abandon this solution in pro of the second and third highest rated solutions. The NEMA11 motor was used in prototypes versions 4 and 5 for motion of large parts, while the NEMA8 was used for motion of smaller parts such as the last carriage of stage V5.

	NEMA15 Belt	SPG1518M0504 Screw	NEMA11 Screw	NEMA8 Screw	B-04F Combo	DC Slider
<b>Picture</b>						
<b>Safety</b>	2	2	2	2	1	1
<b>Robustness</b>	2	3	3	3	1	1
<b>Ease of Use</b>	2	3	3	3	3	3
<b>Portability</b>	2	3	2	3	3	2
<b>Total</b>	8	11	10	11	8	7

Table 4.1: Decision matrix for stage motor selection. Ratings range from 1 (worst) to 3 (best).

### Stage – Version 1

The first version of the stage was not a functional prototype, instead, it aimed at demonstrating the intended size for the final product as well as the notion of how it would interact with the patients arm. Figure 4-2 shows the prototype. Future iterations of the device got progressively larger than the original due to restriction in manufacturing capabilities.

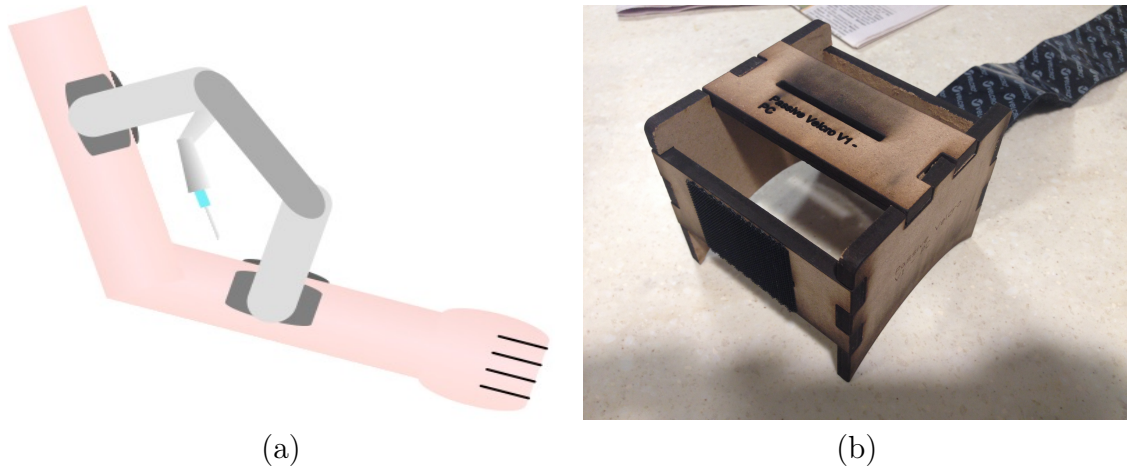


Figure 4-2: (a) Stage V1 depiction. (b) Realization of stage V1.

### Stage – Version 2

The second version of the stage introduced the use of a cartesian stage to move the needle insertion mechanism. The prototype can be observed in figure 4-3.

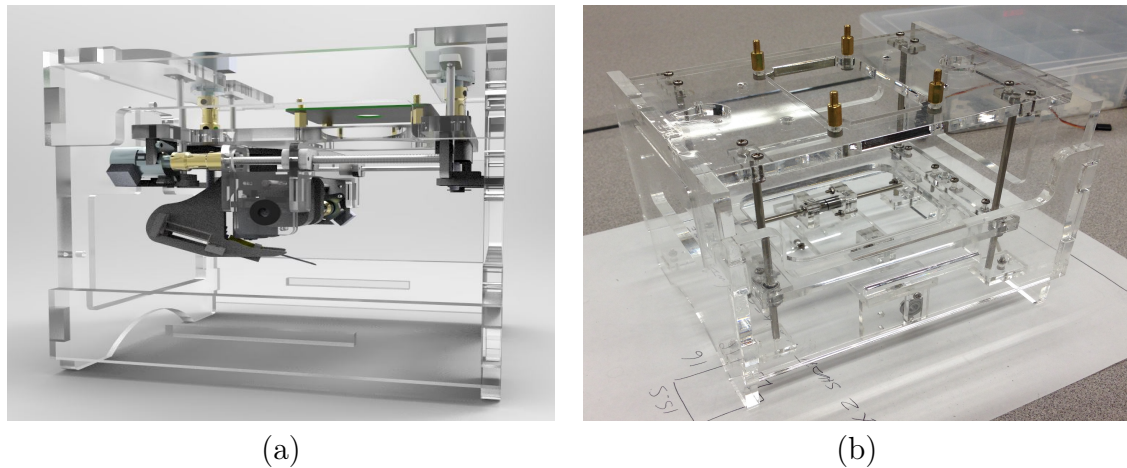


Figure 4-3: (a) Stage V2 3D model. (b) Realization of stage V2.

### Stage – Version 3

The third version of the stage was the first functional version of the prototype. It used the highest rated actuation scheme a Nanotec SPG motor with screw drive (rating shown in table 4.1). The use of a screw for motion no longer allowed for backdriving of the prototype. While being unable to backdrive negatively affected safety, the

prototype could now power the motors off during the procedure as well as reduce the backlash to, effectively, zero. These new abilities were deemed to be more positive than the lack of backdriving was negative. The prototype can be observed in figure 4-4.

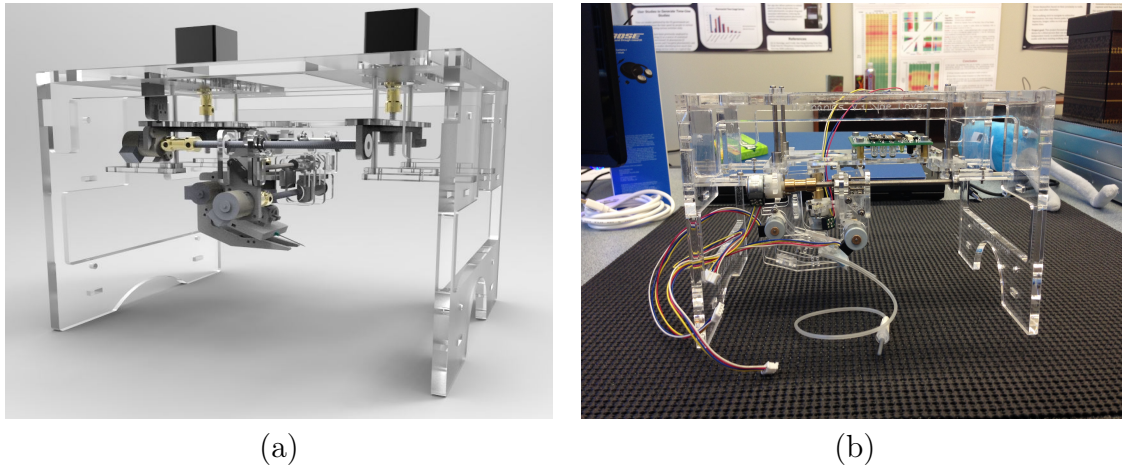


Figure 4-4: (a) Stage V3 3D model. (b) Realization of stage V3.

#### Stage – Version 4

The fourth version of the stage was an almost complete departure from previous designs. Instead of sitting on the patient's arm, as did the previous 3 versions, the patient would instead place his arm inside the device. The prototype also made use of a high quality linear rail for motion colinear with the arm. The linear Z axis (motion that changes distance from arm) was replaced with a 4-bar mechanism which allowed the motion to occur without linear motion. Notice that linear motion had always proven hard to achieve reliably up to this point.

Given the design was mostly redone, several issues arose when constructed. The 4-bar mechanism responsible for motion along the Z-axis proved very unreliable. It had a large backlash, and proved hard to force both sides to move simultaneously. Another issue was due to the use of a single rail for motion along the arm. Although the rail proved steady, the 3mm acrylic deformed leading the NIM to have a significant amount of sideways wobble. Although the design had several flaws, it served as ground for building the more reliable and presentation ready version 5 of the stage.

Figure 4-5 shows the CAD model as well as the realization of the prototype.

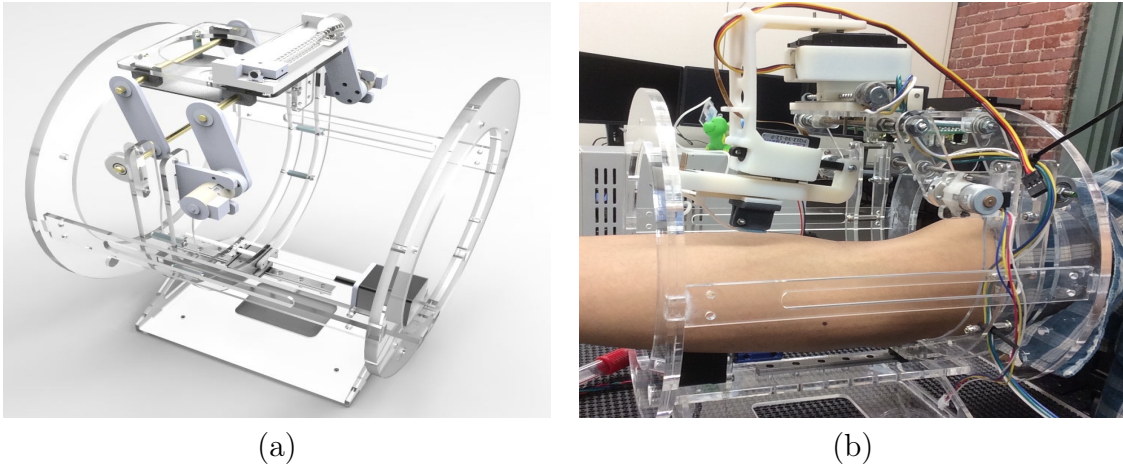


Figure 4-5: (a) Stage V4 3D model. (b) Realization of stage V4.

### Stage – Version 5

The fifth version of the stage is the culmination of all previous prototypes. It consolidates several of the positive features of previous versions, and through a more robust design eliminates several of the issues the previous versions presented.

Improvements in this version include changes to the structure, motorization and kinematic mechanisms. All structural components in this version were built using 6mm acrylic instead of the lighter, but less rigid 3mm acrylic. All the linear axis makes use of high quality carriages and rails with two of the main axis being supported by two of these carriages to reduce reliance of the acrylic. The four-bar linkage was switched over to linear rails for the upward motion and the B-04F combo (lowest rated actuation mechanism as of table 4.1) was replaced by a NEMA8 motor with a lead screw and carriage.

An interesting addition to this prototype was the on-board user interface. With a 24x4 character display and two tactile encoders, the user could directly control the prototype. A larger base also allowed for the electronics to fit within the prototype.

Over the course of a few weeks of testing, the last carriage, responsible for motion perpendicular to the arm, failed. It prompted a redesign of the last carriage which



was replaced with a more robust completely 3D printed model. The new carriage is in use in the presentation version of device and can be observed in figure 4-6.

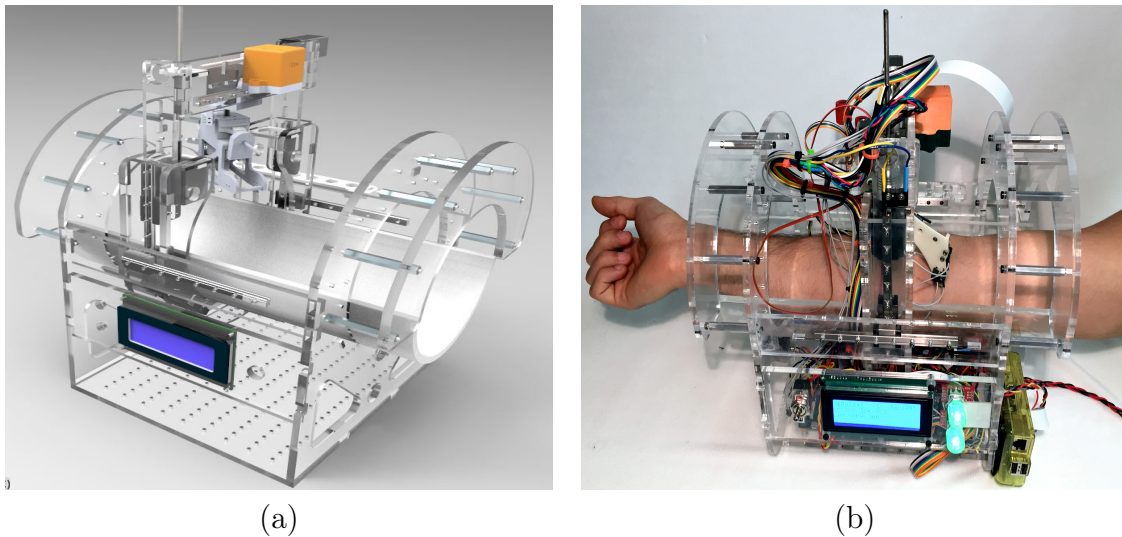


Figure 4-6: (a) Stage V5 3D model. (b) Realization of stage V5.

#### 4.2.5 Future Direction

The stage was developed from ground to a stable build. However, several changes are warranted in order for the device to scale in manufacturing and adhere to medical-grade quality. These changes can include both short term (simple changes) and long term (complete redesign) changes.

Several short term changes to the stage should be performed. A second motor (parallel) motor should be added to the z-axis in order to solve an issue where said axis can be forced to tilt. The half-tube that supports the patients arm on the prototype should be made opaque to simplify vein detection by eliminating some of the unnecessary background. The height of the electronics compartment of the prototype should be increased to leave more space for the electronics and the base plate widened to the total width of the prototype. The position of the camera should be altered to better the field of view which is now occluded by the NIM. Notice that most of these changes have already been caded and can be observed in figure 4-7. Another change which can be easily applied if the prototype is rebuilt, is better cable

management.

Several long term changes to the prototype are required to achieve a more manufacturable design which can survive abuse from long term use. The most important redesign is to switch the stage material, currently acrylic which was selected due to its transparency making it ideal for a prototype, to aluminum or injection molded plastic. By doing so, much of the issues with deformation of the acrylic under forces would be solved making the prototype more accurate.

The proposed changes to the stage would allow for a more robust prototype which could withstand field use. It would also become possible to manufacture and assemble it without the significant overhead, from construction time and material misuse, involved in the current design.

## **4.3 Needle Insertion Mechanism (NIM)**

### **4.3.1 Summary**

The needle insertion mechanism (NIM) is responsible for performing the insertion of the needle into the patient's limb. This chapter will introduce the system requirements and explore the development of the mechanism by detailing each of its 7 major revisions.

### **4.3.2 System Requirements**

The mechanical requirements for the needle insertion mechanism are perhaps the most stringent in the development of the entire system. Since the insertion axis is the final motion axis that puts the patient in contact with the robot, it has to be mechanically precise, sturdy, safe and limited in its range of motion. A study characterized the typical vein diameters in the antecubital region found across a sample of over two and a half thousand subjects. The mean vein diameter was found to be  $2.7 \pm 1.6$  mm. [34] Based on this, the team estimated that a bevel tip needle requires a positional accuracy of 200 microns along the insertion axis to maximize the cross-

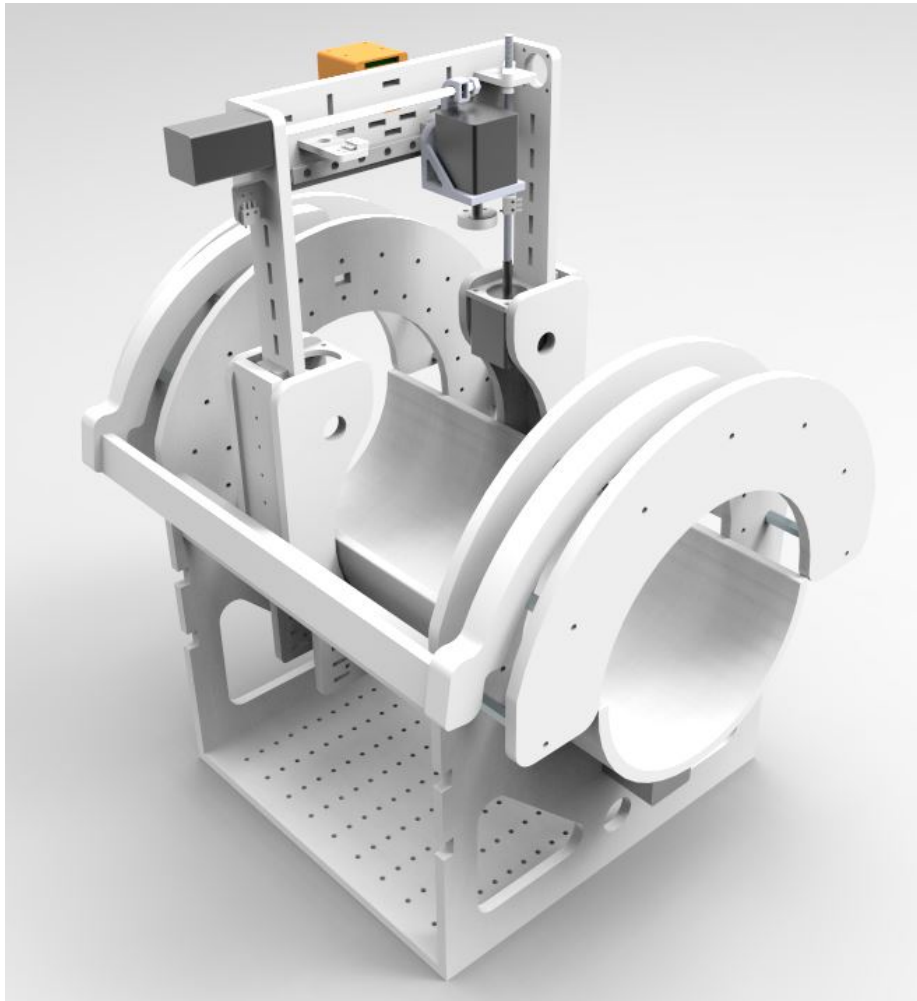


Figure 4-7: 3D model rendering for short term modifications of the Phlebot as outlined in future direction.

sectional circular error probable (CEP) while guiding the needle into the vein.

There must be a way to sense when both the needle insertion mechanism and the needle are in contact with the patients arm and register the force on the needle tip to drive to the needle insertion controller. Moreover, it requires a way to be able to quickly replace used needles with new ones between procedures. With all of these tight design requirements in mind, the team went through several iterations of the needle insertion mechanism, incrementally improving the design, validating the improvements and integrating it with the motion stage that comprises the rest of the robot. The next section focuses on this development process and features of each of the iterations.

### 4.3.3 System Development

The Needle insertion mechanism underwent a total of 5 iterations. With every iteration, a novel concept was tested and an existing one refined. Different manufacturing processes were experimented with in order to assess and hone the mechanical precision of the NIM at each stage.

#### NIM – Version 1

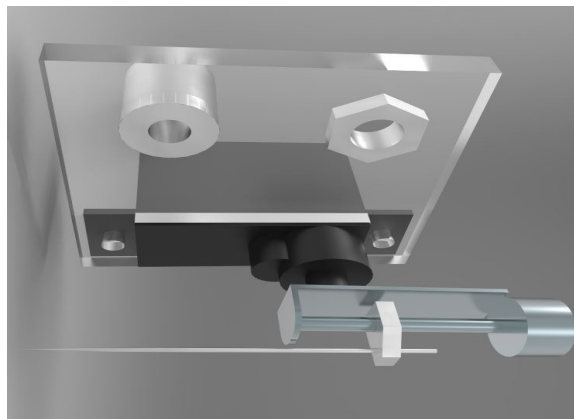


Figure 4-8: NIM – Version 1

The very first version of the NIM, shown in figure 4-8, was purely conceptual and was not manufactured to completion. Rudimentary in nature, it consisted of a servo

motor to pitch a linear stepper motor assembly (obtained from hard drive armatures) on whose carriage rides a sewing needle.

### **NIM – Version 2**

The second version of the NIM attempted to use two of the hard drive stepper motors from NIM version 1. The gooseneck design of this NIM emerged from a space constraint that forced the motor casing to ride with the NIM. This NIM was laser cut from 3mm and 2mm thick acrylic. Although original in design, this NIM was unacceptably inaccurate due to mechanical backlash and demanded new manufacturing techniques and components. The two feet straddling the needle were meant to stabilize the skin and prevent roll of the vein during needle insertion. This design was inspired by a similar mechanism used in sewing machines to stabilize the fabric being stitched.

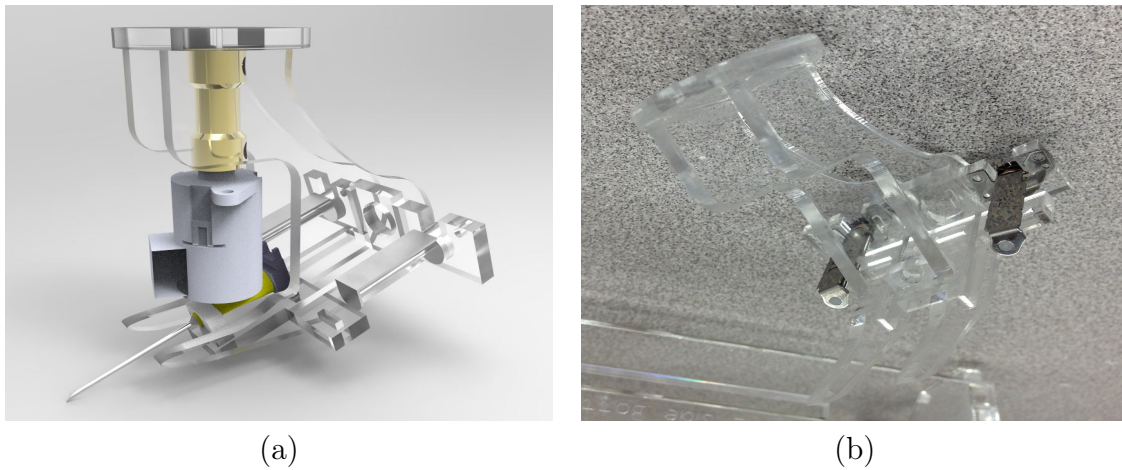


Figure 4-9: NIM Version 2. (a) CAD Model. (b) Realization of mechanism.

### **NIM – Version 3**

The third version of the NIM employed 2 Nanotec stepper motors, one used for the yaw and the other for insertion (see figure 4-10). The insertion motor is coupled to the needle holder, which slides in an acrylic channel, through a slotted-bar cam mechanism. It borrows the gooseneck design and the feet from NIM V2. This NIM was the first to be mated to a Stage to have its work envelope analyzed.

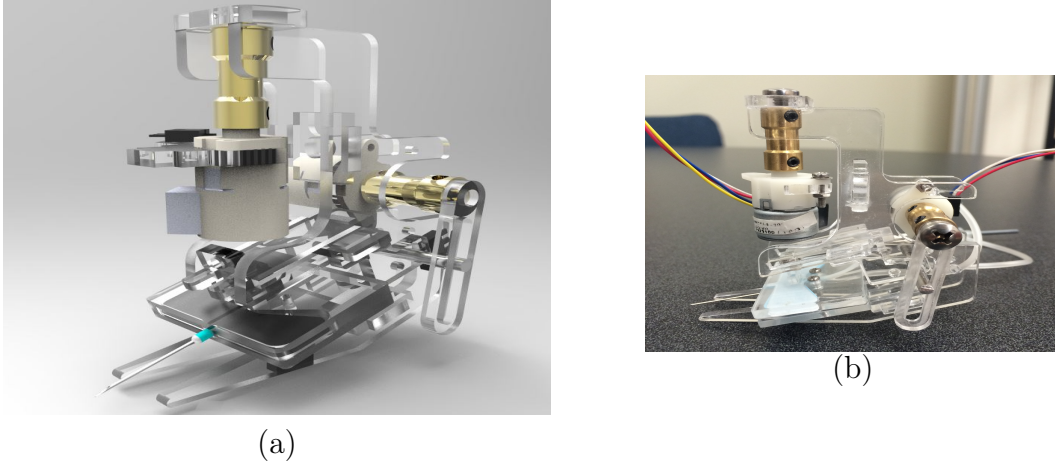


Figure 4-10: NIM Version 3. (a) CAD Model. (b) Realization of mechanism.

#### NIM – Version 4

The fourth version of the NIM, shown in figure 4-11, borrowed the space-saving gooseneck design from its predecessors. This NIM represented the biggest leap in terms of mechanical accuracy. Ultra-small ball-bearing carriages and 2mm stainless steel rails were used for linear motion of the needle holder. This aided in achieving a near-perfect collimation of the needle with the insertion axis. The actuators used on this version of the NIM included a low-profile HiTec servo for the yaw axis and a Firgelli linear servo actuator with a 20mm stroke length for the insertion axis. The actuators worked satisfactorily but lack of position feedback on the yaw axis was a potential safety problem. The NIM itself consisted of 2 main parts that were 3D printed besides the gooseneck – the primary carriage and the secondary carriage. The primary carriage held a rear-mounted Honeywell FSG high-resolution force sensor and was directly coupled to the linear servo actuator. This allowed the gross motion of the needle along the insertion axis. The primary carriage and the secondary carriage were coupled through another set of linear bearings. This design affords a small degree of relative motion between the needle and the force sensor. This forms the redundant axis within the underactuated system to ensure that forces registered by the sensor at the needle tip are only associated with the insertion process.



Figure 4-11: NIM Version 4. (a) CAD Model. (b) Realization of mechanism.

### NIM – Version 5

The fifth version of the NIM was also 3D printed but used a significantly more compact structure. It incorporated a Maxon GP6S Spindle Drive Motor for the needle insertion. The needle adapter was magnetically attached to the motion carriage. This is a safety feature that enables a quick release of the needle without powering on the device in case of a critical procedural failure. This can be seen in figure 4-12 . Some of the drawbacks of this highly capable version included its high price due to the dual carriage design and difficulty of mechanical assembly.

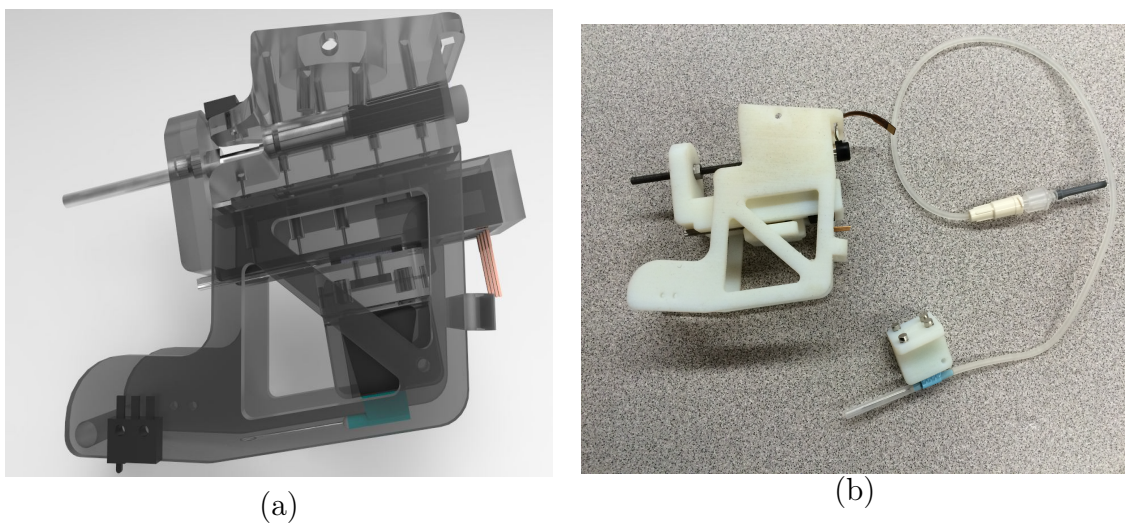


Figure 4-12: NIM Version 5. (a) CAD Model. (b) Realization of mechanism.

#### 4.3.4 NIM – Version 6

The sixth and final version of the needle insertion mechanism, shown in figure 4-13, achieved the same mechanical precision of its predecessors but at a lower price point by using only a single linear carriage and improved ease of manufacturability due to the open design. The design was validated using finite element analysis (FEA) to ensure that the mechanism does not flex under the load of insertion. The NIM also included an end stop to aid in the calibration of the insertion axis motor. The NIM was mated with Stage V5 and was used to successfully perform insertion on phantoms.

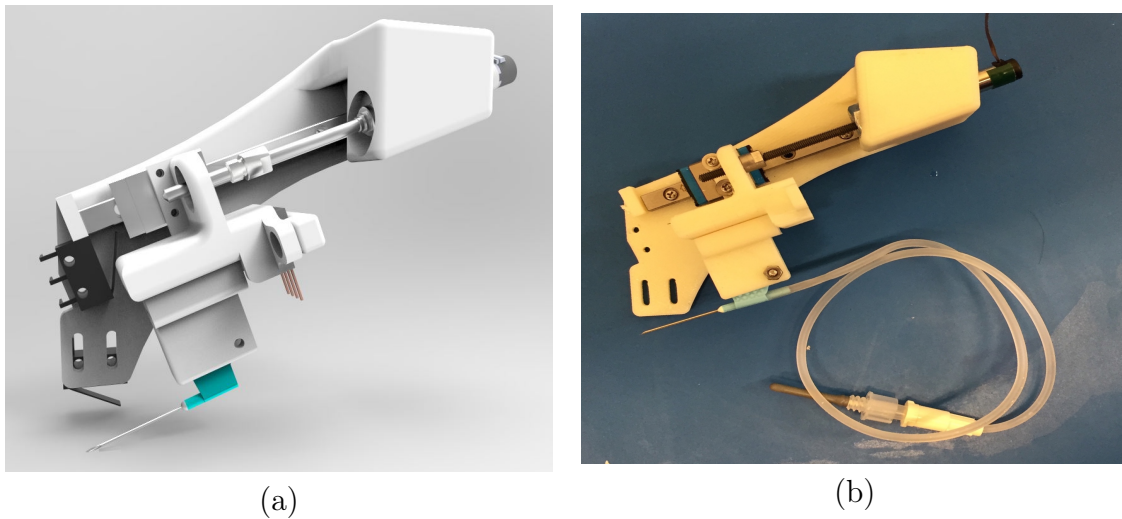


Figure 4-13: NIM Version 6. (a) CAD Model. (b) Realization of mechanism.

#### 4.3.5 Future Direction

Several important design lessons were learned from the various iterations of the NIM in terms of compactness, ease of assembly and mechanical robustness. With NIM V5 and V6 having met all necessary design goals, future improvements to the NIM would only be incremental and focus on miniaturization of the mechanism. Features that the team intends to include in future revisions of the NIM are automatic needle sheathing/resheathing and automatic needle swapping using a custom-designed needle magazine.



## **4.4 Attachment Mechanism**

### **4.4.1 Summary**

An important feature of the device is its ability to comfortably, yet securely, hold the patients arm during the procedure. To this end, several attachment mechanisms were devised and tested. This section will present each of the developed mechanisms and the rationale for the iteration. Finally, the final design will be presented.

### **4.4.2 System Background**

The attachment mechanism is responsible for comfortably, yet securely, fixing the patient and prototype under the same inertial frame. This is important since motion during a procedure can result in injury. In holding the arm, it cannot block the workspace of the device or interfere with bloodflow. Moreover, the device should be comfortable to use and should not inflict pain on the user if during long procedures.

### **4.4.3 System Requirements**

The prototype specifications determined that it should be safe, robust, easily used and portable. To meet these standards, the attachment mechanism was designed to derivatives of these standards, namely: Secureness; robustness, ease of use and portability.

### **4.4.4 System Development**

A total of 5 attachment mechanisms were constructed for testing, namely: Passive velcro, N-Linkage, motorized tensioning string (MTS), Active Belt and cuffs. The decision matrix presents in table 4.2 presents a summary of the specification fulfillment for each of the prototypes. A 0 specifies that the attribute is poorly fulfilled, a 1 means its partially fulfilled and a 2 specifies it excels in the given criteria. The following subsections will present each of the devices including their modeling and realization.

	Secureness	Robustness	Ease of Use	Portability	Total
<b>Passive Velcro</b>	1	1	0	2	<b>4</b>
<b>N-Linkage</b>	1	2	2	2	<b>7</b>
<b>MTS</b>	1	1	2	2	<b>6</b>
<b>Active Belt</b>	2	1	1	2	<b>6</b>
<b>Cuff</b>	2	2	2	1	<b>7</b>

Table 4.2: Decision matrix for selection of attachment mechanism.

### N-Bar Linkage

The N-Linkage attachment was the most complex attachment mechanism tested. The design was based on four 4-bar linkages actuated by two large 3D printed racks. Each of these racks extrude to the bottom of the prototype when it is not applied on a patient's arm. When placed on the arm, the racks are force up and actuate the 4-bar linkages which embrace the arm securing the device in place. The model and actual device can be observed in figure 4-14.

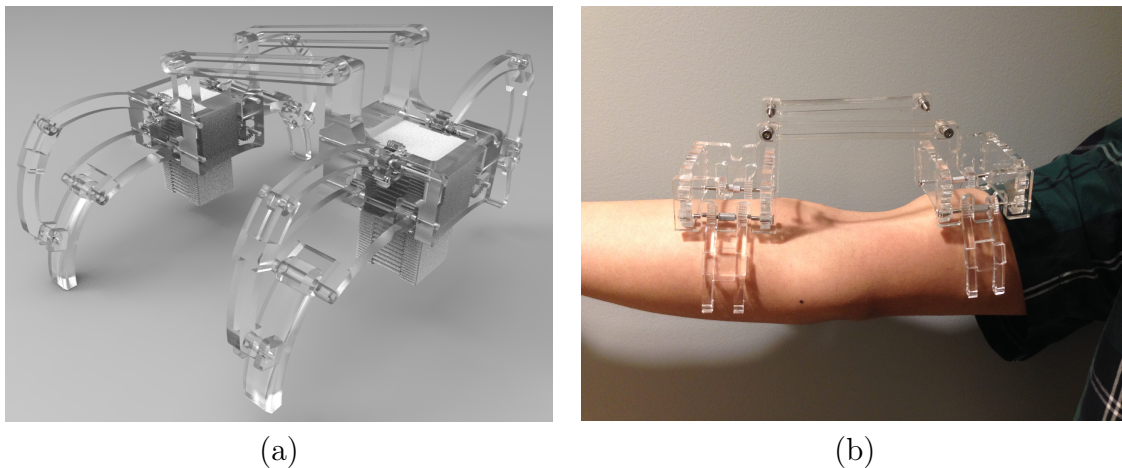


Figure 4-14: (a) N-linkage 3D model (b) Realization of N-linkage attachment mechanism.

### Motorized Tensioning Band

The motorized tensioning band is similar in concept to the active belt attachment mechanism. The CAD model and its realization can be observed in figure 4-15. In this design, small Pololu motors spool a narrow band which tightens around the patient's arm. One of the main issues with this version of the attachment is that for a material

to be able to reliably spool it has to be thin, thus it is inherently uncomfortable for the patient.

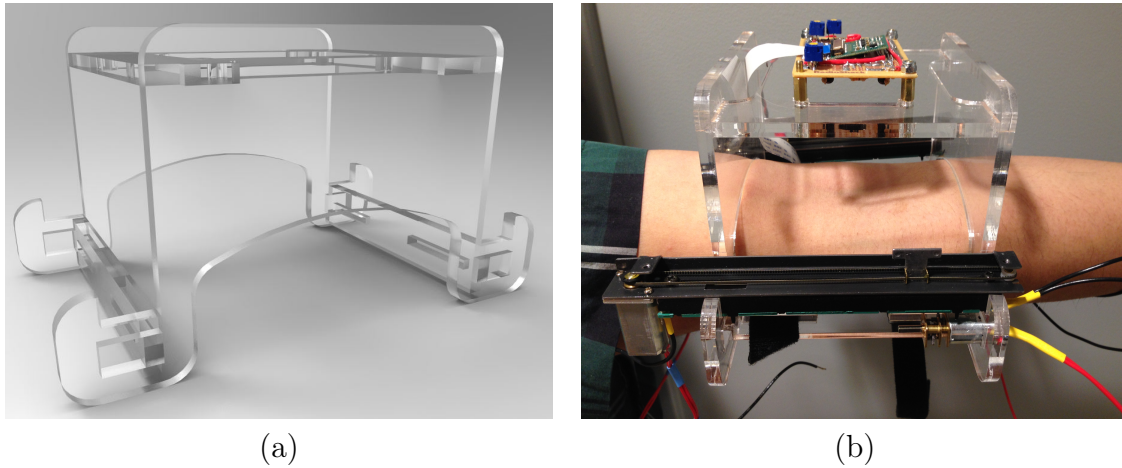


Figure 4-15: Motorised tensioning band attachment mechanism. (a) CAD model. (b) Realization.

### **Active Belt**

The active belt attachment was one of the descendants of the passive velcro attachment. In this version of the device, a webbing-type belt (similar to those used in seat belts) had a 6mm rod sown to both of its ends. One end was held in place in the device with U-shaped brackets. Once the device was placed on the patient's arm, the other side of the belt could be slid into another U-shaped bracket at the end of a lever actuated by two motors. Once in place, the prototype would actuate the motors forcing the band to tighten around the patient's arm. Figure 4-16 shows both the realization of the device.

### **Manual Velcro Strap**

The manual velcro strap attachment was the first proposed design for the Phlebot. In it, the prototype, represented by the wooden box in figure 4-17, would be placed on the patients arm and a high adhesion velcro would be manually tightened. This design presented a good starting point for the project since it did not require any active components. However, its simplicity came at the cost of repeatability which

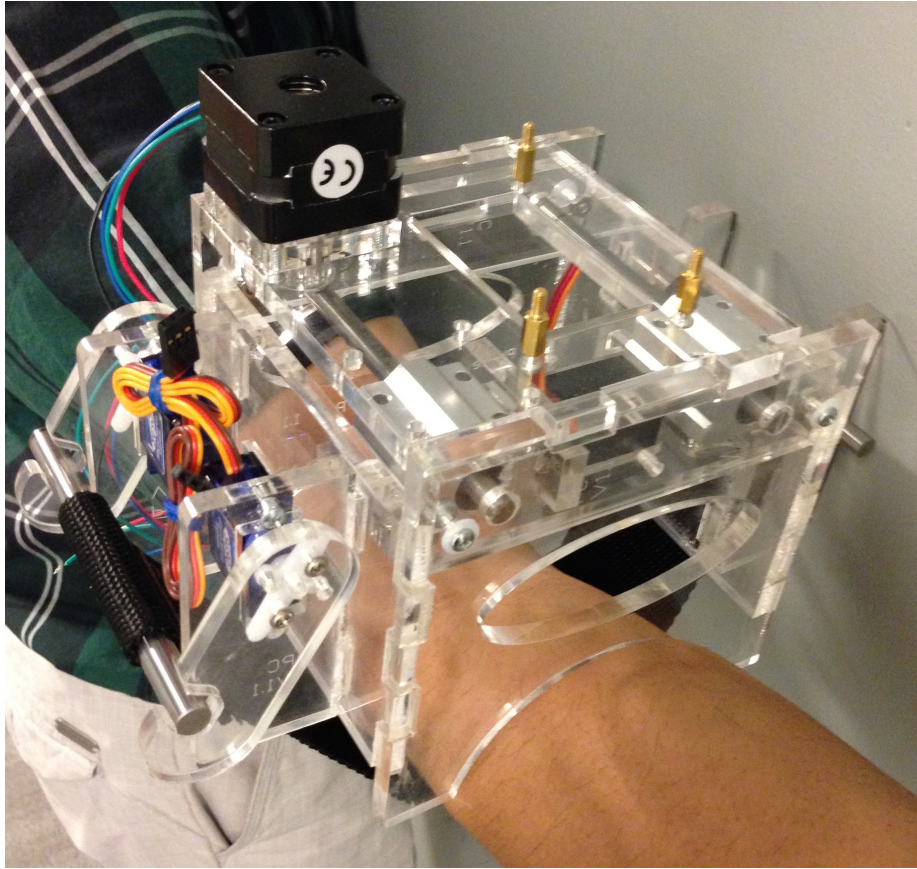


Figure 4-16: Active belt attachment mechanism realization.

resulted in a lower score for secureness since it is operator dependent. Its requirement for an operator also resulted in the lowest score for ease of use. The full scoring for the prototype can be observed in table 4.2.

### **Inflatable Cuff**

The inflatable cuff was deemed the best attachment mechanism according to the decision matrix of table 4.2. In it, a toroidal shaped cuff would inflate around the patient's arm, holding it in place.

Even though this method had the highest rating, it also proved to be the hardest to realize. Initially the team attempted to construct the cuff using heat soldering and the plastic used in inflatable mattresses. The solder and the resulting cuff can be observed in figure 4-18. However, the toroidal shape required for the cuff turned out to be unreproducible using the heat solder. For that reason, the team turned

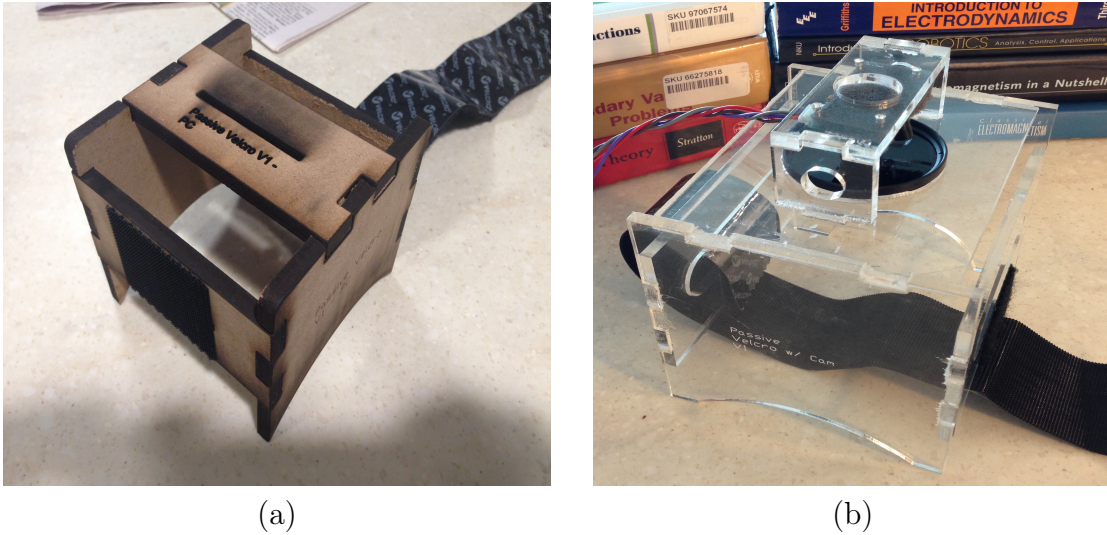


Figure 4-17: (a) First realization of the passive velcro attachment mechanism. (b) Second realization of the passive velcro attachment mechanism.

its attention to determining a rubber and glue combination that could outperform the previous material. With this in mind a study was conducted on 52 combinations of materials and glues. Four of the combinations were selected as viable candidates for manufacturing of a cuff. See appendix A for a complete description of the study. However, when attempting to manufacture the cuff the team was unable to construct one that could reliably survive more than 3 inflation and deflation cycle at 3 PSI. During operation, the cuff would have to reliably operate at pressures from 1-4 PSI. Finally, the team resorted to modifying a 12.5x1.5-2.2 5 Kenda Inflatable chamber of a bicycle tire to manufacture of the cuff. Even though the chamber did not have a uniform diameter when inflated it could be modified into an effective cuff.

#### 4.4.5 Future Direction

The inflatable cuff manufactured from bicycle tubing turned out to create a successful cuff. However, much work is needed to create a more elegant and reliable solution. Future work on the cuff would depend on the overall procedure for attaching the device. If a Phlebot with a stage V5-like attachment in which the patient places their arm inside the device is chosen, the team would recommend continuing work on inflatable cuff. Either outsourcing, or developing in-house the method to manufacture

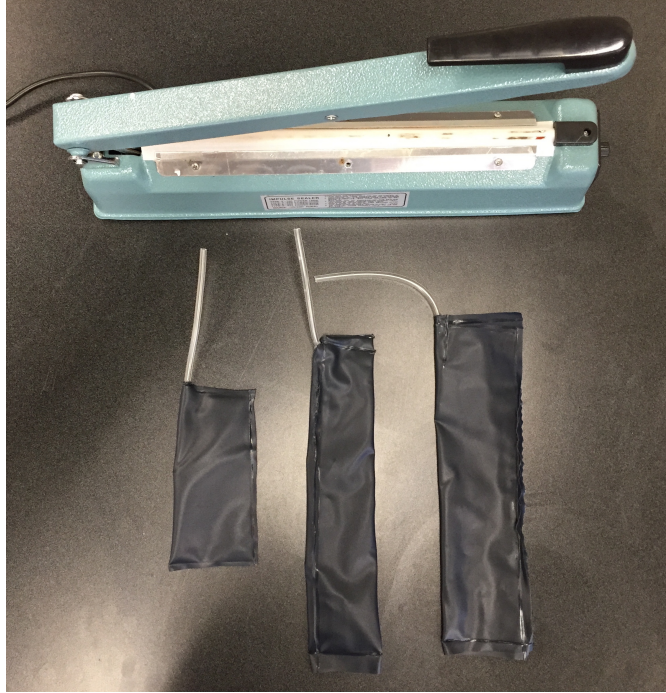


Figure 4-18: Inflatable cuffs development using heat soldering and air-mattress material.

a uniform, reliable and consistent cuff. However, if the device is intended to be placed on the patient's arm, the team would recommend re-exploring the N-linkage attachment due to its effectiveness and lack of external parts.

# Chapter 5

## Electronics Design

### 5.1 Chapter Summary

The development, construction and testing of the electronics will be presented. This includes the three versions of the IRRig which was developed to provide several wavelengths of IR illumination during testing and then settled on a single wavelength in its production version, as well as both versions of the Main Board which control the prototype. Due to the very different nature of the Main Board and the IRRig board, most of the chapter will be divided into a subsection for each of the two board types.

### 5.2 Background

The Main Board (originally referred to as Electronics Module) is a single board that contains all the peripherals required to control, power and sense the PhleBot. It pairs with the IRRig board to provide multiple wavelength illumination of variable intensity. Together, they account for all custom electronics of the PhleBot.

## 5.3 Main Board

### 5.3.1 System Requirements

Table 5.1 provides a comparison between the requirements of the two versions of the main board. Apart from the specific requirements, the boards were also to be developed in order to meet the global criteria of safety, ease of use, robustness and portability.

In order to meet the safety criteria the boards were to operate at a low voltage (less than 18 volts) such that patient contact with any exposed circuit would not result in a shock. Special attention would also have to be placed on the failure conditions. In no condition should a failed board result in motion of the actuators or physical damage. In abiding to these guidelines a board would be deemed safe.

The remaining three criteria namely ease of use, portability and robustness had similarly specific guidelines. To be easy to use a board should have the minimum amount of inputs and buttons to be operational. In order to be portable the board should be as small as possible without compromising quality while simultaneously being as self contained as possible (ex on-board Raspberry Pi). To be robust a board should be able to operate for extended periods of time without failure. This final criteria, requires engineering the board with large tolerances such as having trace thicknesses that exceed required current rating and components that are operating at or under maximum nominal limits.

	Main Board V1	Main Board V2
Features	Completely self contained including on board Raspberry Pi Compute Module. Probing points for debugging. Board should be able to sense attitude. Switching power regulation.	Modular design. Probing points and LEDs for debugging. Board should be able to sense attitude. Linear power regulation.
Connect/Drive	6 Stepper Motors Force Sensor EthernetCamera IR LEDs End Stops	4 Stepper Motors 2 DC Motors Force Sensor LCD Display Maxon motor controller IR LEDs Pressure sensor

Table 5.1: Summary of requirements for Main Board V1 and Main Board V2 for the Phlebot MQP.



### 5.3.2 System Development

The requirements outlined in the previous section, summarized in table 5.1, led to the determination that the board should have the set of features outlined in table 5.2. Notice that the table places the features of both boards side by side for easier comparison.

The set of features outlined above were used in selecting the components and final design of the PCBs. The major components and the motivation in their selection will be explored in the subsections to follow. Notice that due to size constraints, whenever available, a component was chosen in its SMD version.

Board Content	Main Board V1	Main Board V2
Inputs	6 End Stops Force Sensor	8 End Stops 2 Encoders Force Sensor
Outputs	6 Stepper Motor Drivers IRRig	5 Stepper Motor Drivers 4 Solenoid Drivers 20x4 LCD Display IRRig
Sensors	Inertial Measurement Unit	3-Axis Accelerometer Temperature Sensor Pressure Sensor LDR
Others	FTDI Ethernet Host USB	FTDI Interface to Maxon Motor Controller
Processing	Compute Module (Primary) ATMEGA2560	ATMEGA2560 (Primary) 2 ATMEGA328P Connects to external Pi

Table 5.2: Comparison of features between Main Board V1 and Main Board V2.

#### Microcontrollers (ATMEGA Family)

For both versions of the board a microcontroller from Atmels ATMEGA family were chosen. Main Board V1 used one ATMEGA2560 as its main microcontroller whilst Main Board V2 used the same main microcontroller with the addition of two ATMEGA328P for support. Table 5.3 summarizes the feature set of each of these mi-

crocontrollers.

Through inspection of the feature list for each of the microcontrollers one can notice that they fulfill all needs for the main boards. Given that these microcontrollers are widely available and coding for them is facilitated during prototyping due to the Arduino libraries, they were selected for use.

ATMEGA2560	ATMEGA328P
Two 8-bit timer and four 16-bit timers.	Two 8-bit timers and one 16-bit timer.
16 PWM Channels	6 PWM Channels
16 10-bit ADC	Eight 10-bit ADC
4 UART	1 UART
256 KB Flash, 8 KB RAM	32 KB Flash, 2 KB RAM

Table 5.3: Feature list of ATMEGA family microcontrollers used in Main Board V2.

### Motor Drivers (DRV8834)

The stepper drivers are an important component of both boards given they are the main means of controlling the Phlebot. Several devices were considered, however, the Texas Instruments DRV8834 came out as a victor. This IC, permits the driving of motors that consume up to 1.5 amps per phase at up to 10.8 volts with microstepping through a simple STEP/DIR type of interface. A fault line can be used to alert the microcontroller in case of fault conditions which provides useful diagnostics for a medical device. The low pin count, allied with the diagnostics features were key in choosing this IC as the motor driver.

### Inertial Measurements Units (IMU)

Version 1 and 2 of the Main Boards diverge in their selected IMU. Table 5.4 provides an overview of the main features provided by each IMU.

Inspection of the feature set for each of the devices reveals that the LSM is clearly more feature rich. However, problems with its use in the first version of the board including a hard to solder LGA package, error in package size specification, and a complicated interface lead the team away from it. The second version of the board

opted for a simpler IMU which did not contain a gyroscope and used an analog interface instead. This decision was made given that the prototype is nearly stationary and therefore will not benefit from a gyroscope. The gained resolution (16-bit versus 10-bit ADC) when using the I2C interface does not justify the added complexity of writing custom libraries to interface with the device and losing clock cycles in the communication.

<b>LSM330DLC - Main Board V1</b>	<b>ADXL337 - Main Board V2</b>
Brand: ST Microcontrollers	Brand: Analog Devices
3-Axis Accelerometer and 3-Axis Gyroscope	3-Axis Accelerometer
3.3V and 1.8V Supply Required	3.3V Supply
I2C or SPI Interface (16-bit)	Analog Interface

Table 5.4: Feature comparison between inertial measurement units of Main Board V1 and V2.

### **Power Regulation (Switching Versus Linear)**

The two versions of the main board contain significant differences in the power regulation. Table 5.5 summarizes the power regulation scheme of each board.

Version 1 of the main board features switching based voltage regulators with an efficiency of almost 93%. However, problems with soldering of the short pins of the device together with their long rising time led to the change to linear based regulators. Notice that the long rising time led to brown-out of the compute module in the Main Board V1. Notice also, that since the Main Board V2 does not contain an onboard Pi, voltage regulation at 1V8 was no longer required.

The long rising time of the voltage rails as well as the power up sequencing were cause of concern on the first version of the Main Board; figure 5-2 illustrates both. The power sequencing required for the compute module is that the 1V8 line powers up after complete powering of the 3V3 voltage rail. To achieve this, the Main Board V1 had a simple delay circuit controlling the shutdown line of the 1V8 regulator as shown in figure 5-1. Unfortunately, the Compute Module documentation failed to note that the device would enter a brown out condition if the rise time of the 3V3

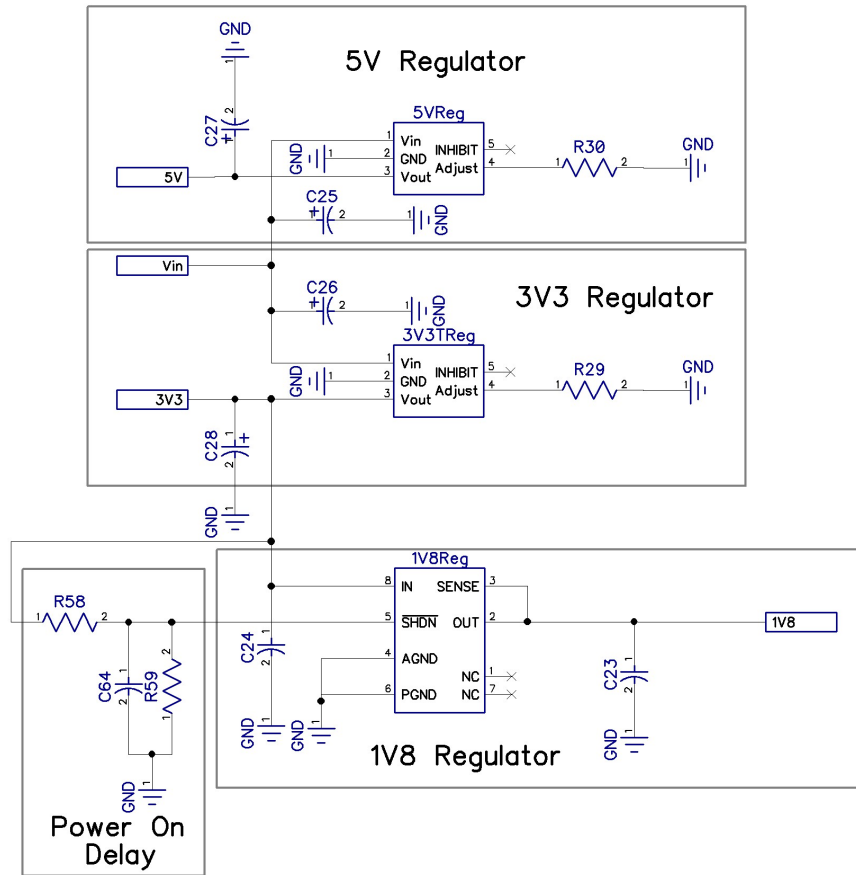


Figure 5-1: Power regulation schematic for Main Board V1

rail was too long. This resulted in the Compute Module being unable to boot in the main board V1.

## Realization

Although changes in the requirements between board versions 1 and 2 elicited a remake of the board, both versions were functional. Figure 5-3 presents the top and bottom views of the assembled PCBs. However, there were some issues with the boards which were tracked during testing. An exhaustive list of these is available in table y. For a complete documentation of the boards including, schematics, PCB art, pin maps and list of components see appendices D and E.

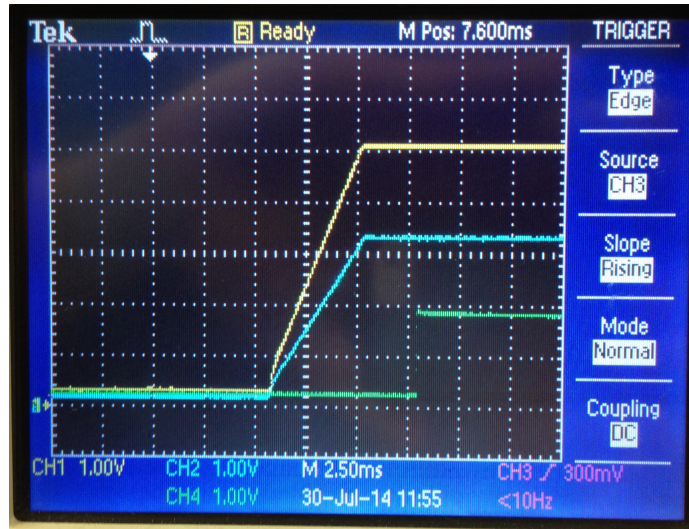


Figure 5-2: Power-up sequence for Main Board V1.

Voltage	Main Board V1	Main Board V2
<b>Vmotor</b>	No regulation or protection	No regulation or protection
<b>5V</b>	Texas Instruments PTH08080W Switching Regulator up to 2.25 amps Input: Main Input	Linear Technology LT1529 Linear Regulator up to 3 amps Input: Main Input
<b>3V3</b>	Texas Instruments PTH08080W Switching Regulator up to 2.25 amps Input: Regulated 5V	Texas Instruments LM3940 Linear Regulator up to 1 amp Input: Regulated 5V
<b>1V8</b>	Linear Technology LT3021 Linear Regulator up to 500mA Input: Regulated 3V3	None

Table 5.5: Comparison of power regulation in Main Board V1 and V2.

### 5.3.3 Future Direction

Since the electronics is a support system which enables the remainder of the prototype to perform, it is highly dependent on the projects specifications. However, under the assumption that the future prototype is to remain similar to the current prototype, a few recommendations include:

1. Switch microcontrollers to an ARM based unit such as the ST32M line of cortex M4. This would significantly decrease the loop time as well as allow for more flexible programming.

2. Add wireless capability either through WIFI in the Raspberry Pi or through an XBee or similar in the Main Board itself.
3. Include electronics for battery charging and management. The current version makes a connector available for this purpose but an actual battery management system was never realized.
4. Return to the monolithic PCB design of Main Board V1 which contains an on-board Raspberry Pi. This makes a more portable design.

Notice that at the time of this writing the team was working on a Main Board V3 which is an improvement on the existing Main Board V2 by:

1. Adds wireless connectivity through use of an Xbee.
2. Removes the on-board UI.
3. Fixes issue of solenoid drivers not being attached to main microcontroller.

## 5.4 Infrared Lighting Rig

### 5.4.1 System Requirements

The requirements for the IRRigs evolved with the project as can be seen in table 5.6. The first version was intended as a platform to test different wavelengths of illumination and the plausibility of vein viewing. With the second version, the team intended to determine the ideal wavelength for illumination. Finally, version 3, would be needed to illuminate only using the ideal wavelength for illumination.

Version 1	Version 2	Version 3
	Provide at least 3 wavelengths.	
Provide at least 3 wavelengths.	Embedded power stage. Use custom connector.	Single wavelength.

Table 5.6: Comparison of requirements between IRRig versions.

## 5.4.2 System Development

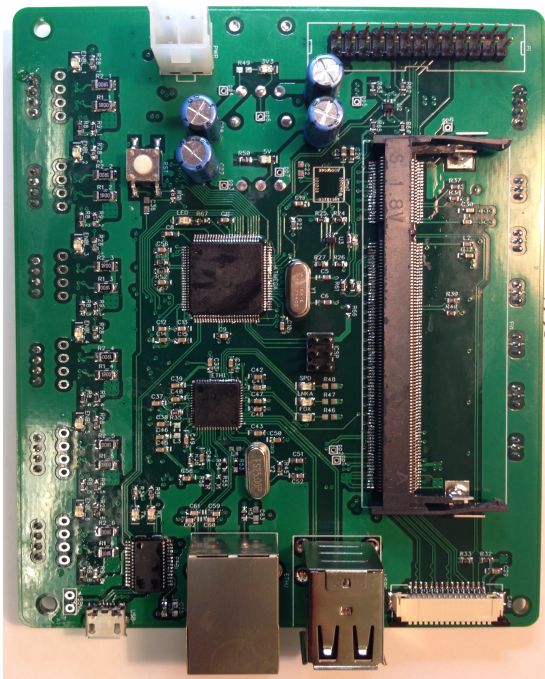
Based on the requirements outlined in the previous section, the feature list of table 5.7 was determined for each of the IRRigs. As can be observed, versions 1 and 2 of the test rig were used for studying the effect of different wavelengths on vein viewing. Their operating wavelengths were chosen based on survey of previous art. By version 3 the imaging wavelength was determined dispensing the need for a custom board. Figure 5-4 shows versions 1 and 2 of the IRRig for comparison.

	Version 1	Version 2	Version 3
<b>General</b>	Potentiometer based intensity adjustment.	MOSFET power stage. PWM Controlled	
<b>Wavelength</b>	850nm,880nm,935nm	740nm,770nm,830nm,850nm,860nm RGB	880nm

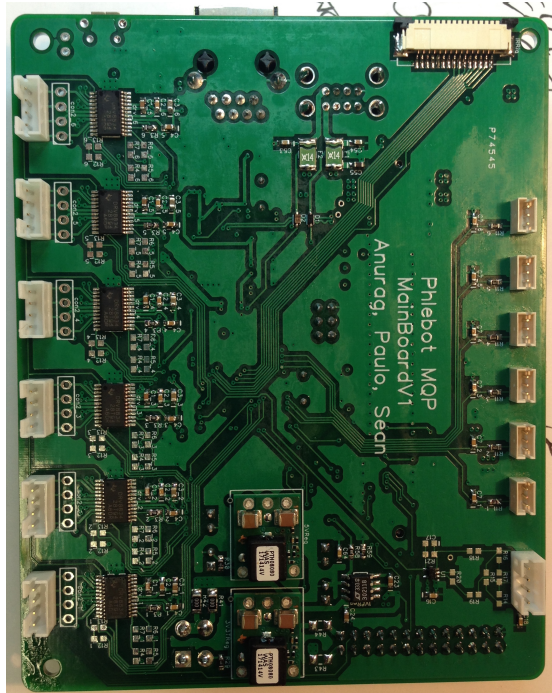
Table 5.7: Feature comparison between IRRig versions.

## 5.4.3 Future Direction

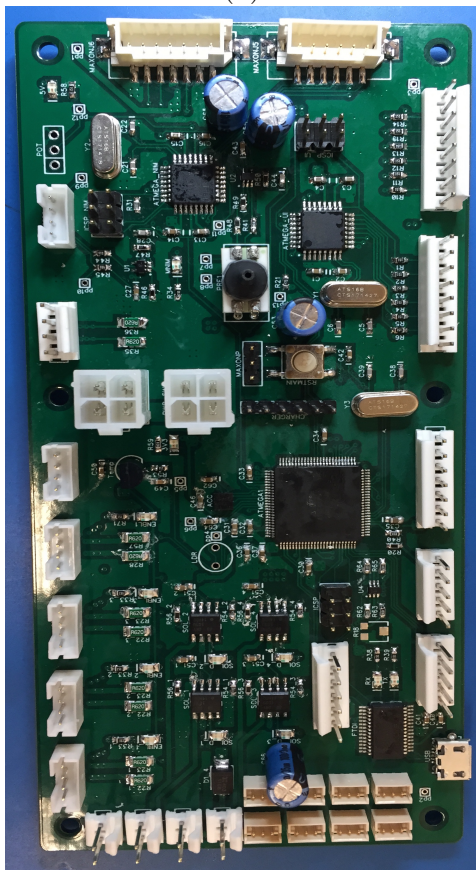
The infrared rig is an area whose development is closely tied to that of the imaging system. For this matter, the future of the IRRig has to be determined based on the direction that is chosen for imaging. If one intends to explore the effect of multiple wavelengths on vein viewing, a rig similar to IRRig version 2 is recommended but much smaller in size. If uniform illumination of a single wavelength is desired, multiple LEDs in 3D printed cases at vantage points around the device would be recommended.



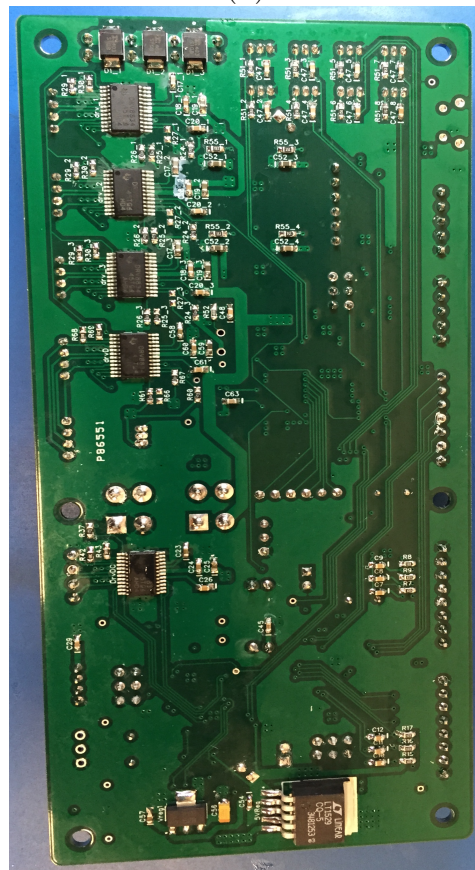
(a)



(b)



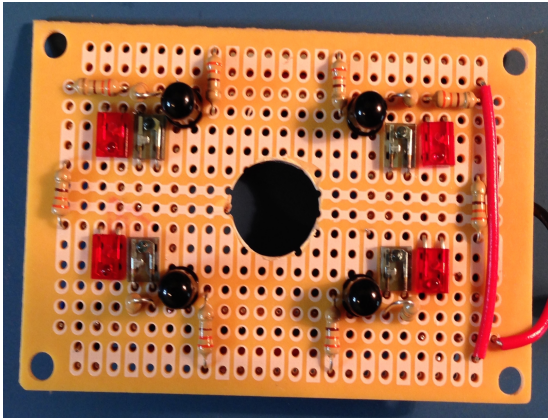
(c)



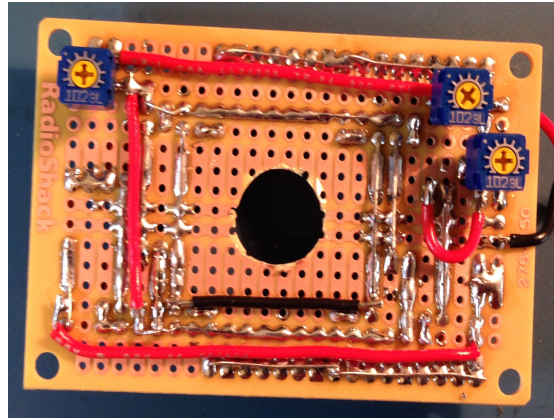
(d)

Figure 5-3: (a) Main Board V1 top view picture. (b) Main Board V1 bottom view picture. (c) Main Board V2 top view picture. (d) Main Board V2 bottom view picture.

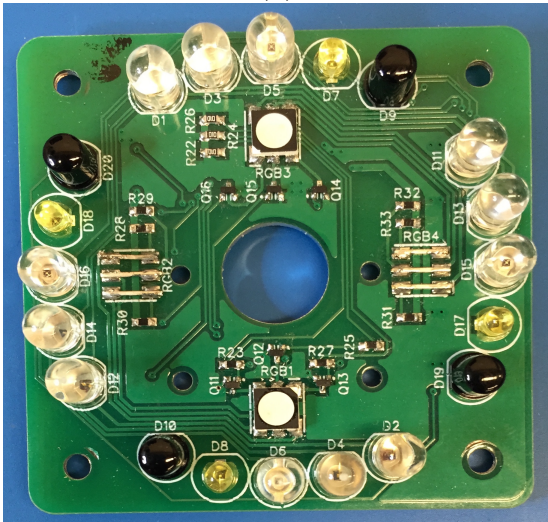




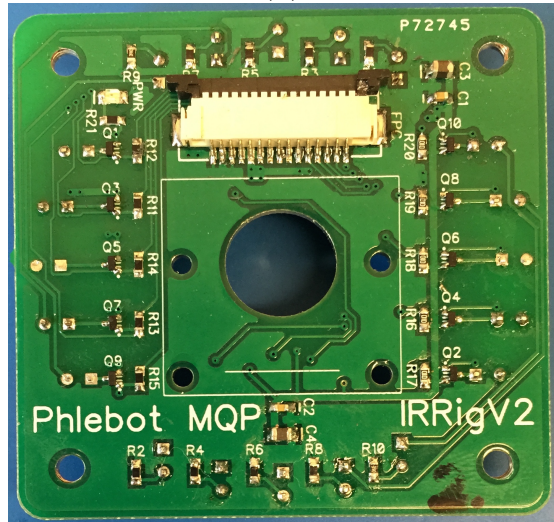
(a)



(b)



(c)



(d)

Figure 5-4: (a) IRRig V1 top view picture. (b) IRRig V1 bottom view picture. (c) IRRig V2 top view picture. (d) IRRig V2 bottom view picture.



# Chapter 6

## Software Design

### 6.1 Chapter Summary

This section will dive into the development and specifications of the final software used in the Phlebot. For this matter, most of the chapter will be split into two sections. The first will deal with the embedded software and the second will deal with the high level software.

### 6.2 Embedded Software

#### 6.2.1 Software Background

The Phlebot contains three microcontrollers each running a unique firmware to control its related subsystem. The main microcontroller controls most of the Phlebot including the motors for the stage and sensors. It also serves as a networking hub which forwards external commands to the secondary microcontrollers. A smaller microcontroller is dedicated to controlling the needle insertion mechanism (NIM); and, another microcontroller is dedicated to the on-board user interface. All software for the Phlebot is designed using an object oriented paradigm so as to remain modular allowing for expansion and removal of features without significant complications.

## 6.2.2 Software Requirements

Robustness was rated the third most important criteria in designing the Phlebot. As such, the software would have to be designed to an object oriented paradigm that would better overall testing ensuring robustness (in the sense of tolerance to failure). Inherent to the object oriented paradigm is modularity which was a driving force in the design of the Phlebot.

Since the firmware is meant to enable all on-board features of the Phlebot, it also has the most specific set of requirements. These requirements are outlined in table 6.1. The requirements are in line with the system architecture of the device in that each microcontroller must control all peripherals connected to it. The criteria of safety is also exemplified in table 6.1 under the row named other. The NIM MCU has to always prioritize control of the NIM such that no blocking action has the potential to lead the system to insert too deeply into the patient’s arm. Similarly, the main code was to be designed such that there are no blocking activities. For these could potentially lead the system to delay an emergency stop.

	<b>MainCode</b>	<b>NIMCode</b>	<b>UICode</b>
<b>Peripherals</b>	End Stops		
	Stage Motors	2 DC Motors	2 Encoders
	Infrared LEDs	Maxon Motor	LCD Display
	Analog Sensors	Force Sensor	
	Reset MCUs		
<b>Communication</b>	NIM MCU		
	UI MCU		
	Raspberry Pi	Main MCU	Main MCU
	Computer		
<b>Other</b>	Non-blocking	NIC Priority	

Table 6.1: Summary of embedded software requirements.

## 6.2.3 Software Development

The MainBoard V2 used in the Phlebot, at the time of this writing, possesses 3 on board microcontrollers. Each of the microcontrollers runs its own firmware: The

ATMEGA2560 runs the MainCode; the NIM ATMEGA328 runs the NIMCode; and, the UI ATMEGA328 runs the UICode. Although each of the firmwares possess very different functions, much of the code is reused between them. The subsections below will explore each of the firmwares in more detail.

In order to fulfill the requirements of robustness and meet the non-blocking criteria, the firmware was designed as an event driven system. In practice this translates to the use of a Status class whose attributes have get, set, tag and tagged methods. Basically each microcontrollers main loop runs an update method from each of its classes. If the class is a sensing class, it sets its related attributes in the Status class and tags them if appropriate. If the class is an actuation class it gets its related attributes from the Status class acts on them and sets them with new values tagging when appropriate. If the class is communication related, it checks which attributes are tagged, untags them if appropriate, and sends them over serial. The communication class also sets the attributes it receives over serial. More simply, when an element is tagged it is marked for sending over serial and is usually sent at the next run of the update method for the communication class.

All embedded software is built in such a way that the main program loop has a single responsibility: To call the update method of each class. Thus, each class in the program requires an update method if it is to perform an action.

### **Main Code - Version 1**

There were two versions of the main code developed for the Phlebot. Version 1 is shown in figure 6-1. Note that this version was abandoned early in the project since the monolithic design of its Status and Comm class violated the robustness criteria of the project and made the code significantly complicated to work with. Since this code was not used it is included here for completeness and will not be described further.

### **Main Code - Version 2**

The base functionality of the version 1 and version 2 code are very similar. The program design, however, is very different. The second version of the code is more



Figure 6-1: UML class diagram for Main Code V1.

modular and makes better use of object oriented design principles. The main changes include redesign of the Comm class and use of abstract data types in the Status class.

Whereas the Comm class, which is responsible for communication, is a monolithic class in the first version of the program, the second version makes use of inheritance.

The use of inheritance allows for separation of the protocol handling and the parsing of the message as can be observed in the UML diagram for main code V2 shown in figure 6-2. This change made maintenance and debugging of the code more reasonable.

The other major change in the code was related to the Status class. Whereas the main code V1 has a Status class which contains get and set methods for each of its attributes, the second version makes use of abstract data types (ADT). Namely TArray, TData and TSensorArray, these abstract data types are template classes (allow for data types of variables within to be defined on creation) that contain all support methods which in the version 1 had to be created for each of the class attributes manually. The use of these ADTs significantly reduced code size making it less likely that errors would be introduced.

An important class for the main code is the Stepper class. This class is responsible for moving the stepper motors. When its update method is called it compares the attribute for desired stepper position with the attribute for the current stepper position and steps the stepper one step in the desired direction. Updating the stepper current position on the end of its execution. Since the class only steps a single step per calling, it abides to the non-blocking paradigm of the program.

An important feature added to this version of the main code was the ability to forward packets. Since the Main MCU is the only interface between the computer (controller) and the NIM MCU (as well as other peripherals), it became clear that the main MCU should have the ability to redirect commands to peripherals connected to it. To this end, the abstract data types that make up the attributes of the status class have forward and forwarded methods. These allow for an attribute to be marked, by calling forward, to be sent to another MCU.

## **User Interface Code**

The UI Code makes use of the same architecture as the main code V2. It also uses the same communication class, however, the inherited parser class is unique to the UI since the way the UI processes information is inherently different than that of the main microcontroller.

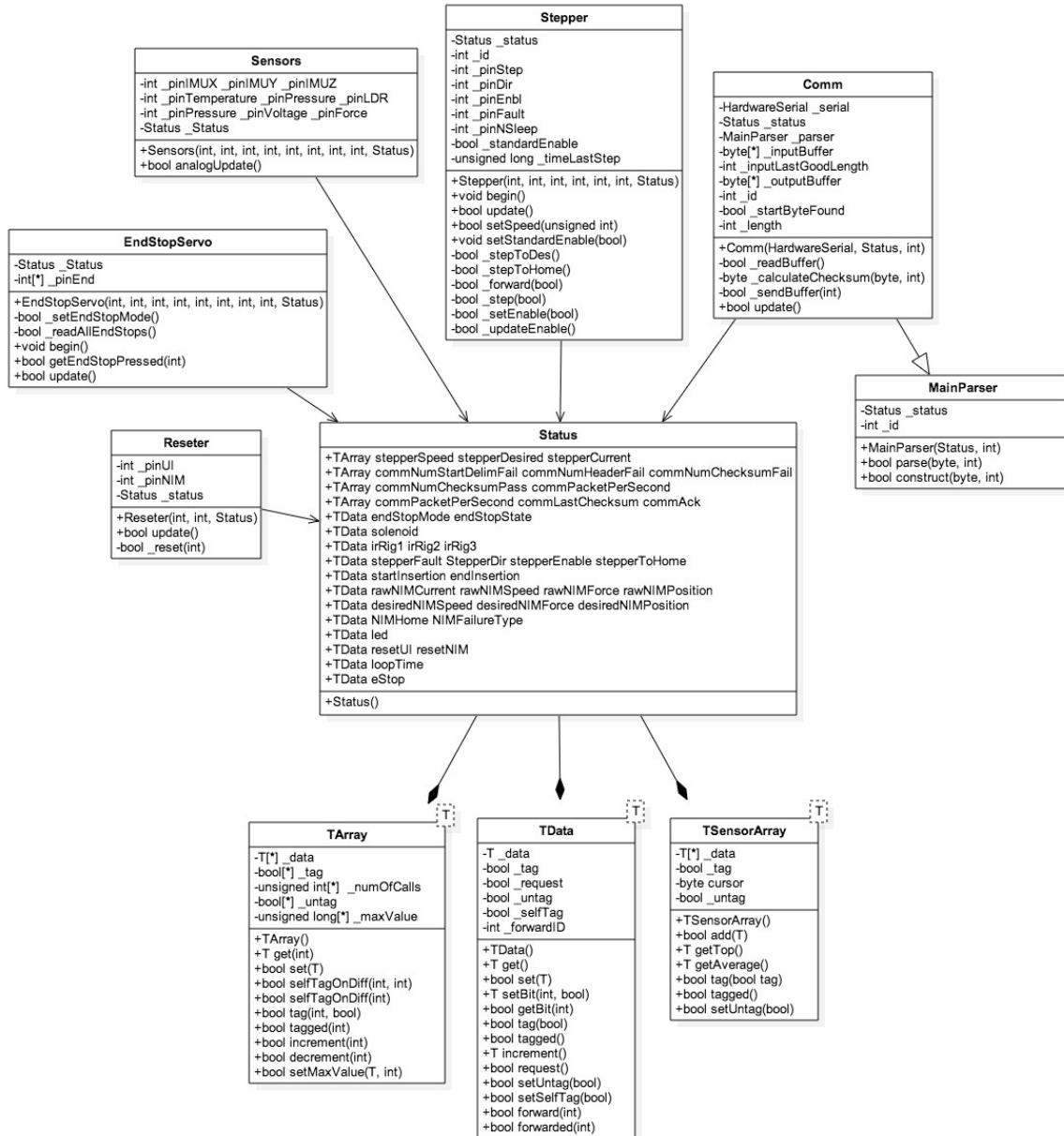


Figure 6-2: UML class diagram for Main Code V2.

The most important class in the UI firmware is the Display class. This class inherits the methods from the Led class which controls the color of the knobs with which the user interacts. It also has an association to the UserInput class which allows it to sense the user commands. The display class is the essence of the onboard user interface, both showing the user the menus and options as well as allowing him to interact with the device. The UML class diagram for the UI Code can be observed



in figure 6-3



Figure 6-3: UML class diagram for UI Code V1.

## Needle Insertion Code

The NIM Controller follows a similar architecture to that of the Main Code V2. For a description of the TArray, TData, TSensorArray, Comm or NIMParser (similar to MainParser) see the Main Code V2 section. The interesting portion of the NIM Code revolves around its NIMController class.

The NIM Controller class is responsible for the procedure of needle insertion. This process includes both updating the estimated position of the needle, as well as running a closed loop with the NIM motor. For more information on the controller see the chapter on the needle insertion controller.

## **6.2.4 Future Direction**

The future direction for embedded software is highly dependent on the future architecture of the prototype. Ideally, a switch to ARM based microcontrollers such as the ST32M series of Cortex-M4s would be recommended. The use of an FPGA could also be explored. Upon completing such change, the firmware could be written on a real time operating system. This would remove several of the restrictions in the current code such as allowing for blocking operations since the operating system scheduler would override them when necessary. Another area of improvement would regard the software engineering aspect of the firmware which should implement more through testing through the use of assertions, unit testing, and coverage to ensure reliable operation.

## **6.3 High-Level Software**

### **6.3.1 Chapter Summary**

The high-level software running on the Raspberry Pi or a tethered laptop is the primary mode of interaction with the robot. It consists of 3 main parts. The first is the Phlebot Control Center which allows real-time monitoring of sensor data and manual control of every function on the device. This is primarily used for debugging and to provide an interface for administrative tasks. The second is the Work-flow Manager which is used to execute pre-defined recipes of actions intended to perform procedures. Medical professionals will primarily interact with the device through this interface. The third part of the device is a data-logging application that is relatively less important for field-usage but was written as a convenience tool during

the prototype's early stages of development.

### **6.3.2 Software Background**

The Phlebot Control center is the primary means of interacting with the robot during the prototyping and debugging phase whereas a medical practitioner would use the Workflow Manager to execute various routines, a typical case of which is shown in figure 6-5.

The high-level software forms the 'brain' of the robot. It is responsible for everything that the robot does such as acquire images, check for the presence of an arm, perform image processing, solve the kinematics and command the motors to move all while monitoring over a dozen sensors in real time. Given all of these functions and depending on the user, the software requires different interfaces, each one exposing different functions and levels of access to the system.

### **6.3.3 System Requirements**

The requirements for the software can be listed as follows:

1. Provide a graphical interface for interacting with the robot's hardware.
2. Manage serial communication with the robot.
3. Image processing capability for enhancing vein contrast.
4. Algorithm for selecting appropriate vein from a set of candidate veins.
5. Solve inverse kinematics for a chosen insertion point.

These requirements force a tight orchestration between various software components.

### **6.3.4 System Development**

The software was written in Python to keep it cross-platform and allow easy portability from the linux development machine to the Raspberry Pi onboard the Phlebot.

There are 3 parts to the high-level software: the image processor, the serial communications manager and the user interface to facilitate interaction with the device.

## **Image Processing**

Initially, all image processing was performed in ImageJ due to its ease of rapid prototyping algorithms and recording processing macros. The images were then manually fed into a Python module for feature extraction and registration to the device coordinate frame. A parallel approach considered rewriting the ImageJ macros in an OpenCV build for the Raspberry Pi in order to allow native interoperability between the image processing and kinematics modules. This approach, though theoretically sound, was not favored due to OpenCV's high processor and memory demands on the Raspberry Pi. The image processing

The Phlebot Control Center allows the operator to perform image acquisition and processing in addition to multi-wavelength illumination pattern control through a simple interface.

## **Serial Communication**

The serial communication for the Phlebot is based on a low-level communication protocol developed by the team for reliable serial communication between the Raspberry Pi, the laptop computer and the 3 on-board microcontrollers (see Appendix F for detailed overview of the protocol and a comprehensive list of serial instructions). The protocol is relatively simple, consisting of a start byte, which signals the start of a packet, followed by a packet header, which defines the message type (such as NIM motor velocity update for example), followed by the message length, followed by the message itself and finally a CRC checksum to ensure data integrity. All message types for sending data to and requesting data from the device are encoded in a serial communications class. The low-level serial communication over USB is implemented by the PySerial library.

## **User Interface**

The off-board user interface followed a systematic iterative design approach. After listing down the UI requirements at each stage of development, a wireframe mock-up was created to structure the GUI and lay out the various controls. After initial experimentation with Qt for front-end development, Qt was abandoned in favor of Python's native tkinter owing to its light weight and ease of use for our application. There were 3 main iterations of the Phlebot Control Center's front end. These are shown in figures 6-6, 6-7 and 6-8

### **6.3.5 Future Direction**

The future of the Phlebot's software will include a complete overhaul of the software and make the code much tighter, incorporate unit testing and code quality monitoring tools. The user interface is quite robust but the serial communication, especially on Macintosh computers, tends to be unreliable in port selection. A web interface for controlling the Phlebot would potentially help in telemedicine applications.

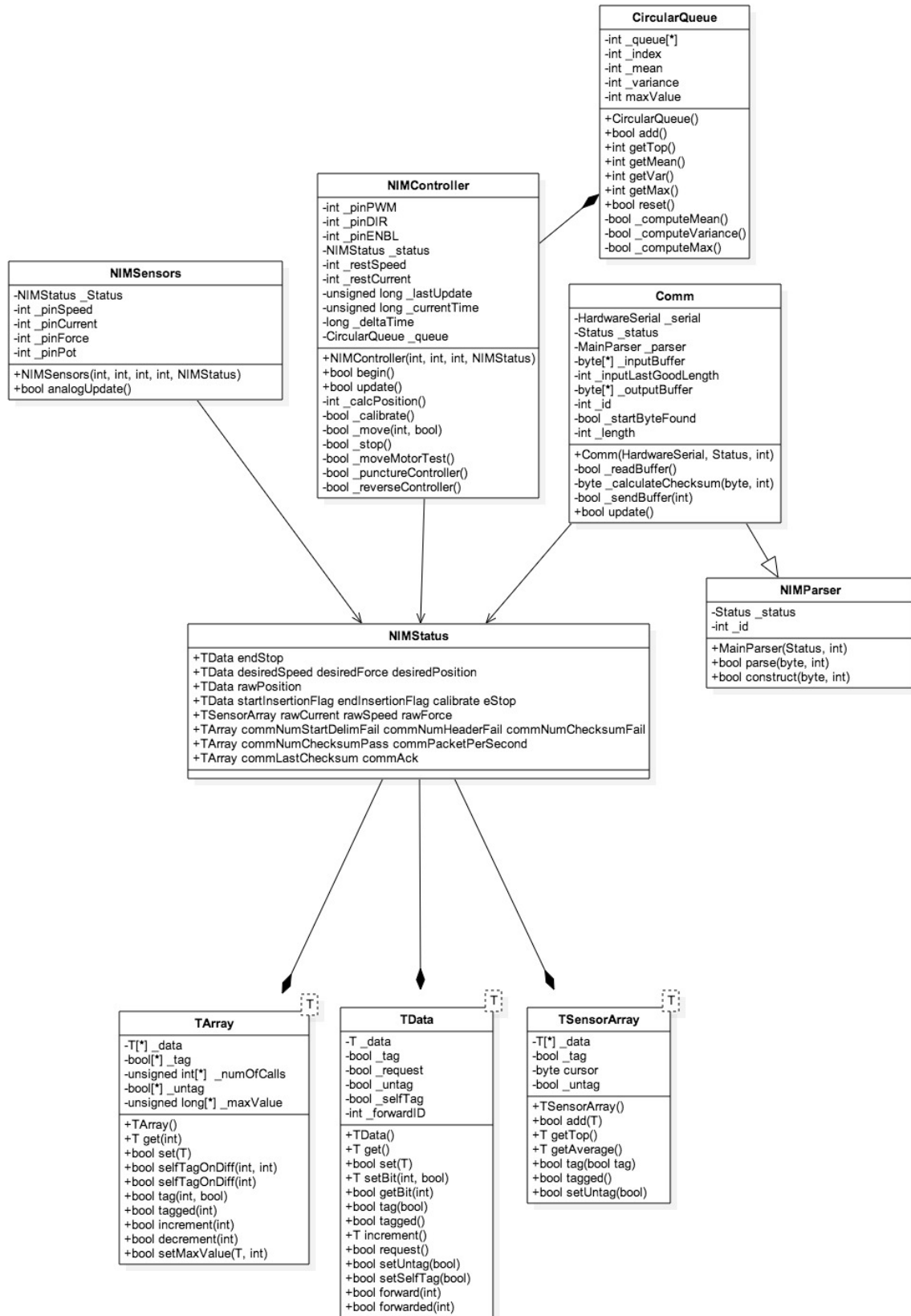


Figure 6-4: UML class diagram for NIM Code V1.

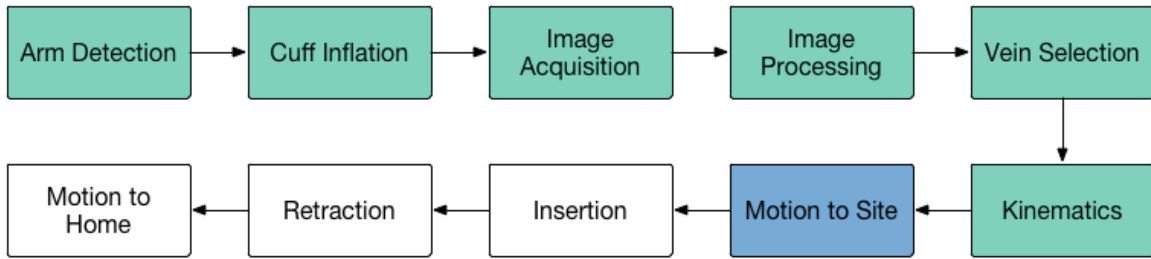


Figure 6-5: Typical Workflow for the Phlebot. Green boxes represent completed steps, blue represents current state and empty boxes steps to be completed.

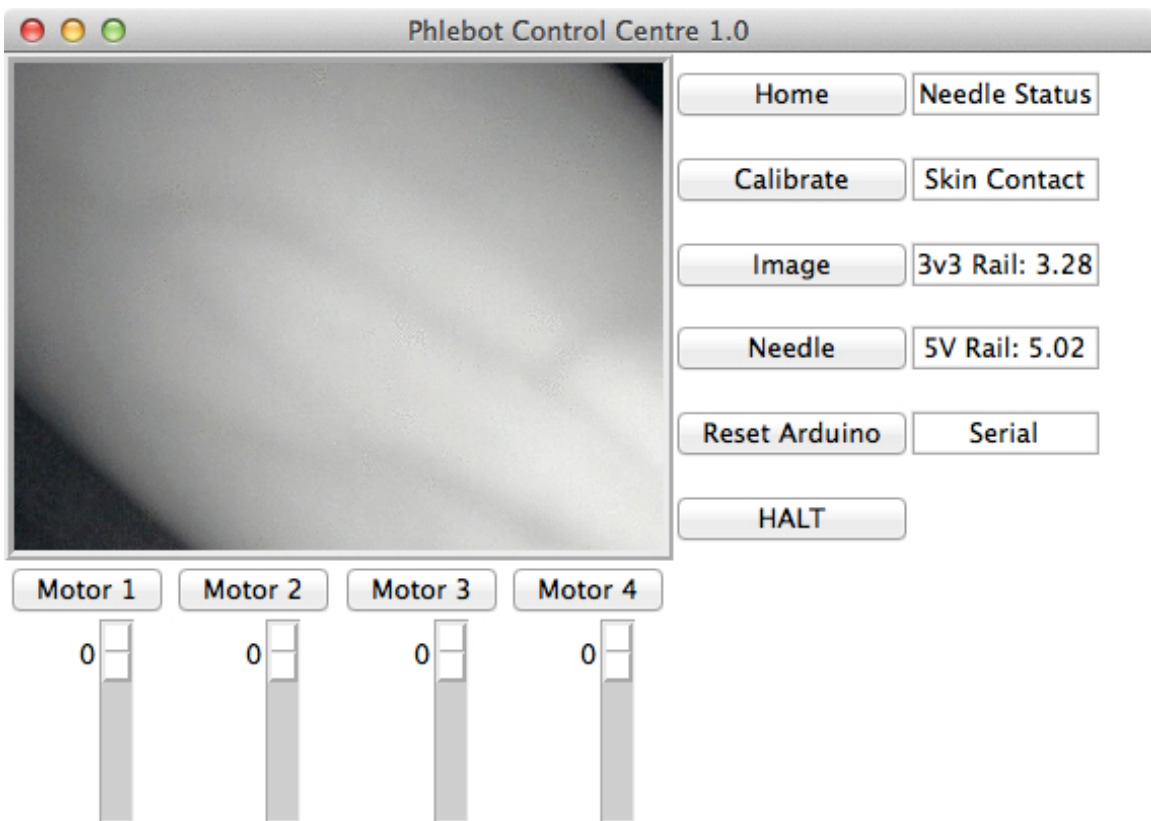


Figure 6-6: Phlebot Control Center V1 with basic motor control and image acquisition.

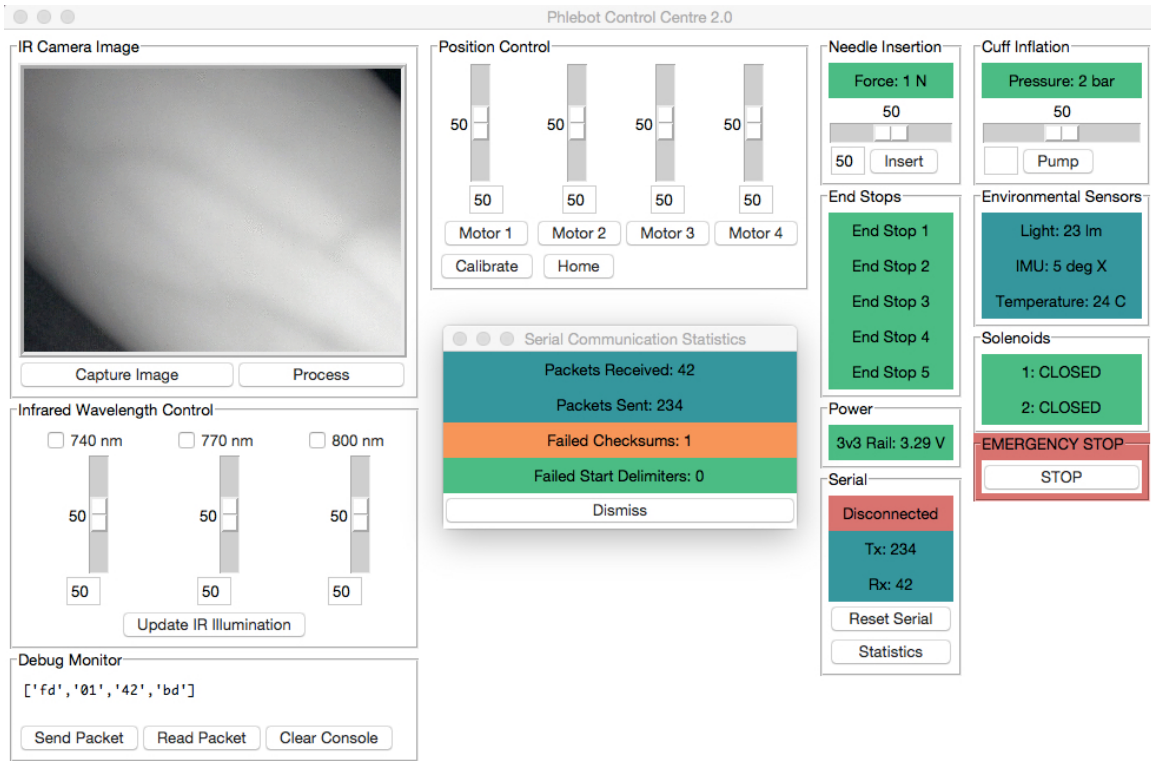


Figure 6-7: Phlebot Control Center V2 with sensor state monitors, communication statistics, and debug console.



Figure 6-8: Phlebot Control Center V3 with Needle Insertion Mechanism control console and live sensor data graphing ability.



# Chapter 7

## Needle Insertion Controller

### 7.1 Summary

Modeling the interaction between end effectors of surgical robots and their tissue targets is frequently complex enough that real time computer modeling of said interactions is not feasible, and reduced complexity models lead to errors in end effector position.

### 7.2 Problem Formulation

### 7.3 Background

There has been a great deal of interest in needle/tissue interaction in percutaneous diagnosis and therapies over the past decade due to the need to improve accuracy in these procedures [35] [2] . This research encompasses tissue mechanics, needle insertion modeling and simulation in both software and hardware, and various control schemes to improve clinical outcomes. Models for needle insertion can be characterized by either deformation models, which fit experimental data to various equations, or fracture mechanics, which models the changes in tissue geometry due to insertion [5]. Most of the recent work is based on the fracture mechanics model presented by Okamura, which relates the force measured at the end of the needle to the cutting

force, friction force, and stiffness force; however many models only take into account the friction and cutting forces [31]. Building on Okamura, there have been numerous simulations proposed to model tissue-needle interactions based on fracture mechanics using various FEM or constraint models to develop needle trajectories offline [3] [13] [33]. Given the time required to solve these models, they are not suitable for realtime needle control. Recently there have been proposals for computational frameworks allowing for real-time FEA simulation, it has not yet been applied to online needle insertion control and is still focused on offline simulation [10]. The trajectories calculated by these simulations have been shown to be effective when applied to tissue phantoms made from soft plastics, they are not able to account for unpredicted needle-tissue interaction and as such do not provide clinically viable solutions [14]. Since the results of [7] demonstrated tactile sense alone is not able to characterize tissue type in most practical applications, methods have been proposed to utilize current medical imaging technology, such as ultrasound and magnetic resonance imaging (MRI), to identify different tissues and generate needle trajectories [4]. However, these trajectories require the use of flexible needles since the desired targets, such as the prostate or liver, are deep in the body. A number of optimal control schemes have been proposed for steering a flexible needle to minimize tissue damage and positioning error such as in [18].

While most of the literature on needle insertion is concerned with percutaneous procedures involving biopsy or treatment, a comparatively small amount of research has been done on blood specimen collection. While it has been theorized for nearly two decades [32] that it is possible to perform venipuncture by monitoring the force profile of insertion, it is only recently that a realistic method has been proposed. By implementing local estimates of cutting and friction forces, Elgezua et. al. were able to create an algorithm able to detect tissue puncture, including venipuncture [14]. While a robotic system was proposed by Zivanovic [40], the device proposed was not sophisticated enough to account for *in vivo* tissue reactions. It is our goal to develop a control algorithm which performs venipuncture while minimizing tissue deformation.

## 7.4 System Development

Since there is limited data available on robot assisted venipuncture, the team investigated the expected tissue forces arising during venipuncture by making tissue phantoms. Numerous tubes of varying material properties were embedded in the phantoms to simulate venipuncture. Insertion was then performed at constant speeds without puncture detection to understand typical force profiles and the effect velocity has on needle force. Next, puncture detection was tested on thin rubber tubes and phantoms.

Before testing surgical robots on tissue either *in vitro* or *in vivo* it is common to first perform studies on synthetic phantoms displaying similar mechanical properties to the tissue(s) under investigation [1]. While phantoms are unable to fully model the mechanical complexity of living tissue, by matching properties such as elastic modulus the cutting force,  $f_{cut}$ , can be adequately modeled. This does not hold for the needle friction,  $f_{frict}$ , which has a more complex needle-tissue interaction than  $F - cut$ . To create phantoms a phantom with the proper elastic modulus for each tissue level, we used liquid polyvinyl chlorid (PVC) and the liquid plasticizer phthalate ester (Super Soft Liquid Plastic, M-F Manufacturing, TX). Increased concentration of liquid plasticizer would cause a decrease in elastic modulus [11]. Five phantoms were made with different concentrations of plasticizer as shown in table7.1. The phantoms

Phantom Number	Percent PVC	Percent Plasticizer
1	100%	0%
2	80%	20%
3	65%	35%
4	50%	50%
5	85%	15%

Table 7.1: Relative Concentrations of PVC and Plasticizer for each test phantom

were then tested on the Instron<sup>TM</sup> 5544 to find the elastic modulus associated with a given concentration. Next, six two layer phantoms were made with the top layer at 100 kPa and the bottom at 40kPa to match the moduli of skin and adipose respectively [20]. Each phantom had tubes of either, white silicone rubber, polyurethane, or

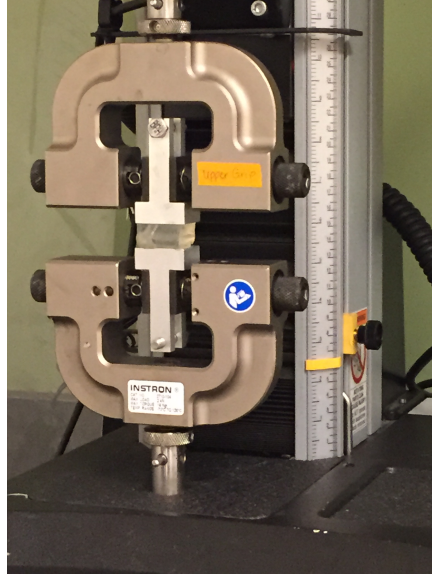


Figure 7-1: Discovering Elastic Moduli of Phantoms

polytetrafluoroethylene (PTFE).

As noted, testing for the modulus of elasticity was performed on the Instron™ 5544 and is shown in figure 7-1. Sections of each phantom were cut, measured, and compressed at three speeds and three loads with three replicates. Not every phantom was tested with each of the  $2^3$  factors. The stress and strain were recorded during the testing and used to find the elastic modulus of the material based on equation 7.1

$$\lambda = \frac{\textit{stress}}{\textit{strain}} \quad (7.1)$$

where  $\lambda$  is the elastic modulus. While the elastic modulus of the phantom is clearly non-linear, a least-squares linear regression was used to approximate the linear modulus. A graph of the stress vs. strain with and the linear fit is shown in figure 7-2. The other graphs may be found in Appendix G. An estimate of the elastic modulus for each phantom sample is shown in table 7.2. There is variability in the elastic depending on the speed the test was performed as well as error in linearizing stress/strain relationship. Should this experiment be performed again a greater number of replicates for each phantom type would need to be used. We decided that the top layer of the second round of phantoms should be made from sample 1, which had an elastic

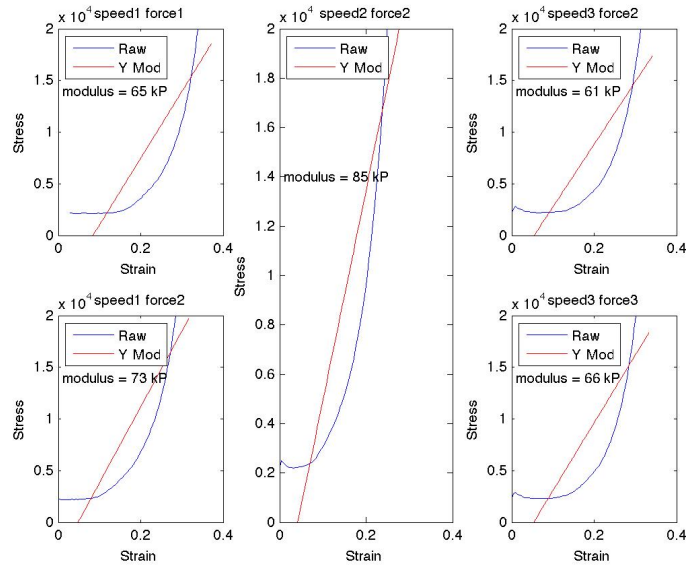


Figure 7-2: Graph of the stress vs strain of phantom sample 3 with regression line. The stress and strain shown is the mean of the three trials performed

modulus of approximately 100 kPa, and the bottom layer made from phantom 4, which had a modulus of 40 kPa. We attempted to make the top layer 2mm thick, but were unable to obtain consistent results given the method used for making the phantoms. The mechanical properties of the phantoms provide an idealized estimate

Phantom Number	Elastic Modulus
1	110 kPa
2	80 kPa
3	65 kPa
4	50 kPa
5	90 kPa

Table 7.2: Elastic modulus for each phantom

of the forces which can be expected should puncture be performed on living tissue.

Next, insertion was done on the phantoms with a constant velocity controller to obtain data on the needle force to guide the development of the NIC. Throughout these trials a 22 gauge butterfly needle was used at a 20° angle of insertion. During insertion the force, speed, and current are monitored by the Phlebot and written to a JSON file for processing at a frequency of 10Hz. Since the microcontroller responsible

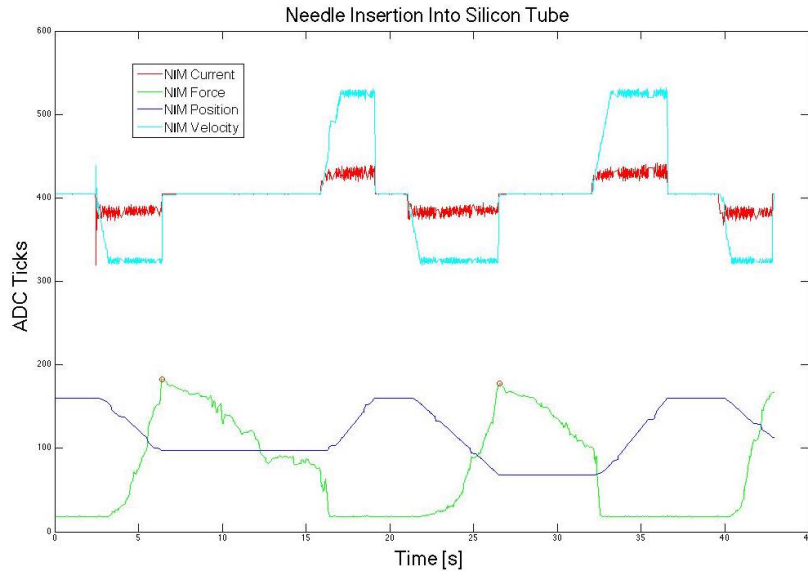


Figure 7-3: Insertion and puncture detection on silicon tube. Red dots mark where puncture is detected. The red line is the current, the cyan is the velocity, green the force, and blue the position.

for the NIC was sampling at 1kHz, the data stored in the file was considered under-sampled and could not be used for reliable tuning of a chosen control algorithm. It was found that of the three tubes used to simulate veins, only the white silicon was amenable to puncture by the Phlebot. The other two materials were too stiff for the Phlebot to reliably puncture.

Before implementing an optimal control law, it was first necessary to implement a suitable puncture detection algorithm. We based our puncture detection on the algorithm developed in [14] with slight modifications to suite implementation on a microcontroller. In this algorithm, a cyclic buffer of force values is stored. The mean, variance, and maximum value of the buffer are calculated at each time step. If  $buffer_{max} - buffer_{new} > K * buffer_{var}$  where  $K$  is a constant, a peak is detected. To test puncture detection, the Phlebot performed insertion at a constant speed, and when puncture occurs the motor is disabled. In figure 7-3 we show the output of the Phlebot when puncturing a silicon tube (2mm diameter). The red dots indicate when puncture has been detected which is closely followed by the motor being disabled.

## 7.5 Future Direction

While the control law currently implemented shows it is possible to use the Phlebot to perform venipuncture, it is not robust enough to be used on a large and varied population nor does it minimize the inevitable pain associated with insertion. Our next step is to modify the puncture detection algorithm presented to take into account other parameters regarding insertion force, such as the time derivative, to provide a more robust detection algorithm. We believe that by implementing a minimum time controller, insertion would be performed at maximum speed while still conforming to all necessary constraints. Increased insertion speed should correlate with decreased patient pain.





# Chapter 8

## Conclusion

The safe and reliable automation of phlebotomy would represent an enormous boon to the healthcare industry. Previous attempts to automate phlebotomy employed ultrasonography and stereoscopic near-infrared (NIR) imaging to locate veins. However, these systems are very expensive and complex to maintain.

We have designed and built Phlebot, a medical robot for the automatic collection of blood samples or intravenous catheterization. The Phlebot uses a combination of monocular NIR imaging and needle tip force monitoring to select an optimal vein for venipuncture and insert the needle into the selected vein, stopping at a safe depth when vein wall puncture is detected. This novel approach makes the system much easier to maintain and significantly more affordable.

Phlebot is designed to be a completely self-contained and portable system. A modular design approach allowed us to independently test and iterate the various subsystems before end-to-end integration. We envision that the Phlebot represents a major step towards more affordable point-of-care testing and diagnostic healthcare systems.

The Phlebot has undergone six major revisions with new concepts tested at each stage and previous concepts improved upon. The robot is currently capable of automatically locating a suitable vein using imaging parameters obtained from an IRB-approved study on 9 subjects. We have validated the needle insertion controller in phantoms that mimic the mechanical properties of the vein and surrounding tissue.

The closed loop controller for insertion ensures complete stopping of the needle within 100 milliseconds of a puncture being detected. These results represent our proof of concept for the technology we are developing.

The Phlebot prototype possesses most of the features in place for further testing. However, some work remains before clinical trials can take place. The vision-based vein detection is presently limited by the assumption of linear veins. This limitation can be tackled using a variation of a well-known algorithm which we are currently developing. The needle insertion controller requires material-dependent parameter tuning and is yet to be clinically tested. The mechanical components need an upgrade since the limited availability of materials and equipment have precluded the creation of a medical grade device.

We have an ASME paper titled Robotic Assistive Device for Phlebotomy accepted for publication in July and are currently working with Professor Gregory Fischer and Todd Keiler to apply for a provisional patent.

# Bibliography

- [1] Momen Abayazid, CL De Korte, S Misra, et al. Effect of skin thickness on target motion during needle insertion into soft-tissue phantoms. In *Biomedical Robotics and Biomechatronics (BioRob), 2012 4th IEEE RAS & EMBS International Conference on*, pages 755–760. IEEE, 2012.
- [2] Niki Abolhassani, Rajni Patel, and Mehrdad Moallem. Needle insertion into soft tissue: A survey. *Medical engineering & physics*, 29(4):413–431, 2007.
- [3] Ron Alterovitz, Kenneth Y Goldberg, Jean Pouliot, and I-C Hsu. Sensorless motion planning for medical needle insertion in deformable tissues. *Information Technology in Biomedicine, IEEE Transactions on*, 13(2):217–225, 2009.
- [4] Ron Alterovitz, Andrew Lim, Ken Goldberg, Gregory S Chirikjian, and Allison M Okamura. Steering flexible needles under markov motion uncertainty. In *Intelligent Robots and Systems, 2005.(IROS 2005). 2005 IEEE/RSJ International Conference on*, pages 1570–1575. IEEE, 2005.
- [5] Toufic Azar and Vincent Hayward. Estimation of the fracture toughness of soft tissue from needle insertion. In *Biomedical simulation*, pages 166–175. Springer, 2008.
- [6] Dana H Ballard. Generalizing the hough transform to detect arbitrary shapes. *Pattern recognition*, 13(2):111–122, 1981.
- [7] Peter N Brett, Andrew J Harrison, and Trevor A Thomas. Schemes for the identification of tissue types and boundaries at the tool point for surgical needles. *Information Technology in Biomedicine, IEEE Transactions on*, 4(1):30–36, 2000.
- [8] Cap.org. College of american pathologists blueprint for blue penciling phlebotomy errors, 2015.
- [9] Alvin Chen, Kevin Nikitczuk, Jason Nikitczuk, Tim Maguire, and Martin Yarmush. Portable robot for autonomous venipuncture using 3d near infrared image guidance. *Technology*, 1(01):72–87, 2013.
- [10] Hadrien Courtecuisse, Jérémie Allard, Pierre Kerfriden, Stéphane PA Bordas, Stéphane Cotin, and Christian Duriez. Real-time simulation of contact and

- cutting of heterogeneous soft-tissues. *Medical image analysis*, 18(2):394–410, 2014.
- [11] Simon P DiMaio and Septimiu E Salcudean. Needle insertion modeling and simulation. *Robotics and Automation, IEEE Transactions on*, 19(5):864–875, 2003.
- [12] Lisa Dugan, Lida Leech, Karen Gabel Speroni, and Joy Corriher. Factors affecting hemolysis rates in blood samples drawn from newly placed iv sites in the emergency department. *Journal of Emergency Nursing*, 31(4):338–345, 2005.
- [13] Christian Duriez, Christophe Guébert, Maud Marchal, Stéphane Cotin, and Laurent Grisoni. Interactive simulation of flexible needle insertions based on constraint models. In *Medical Image Computing and Computer-Assisted Intervention–MICCAI 2009*, pages 291–299. Springer, 2009.
- [14] Inko Elgezua, Yo Kobayashi, and Masakatsu G Fujie. Estimation of needle tissue interaction based on non-linear elastic modulus and friction force patterns. In *Intelligent Robots and Systems (IROS 2014), 2014 IEEE/RSJ International Conference on*, pages 4315–4320. IEEE, 2014.
- [15] Harold J Galena. Complications occurring from diagnostic venipuncture. *The Journal of family practice*, 34(5):582–584, 1992.
- [16] MD Gerry Greenstone. The history of bloodletting, jan 2010. <http://www.bcmj.org/premise/history-bloodletting>.
- [17] M.D. Gilbert R. Seigworth. A brief history of bloodletting. <http://www.pbs.org/wnet/redgold/basics/bloodlettinghistory.html>.
- [18] Kris Hauser, Ron Alterovitz, Nuttapong Chentanez, Allison Okamura, and Ken Goldberg. Feedback control for steering needles through 3d deformable tissue using helical paths. *Robotics science and systems: online proceedings*, page 37, 2009.
- [19] Min Joung Kim, Joon Min Park, Nuga Rhee, Sang Mo Je, Seong Hee Hong, Young Mock Lee, Sung Phil Chung, and Seung Ho Kim. Efficacy of VeinViewer in pediatric peripheral intravenous access: a randomized controlled trial, 2012.
- [20] Xing Liang and Stephen A Boppart. Biomechanical properties of in vivo human skin from dynamic optical coherence elastography. *Biomedical Engineering, IEEE Transactions on*, 57(4):953–959, 2010.
- [21] Giuseppe Lippi, Jeffrey J Chance, Stephen Church, Paola Dazzi, Rossana Fontana, Davide Giavarina, Kjell Grankvist, Wim Huisman, Timo Kouri, Vladimir Palicka, et al. Preanalytical quality improvement: from dream to reality. *Clinical chemistry and laboratory medicine*, 49(7):1113–1126, 2011.

- [22] Giuseppe Lippi, Gian Luca Salvagno, Martina Montagnana, Massimo Franchini, and Gian Cesare Guidi. Phlebotomy issues and quality improvement in results of laboratory testing. *Clinical laboratory*, 52(5-6):217–230, 2006.
- [23] Glynnis Lowe, Rose Stike, Marc Pollack, Jenny Bosley, Patti O’Brien, Amy Hake, Greta Landis, Natalie Billings, Pam Gordon, Steve Manzella, et al. Nursing blood specimen collection techniques and hemolysis rates in an emergency department: analysis of venipuncture versus intravenous catheter collection techniques. *Journal of Emergency Nursing*, 34(1):26–32, 2008.
- [24] T. Maguire, K. Nikitzuk, M. Yarmush, E. Novik, and S. Dunn. Automated vessel puncture device using three-dimensional(3d) near infrared (nir) imaging and a robotically driven needle, December 8 2011. US Patent App. 13/124,324.
- [25] MedTech. The complete history and progression of bloodletting. <http://www.medtech.edu/blog/the-history-progression-and-modern-stance-on-bloodletting>.
- [26] Roberto Kasuo Miyake, Herbert David Zeman, Flavio Henrique Duarte, Rodrigo Kikuchi, Eduardo Ramacciotti, Gunnar Lovhoiden, and Carlos Vrancken. Vein imaging: a new method of near infrared imaging, where a processed image is projected onto the skin for the enhancement of vein treatment. *Dermatologic surgery : official publication for American Society for Dermatologic Surgery [et al.]*, 32:1031–1038, 2006.
- [27] Sheshadri Narayanan. The preanalytic phase an important component of laboratory medicine. *American journal of clinical pathology*, 113(3):429–452, 2000.
- [28] Nhlbi.nih.gov. Types of blood tests - nhlbi, nih, 2015.
- [29] S. Nicholson, L.S. Paul, and T.P. Pawelko. Method, system and apparatus for projecting visible and non-visible images, January 12 2011. EP Patent App. EP20,090,174,426.
- [30] United States Department of Labour. Healthcare wide hazards. Hospital ETool: Healthcare Wide Hazards - Needlestick/Sharps Injuries.
- [31] Allison M Okamura, Christina Simone, and Mark D O’Leary. Force modeling for needle insertion into soft tissue. *Biomedical Engineering, IEEE Transactions on*, 51(10):1707–1716, 2004.
- [32] Daisaku Okuno, Tatsuo Togawa, Hirokazu Saito, and Kiichi Tsuchiya. Development of an automatic blood sampling system: control of the puncturing needle by measuring forces. In *Engineering in Medicine and Biology Society, 1998. Proceedings of the 20th Annual International Conference of the IEEE*, volume 4, pages 1811–1812. IEEE, 1998.

- [33] Igor Peterlik, Mourad Nouicer, Christian Duriez, Stephane Cotin, and Abderahmane Kheddar. Constraint-based haptic rendering of multirate compliant mechanisms. *Haptics, IEEE Transactions on*, 4(3):175–187, 2011.
- [34] D. E. Spivack, P. Kelly, J. P. Gaughan, and P. S. van Bemmelen. Mapping of superficial extremity veins: normal diameters and trends in a vascular patient-population. *Ultrasound Med Biol*, 38(2):190–194, Feb 2012.
- [35] Dennis J van Gerwen, Jenny Dankelman, and John J van den Dobbelsteen. Needle–tissue interaction forces—a survey of experimental data. *Medical engineering & physics*, 34(6):665–680, 2012.
- [36] Elizabeth A Wagar, Ana K Stankovic, Stephen Raab, Raouf E Nakhleh, and Molly K Walsh. Specimen labeling errors: a q-probes analysis of 147 clinical laboratories. *Archives of pathology & laboratory medicine*, 132(10):1617–1622, 2008.
- [37] F. Wood, R. Goldman, S. Conlon, and V. Luciano. Laser vein contrast enhancer, February 21 2008. US Patent App. 11/807,359.
- [38] Kouji Yamada, Keiki Yamada, Ituro Katsuda, and Takehiko Hida. Cubital fossa venipuncture sites based on anatomical variations and relationships of cutaneous veins and nerves. *Clinical anatomy (New York, N.Y.)*, 21(4):307–13, May 2008.
- [39] D Yücel and K Dalva. Effect of in vitro hemolysis on 25 common biochemical tests. *Clinical chemistry*, 38(4):575–577, 1992.
- [40] Aleksandar Zivanovic and Brian L Davies. A robotic system for blood sampling. *Information Technology in Biomedicine, IEEE Transactions on*, 4(1):8–14, 2000.

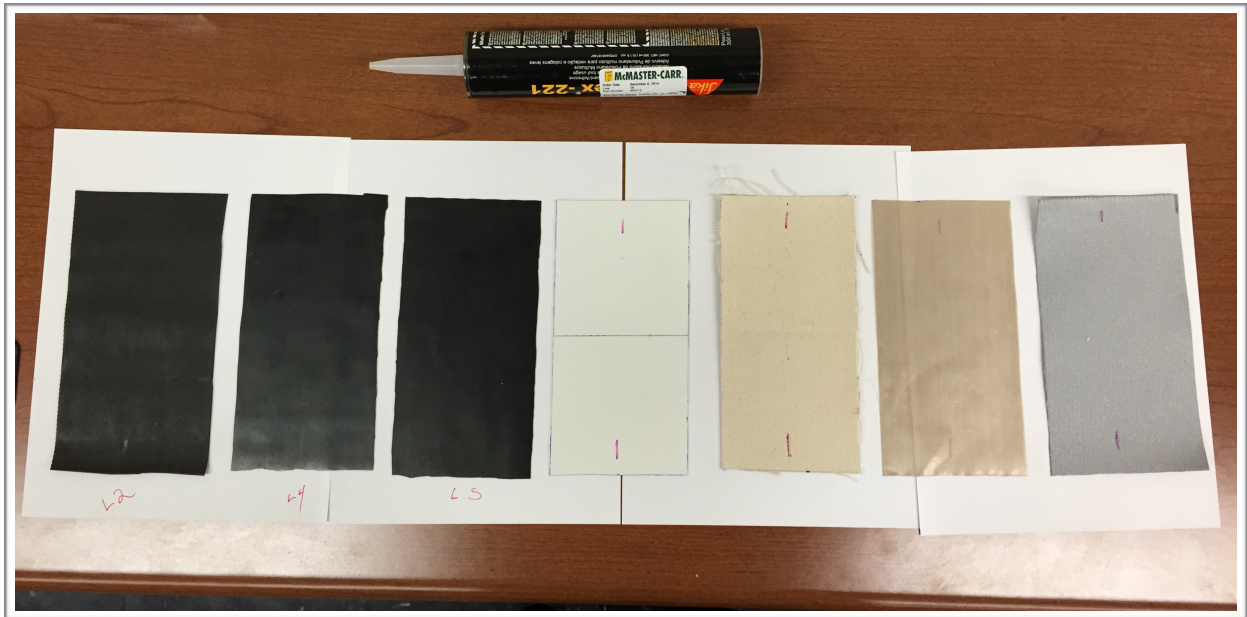
# Appendix A

## Cuff Study: Materials and Glue

# Phlebot MQP Cuff Study

## *Part 1: Materials and Glue*

### Phlebot MQP



Fall 2014



# Phlebot MQP Cuff Study

## *Part 1: Materials and Glue*

### Objective

Determine the best material and adhesive for manufacture of the inflatable cuff.

### Overview

A selection of 18 materials and 9 glues were chosen for the study. A standard cuff and glue pattern was applied on all relevant combinations from which the material with McMaster reference 9455K52 and glues LOC409 and 3MCA4 were determined to be the best combinations to be used when manufacturing the inflatable cuff.

### Materials and Methods

The selected materials are summarized in the table 1. Materials marked with a strikethrough were not used in the study as a cuff could not realistically be manufactured from them.

Material Identifier	McMaster Reference	Material Description
Rubber 1	9109K61	Super-Soft Neoprene Rubber, 1/16" Thick, 6" X 6", 10A Durometer
FDA Rubber 1	86795K21	FDA-Compliant Oil-Resistant Buna-N Rubber, White, Plain Back, 1/16" Thickness, 12" X 12", 60A Durometer
<del>Shim</del>	<del>9513K42</del>	<del>Color-Coded Plastic Shim Stock, 15 Pieces, Assortment of 5" X 20"</del>
<del>PTFE + Fiberglass 1</del>	<del>5739T11</del>	<del>Adhesive-Backed PTFE-Coated Fiberglass Sheet, .003" Thick, 12" X 12"</del>
PTFE + Fiberglass 2	8876K81	Tear-Resistant PTFE-Coated Fiberglass Fabric, .003" Thick, 37-1/2" Width, 1' Length
Tyvek	1650T11	Lightweight Tyvek Fabric, .007" Thick, 24" Wide, 15' Long
Silicon Coated Fiberglass	87815K1	Silicone-Coated Fiberglass Fabric, .017" Thick, 60" Width, Gray, 1' Length
Cotton Fabric	8778K1	Cotton Fabric .026" Thick, 36" Width, 8 Ounces Per Square Yard, 2 ft. Length
<del>Polysterene 1</del>	<del>8734K31</del>	<del>Easy-to-Machine Polystyrene Sheet, 1/32" Thick, 12" X 24"</del>
<del>Polysterene 1</del>	<del>8734K32</del>	<del>Easy-to-Machine Polystyrene Sheet, 1/16" Thick, 12" X 24"</del>
<del>Kapton</del>	<del>2271K1</del>	<del>Kapton (R) Polyimide Film, .001" Thick, 12" X 12"</del>

Material Identifier	McMaster Reference	Material Description
<del>PEEK</del>	8504K11	<del>PEEK Film, .003" Thick, 6" X 6"</del>
Rubber 2	9109K42	Super-Soft Neoprene Rubber, 1/16" Thick, 12" X 24", 10A Durometer
<del>Rubber 3</del>	<del>8630K168</del>	<del>Neoprene Spring Rubber, 1/16" Thickness, 12" W X 12" L, 70A Durometer</del>
Rubber 4	9455K52	Medium-Strength Neoprene Rubber, Plain Back, 1/32" Thick, 12" X 24", 30A Durometer
Rubber 5	9455K52	Medium-Strength Neoprene Rubber, Plain Back, 1/32" Thick, 12" X 24", 40A Durometer
Rubber 6	86435K41	Super-Soft Silicone Rubber, .010" Thick, 12" X 12", 10A Durometer
FDA Rubber 2	86915K12	FDA-Compliant Silicone Rubber, Plain Back, .020" Thickness, 12" X 12", Transparent

**Table 1: Materials selected for study.**

The selected glues are summarized in table 2. Glues with a strikethrough were not used in study as their properties were deemed insufficient for creation of a cuff.

Glue Identifier	McMaster Reference	Glue Description
Silicon1	7606A49	Flexible Sealant, Super Flexible, 10.1-Ounce Size, Black
<del>Silicon2</del>	<del>7322A31</del>	<del>Flexible Sealant, for Plastics, 10.1-Ounce Size</del>
Sika221	6937T2	Sika Flexible Sealant, Number 221, 10.1 Ounce Cartridge, Aluminum
<del>Cord</del>	<del>9408T17</del>	<del>Sealing Cord, 45 ft Long</del>
LOC409	7608A56	Loctite Instant-Bonding Adhesive, #409, 0.1 oz Tube
3MCA4	75445A71	3M Instant-Bonding Adhesive, #CA4, 0.07 oz Tube
Pliobond	7468A61	Pliobond Contact Adhesive, #25, 3 oz Brush-Top Bottle
Epoxy 1	—	Loctite 1363118 (From Amazon). Epoxy.
G1	7628A52	VHB Glue-on-a-Roll
G2	7628A68	Glue-on-a-Roll for Slippery Plastics

**Table 2: Glues/Sealants used for study.**

For all tests, a standard cuff was manufactured following the procedure outlined below:

1. If required, material was washed with running water and detergent.

2. The selected material was cut into a 20cm by 10cm rectangle.
3. Center of each of the 10cm edges were marked for appropriate localization of the tube.
4. Glue was applied with the following procedure: (Figure 1 shows example of glue pattern)
  - 4.1. Starting 1 cm below the half length of the 20cm edge, glue was applied towards the furthest 10cm edge. Notice that attempt was made to keep glue 5mm away from any edge.
  - 4.2. Continuing on previous movement glue was applied along the 10 cm edge and then down the opposing 20cm edge. Notice that, here also, glue was maintained 5mm away from edges.
  - 4.3. At the center of the 10cm edge where glue was now applied, a 1.5cm line was placed perpendicular to the edge.
  - 4.4. On the side where no glue was as of yet applied, a T was created keeping 5mm away from edge and with the crossing part being 2cm in length.
5. A 1/8 silicon tube was prepared as follows:
  - 5.1. Cut to 20cm length
  - 5.2. 3cm Axial cut created on one side
  - 5.3. 5cm marked with marker
6. Tube was placed on with 5cm mark on edge of material on the side with continuous glue application.
7. After tube appeared to have gained adherence to material, the opposite edge was brought over the tube. Figure 2 shows picture of construction up to this point.
8. Material on sides of tube were pinched as to force a tight seal with the tube.
9. After material at pinching site gained adherence to the tube, sides were pressured together and force was applied until formation of seal was confirmed.

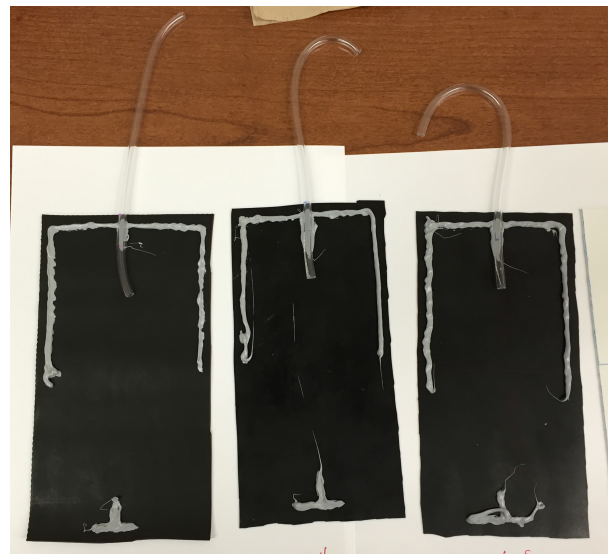
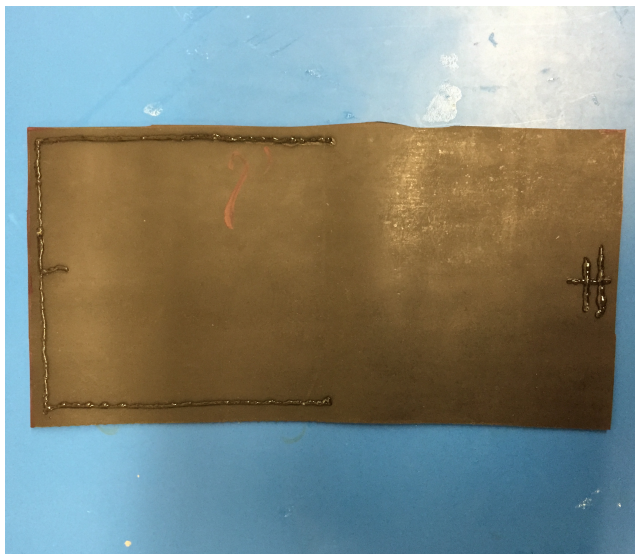


**Figure 1 (Left) shows glue applied on material. Figure 2 (Right) shows the tube placed on the material.**

Cuffs were inspected and the ones in which prohibiting conditions (see results) were not noticed were tested following the procedure below:

1. A pressure system was assembled to contain the following:
  - 1.1. Pump E129-13-120 was connected to a 8-way valve splitter with a 1/8” silicon tube.
  - 1.2. The main output of the splitter a 1/4” tube was connected to a Winters pressure gauge (part number PEM136) and a pressure relief valve.
2. Cuff were independently tested by attaching their tube to one of the valves in the 1/8 inch splitter.
3. The pump was then powered on and the inflation of the cuff as well as the pressure on the gauge were monitored and filmed.

## Results and Discussion

Table 3 matches each combination of material and glue to an identifier. The table also notes if the cuff was eliminated by inspection or if it proceeded to full testing.

Identifier	Material	Glue	Inspection Result
1	Cotton Fabric	LOC409	Fail: Adherence = 3. Material leaks.
2	Cotton Fabric	3MCA4	Fail: Adherence = 3. Material leaks.
3	FDA Rubber 1	LOC409	Passed: Adherence = 3
4	FDA Rubber 1	3MCA4	Passed: Adherence = 3
5		LOC409	Fail: Adherence = 0
6		3MCA4	Fail: Adherence = 0
7	Silicon Coated Fiberglass	LOC409	Fail: Adherence = 0
8	Silicon Coated Fiberglass	3MCA4	Fail: Adherence = 0
9	Tyvek	3MCA4	Fail: Adherence = 0
10	Tyvek	LOC409	Fail: Adherence = 0
11	Rubber 2	3MCA4	Passed: Adherence = 1. Manufacture defects.
12	Rubber 2	LOC409	Passed: Adherence = 2
13	Rubber 4	3MCA4	Passed: Adherence = 3

Identifier	Material	Glue	Inspection Result
14	Rubber 4	LOC409	Passed: Adherence = 2
15	Rubber 5	3MCA4	Passed: Adherence = 2. Manufacture defects near tube.
16	Rubber 5	LOC409	Passed: Adherence = 2
17	Rubber 2	SIKA221	Failed: Adherence = 1. Good seal.
18	Rubber 4	SIKA221	Failed: Adherence = 1. Good seal.
19	Rubber 5	SIKA221	Failed: Adherence = 1. Good seal.
20	FDA Rubber 1	SIKA221	Passed: Adherence = 1. Good seal.
21	Silicon Coated Fiberglass	SIKA221	Failed: Adherence = 0. Good seal.
22		SIKA221	Failed: Adherence = 0. Good seal.
23	Cotton Fabric	SIKA221	Failed: Adherence = 3. Good seal. Material leaks.
24	Rubber 5	Silicon1	Failed: Adherence = 1. Good seal.
25	Rubber 2	Silicon1	Failed: Adherence = 1. Good seal.
26	Rubber 4	Silicon1	Passed: Adherence = 1/2 Good seal.
27	FDA Rubber 1	Silicon1	Passed: Adherence = 2. Good seal. Manufacture defect on corner.
28	Silicon Coated Fiberglass	Silicon1	Passed: Adherence = 3. Good seal. Manufacture defect on corner.
29			Fail: Adherence = 0
30	Rubber 6	3MCA4	Failed: Adherence = 1. Manufacture defects.
31	FDA Rubber 2	3MCA4	Failed: Adherence = 1.
32	Rubber 4	Pliobond	Failed: Adherence = 1. Manufacture defects. (Should be tested for completeness)
33	Rubber 2	Pliobond	Failed: Adherence = 1. Manufacture defects.
34	Rubber 5	Pliobond	Failed: Adherence = 1. Manufacture defects.
35	FDA Rubber 2	Pliobond	Failed: Adherence = 1. Manufacture defects.
36	Silicon Coated Fiberglass	Pliobond	Failed: Adherence = 1. Manufacture defects.
37	Rubber 6	Pliobond	Failed: Adherence = 0/1. Manufacture defects.
38	Rubber 6	Silicon1	Passed. Adherence = 1. Good seal.
39	FDA Rubber 2	Silicon1	Passed. Adherence = 1. Good seal. ERRATA: Adherence increased to 3 after sealant was allowed to dry for 4 weeks.

Identifier	Material	Glue	Inspection Result
40	Rubber 4	Epoxy 1	Passed. Adherence = 2.
50	Rubber 2	G1	Fails. Adherence = 1.
51	Rubber 5	G2	Passed. Adherence = 2.
52	FDA Rubber 2	G2	Fails. Adherence = 1.

**Table 3: Manufactured cuffs and results from their inspection.**

The adherence Scale used in table 3 corresponds to the following levels of adherence: 0 - no adherence; 1 - Poor adherence, can be easily peeled. 2 - acceptable adherence, can be peeled with difficulty; 3 - good adherence, very hard to peel.

Table 4 summarizes the results from the second phase of the study. Notice that only the materials that passed inspection were analyzed in this phase. Cuffs with identifiers 4, 13, 14, 15, 27, 28, passed the phase two of testing.

Although cuffs with identifiers 4 and 27 passed both phases of testing they will not be used in further cuff manufacturing. The reason being that they do not expand upon inflation and due to space constraints a material that expands when inflated is required. For the same reason the material composing cuff 28 will also be eliminated.

ERRATA: Cuff of identifier 29 passed both phases of testing.

Identifier	Max Pressure (PSI)	Result and Notes
3	0	Undetermined. Several manufacturing related leakages impeded testing.
4	7	Passed. Does not grow significantly from original size. Did not leak even at highest recorded pressure. Maintains pressure at 3.5 (max pump pressure)
11	0	Failed. Had a manufacture defect that when sealed caused cuff seal to break at another place.
12	3.5	Failed. Inflated to a few time its original size. Deflated to original size when pressure was removed. Seal failed at max recorded pressure wit addition of significant force.
13	5	Passed. Inflated to many times its original size. When untouched pressure remained at about 1 PSI; probably due to a manufacture related leak. Did not show major leaks even at maximum recorded pressure.
14	3	Passed. Inflated to a few times its original size. Did not have additional leaks even at the maximum recorded pressure.
15	0	Passed. Undetermined. Material had a hole.
16	1.5	Undetermined/Failed. Increases in size at 0 recorded pressure. Upon sealing leakage by applying pressure achieved maximum recorded pressure without new leakages.
20	1.5	Failed. Ruptures at MRP.
26	0	Failed. Seal ruptures without recording pressure.
27	6	Passed. Upon applying pressure to manufacture defects, cuff inflates to a stable 3.5 PSI. No ruptures noticed even when compressing cuff causing pressure to increase to maximum recorded pressure.
28	6	Passed. Manufacture defect was sealed by applying pressure. No additional leaks even at maximum recorded pressure. Material did not show expansion.
32	0	Failed. Manufacturing defects were sealed by applying pressure on the leakages without success.
38	0	Failed. Increased significantly in size without registering pressure until failure of seal. Pressure was applied on ruptured area and a second failure occurred.
39	0	Failed/ERRATA:Passed (After 4 weeks of drying). Seal was broken even without pressure being registered on the gauge.
40	1	Failed. Acquired significant size follows by failure of seal at maximum recorded pressure. Pressure was applied on ruptured area and a second failure occurred.
51	0	Failed. Seal ruptured without recording pressure.

Table 4: Result from phase 2 of the study.

## Conclusion

The two phase study concludes that rubber 4 (9455K52 30A) when paired with either LOC409 of 3MCA4 as well as rubber 5 (9455K52 40A) when paired with 3MCA4 yield the best candidates for manufacturing of the cuff. In determining this conclusion, the results from the study were taken into account as well as the requirements of expansion, flexibility and comfort.

ERRATA: Cuff of identifier 29 (86915K12) passed both phases of testing.



# Appendix B

## Financial Summary

Intended For	Description	Store	Date	Total Price	Ordered By	Payed By
Imaging	JPEG + Raspberry Pi cameras	Sparkfun	3/17/2014	79.9	Paulo	Paulo
Mechanical Prototype (PC Trial 1)	6mmx300mm Cylinder Shaft	Ebay	4/12/2014	6.68	Paulo	Paulo
Mechanical Prototype (PC Trial 1)	8mmx100mm Cylinder Shaft	Ebay	4/12/2014	7	Paulo	Paulo
Mechanical Prototype (PC Trial 1)	8mm Linear Bearing with Case	Ebay	4/12/2014	8.54	Paulo	Paulo
Mechanical Prototype (PC Trial 1)	6mm Linear Bearings	Ebay	4/12/2014	7.3	Paulo	Paulo
Mechanical Prototype (PC Trial 1)	6mm Linear Bearings With Case	Ebay	4/12/2014	12.76	Paulo	Paulo
Mechanical Prototype (PC Trial 1)	6mm Shaft Support	Ebay	4/12/2014	13.78	Paulo	Paulo
Mechanical Prototype (PC Trial 1)	Hitec Low Profile Servo	Amazon	4/12/2014	24.49	Paulo	Paulo
Mechanical Prototype (PC Trial 1)	Slide Rail Linear 6.5 inches long	Amazon	4/12/2014	13.01	Paulo	Paulo
Mechanical Prototype (PC Trial 1)	Flange Ball Bearings F608ZZ	Ebay	4/12/2014	9.67	Paulo	Paulo
Mechanical Prototype (PC Trial 1)	Ball Bearing 608ZZ	Ebay	4/12/2014	7.77	Paulo	Paulo
Mechanical Prototype (PC Trial 1)	GT2 Timing Belt 2m + 2 Pulleys	Ebay	4/12/2014	13.49	Paulo	Paulo
Imaging	Raspberry Pi NoIR	Amazon	4/14/2014	38.75	Anurag	Anurag
Electronics	Raspberry Pi Model B SBC	Amazon	2/5/2014	40	Anurag	Anurag
Imaging	850nm IR filter	Amazon	2/5/2014	13.95	Anurag	Anurag
Electronics	SD card for Raspberry Pi	Amazon	2/5/2014	6.95	Anurag	Anurag
Mechanical Prototype (AK Trial 1)	Motorized Linear Slides x 2	Vetco	4/12/2014	35.75	Anurag	Anurag
Mechanical Prototyping Raw Material	Acrylic - 5 sheets	ebay	4/1/2014	64.73	Anurag	Anurag
Sensor	Load Cell	Robotshop	4/15/2014	7	Anurag	Anurag
Imaging	IR LEDs - assorted wavelengths	Digikey	4/6/2014	43.17	Anurag	Anurag
Electronics	12VDC power supply	Amazon	4/23/2014	5	Anurag	Anurag
Mechanics	Raspi case	Amazon	4/21/2014	7.79	Anurag	Anurag
Electronics	7" TFT Display for Raspi	Amazon	4/21/2014	31.48	Anurag	Anurag
Actuators	Assorted Servos	HobbyKing	4/16/2014	39.96	Anurag	Anurag
Mechanical Prototype (PC Trial 1)	25 Yards Webbing	Amazon	4/24/2014	15.95	Paulo	Paulo
Mechanical Prototype (PC Trial 1)	Velcro	Amazon	4/24/2014	8.98	Paulo	Paulo
Mechanical Prototype (PC Trial 1)	10x 6mm Shaft (10cm)	Amazon	4/26/2014	9.43	Paulo	Paulo
Mechanical Prototype (PC Trial 1)	2x Adicore Mini Servo	Amazon	4/26/2014	7.48	Paulo	Paulo
All Mechanical Prototypes	Screws, Nuts, Washers, Organizer	Amazon	4/27/2014	47.07	Paulo	Paulo
All Mechanical Prototypes	8mm by 200mm Rod	Ebay	4/23/2014	6	Paulo	Paulo
All Mechanical Prototypes	2x XL Timing Pulley	Ebay	4/23/2014	13.99	Paulo	Paulo
All Mechanical Prototypes	8mm x 500mm Rod	Ebay	4/23/2014	9.92	Paulo	Paulo
All Mechanical Prototypes	10x Brass Standoff M3x20mm	Ebay	5/1/2014	5.5	Paulo	Paulo
All Mechanical Prototypes	6in 1/2-10 Lead Screw	Ebay	5/1/2014	10	Paulo	Paulo
All Mechanical Prototypes	5V Stepper with Driver	Ebay	5/1/2014	3.83	Paulo	Paulo
All Mechanical Prototypes	Bipolar Stepper with Slider	Ebay	5/1/2014	3.92	Paulo	Paulo
All Mechanical Prototypes	Maxon DC 22mm + Encoder	Ebay	5/1/2014	49	Paulo	Paulo
All Mechanical Prototypes	Coupler 5mm to 8mm	Ebay	5/1/2014	4.49	Paulo	Paulo
All Mechanical Prototypes	Linear Bearing Assortment	Ebay	5/1/2014	24.58	Paulo	Paulo
All Mechanical Prototypes	Coupler 4/4mm and 3/3mm	Ebay	5/1/2014	9	Paulo	Paulo
All Mechanical Prototypes	Bearing Assortment	Ebay	5/1/2014	29.91	Paulo	Paulo
All Mechanical Prototypes	Gear 11184 and 111119	Ebay	5/11/2014	8.49	Paulo	Paulo
All Mechanical Prototypes	1x Titanium 3mmX10mm Rod	Ebay	5/23/2014	6.99	Paulo	Paulo
All Mechanical Prototypes	5x 4mmX300mm Brass Rod	Ebay	5/23/2014	17.98	Paulo	Paulo
All Mechanical Prototypes	10x 3mmX300mm Steel Rod	Ebay	5/23/2014	14.81	Paulo	Paulo
All Mechanical Prototypes	2M542 Stepper Driver	Ebay	5/23/2014	36.99	Paulo	Paulo
All Mechanical Prototypes	NEMA23 270oz Stepper	Ebay	5/23/2014	45	Paulo	Paulo
All Mechanical Prototypes	Assortment of Mini Coupler	Ebay	5/23/2014	17.88	Paulo	Paulo
All Mechanical Prototypes	8x A2 Steel M4x100mm	Ebay	5/26/2014	14.98	Paulo	Paulo
All Mechanical Prototypes	8x LM3UU	Ebay	5/26/2014	17.19	Paulo	Paulo
All Mechanical Prototypes	3x Timing Belt	Ebay	5/26/2014	24.9	Paulo	Paulo
All Mechanical Prototypes	2x M3x1m Threaded Rod	Ebay	5/26/2014	15.86	Paulo	Paulo
All Mechanical Prototypes	10x 4x10x4 Flanged Bearing	Ebay	5/26/2014	7.85	Paulo	Paulo
All Mechanical Prototypes	3/4mm coupler	Ebay	5/26/2014	4.96	Paulo	Paulo
All Mechanical Prototypes	8x LM3UU	Ebay	5/26/2014	17.19	Paulo	Paulo
All Mechanical Prototypes	M4 Threaded Rod (100mm)	Ebay	6/11/2014	14.2	Paulo	Paulo
All Mechanical Prototypes	0.236inx12inx12in (8 pack)	Amazon	6/6/2014	48	Paulo	Anurag
All Mechanical Prototypes	5x 6mmx100mm Threaded Rod	Amazon	5/26/2014	7.86	Paulo	Paulo
All Mechanical Prototypes	0.118inx12inx12in (8 pack)	Amazon	5/26/2014	29	Paulo	Paulo
All Mechanical Prototypes	Screws Assortming M1-M1.6	Amazon	5/23/2014	10.94	Paulo	Paulo
All Mechanical Prototypes	Acrylic 1mm, 2mm	Ebay	6/24/2014	42.59	Paulo	Paulo
Software Development Platform	2 x Raspberry Pi	Amazon	5/20/2014	73.8	Anurag	Anurag
Software Development Platform	2 x RasPi cases	Amazon	5/20/2014	13	Anurag	Anurag

Software Development Platform	2 x Micro USB for Pi	Amazon	5/20/2014	7.46	Anurag	Anurag
Imaging	Raspberry Pi NoIR	Amazon	6/18/2014	26.89	Anurag	Anurag
All Mechanical Prototypes	Assortment of Linear Stepper	Ebay	6/20/2014	48.57	Paulo	Paulo
All Mechanical Prototypes	2 x bad steppers	Ebay	6/5/2014	5.48	Anurag	Anurag
Imaging	Lens	Edmund Optics	6/25/2014	59.5	Sean	Sean
Imaging	2 x Filter	Edmund Optics	6/25/2014	100	Sean	Sean
Medical Supplies	Assorted Needles	Allegro Medical	6/15/2014	62.31	Sean	Sean
Imaging	RasPi Accessories	Adafruit	6/19/2014	21.15	Sean	Sean
Software Development Platform	RasPi Compute DevKit	Newark	6/26/2014	215	Sean	Sean
Tester Dev	RasPi Kit + Noir Camera	Amazon	6/26/2014	85	Sean	Sean
IRRIgV2	3 PCBs	4PCB	6/28/2014	118.91	Paulo	Paulo
All Mechanical Prototypes	Assorted Steppers	Ebay	7/1/2014	30.95	Paulo	Paulo
Imaging	Diffusers	Edmund Optics	7/6/2014	70	Sean	Sean
Imaging	2 x Lenses	Edmund Optics	7/6/2014	190	Sean	Sean
Electronics	IRRIgV2	Digikey	7/6/2014	157.06	Anurag	Anurag
Electronics	STK500 Programmer	Amazon	7/2/2014	50	Anurag	Anurag
Software Development Platform	SD Card 16GB	Amazon	7/1/2014	9.2	Anurag	Anurag
Electronics	9V batteries	Amazon	7/1/2014	7.45	Anurag	Anurag
Software Development Platform	Display for Pi	Amazon	6/20/2014	79.8	Anurag	Anurag
Electronics	Power Regulators	Newark	7/12/2014	74.2	Sean	Sean
Electronics	Missing Components 1 IRRIgV2	Digikey	7/14/2014	44.85	Paulo	Paulo
All Mechanical Prototypes	M1.6 Screws, washers, and nuts	McMaster	7/18/2014	20	Sean	Sean
All Mechanical Prototypes	Acrylic	Amazon	7/17/2014	34.4	Anurag	Anurag
All Mechanical Prototypes	Flanged bearings	Ebay	7/20/2014	7.79	Anurag	Anurag
Electronics	Electronics V1	Digikey	7/17/2014	267.74	Anurag	Anurag
All Mechanical Prototypes	Stepper screw with nut slider	Ebay	7/15/2014	21.48	Anurag	Anurag
All Mechanical Prototypes	Stepper screw with nut slider	Ebay	7/15/2014	9.78	Anurag	Anurag
Needle Insertion Mechanism	Force Sensor	Mouser	7/19/2014	207	Sean	Sean
Electronics	USB hub for Pi	Amazon	7/15/2014	6.99	Anurag	Anurag
Electronics	SD card	Amazon	7/15/2014	17.49	Anurag	Anurag
All Mechanical Prototypes	Firgelli micro linear actuator	Firgelli	7/24/2014	100.43	Anurag	Anurag
All Mechanical Prototypes	3x8x3mm flanged bearings	Ebay	7/19/2014	7.79	Anurag	Anurag
Electronics	Main Board V1 Missing Components	Digikey	7/24/2014	40.99	Paulo	Paulo
All Mechanical Prototypes	NEMA 11 Stepper (2 Units)	Ebay	7/24/2014	45.48	Paulo	Paulo
Mechanics V4 and NIM V4?	Carriages and rails, etc	McMaster	9/9/2014	348.33	Paulo	Paulo
Mechanics V4	Threaded Rod M4	McMaster	9/14/2014	9.05	Paulo	Paulo
Tester Dev	Materials for Building Tester	McMaster	8/25/2014	601.46	Sean	Sean
Imaging	Filters for Tester	Edmund Optics	10/5/2014	60	Sean	Sean
Mechanics V5	Motors and Coupler	Ebay	10/13/2014	45.48	Paulo	Paulo
Electronics V2	Know, Buttons	Sparkfun	10/18/2014	47.17	Paulo	Paulo
Cuff Study Part 1	Materials + Glue	McMaster	12/10/2014	90.66	Paulo	Paulo
Cuff Study Part 1	Materials + Glue	McMaster	12/6/2014	201.28	Paulo	Paulo
IRRIgV3	Medical Imaging LEDs	Digikey	2/9/2015	136.64	Paulo	Paulo
MainBoardV3	MainBoardV3	4PCB	3/23/2015	86.39	Paulo	Paulo
<b>Total By Person</b>						
Anurag	1286.56					
Paulo	2113.85					
Sean	1765.62					
<b>Overall</b>	<b>5166.03</b>					



# Appendix C

## Interface Document: IRRigV2



# INTERFACE DOCUMENT

IRRIg V2

## Abstract

This document contains all necessary information for assembly and operation of the IRRIg V2 for the Phlebot MQP.

Phlebot MQP  
phlebot@wpi.edu

## Contents

Table of Figures.....	2
Board Description .....	3
Pin Mapping .....	4
FPC Connector.....	4
Schematic.....	5
PCB Art .....	6
Top Layer.....	6
Bottom Layer.....	7
Mechanical Drawing .....	8
Component List.....	9
Errata.....	10

## Table of Figures

Table 1: Pin mapping for FPC Connector. ....	4
Figure 1:Schematic For IR Rig V2 .....	5
Figure 2: Top PCB Art. ....	6
Figure 3: Bottom PCB Art. ....	7
Figure 4: Mechanical drawing for the IRRig V2.....	8
Table 2: List of Components for IRRig V2.....	9



## Board Description

The IRRig V2 is a five IR wavelength + RGB illuminator mechanically compatible with the raspberry pi No-IR camera for use in the small and large scale study of the Phlebot MQP. The board is also compatible with the Velcro based Cartesian stage V2 and an attempt will be made to use it in further versions of the prototypes.

The board contains no on board “intelligence” and is instead controlled completely by 8 GPIO broken out by a 15 pin FPC cable. See further sections for details.

## Pin Mapping

### FPC Connector

The 15 pin 1-84953-5 FPC connector interfaces the board with the controller. Breaks out all IR MOSFET gates after appropriate supporting circuitry.

*Table 1: Pin mapping for FPC Connector.*

Pin #	Pin Name	Connected To	Description
1	LED740	MOSFET Gate Through R12	Active HIGH IR Control Line
2	LED770	MOSFET Gate Through R11	Active HIGH IR Control Line
3	LED830	MOSFET Gate Through R14	Active HIGH IR Control Line
4	LED850	MOSFET Gate Through R13	Active HIGH IR Control Line
5	LED860	MOSFET Gate Through R15	Active HIGH IR Control Line
6	RGBB	MOSFET Gate Through R27	Active HIGH IR Control Line
7	RGBG	MOSFET Gate Through R25	Active HIGH IR Control Line
8	RGBR	MOSFET Gate Through R23	Active HIGH IR Control Line
9	--	--	--
10	GND	GND	Ground Feed
11	GND	GND	Ground Feed
12	GND	GND	Ground Feed
13	VCC	VCC	Power Feed
14	VCC	VCC	Power Feed
15	VCC	VCC	Power Feed

# Schematic

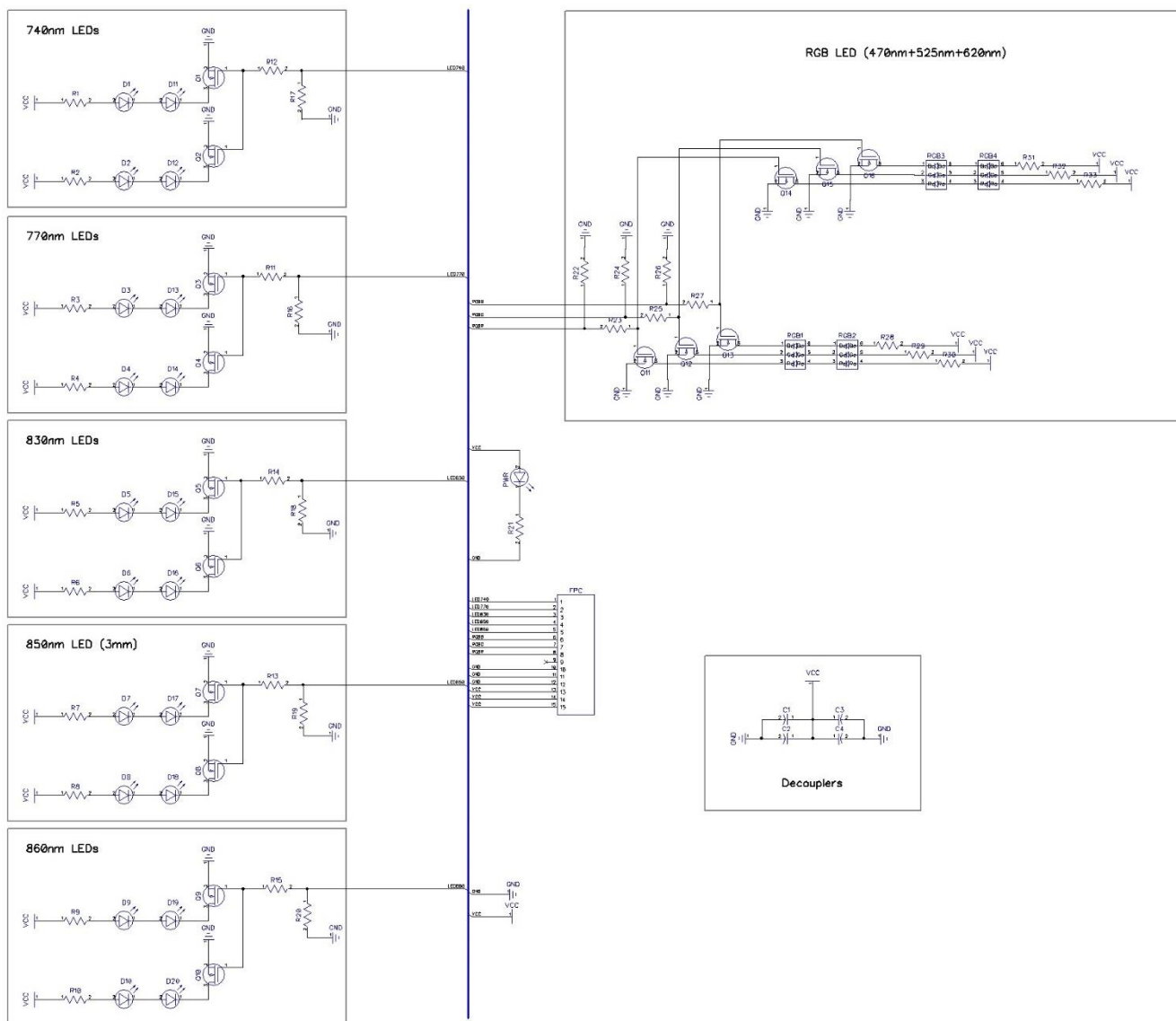


Figure 1: Schematic For IR Rig V2

PCB Art  
Top Layer

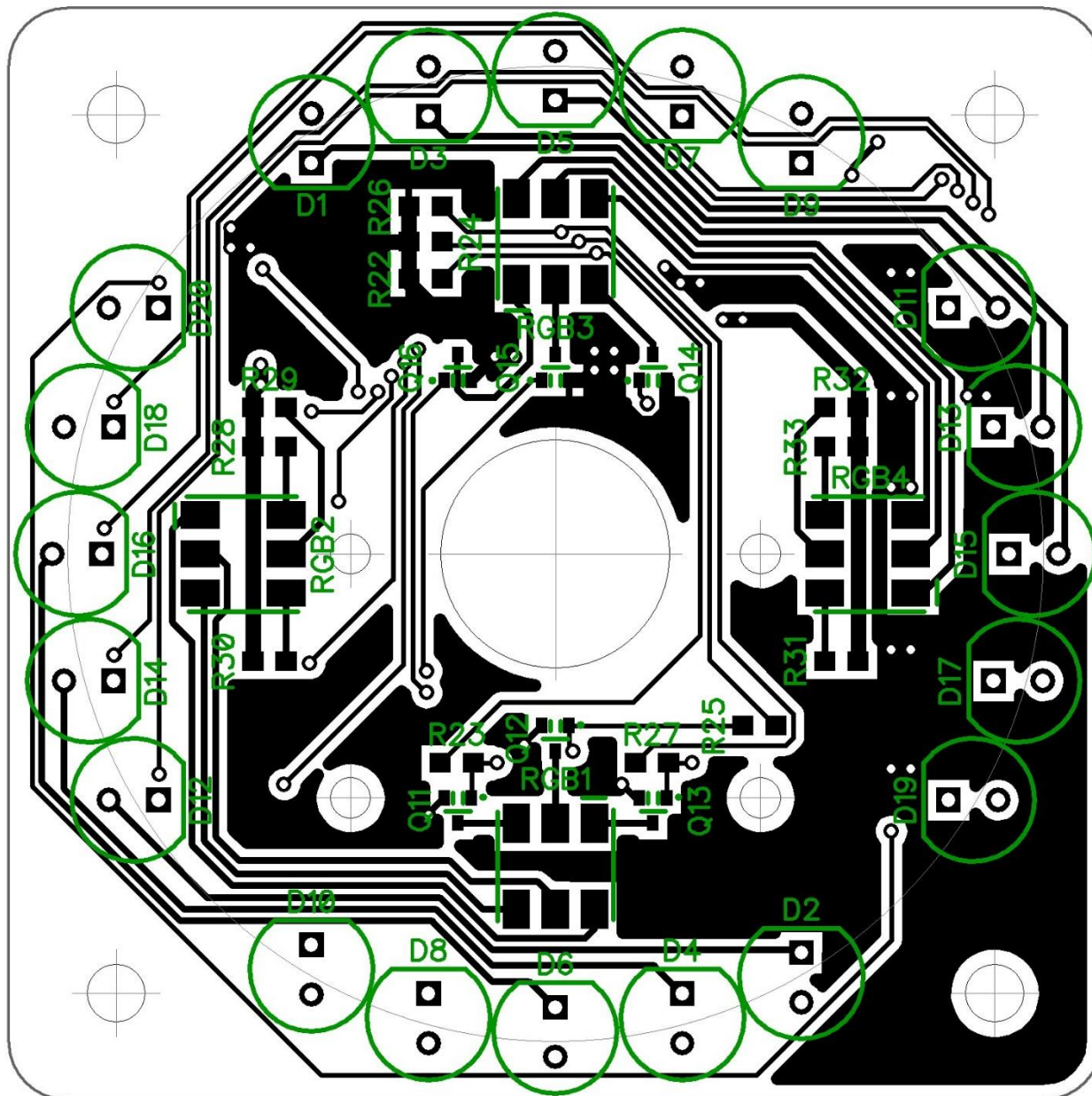


Figure 2: Top PCB Art.

## Bottom Layer

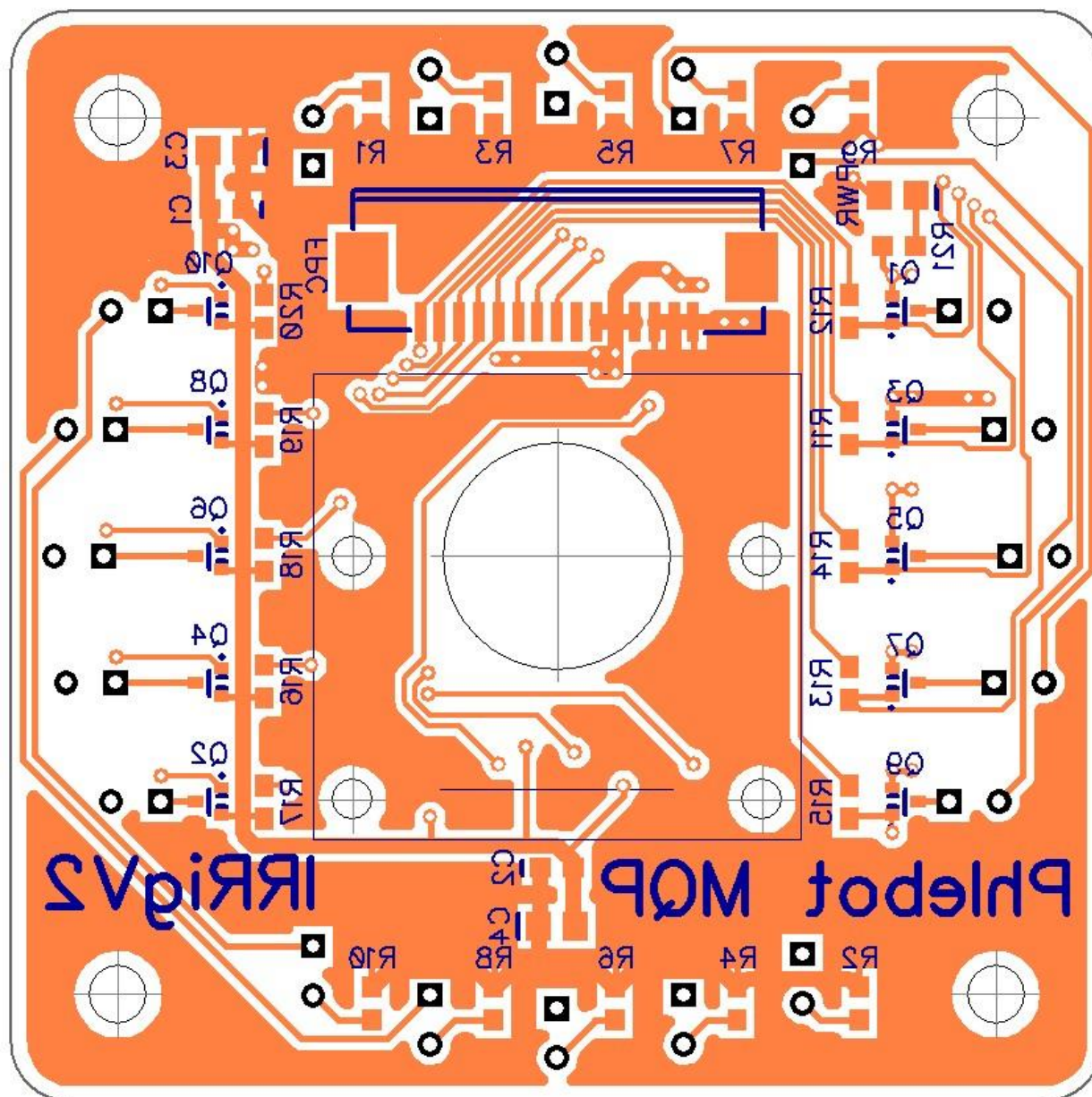


Figure 3: Bottom PCB Art.

## Mechanical Drawing

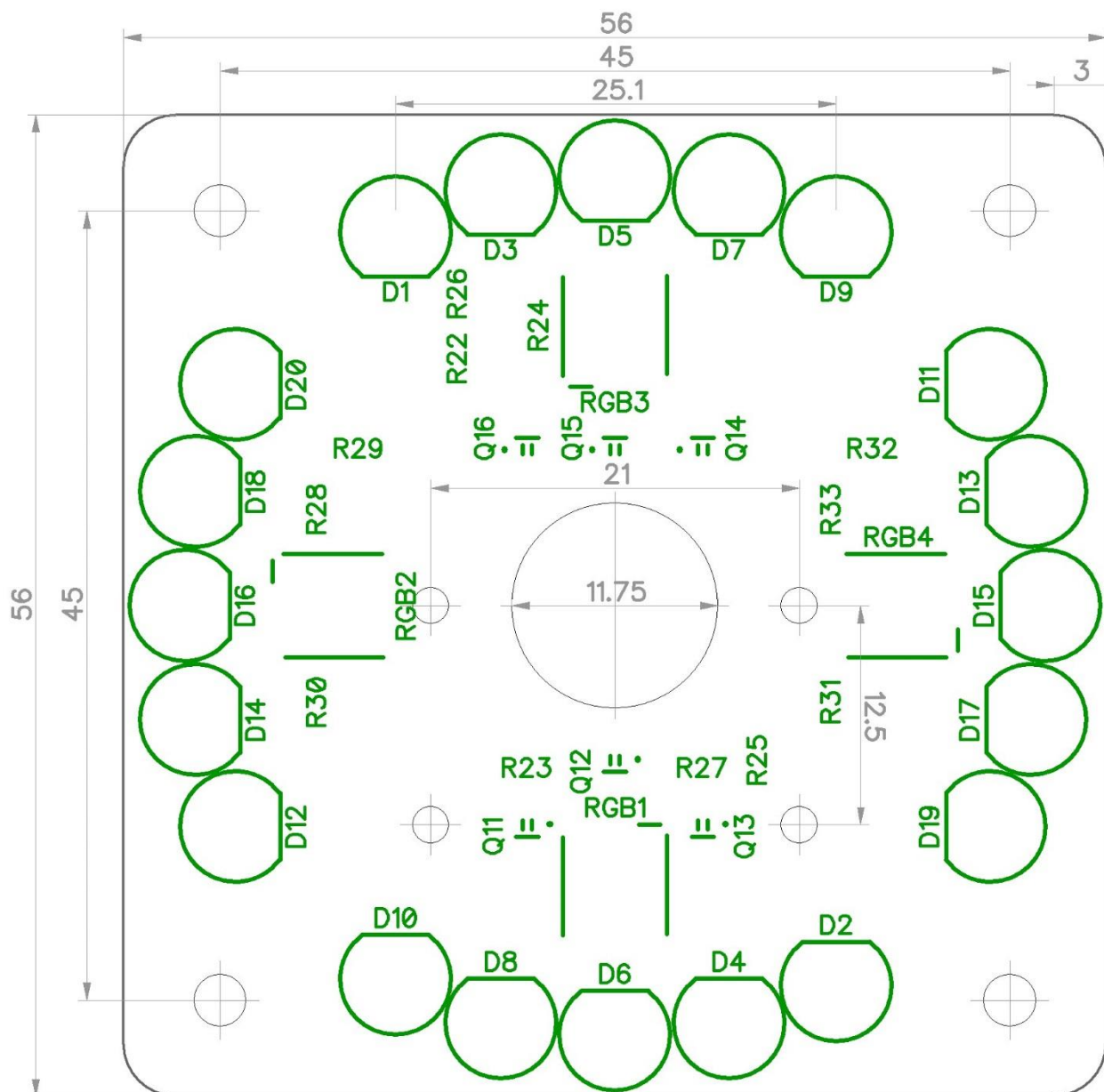


Figure 4: Mechanical drawing for the IRRig V2.

## Component List

Lists all components for assembly of the IRRig V2. Notice that the values are based on the chosen LEDs as of 6/30/2014. Adapt resistors as necessary if different IR LEDs are used. All resistor values are given for operation of board at 5V DC.

Table 2: List of Components for IRRig V2.

Reference	Type	Value	Description
C1-C2	CAP C 0603	100 nF	Decoupling Capacitor
C3-C4	CAP C 0805	47 uF	Decoupling Capacitor
D1,D2,D11,D12	740nm IR	MTE1074N1-R	IR LED
D3,D4,D13,D14	770nm IR	MTE1077N1-R	IR LED
D5,D6,D15,D16	830nm IR	TSHG8400	IR LED
D7,D8,D17,D18	850nm IR	HIR204/H0	IR LED
D9,D10,D19,D20	860nm IR	SFH 4557	IR LED
RGB1,RGB3	PLCC-6 LED	QBLP679E-RGB	RGB LED
RGB2,RGB4	Jumper	--	Bypass with wire jumper*
Q1-Q16	N MOSFET	DMN26D0UT	LED Driving MOSFET
PWR	0805 LED	SMD LED	Indicator LED for Board Power On
R1,R2	0603 RES	24 OHMS	Current Limitng Resistor for IR LED
R3,R4	0603 RES	24 OHMS	Current Limitng Resistor for IR LED
R5,R6	0603 RES	24 OHMS	Current Limitng Resistor for IR LED
R7,R8	0603 RES	150 OHMS	Current Limitng Resistor for IR LED
R9,R10	0603 RES	40 OHMS	Current Limitng Resistor for IR LED
R28,R31	0603 RES	100 OHMS	Current Limitng Resistor for IR LED
R29,R32	0603 RES	100 OHMS	Current Limitng Resistor for IR LED
R30,R33	0603 RES	150 OHMS	Current Limitng Resistor for IR LED
R16- R20,R22,R24,R26	0603 RES	100K OHM	Pull Down for MOSFET Gates. Keeps IR LEDs OFF
R11- R15,R23,R25,R27	0603 RES	100 OHM	Current Limiter for MOSFET Gates
R21	0603 RES	See Table 3	Current Limiting Resistor for Power LED
FPC	Connector	1-84953-5	15 Pin FPC Connector for Board Interface

\*Due to error in design selected RGB LEDs cannot be used in series due to high Vdrop. See errata.

## Errata

<b>Error</b>	<b>Description</b>	<b>Date</b>
RGB LED high V drop	QBLP679E-RGB has 3V3 voltage drop on B and G channel. Cannot be used in series. Either replace for different component with lower V drop or short one LED per channel.	Jul 1, 2014



# Appendix D

## Interface Document: Main Board V1



# INTERFACE DOCUMENT

## Main Board V1

### [Abstract](#)

Contains all information necessary for assembly and operation of the main board V1 for the Phlebot MQP.

Phlebot MQP  
phlebot@wpi.edu

## Contents

Table of Figures.....	2
Description.....	3
Pin Mapping.....	4
ATMEGA: ATMEGA2560.....	4
Pi1: Compute Module.....	6
Pi: Connector for External Raspberry Pi.....	6
Schematic Diagrams.....	8
Main Block.....	8
FTDI Schematic.....	9
Decoupler Schematic.....	10
IMU Schematic.....	11
Mechanical End Stop Schematic.....	12
Level Shifter Schematic.....	13
Power Regulation.....	14
Force Sensor.....	15
Motor Driver Schematic.....	16
LAN and USB Schematic.....	17
PCB Art.....	18
Top Layer.....	18
Inner Layer 1.....	19
Inner Layer 2.....	20
Bottom Layer.....	21
Mechanical Drawing.....	22
Table of Components.....	23
Stepping Size Selector Resistors.....	25
Errata.....	26

## Table of Figures

Figure 1: Main schematic block .....	8
Figure 2: FTDI schematic .....	9
Figure 3: Decoupler schematic.....	10
Figure 4: IMU Schematic.....	11
Figure 5: Mechanical end stop schematic.....	12
Figure 6: Level shifter schematic .....	13
Figure 7: Power regulation schematic .....	14
Figure 8: Force sensor schematic.....	15
Figure 9: Motor driver schematic .....	16
Figure 10: LAN and USB schematic .....	17
Figure 11: Top layer PCB art.....	18
Figure 12: Inner layer 1 PCB art containing ground plane.....	19
Figure 13: Inner layer 2 PCB art containing 3V3 and 5V planes.....	20
Figure 14: Bottom layer of PCB.....	21
Figure 15: Mechanical drawing for phlebot main board V1.....	22

DRAFT

## Description

The Phlebot Main Board V1 is the main control board for the first iteration of the phlebotomist robot. The board will contain all processing, power regulation and management for the first prototype series.

All onboard processing is separated into two entities: The Raspberry Pi Compute Module and an ATMEGA2560. The compute module connects to the board through an SODIMM connector and directly attaches to the camera. A LAN9512 serves as interface between the module and the world providing two USB host ports as well as an Ethernet connector. The compute module interfaces with the ATMEGA2560 through a UART link. The ATMEGA provides all low level control over the prototype including providing signals for the 6 onboard DRV8834 stepper motor drivers.

In case some mistake with the board causes the compute module to be unusable, the board can also be controlled using a model B or B+ raspberry pi connected through an IDC connector at the top left corner. In this case onboard ethernet, USB and camera connector would all be rendered unused as the standard raspberry pi contains all of the above.

For easier debugging, the board is equipped with 7 probing point, an extra connector for each motor driver as well as an LED attached to the ATMEGA. End stops and force sensor attach to the board using JST connectors.

## Pin Mapping

### ATMEGA: ATMEGA2560

The table below reports all connections to the ATMEGA2560 microcontroller. For easier pin identification when programming in an Arduino compatible environment, Arduino specific nomenclature is provided on the third column.

Pin #	Pin Name	Arduino	Connected To	Description
1	PG5(OC0B)	DIO4	IRRig1	Connects to IRRig FPC Header
2	PE0(RXD0)	DIO0(RX0)	MCU_Din	Data out from FTDI into MCU
3	PE1(TXD0)	DIO1(TX0)	MCU_Dout	Data in to FTDI to MCU
4	PE2	--	--	--
5	PE3(OC3A)	DIO5	IRRig2	Connects to IRRig FPC Header
6	PE4(OC3B)	DIO2	IRRig3	Connects to IRRig FPC Header
7	PE4(OC3C)	DIO3	IRRig4	Connects to IRRig FPC Header
8	PE6	--	--	--
9	PE7	--	--	--
10	VCC	--	+5V	--
11	GND	--	GND	--
12	PH0(RXD2)	DIO17(RX2)	--	--
13	PH1(TXD2)	DIO16(TX2)	--	--
14	PH2	--	--	--
15	PH3(OC4A)	DIO6	IRRig5	Connects to IRRig FPC Header
16	PH4(OCAB)	DIO7	IRRig6	Connects to IRRig FPC Header
17	PH5(OC4C)	DIO8	IRRig7	Connects to IRRig FPC Header
18	PH6(OC2B)	DIO9	IRRig8	Connects to IRRig FPC Header
19	PB0	DIO53	GYR_INT	Triggers on gyro related interrupts
20	PB1(SCK)	DIO52(SCK)	ICSP_SCK	ICSP programming pin
21	PB2(MOSI)	DIO51(MOSI)	ICSP_MOSI	ICSP programming pin
22	PB3(MISO)	DIO50(MISO)	ICSP_MISO	ICSP programming pin
23	PB4	DIO10	GYRO_EN	
24	PB5	DIO11	EndStop6	Connects to an end stop sensor
25	PB6	DIO12	EndStop5	Connects to an end stop sensor
26	PB7	DIO13	EndStop4	Connects to an end stop sensor
27-29	--	--	--	--
30	RST	--	--	Active LOW reset
31	VCC	+5V	--	Power Supply
32	GND	GND	--	Power Supply
33	XTAL	--	--	16 MHz crystal
34	XTAL	--	--	16 MHz crystal
35	PL0	DIO49	EndStop3	Connects to an end stop sensor
36	PL1	DIO48	EndStop2	Connects to an end stop sensor
37	PL2	DIO47	EndStop1	Connects to an end stop sensor
38	PL3(OC5A)	DIO46	MOT_nSLEEP	Places all motor drivers in sleep. Active LOW
39	PL4(OC5B)	DIO45	MOT1_DIR	Sets stepper motor direction
40	PL5(OC5C)	DIO44	MOT1_nENBL1	Enables stepper motor. Active LOW

41	PL6	DIO43	MOT1_nFAULT	LOW if stepper motor driver is at fault
42	PL7	DIO42	MOT1_STEP	Edge triggered stepper motor step
43	PD0(SCL)	DIO21(SCL)	MCU_SCL	Interfaces IMU through a level shifter
44	PD1(SDA)	DIO20(SDA)	MCU_SDA	Interfaces IMU through a level shifter
45	PD2(RXD1)	DIO19(RX1)	Net 191	UART from MCU to Pi through level shifter
46	PD3(TXD1)	DIO18(TX1)	Net 192	UART from Pi to MCU through level shifter
47-49	--	--	--	--
50	PD7	DIO38	MOT2_DIR	Sets stepper motor direction
51	PG0	DIO41	MOT2_nENBL1	Enables stepper motor. Active LOW
52	PG1	DIO40	MOT2_nFAULT	LOW if stepper motor driver is at fault
53	PC0	DIO37	MOT2_STEP	Edge triggered stepper motor step
54	PC1	DIO36	MOT3_DIR	Sets stepper motor direction
55	PC2	DIO35	MOT3_nENBL1	Enables stepper motor. Active LOW
56	PC3	DIO34	MOT3_nFAULT	LOW if stepper motor driver is at fault
57	PC4	DIO33	MOT3_STEP	Edge triggered stepper motor step
58	PC5	DIO32	MOT4_DIR	Sets stepper motor direction
59	PC6	DIO31	MOT4_nENBL1	Enables stepper motor. Active LOW
60	PC7	DIO30	MOT2_nFAULT	LOW if stepper motor driver is at fault
61	VCC	--	+5V	Voltage supply
62	GND	--	GND	Voltage supply
63	PJ0(RXD3)	DIO15(RX3)	--	--
64	PJ1(TXD3)	DIO14(TX3)	LED1	Indicator LED
65-69	--	--	--	--
70	PG2	DIO39	MOT4_STEP	Edge triggered stepper motor step
71	--	--	MOT5_DIR	Sets stepper motor direction
72	PA6(AD6)	DIO28	MOT5_nENBL1	Enables stepper motor. Active LOW
73	PA5(AD5)	DIO27	MOT5_nFAULT	LOW if stepper motor driver is at fault
74	PA4(AD4)	DIO26	MOT5_STEP	Edge triggered stepper motor step
75	PA3(AD3)	DIO25	MOT6_DIR	Sets stepper motor direction
76	PA2(AD2)	DIO24	MOT6_nENBL1	Enables stepper motor. Active LOW
77	PA1(AD1)	DIO23	MOT6_nFAULT	LOW if stepper motor driver is at fault
78	PA0(AD0)	DIO22	MOT6_STEP	Edge triggered stepper motor step
79	PJ7	-	--	--
80	VCC	--	+5V	Voltage Supply
81	GND	--	GND	Voltage Supply
82	PK7(ADC15)	AI15	ForceSense	Analog input from force sensor differential amplifier.
83	PK6(ADC14)	AI14	1V8	Analog input from 1V8 for voltage measuring
84	--	--	3V3	Analog input from 3V3 for voltage measuring
85-97	--	--	--	--
98	AREF	--	+5V	Voltage reference for analog inputs
99	GND	--	GND	Voltage Supply
100	AVCC	--	+5V	Voltage Supply

## Pi1: Compute Module

Table below contains all the data pins connected to the compute module SODIMM connector. Note that power pins will be omitted there is a significant number of such pins. For power related information see the schematics in their appropriate sections.

Pin #	Pin Name	Connected To	Description
9	GPIO2	CAM_SDA1	Camera I2C Interface
11	GPIO3	CAM_SCL1	Camera I2C Interface
15	GPIO4	MOT1_ENBL2	Enables stepper motor. Active LOW
17	GPIO5	CAM_CLK	Camera clock line
21	GPIO6	LAN_RUN	Reset for LAN9512 ethernet controller
23	GPIO7	MOT2_ENBL2	Enables stepper motor. Active LOW
27	GPIO8	MOT3_ENBL2	Enables stepper motor. Active LOW
29	GPIO9	MOT4_ENBL2	Enables stepper motor. Active LOW
34	GPIO30	MOT6_ENBL2	Enables stepper motor. Active LOW
36	GPIO31	MOT5_ENBL2	Enables stepper motor. Active LOW
51	GPIO14	PI_DOUT	UART to ATMEGA2560
53	GPIO15	PI_DIN	UART to ATMEGA2560
89	GPIO27	CAM_GPIO	Camera related GPIO
147	CAM1_CP	CAM1_CP	Camera related data lin
149	CAM1_CN	CAM1_CN	Camera related data lin
153	CAM1_DP1	CAM1_DP1	Camera related data lin
155	CAM1_DN1	CAM1_DP1	Camera related data lin
159	CAM1_DP0	CAM1_DP0	Camera related data lin
161	CAM1_DN0	CAM1_DN0	Camera related data lin
165	USB_DP	PI_USBDP	USB to LAN9512 ethernet controller
167	USB_DN	PI_USBDM	USB to LAN9512 ethernet controller

## Pi: Connector for External Raspberry Pi

In case the onboard compute module is not operational or quicker debugging can be made on an off board Raspberry Pi, this connector allows its connection to the board. All necessary IO lines are made available, thus there is no loss of function due to its use.

Pin #	Pin Name on Pi Model B	Connected To	Description
1	3V3	3V3 Through R44	3V3 power supply to Rasp Pi. Can be disabled by not soldering R44.
2	5V	5V Through R43	5V power supply to Rasp Pi. Can be disabled by not soldering R43.
3	GPIO2	MOT1_nENBL2	Enables stepper motor. Active LOW
4	5V	5V Through R43	5V power supply to Rasp Pi. Can be disabled by not soldering R43.
5	GPIO3	MOT2_nENBL2	Enables stepper motor. Active LOW
6	GND	GND	GND connection
7	GPIO4	--	--
8	GPIO14	PI_DOUT	UART connection to MCU



9	GND	GND	GND Connection
10	GPIO15	PI_DIN	UART connection to MCU
11	GPIO17	MOT3_nENBL2	Enables stepper motor. Active LOW
12	GPIO18	--	--
13	GPIO27	MOT4_nENBL2	Enables stepper motor. Active LOW
14	GND	GND	GND Connection
15	GPIO22	MOT5_nENBL2	Enables stepper motor. Active LOW
16	GPIO23	MOT6_nENBL2	Enables stepper motor. Active LOW
17	3V3	3V3 Through R44	3V3 power supply to Rasp Pi. Can be disabled by not soldering R44.
18	GPIO24	--	--
19	GPIO10	--	--
20	GND	GND	GND Connection
21-24	--	--	--
25	GND	GND	GND Connection
26	GPIO7	--	--

DRAFT

# Schematic Diagrams

## Main Block

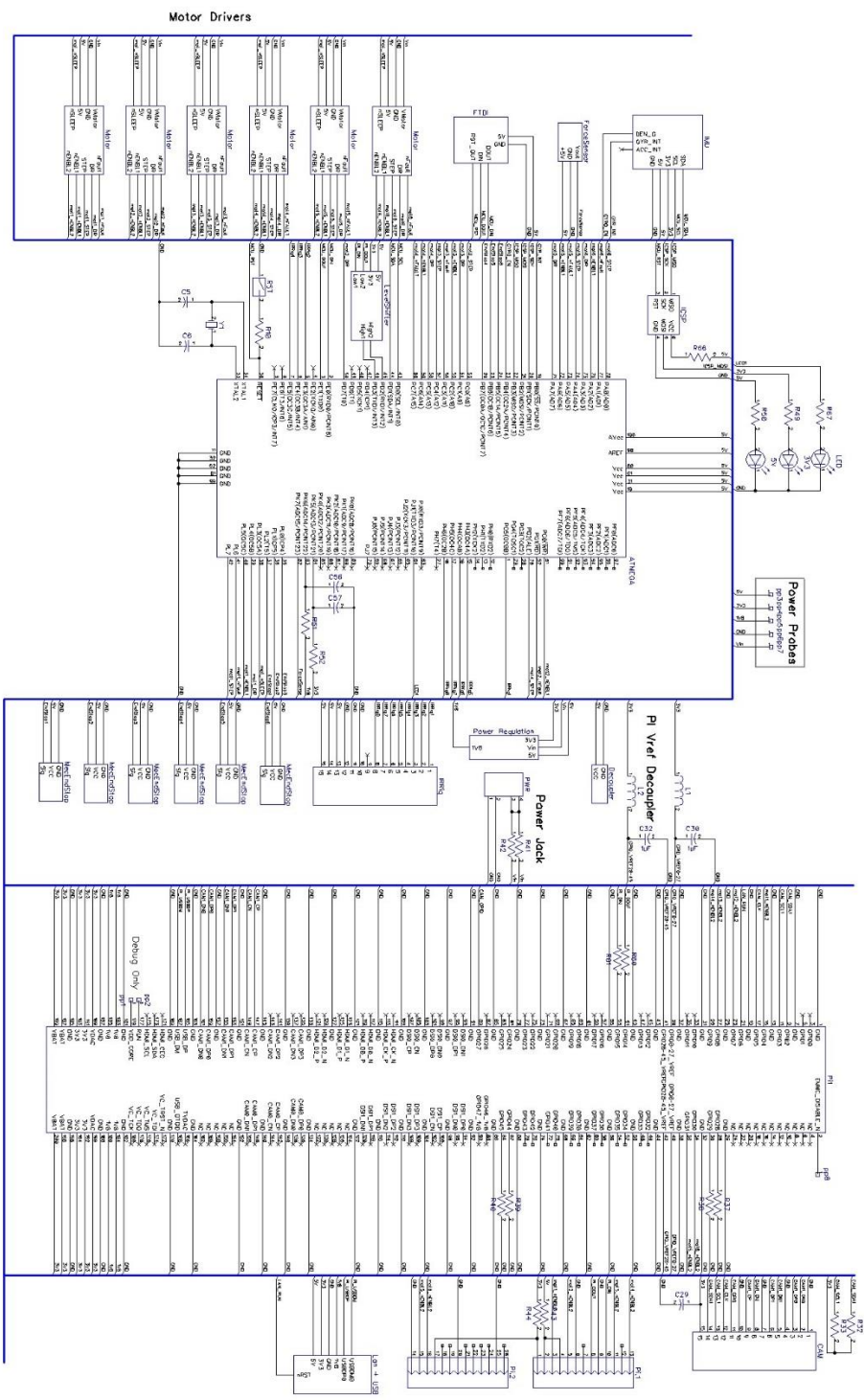


Figure 1: Main schematic block

# FTDI Schematic

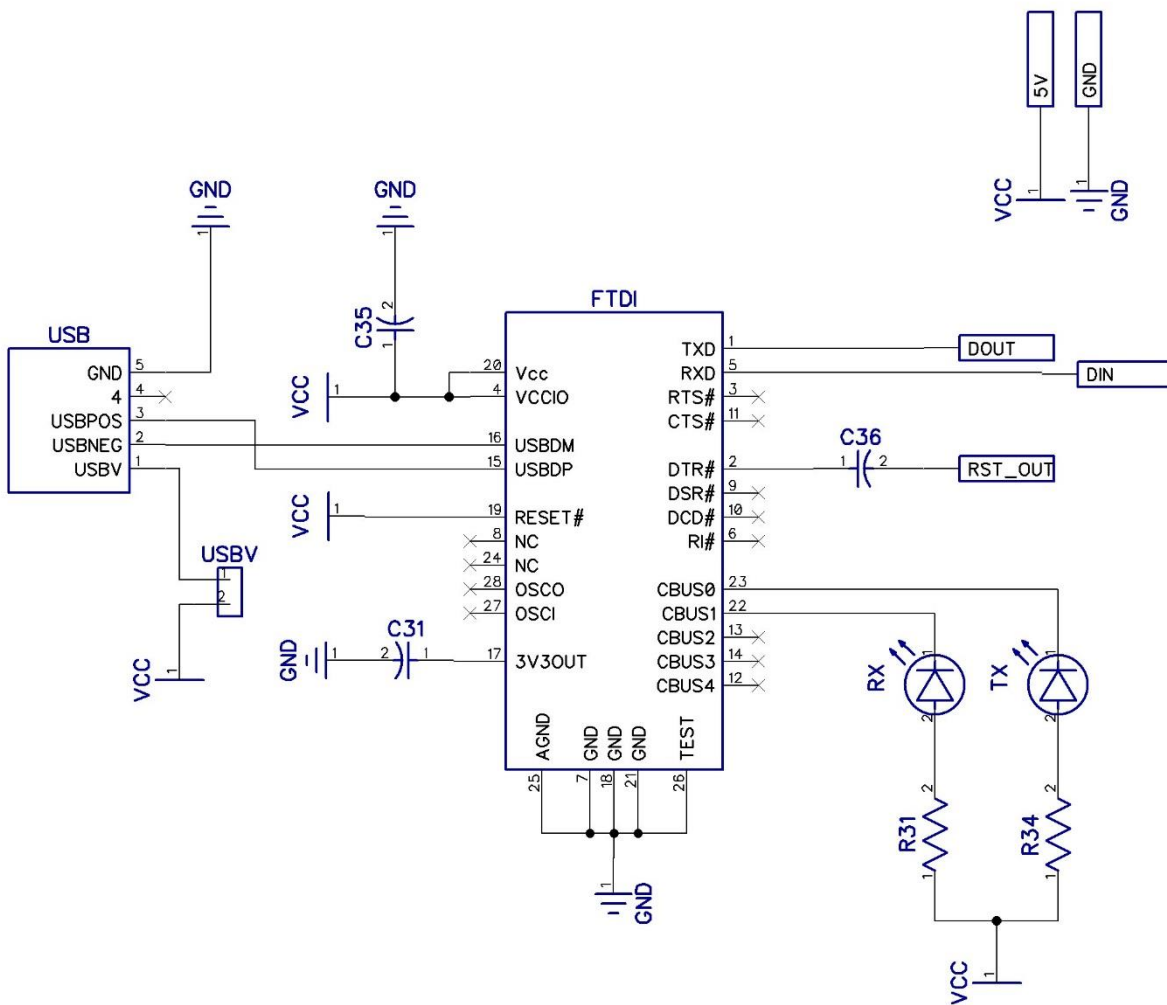


Figure 2: FTDI schematic

### Decoupler Schematic

Note that each analog pin makes use of 2 decoupling capacitors while each digital pin uses a single decoupling capacitor.

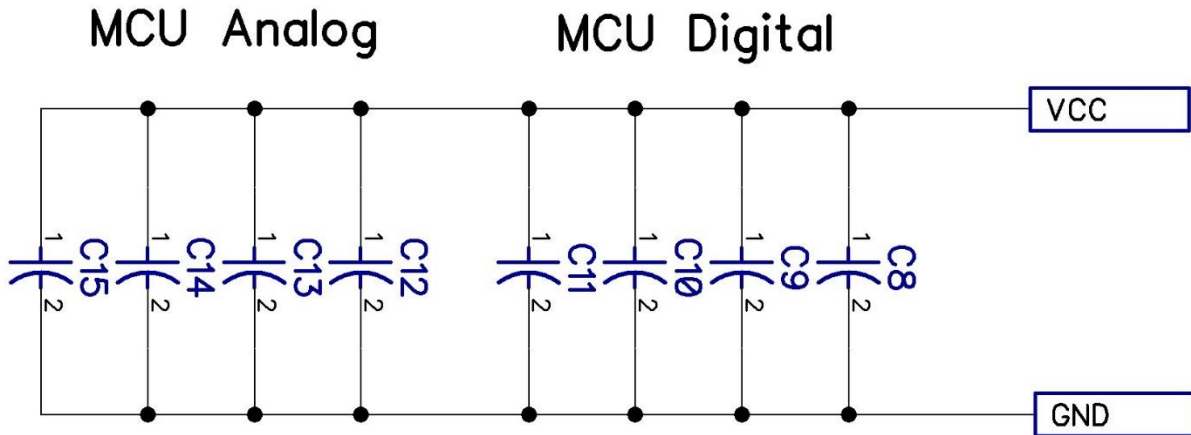


Figure 3: Decoupler schematic

### IMU Schematic

The LSM330DLC 6-DOF inertial sensor is used. It contains a 3-Axis accelerometer and a 3-Axis gyroscope. Due to its operation at 3V3, a level shifter is required for connecting to the ATMEGA which operates at 5V.

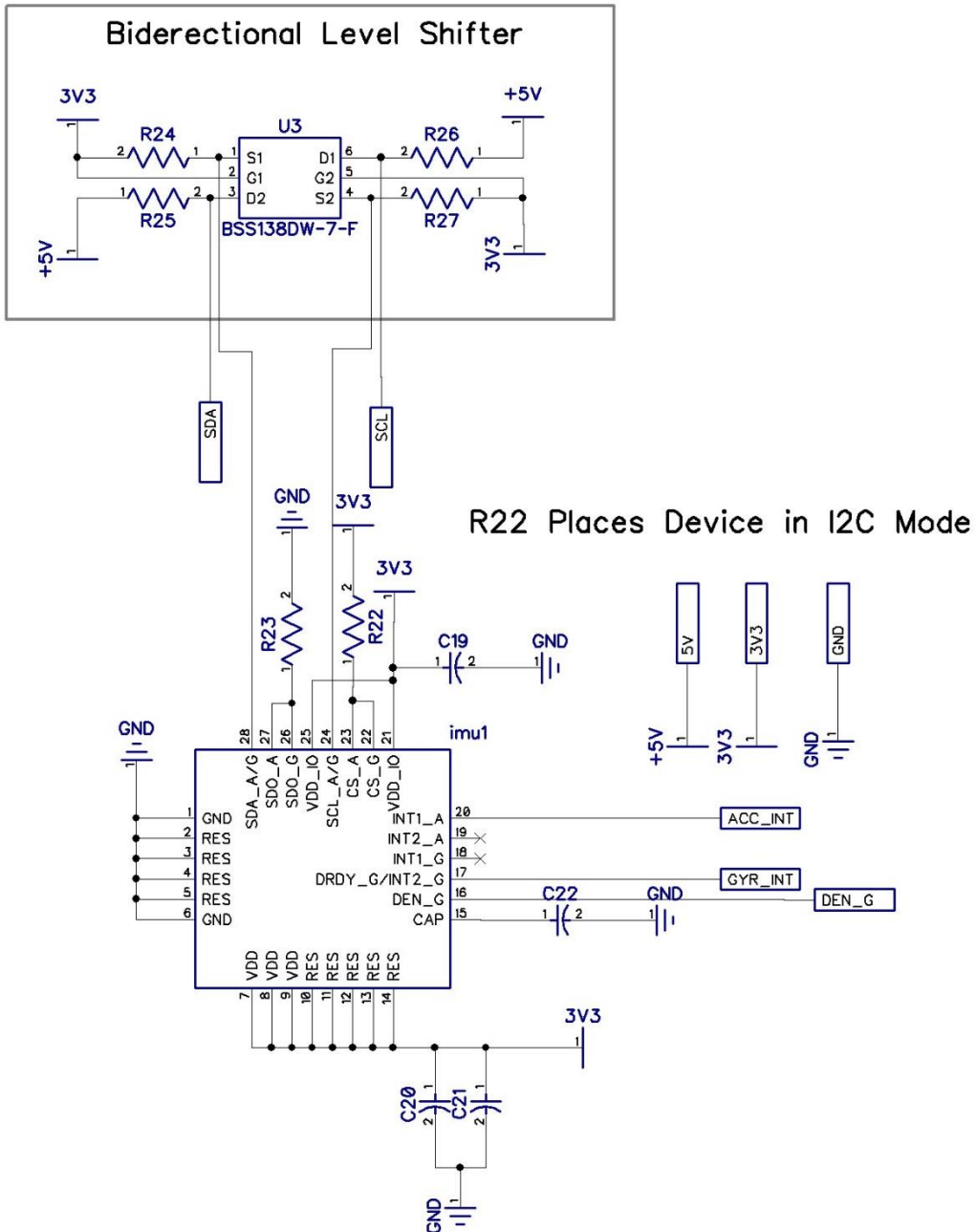


Figure 4: IMU Schematic

### Mechanical End Stop Schematic

End stop sensor and debouncing circuitry are shown below.

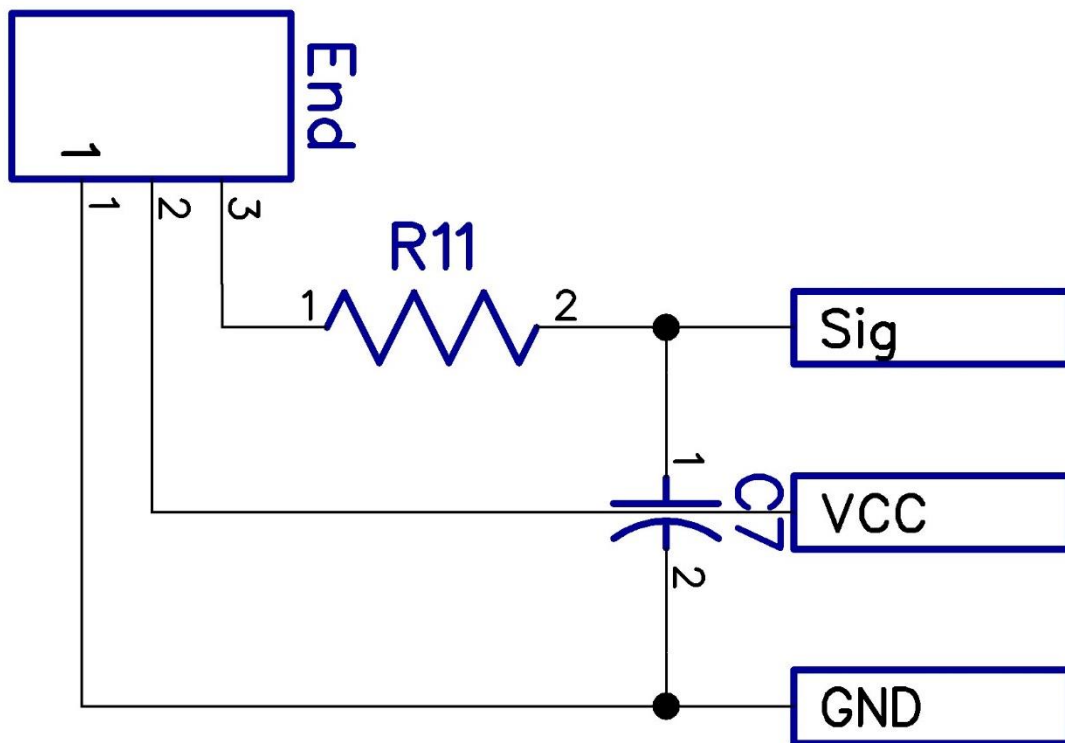


Figure 5: Mechanical end stop schematic

### Level Shifter Schematic

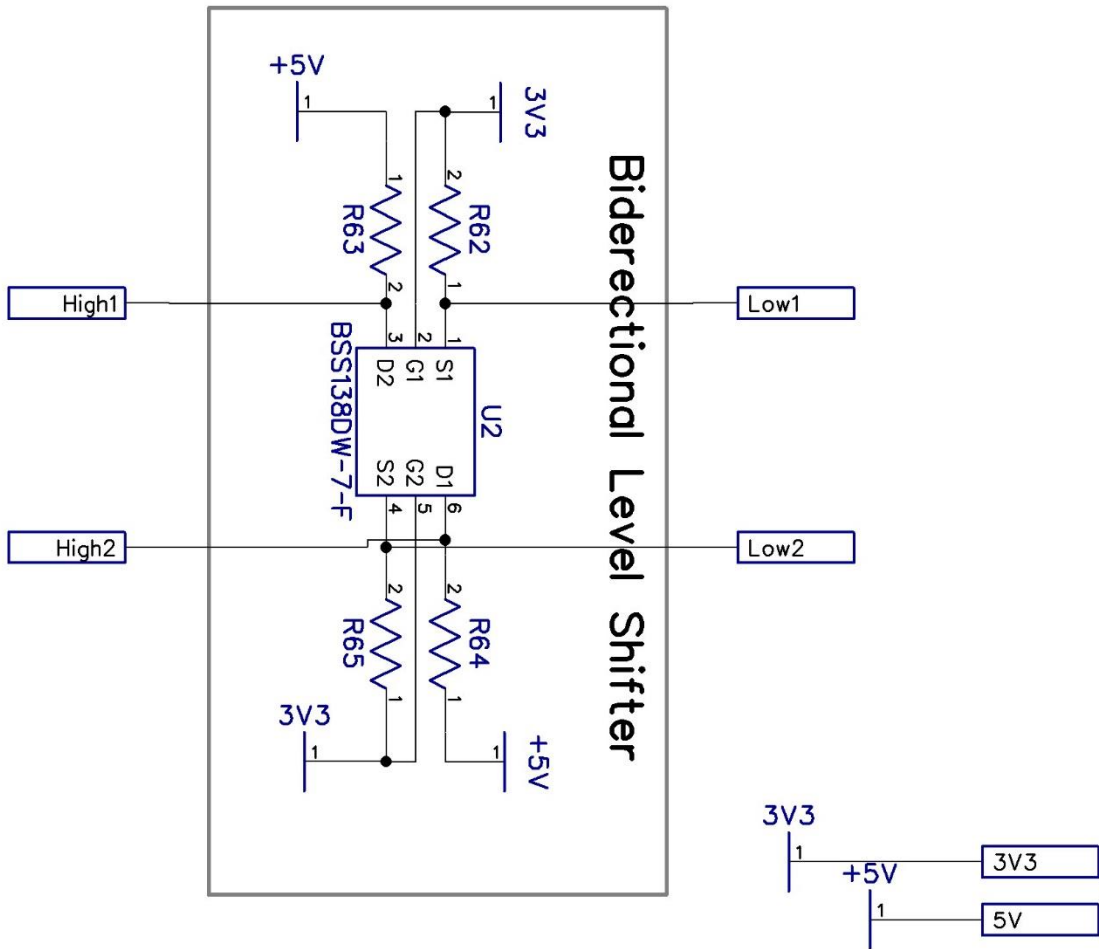


Figure 6: Level shifter schematic

## Power Regulation

The board counts with 3 onboard voltage regulators. The 5V and 3V3 are PTH08080WAS switching voltage regulators. The 1V8 line originates from the 3V3 regulator through a linear LT3021 regulator. As the compute module requires higher voltages to be powered first, the 1V8 regulator has a power-on delay circuitry which allows it to begin operation only after the 3V3 line has stabilized.

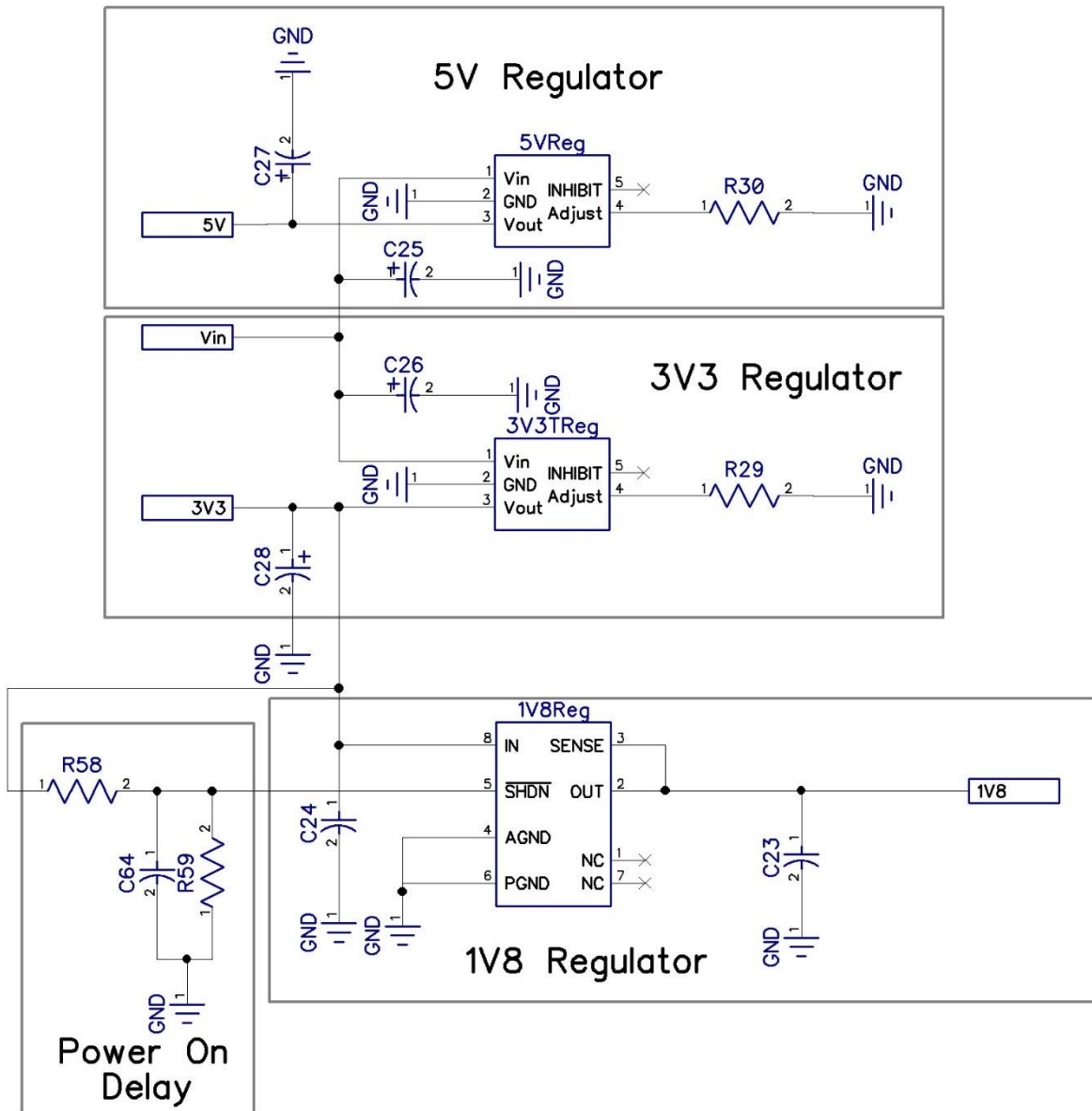


Figure 7: Power regulation schematic



Force Sensor

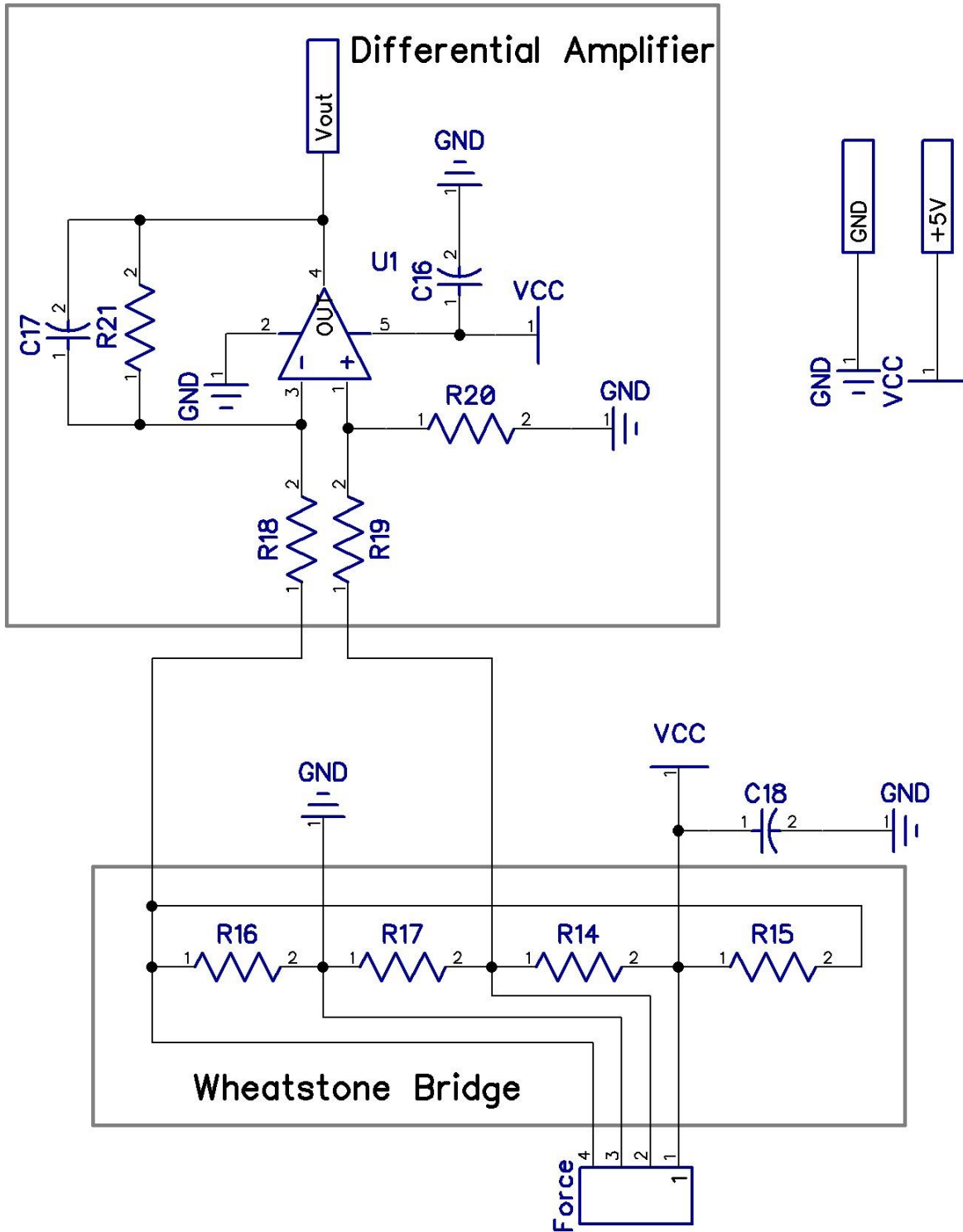


Figure 8: Force sensor schematic

### Motor Driver Schematic

The schematic for the DRV8834 microstepping motor drivers is shown below. Note that there are two enable sources: That allows selecting between the Raspberry Pi or the ATMEGA as the source for enabling the drivers. R4-R7 serve as a microstepping selector, solder only the appropriate resistors.

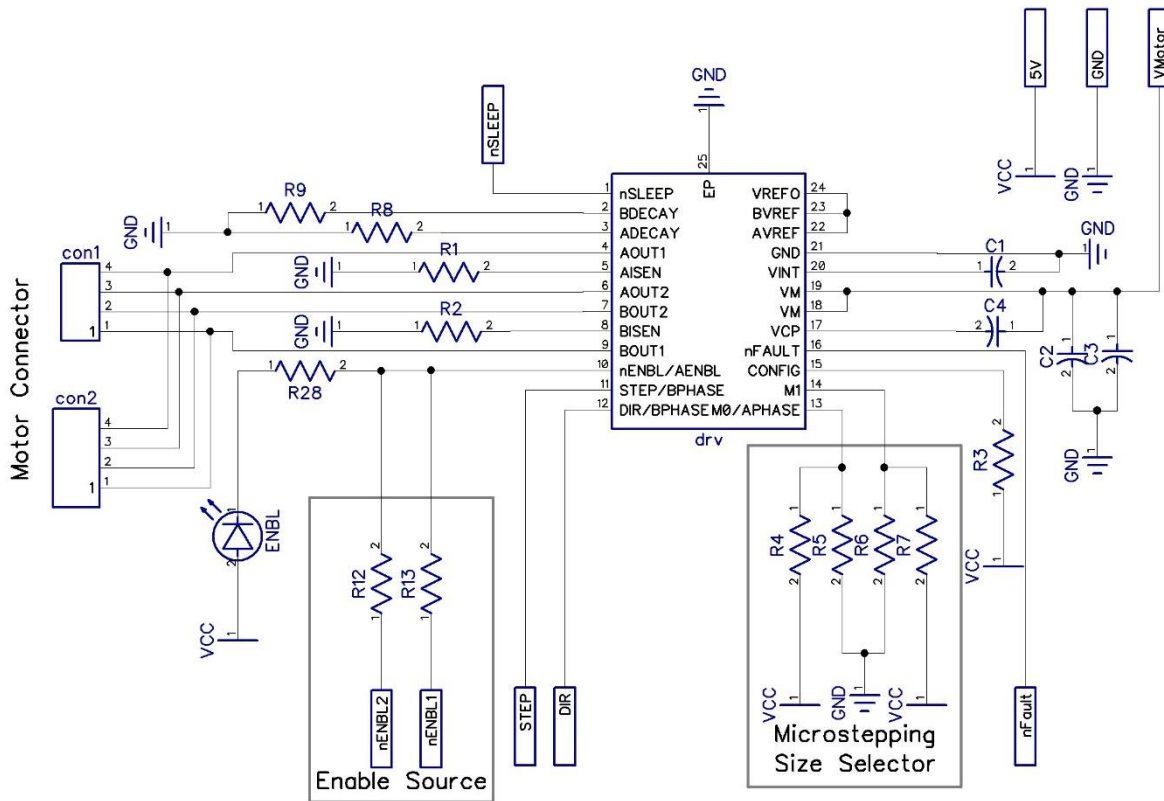


Figure 9: Motor driver schematic

# LAN and USB Schematic

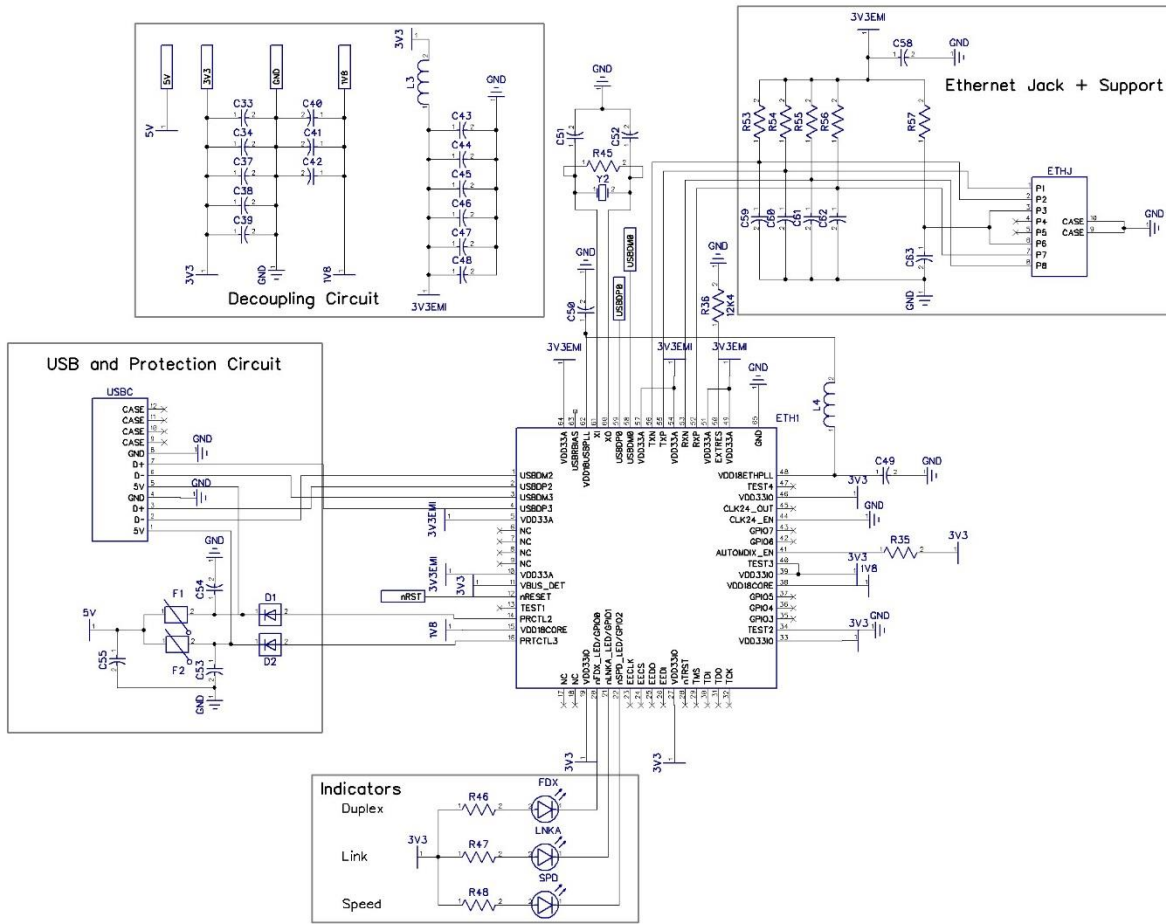


Figure 10: LAN and USB schematic

# PCB Art

## Top Layer

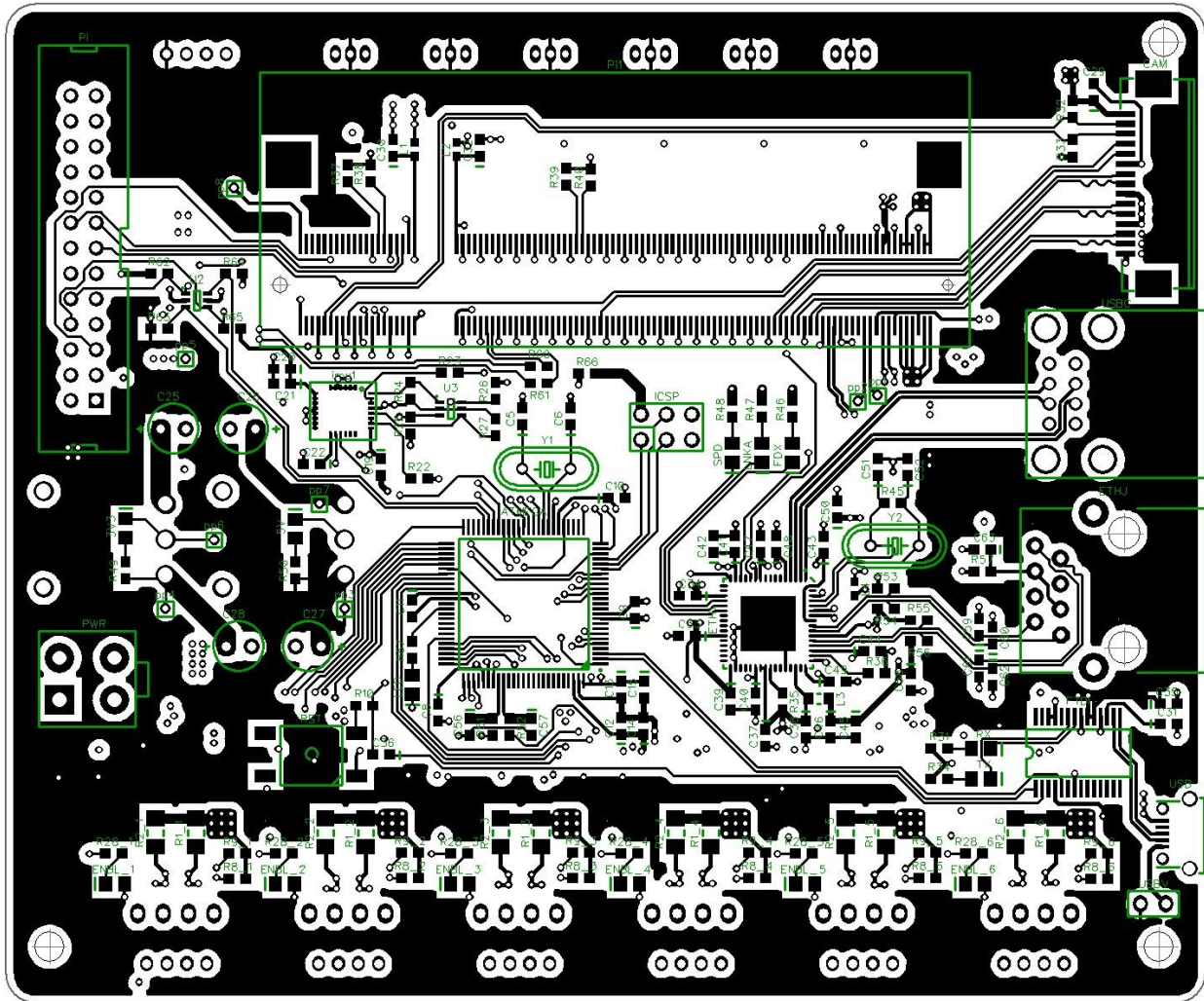


Figure 11: Top layer PCB art

## Inner Layer 1

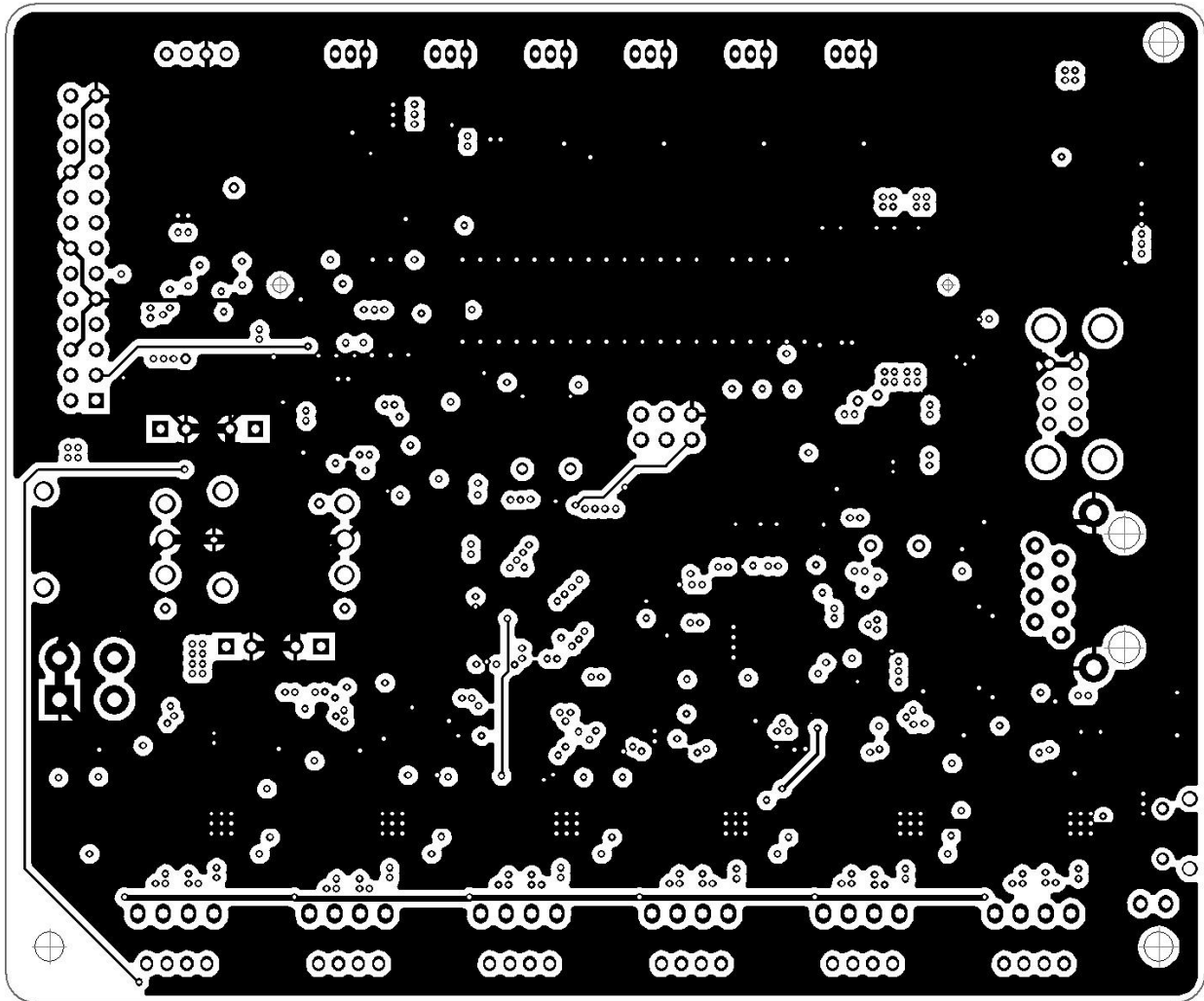


Figure 12: Inner layer 1 PCB art containing ground plane

## Inner Layer 2

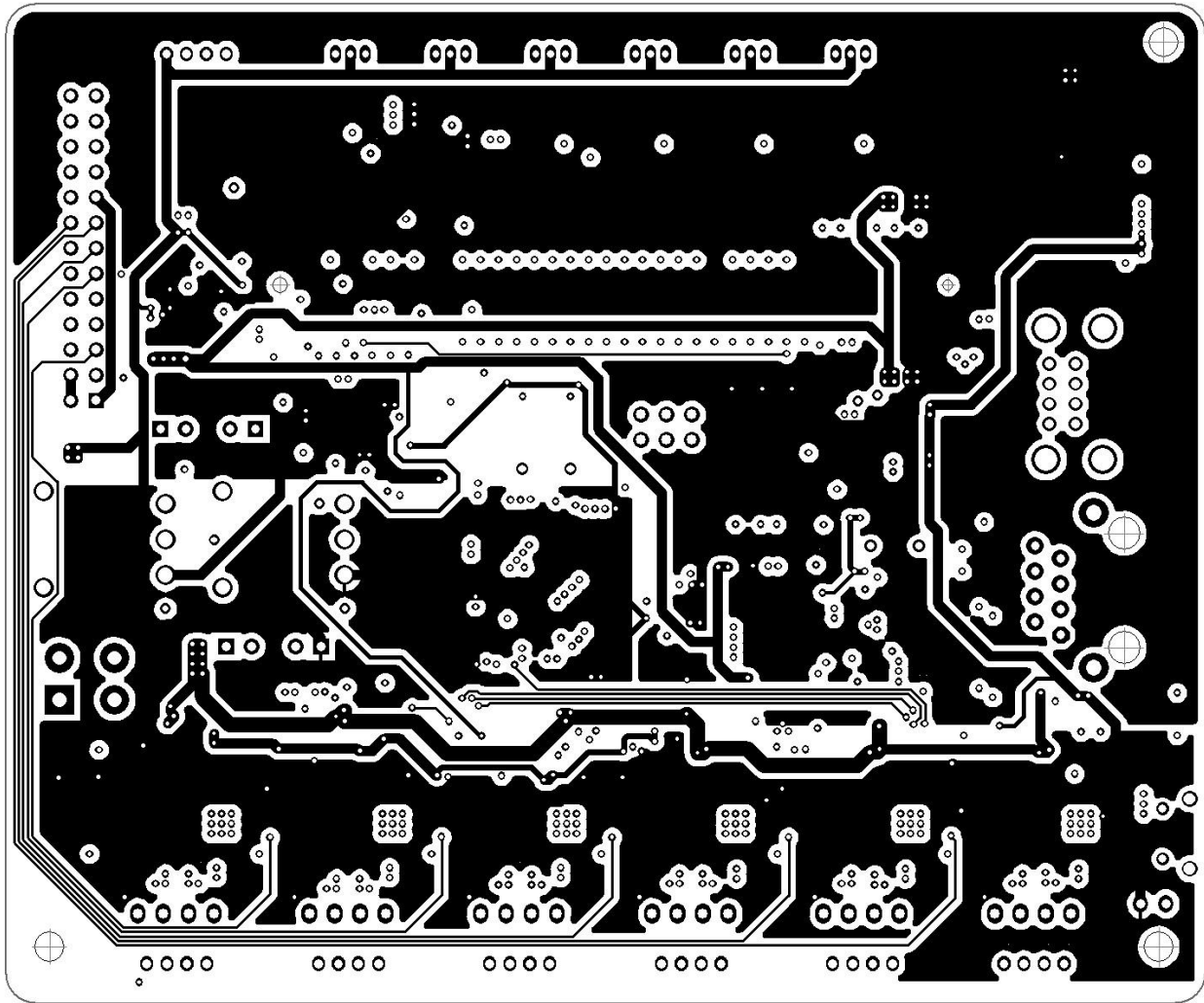


Figure 13: Inner layer 2 PCB art containing 3V3 and 5V planes

Bottom Layer

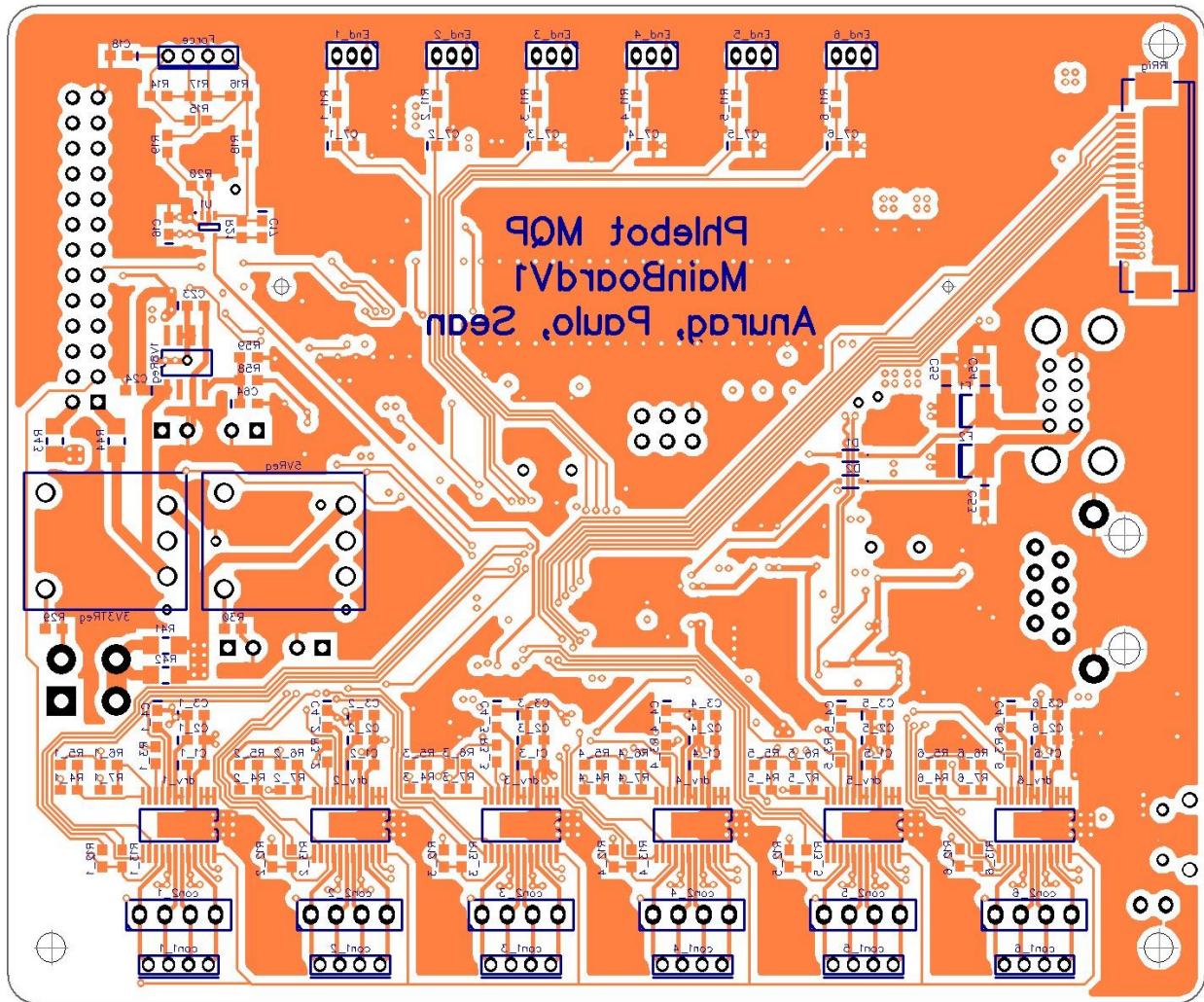


Figure 14: Bottom layer of PCB

# Mechanical Drawing

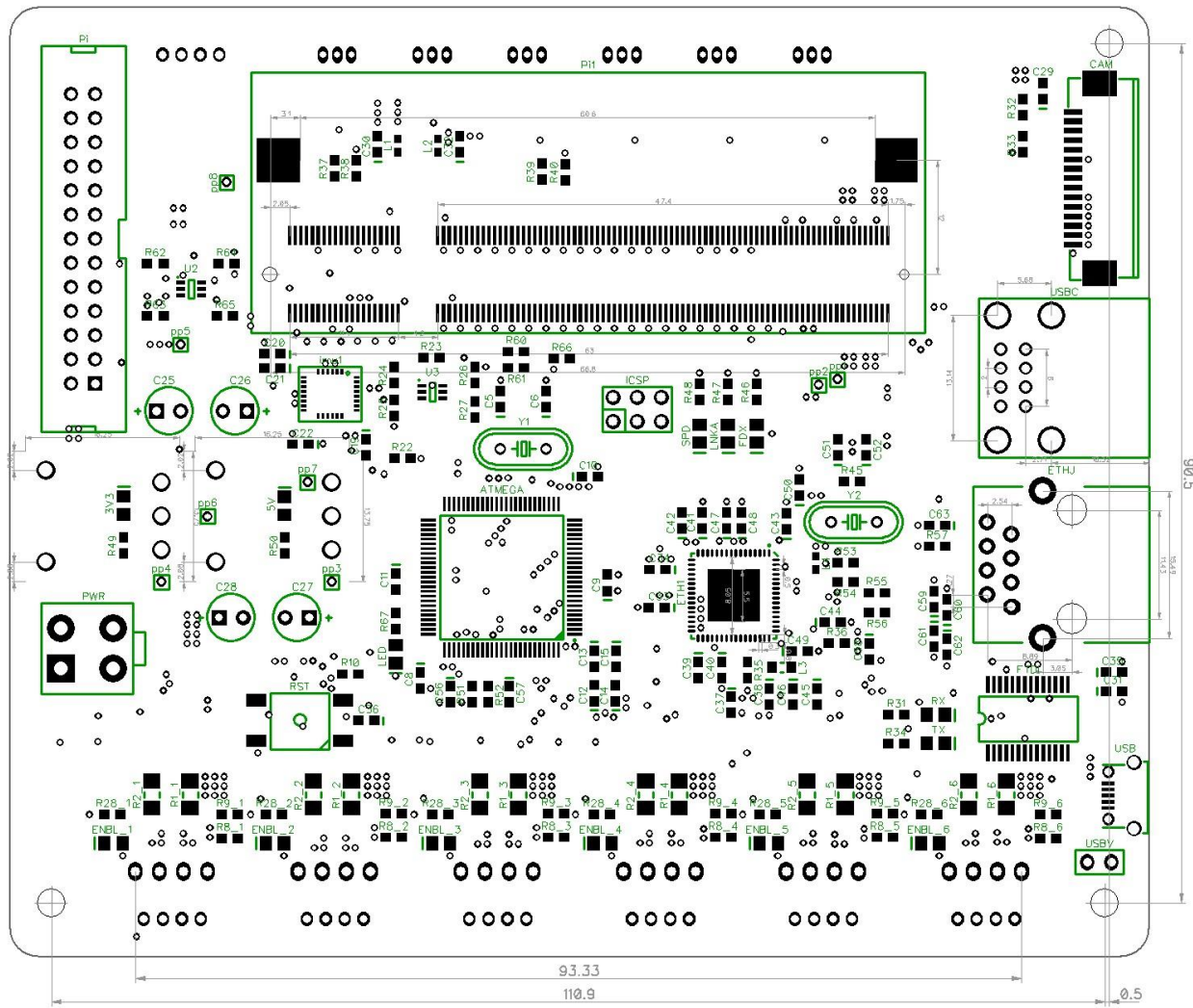


Figure 15: Mechanical drawing for phlebot main board V1



## Table of Components

The table below summarizes the function and lists all components required for proper assembly of the board.

Reference	Type	Value	Description
1V8Reg	Vreg	LT3021ES8-1.8	1V8 voltage regulator for Rap Pi and LAN9512
3V3,5V, ENBL_n, LED	LED 0805	--	Indicator LEDs
3V3TReg,5VReg	Vreg	PTH08080WAS	Main voltage regulators from Vin to 5V and 3V3
ATMEGA	uC	ATMEGA2560	Microcontroller for low level board control
C1_n	CAP C 0603	2.2 uF	Decoupler for internal regulator of stepper driver
C2_n	CAP C 0603	10 nF	Decoupler for stepper driver Vm
C3_n	CAP C 0603	10 uF	Decoupler for stepper driver Vm
C4	CAP C 0603	10 nF	Part of charge pump for stepper driver
C5,C6	CAP C 0603	20 pF	Load for MCU Crystal
C7	CAP C 0603	10 nF	End stop debouncing capacitor
C8-C11	CAP C 0603	100 nF	MCU digital supply decoupler
C12,C13	CAP C 0603	100 nF	MCU analog supply decoupler
C14,C15	CAP C 0603	1 uF	MCU analog supply decoupler
C16,C18	CAP C 0603	100 nF	Decoupler for force sensor and op-amp
C17	CAP C 0603		Low pass filter for force sensor amplifier
C19,C20	CAP C 0603	100 nF	Decoupler for IMU
C21	CAP C 0603	10 uF	Decoupler for IMU
C22	CAP C 0603	10 nF	Internal decoupler for IMU
C23	CAP C 0603	4.7 uF	Output capacitor for 1V8 Regulator
C24	CAP C 0603	4.7 uF	Input Capacitor for 1V8 Regulator
C25,C26,C27,C28	CAP E	100 uF 20V	Capacitors for large voltage regulators (3V3, 5V)
C29	CAP C 0603	100 nF	Decoupler for camera FPC connector
C30, C32	CAP C 0603	1 uF	Part of GPIO Vref Filter for Rasp Pi
C31	CAP C 0603	100 nF	Decoupler of 3V3out for FTDI chip
C33,C34,C37-C39	CAP C 0603	100 nF	LAN9512 3V3 input decouplers
C40-C42	CAP C 0603	100 nF	LAN9512 1V8 input decouplers
C43-C48	CAP C 0603	100 nF	LAN9512 3V3EMI input decouplers (After L3)
C49	CAP C 0603	100 nF	LAN9512 ETH_PLL Decoupler
C50	CAP C 0603	1 uF	LAN9512 USB_PLL Decoupler
C51,C52	CAP C 0603	20 pF	LAN9512 load for crystal
C53,C54	CAP C 0603	100 nF	USB power out decoupler
C55	CAP C 0603	22 uF	USB power out main decoupler
C56,C57	CAP C 0603	10 nF	Low pass filter for voltage measurements
C58	CAP C 0603	100 nF	Part of Ethernet transmission lines
C59-C62	CAP C 0603	15 pF	Part of Ethernet transmission lines
C63	CAP C 0603	22 nF	Part of Ethernet transmission lines
C64	CAP C 0603		Part of delay circuit for 1V8 regulator
CAM	FPC 15 POS	1-84953-5	Connector for camera
Con1_n	JST 4 POS	B4B-PH-K-S	Style 1 motor connectors
Con2_n	Header	4 Pin 2.54mm	Style 2 motor connectors

D1,D2	Diode	BAS16J	Part of USB power circuitry
Drv_n	Motor Dri	DRV8834	Micro stepping stepper motor driving IC
End_n	JST 3 POS	B3B-ZR	Connector for end stop sensors
ETH1	IC	LAN9512	Ethernet and USB IC
ETHJ	Conn	A63-113-300P131	Ethernet RJ45 connector with magnetics
F1,F2	Fuse	miniSMDC014F	Current control for USB connectors
FDX,LNKA,SPD	LED 0805	--	Indicator LEDs for LAN9512
Force	JST 4 POS	B4B-PH-K-S	Connector for force sensor
FTDI	IC	FT232RL	UART to USB converted to ATMEGA2560
ICSP	Header	2X3 POS 2.54mm	Connector for ICSP programming
Imu1	IC	LSM330DLC	Inertial sensing unit
IRRIg	FPC	1-84953-5	Connector for IRRig board
L1,L2	RES 0603	0 OHM	Powers the GPIO of Pi
Pi	Conn	13X2 Pin 2.54mm	Connector for backup pi
Pi1	SODIMM	609-4371-ND	Connector for compute module
PPn	ProbePoint	--	Points for probing signals and power
PWR	Connector		Connector for powering board
R1_n,R2_n	RES 1206	1 OHM 1 %	Shunt for motor driver current sensing
R3_n	RES 0603	1 KOHM	When soldered puts device in indexer mode. HIGH
R4_n-R7_n	RES 0603	10 KOHM	Microstepping size selector. Solder as appropriate
R8,R9	RES 0603	49K9 OHM	Decay rate selector for stepper motor driver
R10	RES 0603	0 OHM	Current limiter for reset button. See errata.
R11	RES 0603	100 OHM	Part of end stop debouncing circuit
R12,R13	RES 0603	0 OHM	Enable source selector for stepper motor. Solder as appropriate
R14-R17	RES 0603		Wheatstone bridge for force sensor
R18,R19	RES 0603		Input resistors to force differential amplifier
R20	RES 0603		Part of gain for force differential amplifier
R21	RES 0603		Part of gain for force differential amplifier
R22, R23	RES 0603	47 KOHM	Chooses appropriate mode for IMU
R24-R27	RES 0603	4K7 OHM	Part of logic level shifter for IMU
R28	RES 0603	200 or 300 OHM	Use 300 Ohm if R13 is soldered. 200 Ohm otherwise
R29	RES 0603	1K87 OHM 1%	Voltage output selector for 3V3 regulator
R30	RES 0603	348 OHM 1%	Voltage output selector for 5V regulator
R31,R34	RES 0603	300 OHM	Current limiter for FTDI indicator LEDs
R32, R33	RES 0603	1K87 OHM 1%	Pull up for camera I2C lines
R35	RES 0603	10 KOHM	Puts LAN9512 in auto speed mode
R36	RES 0603	12K4 OHM	LAN9512 external resistor
R37-R40	RES 0603	100 KOHM	Pull down for Rasp Pi booting lines
R41, R42	RES 1206	0 OHM	Allows board to be powered from power connector
R43,R44	RES 1206	0 OHM or NC	Solder only if external rasp pi will not receive power
R45	RES 0603	1 MOHM	Load for LAN9512 Crystal
R46-R48	RES 0603	1 KOHM ???	Current limiter for LAN9512 indicator LEDs
R49	RES 0603	200 OHM	Current limiter for 3V3 ON indicator LED
R50	RES 0603	300 OHM	Current limiter for 5V ON indicator LED
R51, R52	RES 0603	100 OHM	Part of low pass filter for voltage sensing

R53-R56	RES 0603	49.9 OHM	Part of Ethernet transmission line
R57	RES 0603	10 OHM	Part of Ethernet transmission line
R58	RES 0603		Part of power on delay for 1V8 regulator
R59	RES 0603	47 KOHM	Pull down for 1V8 power on delay
R60,R61	RES 0603	100 OHM	Connects UART to compute module
R62-R65	RES 0603	10 KOHM	Part of logic level shifter for Rasp Pi UART to MCU
R66	RES 0603	0 OHM or NC	If soldered allows ICSP to power board
R67	RES 0603	300 OHM	Indicator Led connected to MCU
RST	Switch	FSMJSMA	Button for resetting ATMEGA2560
RX, TX	LED 0805	--	Indicator LED for FTDI
U1	Op Amp	LMV321	Op Amp for differential amplifier for force sensor
U2,U3	MOSFET	BSS138DW-7-F	Level shifter for communication lines
USB	Connector	609-4618-1-ND	Micro USB Connector for FTDI
USBC	Connector	1175-1018-ND	2 USB A port connector for LAN9512
USBV	Jumper	2.54mm	Jumper for enabling USB to power board
Y1	Crystal	16 MHz 20 pF	Crystal for ATMEGA2560
Y2	Crystal	25 MHz	Crystal for LAN9512

### Stepping Size Selector Resistors

The table below aids in determining the appropriate combination of microstepping resistors. Note that a 0 denotes resistor is not soldered while a 1 implies it is preset on the board.

Step Mode	M0: R4_n (5V)	M0: R5_n (GND)	M1: R6_n (GND)	M1: R7_n (5V)
Full Step (M0=M1=0)	0	1	1	0
Half Step (M0=1,M1=0)	1	0	1	0
Quarter Step (M0=Z,M1=0)	0	0	1	0
1/8 Step (M0=0,M1=1)	0	1	0	1
1/16 Step (M0=M1=1)	1	0	0	1
1/32 Step (M0=Z,M1=1)	0	0	0	1

## Errata

<b>Error</b>	<b>Description</b>	<b>Date</b>
Missing RST pull Up	There should be a pull up in the reset pin of the ATMEGA2560. Resistor was instead placed as a current limiter. Internal pull up should do the job and hopefully there won't be any sporadic resets.	7/17/14

DRAFT

# Appendix E

## Interface Document: Main Board V2



# INTERFACE DOCUMENT

Phlebot MQP: MainBoardV2

## Abstract

Contains all necessary information for assembly and safe operation of the MainBoardV2 for the Phlebot MQP.

Phlebot MQP  
phlebot@wpi.edu

## Contents

Table of Figures.....	2
Description.....	3
Overall.....	3
Power Requirements .....	3
Pin Mapping.....	4
ATMEGA: ATMEGA2560.....	4
ATMEGA_NIM: ATMEGA328P.....	6
ATMEGA_UI: ATMEGA328P .....	7
Schematic Diagrams.....	8
Main Level.....	8
NIM Controller .....	9
UI Controller.....	10
Stepper Motor Driver.....	11
Double Stepper Motor Driver .....	12
Double DC Motor Driver .....	13
Forcer Sensor .....	14
FTDI .....	15
Power Regulation.....	16
Level Shifter .....	17
Pressure Sensor.....	18
End Stop.....	19
LDR .....	20
IMU .....	21
Solenoid .....	22
PCB Art .....	23
Top Layer.....	23
Inner Layer 1: GND.....	24
Inner Layer 2: Power + Data.....	25
Bottom Layer.....	26
Table of Components.....	27
Errata.....	30

## Table of Figures

Figure 1: Main schematic level .....	8
Figure 2: NIM Controller Schematic.....	9
Figure 3: UI Controller Schematic .....	10
Figure 4: Stepper motor driver schematic.....	11
Figure 5: Double stepper motor driver schematic.....	12
Figure 6: Double DC motor driver schematic.....	13
Figure 7: Schematic for force sensor. ....	14
Figure 8: Schematic for FTDI. ....	15
Figure 9: Schematic power regulation. ....	16
Figure 10: Level shifter schematic. ....	17
Figure 11: Pressure sensor schematic.....	18
Figure 12: End stop schematic. ....	19
Figure 13: LDR Schematic.....	20
Figure 14: IMU Schematic. ....	21
Figure 15: Solenoid schematic. ....	22
Figure 16: Top layer PCB art.....	23
Figure 17: Inner layer 1 of PCB art. ....	24
Figure 18: Inner layer 2 of PCB art. ....	25
Figure 19: Bottom layer of PCB art. ....	26



## Description

### Overall

The Main Board V2 is the principal controller for the Phlebot MQP. The board has three microcontrollers grouped to specific peripherals as outlined below:

1. ATMEGA2560: Main MCU
  - a. 4 Solenoid drivers
  - b. 4 Stepper motor drivers
  - c. 8 End stop input or servo outputs
  - d. 3-Axis accelerometer
  - e. FTDI
  - f. Temperature Sensor
2. ATMEGA328P: UI MCU
  - a. 20x4 LCD Display
  - b. 2 Encoders with push button and RGB LED
3. ATMEGA328P: NIM MCU
  - a. Interface to Maxon Controller
  - b. Stepper driver (also dual DC driver)

### Power Requirements

The table below summarizes all the power requirements and limits for the board. Note that using the board outside these specification may lead to permanent damage.

Name	Range	Units	Description
Power Supply	8-10.5	Volts	Provides power to the entire board. Over voltage could cause damage to stepper drivers.
Power Supply	2.0	Amps	Supply should be able to supply given current continuous.

## Pin Mapping

### ATMEGA: ATMEGA2560

The table below reports all connections to the ATMEGA2560 microcontroller. For easier pin identification when programming in an Arduino compatible environment, Arduino specific nomenclature is provided on the third column.

Pin #	Pin Name	Arduino	Connected To	Description
1	PG5(OC0B)	DIO4	--	--
2	PE0(RXD0)	DIO0(RX0)	FTDI_DOUT	UART from FTDI to MCU
3	PE1(TXD0)	DIO1(TX0)	FTDI_DIN	UART from MCU to FTDI
4	PE2	--	--	--
5	PE3(OC3A)	DIO5	--	--
6	PE4(OC3B)	DIO2	END1	End Stop 1 (Interrupt Capable). Requires Pull-Up.
7	PE4(OC3C)	DIO3	END2	End Stop 2 (Interrupt Capable). Requires Pull-Up.
8	PE6	--	--	--
9	PE7	--	--	--
10	VCC	--	+5V	--
11	GND	--	GND	--
12	PH0(RXD2)	DIO17(RX2)	LevelShifter_High2	UART from Raspberry Pi to MCU through level shifter
13	PH1(TXD2)	DIO16(TX2)	LevelShifter_High1	UART to Raspberry Pi from MCU through level shifter
14-19	--	--	--	--
20	PB1(SCK)	DIO52(SCK)	ICSP_SCK	Part of programming header
21	PB2(MOSI)	DIO51(MOSI)	ICSP_MOSI	Part of programming header
22	PB3(MISO)	DIO50(MISO)	ICSP_MISO	Part of programming header
23	PB4	DIO10	IRRIG1	Connects to the IRRIG header
24	PB5	DIO11	IRRIG2	Connects to the IRRIG header
25	PB6	DIO12	IRRIG3	Connects to the IRRIG header
26-29	--	--	--	--
30	RST	--	ICSP, R40, FTDI	Resets the MCU. Resets when LOW.
31	VCC	+5V	--	--
32	GND	GND	--	--
33	XTAL	--	--	--
34	XTAL	--	--	--
35	PL0	DIO49	MOT3_nFAULT	Motor at fault line. Mode: INPUT_PULLUP
36	PL1	DIO48	MOT3_DIR	Motor direction selection line
37	PL2	DIO47	MOT3_STEP	Motor step selection line
38	PL3(OC5A)	DIO46	MOT3_nENBL	Motor driver enable line
39	PL4(OC5B)	DIO45	MOTD_nENBL	Motor driver enable line
40	PL5(OC5C)	DIO44	MOTD_STEP	Motor step selection line
41	PL6	DIO43	MOTD_DIR	Motor direction selection line
42	PL7	DIO42	MOTD_nFAULT	Motor at fault line. Mode: INPUT_PULLUP

43	PD0(SCL/INT0)	DIO21(SCL)	END3	End Stop 3 (Interrupt Capable). Requires Pull-Up.
44	PD1(SDA/INT1)	DIO20(SDA)	END4	End Stop 4 (Interrupt Capable)
45	PD2(RXD1)	DIO19(RX1)	NIM_DOUT	UART from the NIM MCU
46	PD3(TXD1)	DIO18(TX1)	NIM_DIN	UART to the NIM MCU
47-49	--	--	--	--
50	PD7	DIO38	MOT_nSLEEP	Common sleep line for all stepper drivers.
51-52	--	--	--	--
53	PC0	DIO37	NIM_RST	Resets the NIM Controller
54	PC1	DIO36	UI_RST	Resets the UI Controller
55	PC2	DIO35	END5	End Stop 5. Requires Pull-Up.
56	PC3	DIO34	END6	End Stop 6. Requires Pull-Up.
57	PC4	DIO33	END7	End Stop 7. Requires Pull-Up.
58	PC5	DIO32	END8	End Stop 8. Requires Pull-Up.
59-60	--	--	--	--
61	VCC	--	--	--
62	GND	--	--	--
63	PJ0(RXD3)	DIO15(RX3)	UI_DOUT	UART from UI Controller
64	PJ1(TXD3)	DIO14(TX3)	UI_DIN	UART to UI Controller
65-70	--	--	--	--
71	PA7	DIO29	MOT2_nFAULT	Motor at fault line. Mode: INPUT_PULLUP
72	PA6	DIO28	MOT2_DIR	Motor direction selection line
73	PA5	DIO27	MOT2_STEP	Motor step selection line
74	PA4	DIO26	MOT2_nENBL	Motor driver enable line
75	PA3	DIO25	MOT1_nFAULT	Motor at fault line. Mode: INPUT_PULLUP
76	PA2	DIO24	MOT1_DIR	Motor direction selection line
77	PA1	DIO23	MOT1_STEP	Motor step selection line
78	PA0	DIO22	MOT1_nENBL	Motor driver enable line
79	--	--	--	--
80	VCC	--	--	--
81	GND	--	--	--
82	PK7(ADC15)	AI15	Pressure	Output from pressure sensor amplifier
83	PK6(ADC14)	AI14	NIM_FORCE	Output from force sensor amplifier
84	PK5(ADC13)	AI13	IMU_X	Analog input from ACC
85	PK4(ADC12)	AI12	IMU_Y	Analog input from ACC
86	PK3(ADC11)	AI11	IMU_ST	ACC self-test line
87	PK2(ADC10)	AI10	IMU_Z	Analog input from ACC
88	PK1(ADC9)	AI9	LDR	Analog Input from LDR
89	PK0(ADC8)	AI8	Temp	Analog Input from Temperature Sensor
90	PF7(ADC7)	AI7	3V3	Senses voltage on 3V3 line
91	PF6(ADC6)	AI6	CHARGER:6	Connects to the charger connector
92	PF5(ADC5)	AI5	CHARGER:5	Connects to the charger connector
93	PF4(ADC4)	AI4	CHARGER:4	Connects to the charger connector
94	PF3(ADC3)	AI3	CHARGER:3	Connects to the charger connector
95	PF2(ADC2)	AI2	CHARGER:2	Connects to the charger connector
96	PF1(ADC1)	AI1	CHARGER:1	Connects to the charger connector

97	--	--	--	--
98	AREF	--	--	--
99	GND	--	--	--
100	AVCC	--	--	--

### ATMEGA\_NIM: ATMEGA328P

The table below reports all connections to the ATMEGA328P microcontroller. For easier pin identification when programming in an Arduino compatible environment, Arduino specific nomenclature is provided on the third column.

Pin #	Pin Name	Arduino	Connected To	Description
1	PD3(OC2B)	DIO3	MAXONJ5:1	Connects to Maxon Digital Header
2	PD4	DIO4	MAXONJ5:3	Connects to Maxon Digital Header
3	GND	--	--	--
4	VCC	--	--	--
5	GND	--	--	--
6	VCC	--	--	--
7	PB6(XTAL1)	--	XTAL	16 MHz Crystal
8	PB7(XTAL2)	--	XTAL	16 MHz Crystal
9	PD5(OC0B)	DIO5(PWM)	MAXONJ5:4	Connects to Maxon Digital Header
10	PD6(OC0A)	DIO6(PWM)	AENBL	Channel A enable for DC Driver
11	PD7	DIO7	BENBL	Channel A enable for DC Driver
12	PB0	DIO8	nFAULT	Fault line from DC Driver
13	PB1	DIO9	MAXONJ6:1	Connects to Maxon Analog Header
14	PB2	DIO10	MAXONJ6:3	Connects to Maxon Analog Header
15	PB3	DIO11	ICSP	Part of programming header
16	PB4	DIO12	ICSP	Part of programming header
17	PB5	DIO13	ICSP	Part of programming header
18	AVCC	5V	--	--
19	ADC6	--	--	--
20	AREF	5V	--	--
21	GND	Ground	--	--
22	ADC7	--	--	--
23	PC0(ADC0)	AI0	BPHASE	Channel B Phase for DC Driver
24	PC1(ADC1)	AI1	APHASE	Channel A Phase for DC Driver
25	PC2(ADC2)	AI2	FORCE	Analog force sensor input
26	PC3(ADC3)	AI3	POT	Analog potentiometer input
27	PC4(ADC4)	AI4	MAXONJ6:6	Connects to Maxon Analog Header
28	PC5(ADC5)	AI5	MAXONJ6:5	Connects to Maxon Analog Header
29	RESET	RESET	MCU1, ICSP, R31	Resets the microcontroller
30	PD0(RXD)	DIO0(RX)	MCU1:TX1	UART line to main MCU
31	PD1(TXD)	DIO1(TX)	MCU1:RX1	UART line to main MCU
32	PD2	DIO2	MAXONJ5:2	Connects to Maxon Digital Header

## ATMEGA\_UI: ATMEGA328P

The table below reports all connections to the ATMEGA328P microcontroller. For easier pin identification when programming in an Arduino compatible environment, Arduino specific nomenclature is provided on the third column.

Pin #	Pin Name	Arduino	Connected To	Description
1	PD3(OC2B)	DIO3	LCD_D:2	Data connector for LCD Display (D6)
2	PD4	DIO4	LCD_D:3	Data connector for LCD Display (D5)
3	GND	--	GND	--
4	VCC	--	5V	--
5	GND	--	GND	--
6	VCC	--	5V	--
7	PB6(XTAL1)	--	Crystal	16 MHz Crystal
8	PB7(XTAL2)	--	Crystal	16 MHz Crystal
9	PD5(OC0B)	DIO5(PWM)	LCD_D:4	Data connector for LCD Display (D4)
10	PD6(OC0A)	DIO6(PWM)	LCD_D:5	Data connector for LCD Display (RS)
11	PD7	DIO7	LCD_D:6	Data connector for LCD Display (EN)
12	PB0	DIO8	R6 → ENC1:7	Encoder 1 Connector (TICK1)
13	PB1	DIO9	R5 → ENC1:6	Encoder 1 Connector (TICK2)
14	PB2	DIO10	R4 → ENC1:5	Encoder 1 Connector (BUTTON)
15	PB3	DIO11	R3 → ENC1:4	Encoder 1 Connector (R LED)
16	PB4	DIO12	R2 → ENC1:3	Encoder 1 Connector (G LED)
17	PB5	DIO13	R1 → ENC1:2	Encoder 1 Connector (B LED)
18	AVCC	5V	5V	Voltage supply
19	ADC6	--	--	--
20	AREF	5V	--	Voltage reference
21	GND	Ground	GND	Ground
22	ADC7	--	--	--
23	PC0(ADC0)	AI0	R14 → ENC2:7	Encoder 2 Connector (TICK1)
24	PC1(ADC1)	AI1	R19 → ENC2:6	Encoder 2 Connector (TICK2)
25	PC2(ADC2)	AI2	R13 → ENC2:5	Encoder 2 Connector (BUTTON)
26	PC3(ADC3)	AI3	R12 → ENC2:4	Encoder 2 Connector (R LED)
27	PC4(ADC4)	AI4	R11 → ENC2:3	Encoder 2 Connector (G LED)
28	PC5(ADC5)	AI5	R10 → ENC2:2	Encoder 2 Connector (B LED)
29	RESET	RESET	--	--
30	PD0(RXD)	DIO0(RX)	MCU1:TX3	UART to MCU 1
31	PD1(TXD)	DIO1(TX)	MCU1:RX3	UART to MCU 1
32	PD2	DIO2	LCD_D:1	Data connector for LCD Display (D7)

# Schematic Diagrams

## Main Level

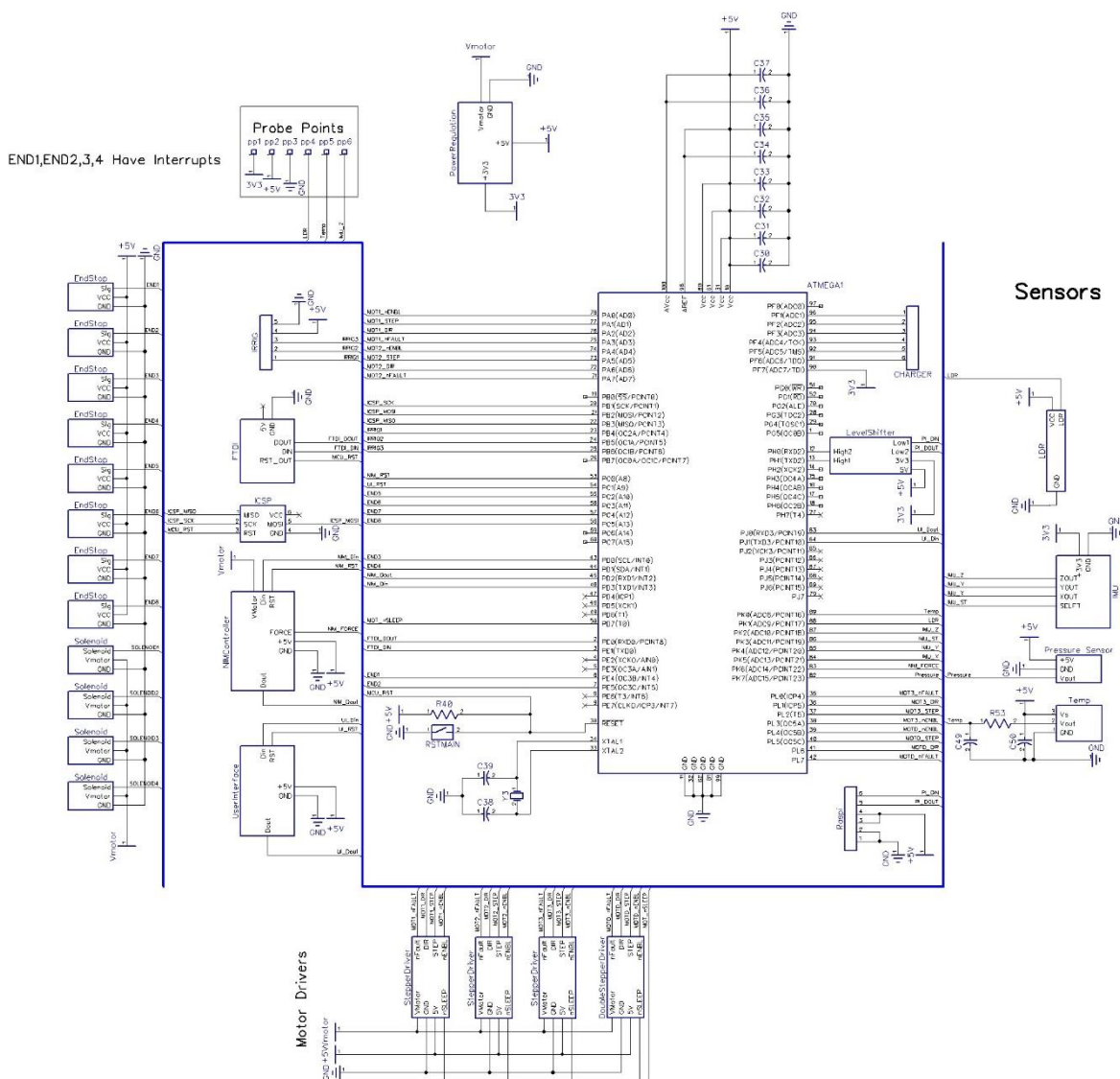


Figure 1: Main schematic level

# NIM Controller

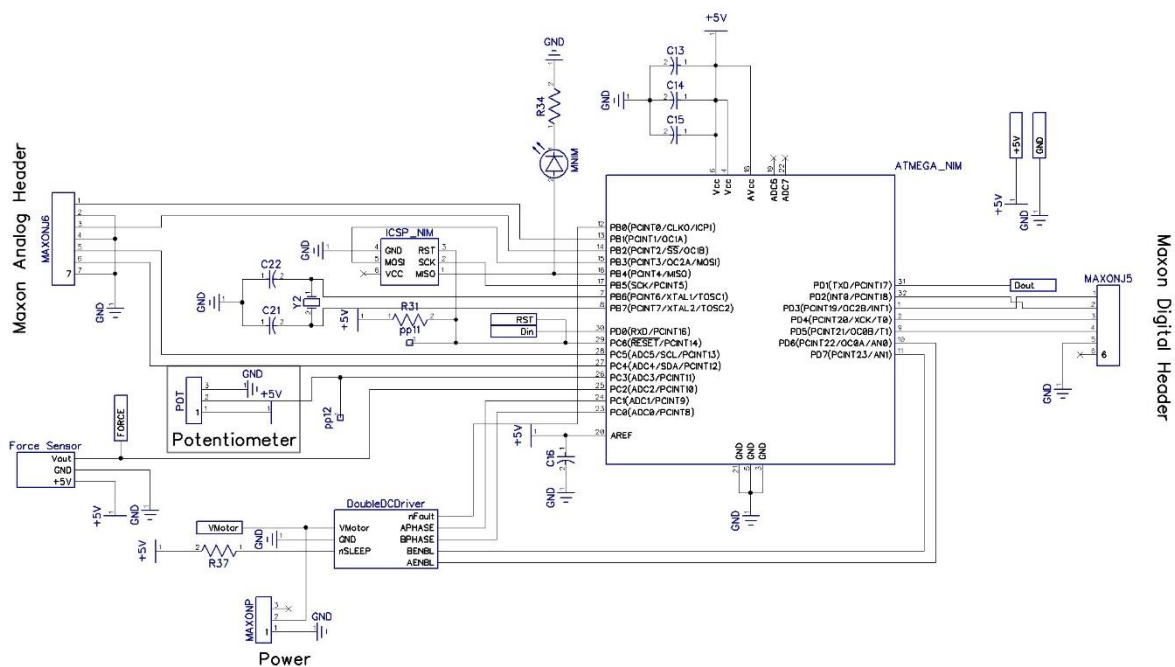


Figure 2: NIM Controller Schematic

# UI Controller

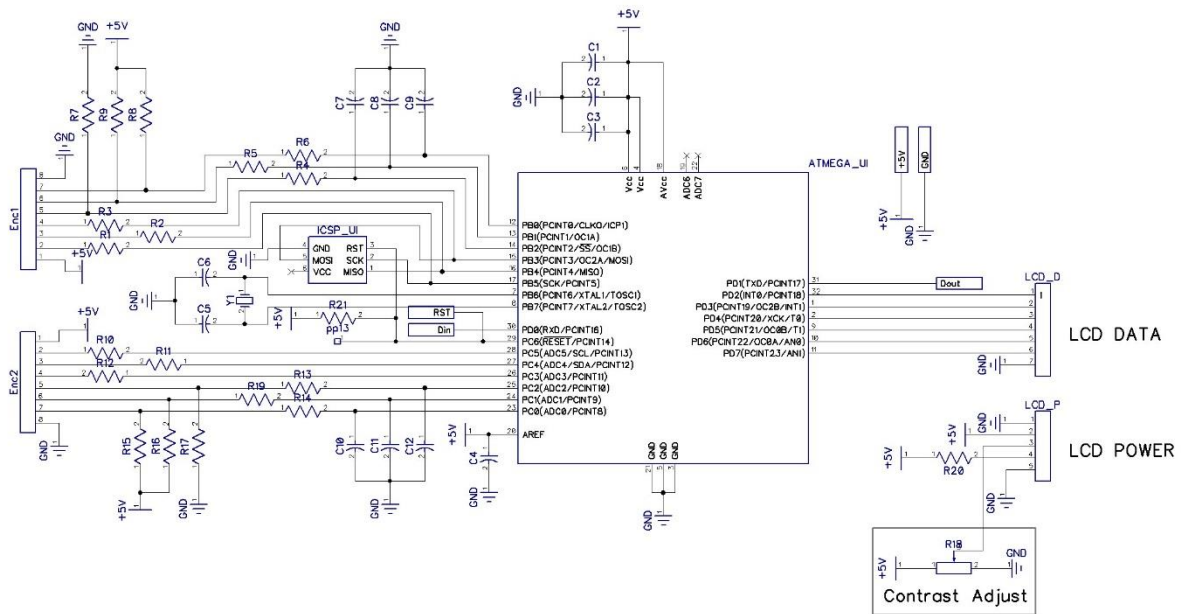


Figure 3: UI Controller Schematic



# Stepper Motor Driver

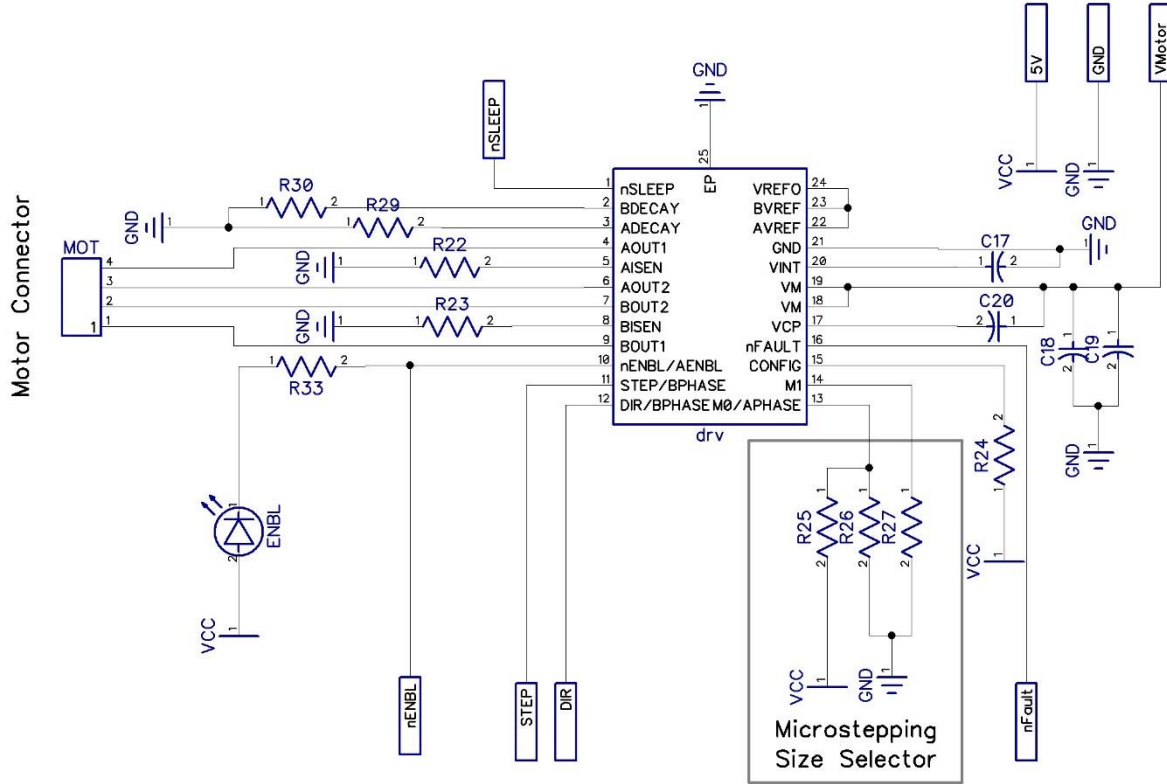


Figure 4: Stepper motor driver schematic.

## Double Stepper Motor Driver

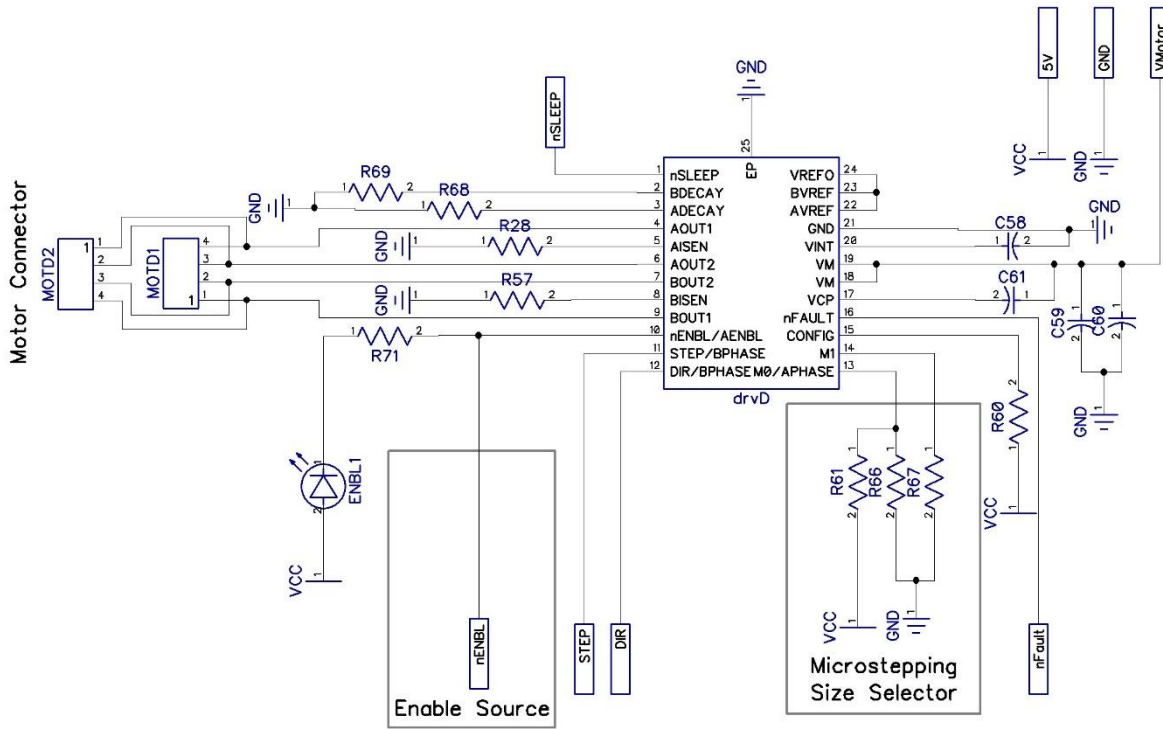


Figure 5: Double stepper motor driver schematic

Double DC Motor Driver

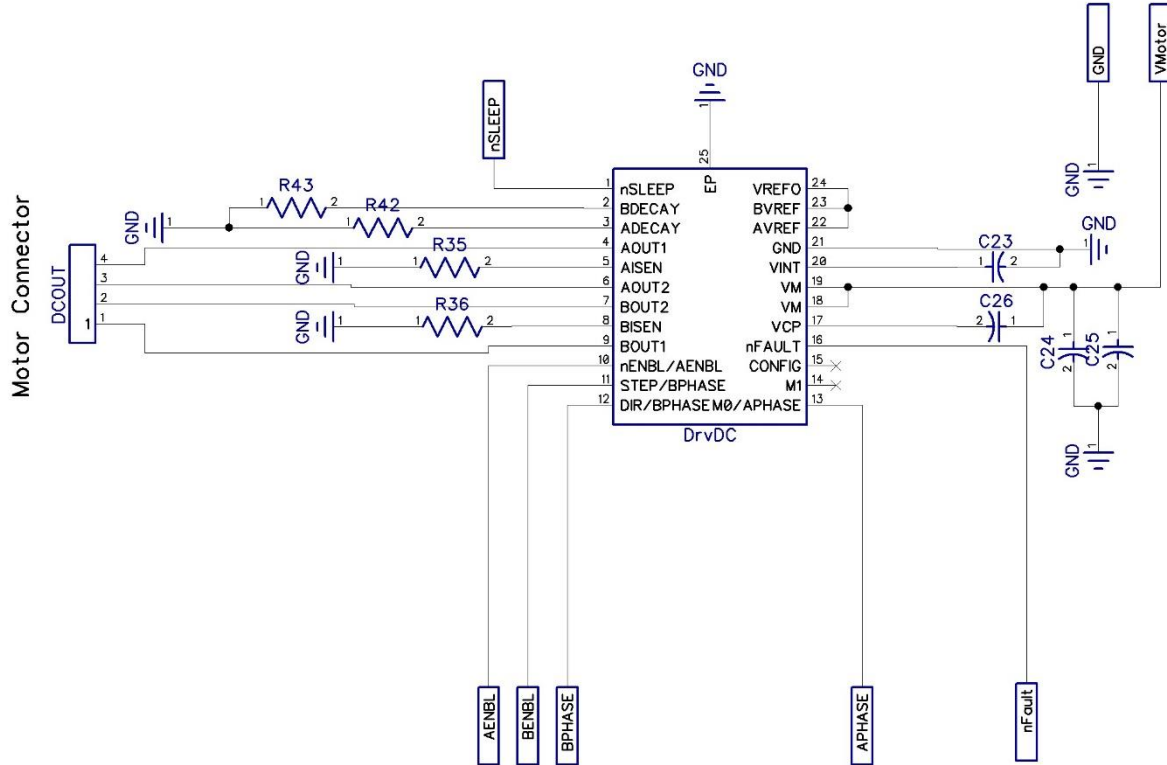


Figure 6: Double DC motor driver schematic.

Forcer Sensor

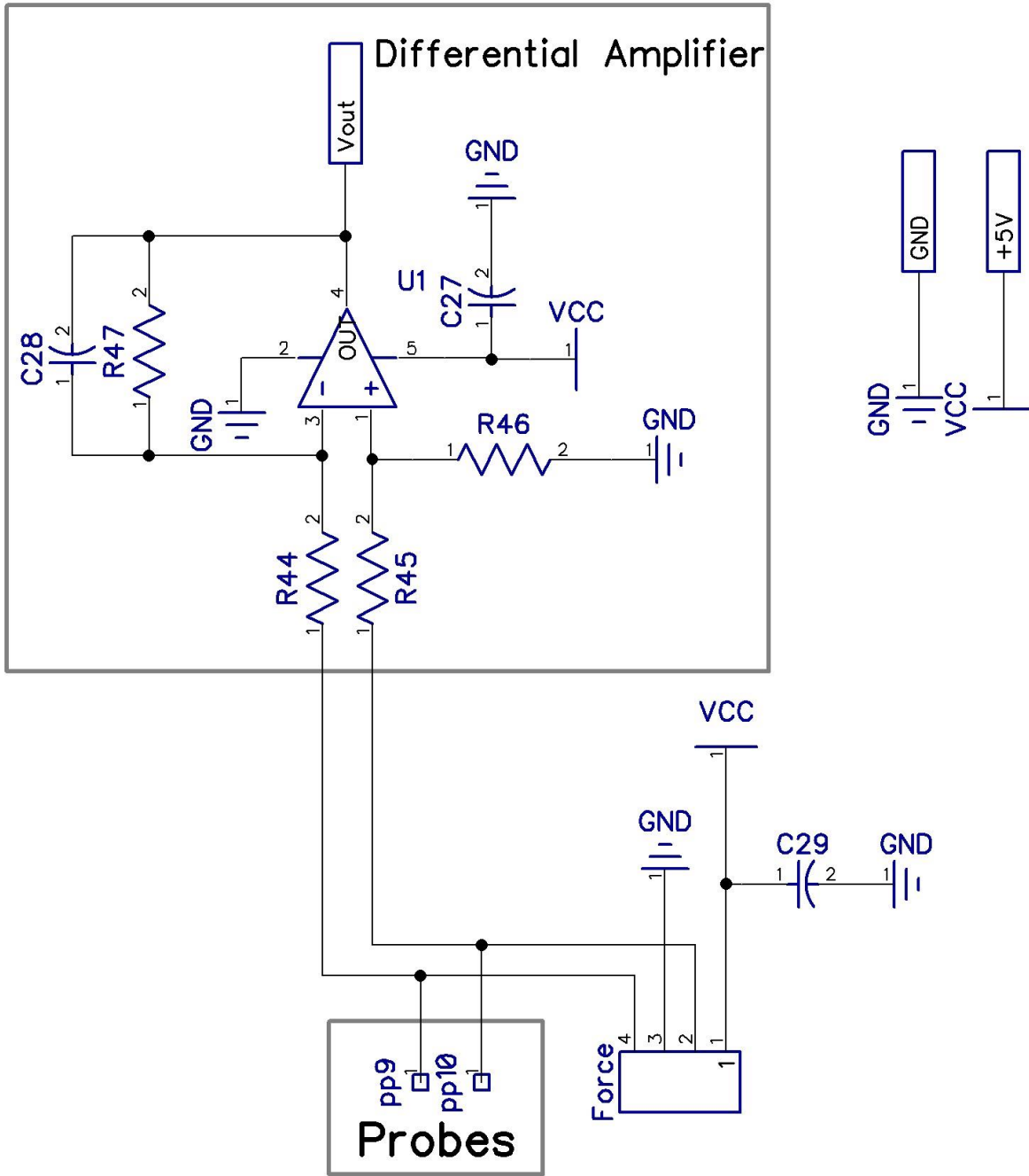


Figure 7: Schematic for force sensor.

# FTDI

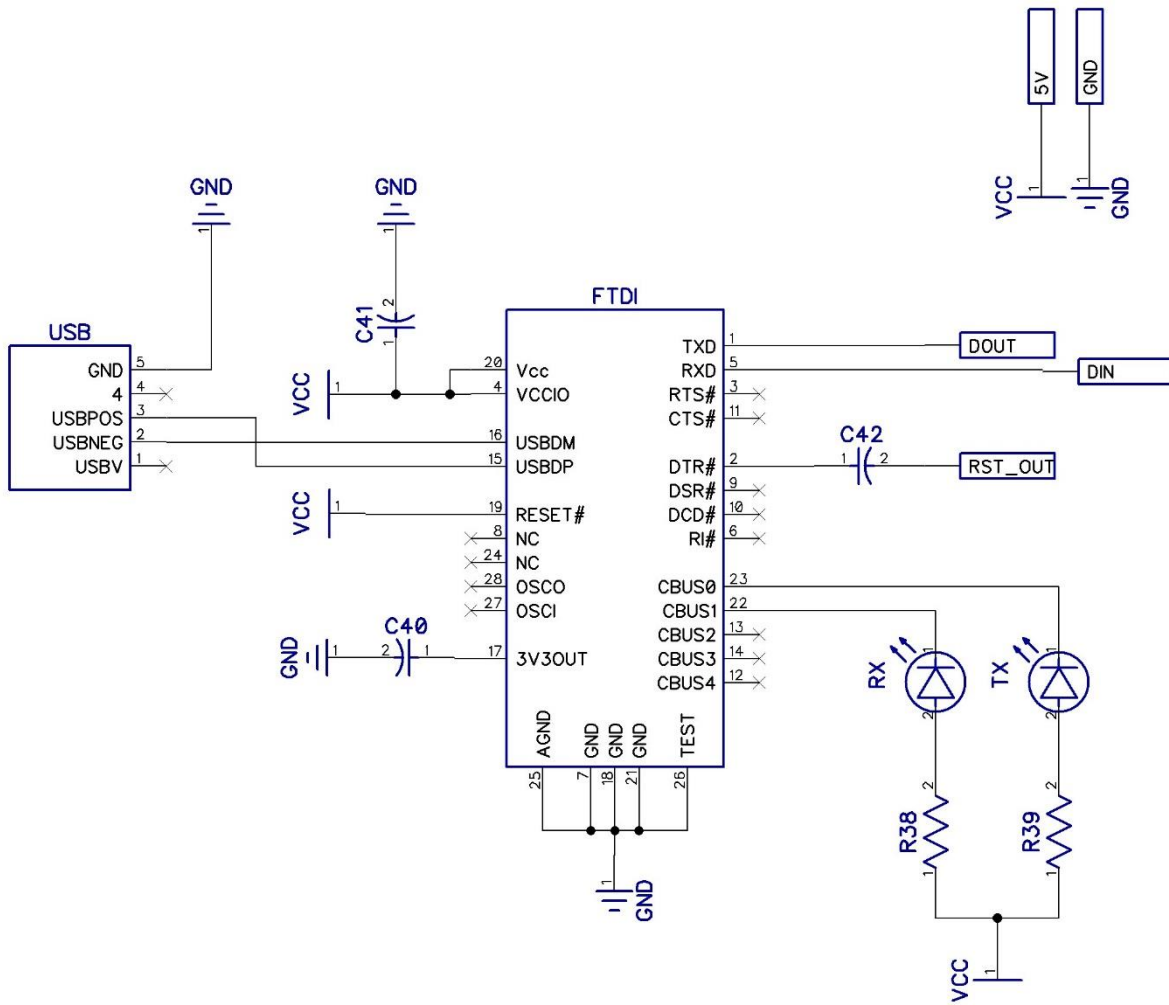


Figure 8: Schematic for FTDI.

Power Regulation

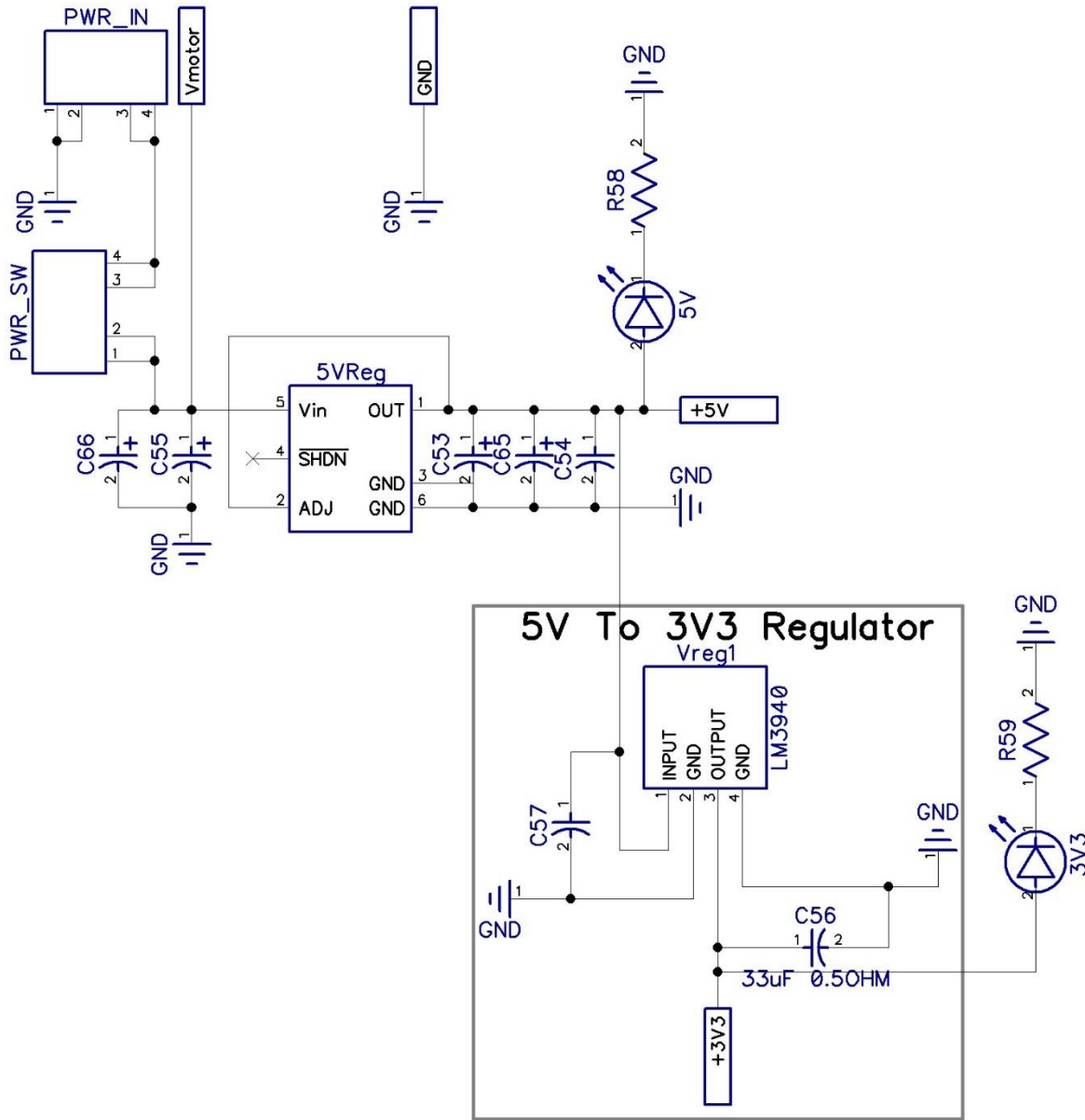


Figure 9: Schematic power regulation.

Level Shifter

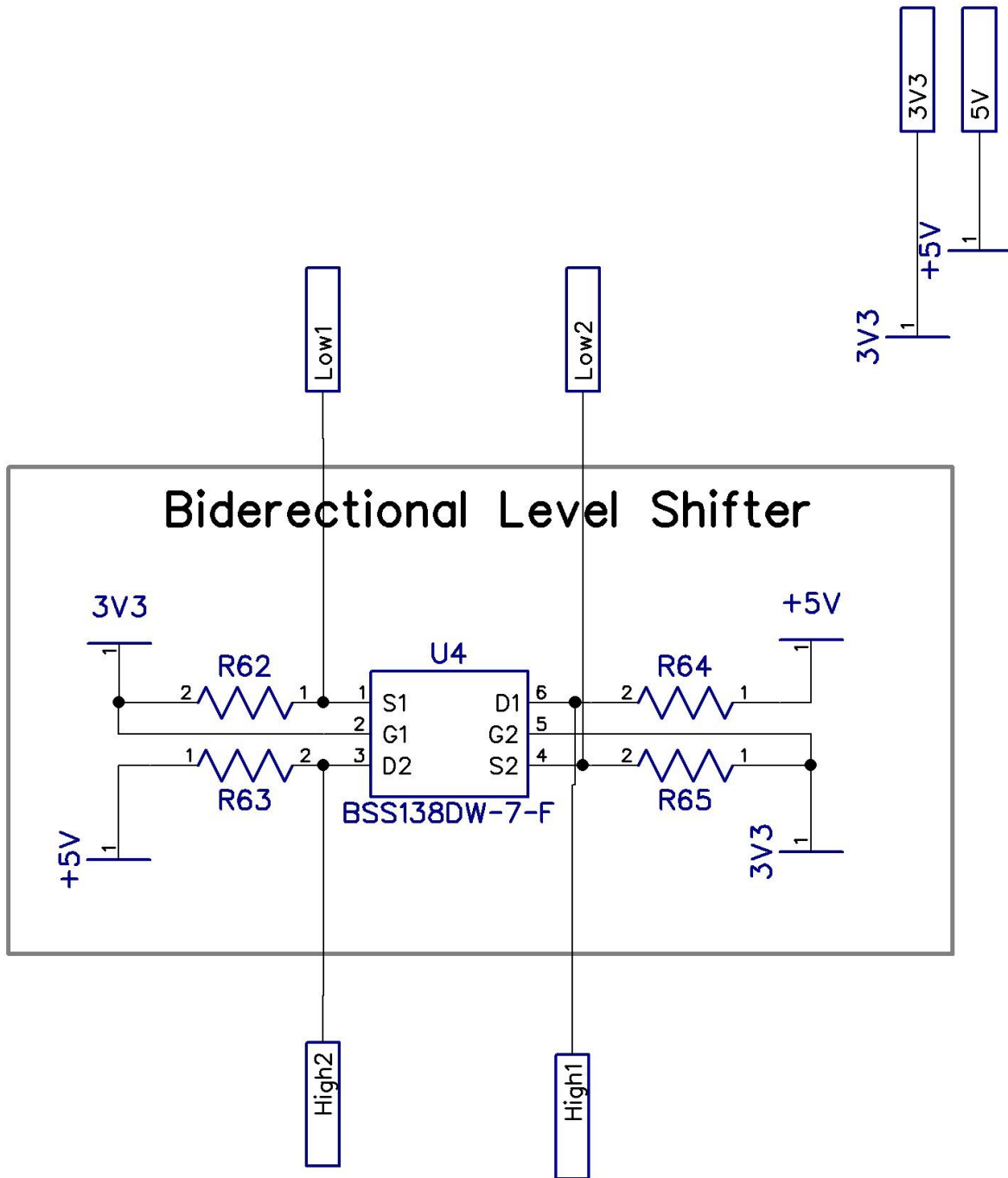


Figure 10: Level shifter schematic.

# Pressure Sensor

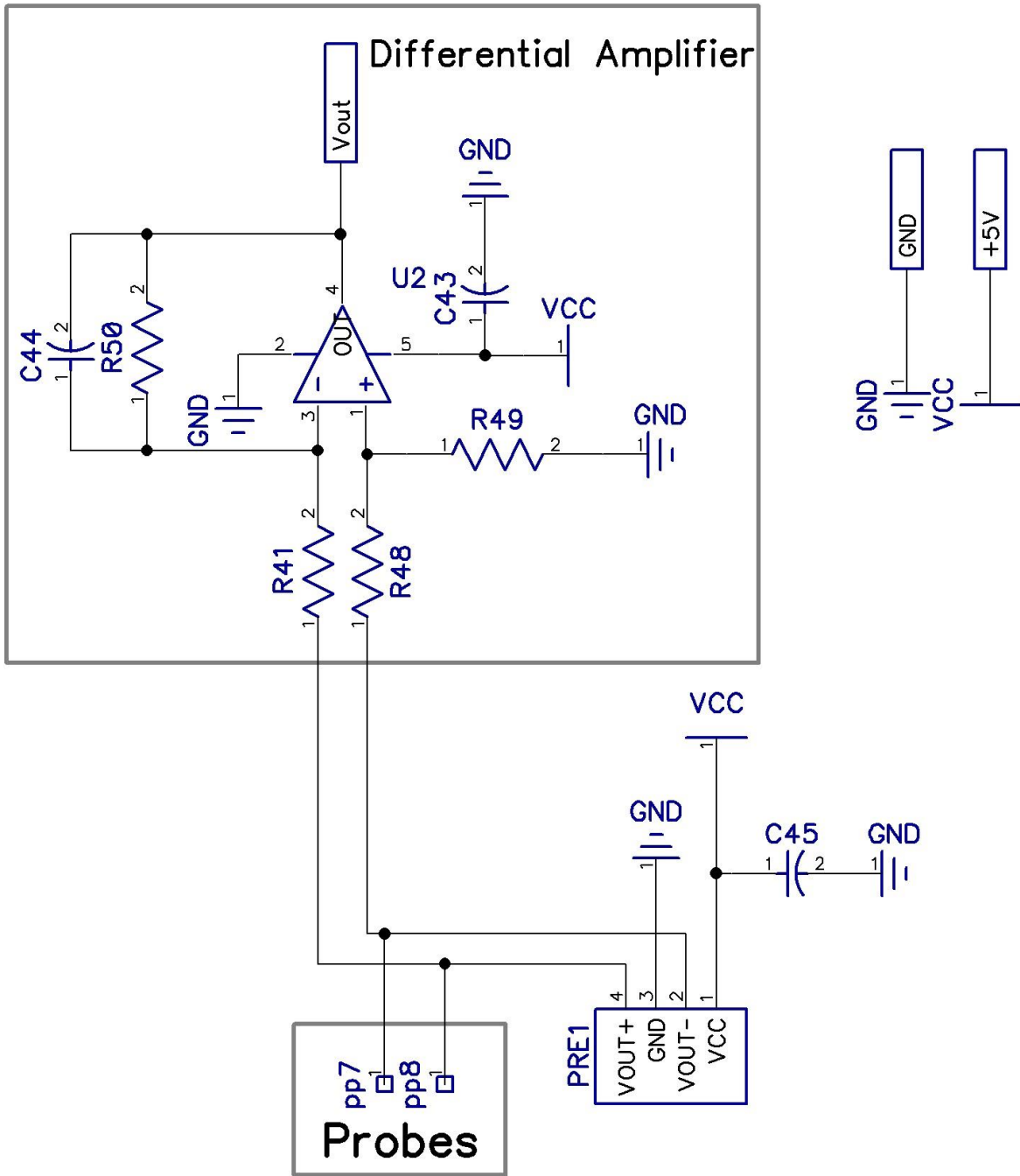


Figure 11: Pressure sensor schematic.



## End Stop

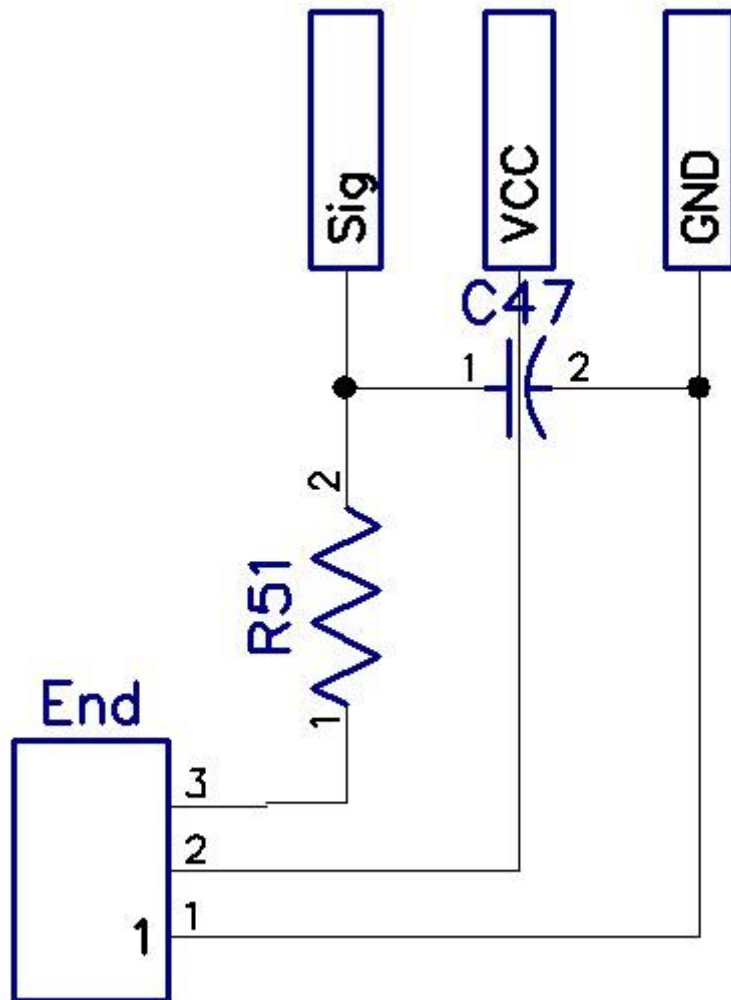


Figure 12: End stop schematic.

# LDR

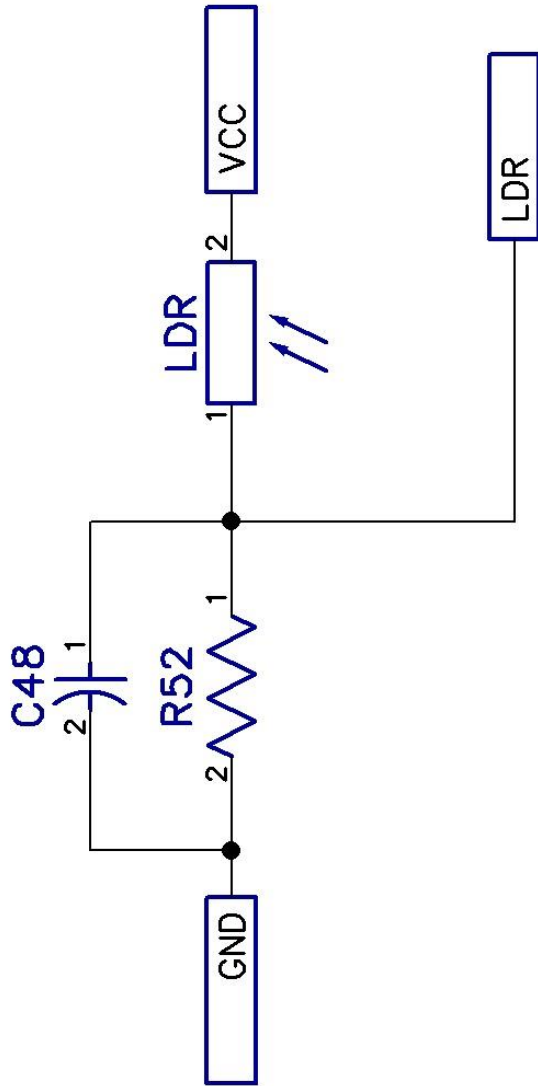


Figure 13: LDR Schematic.

# IMU

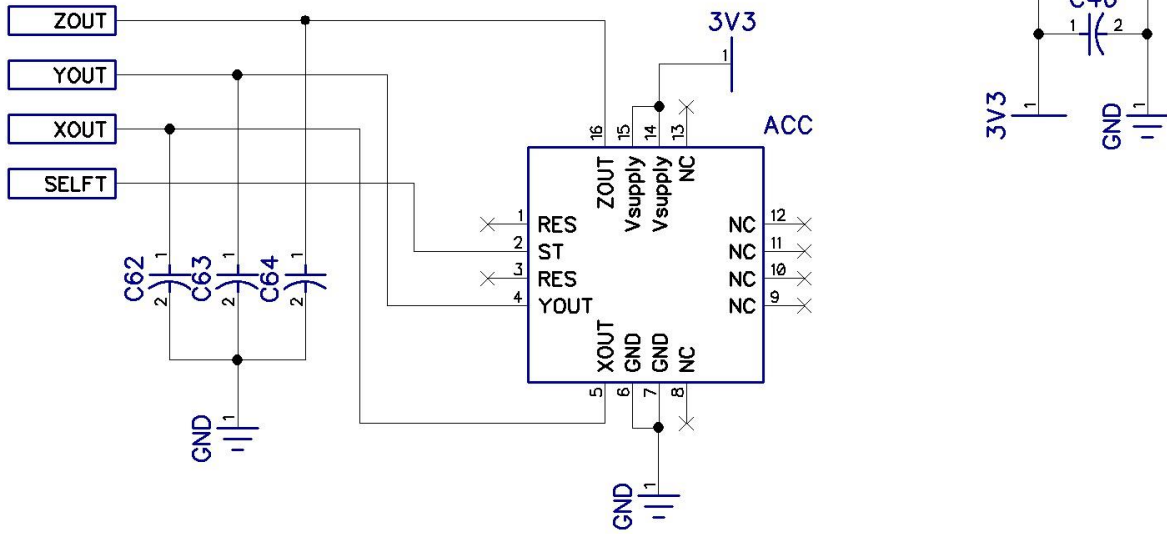


Figure 14: IMU Schematic.

# Solenoid

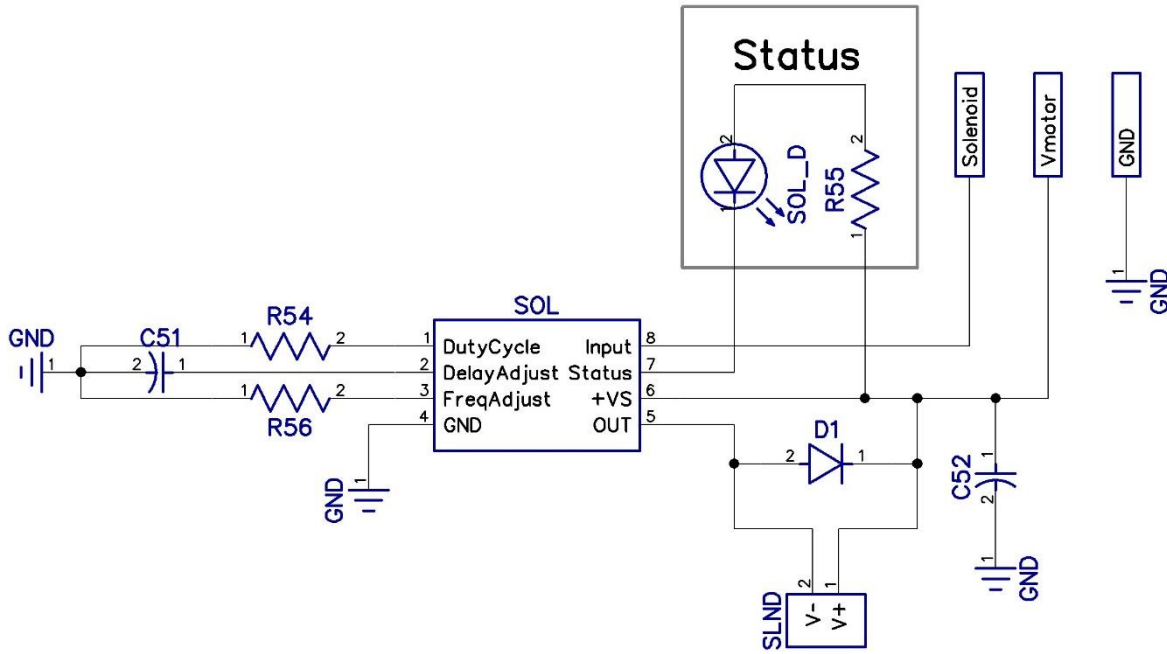


Figure 15: Solenoid schematic.

# PCB Art

## Top Layer

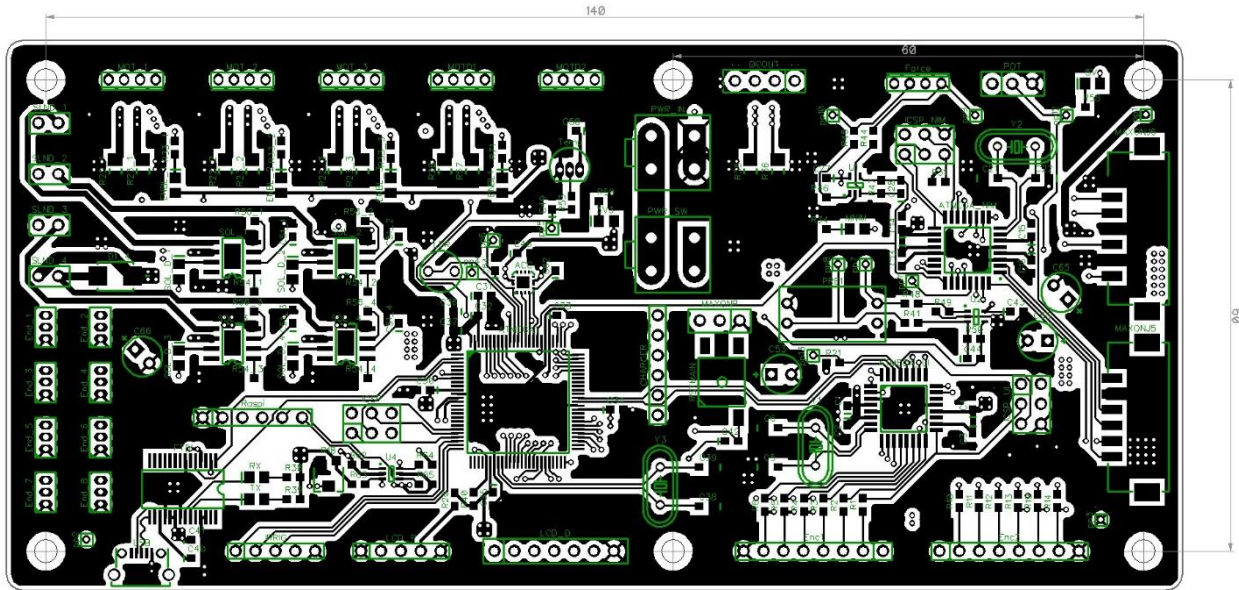


Figure 16: Top layer PCB art.

## Inner Layer 1: GND

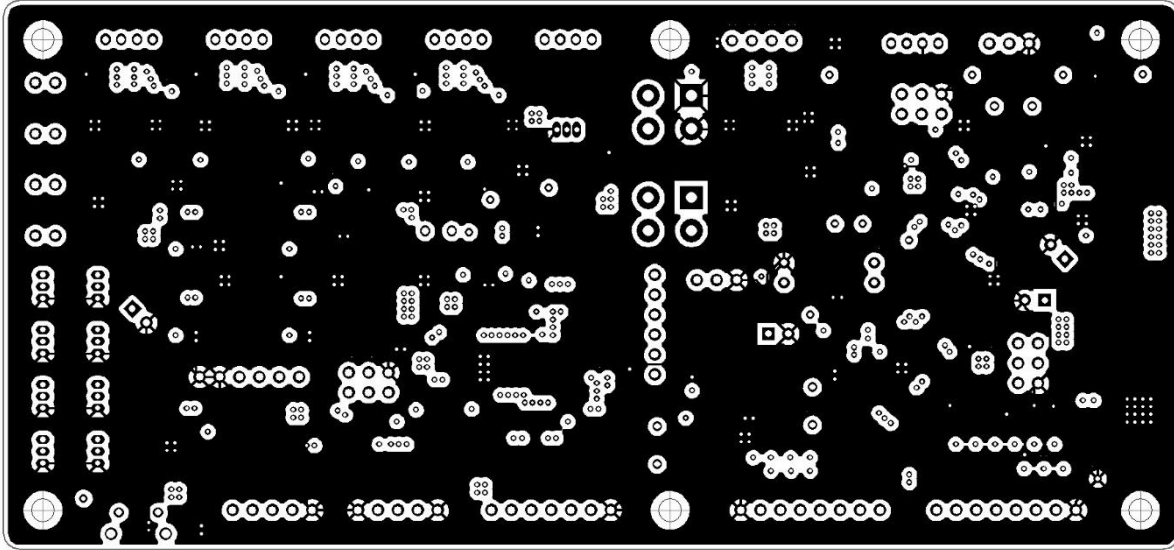


Figure 17: Inner layer 1 of PCB art.

## Inner Layer 2: Power + Data

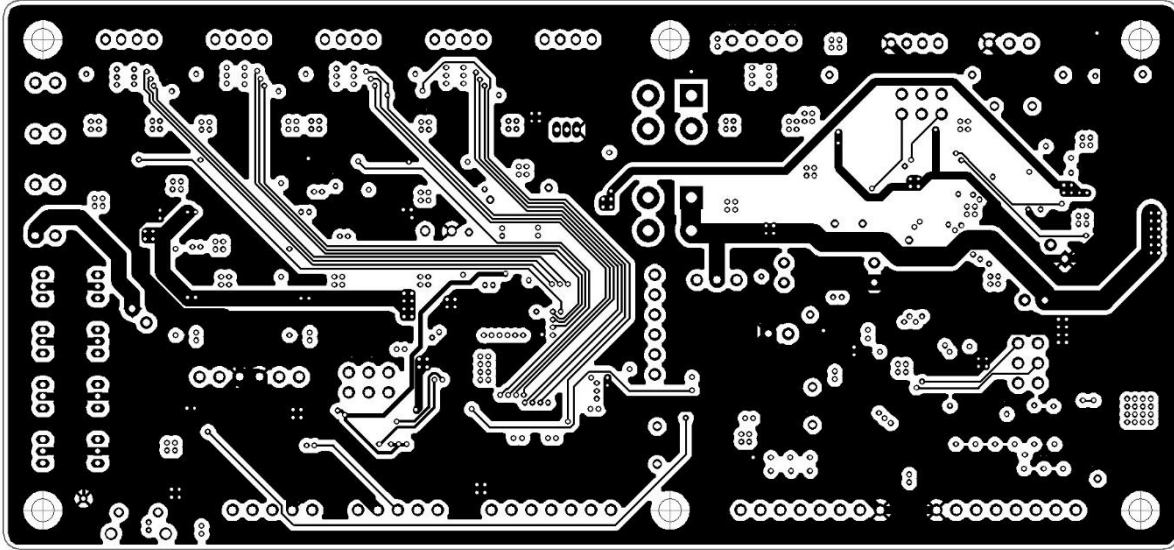


Figure 18: Inner layer 2 of PCB art.

## Bottom Layer

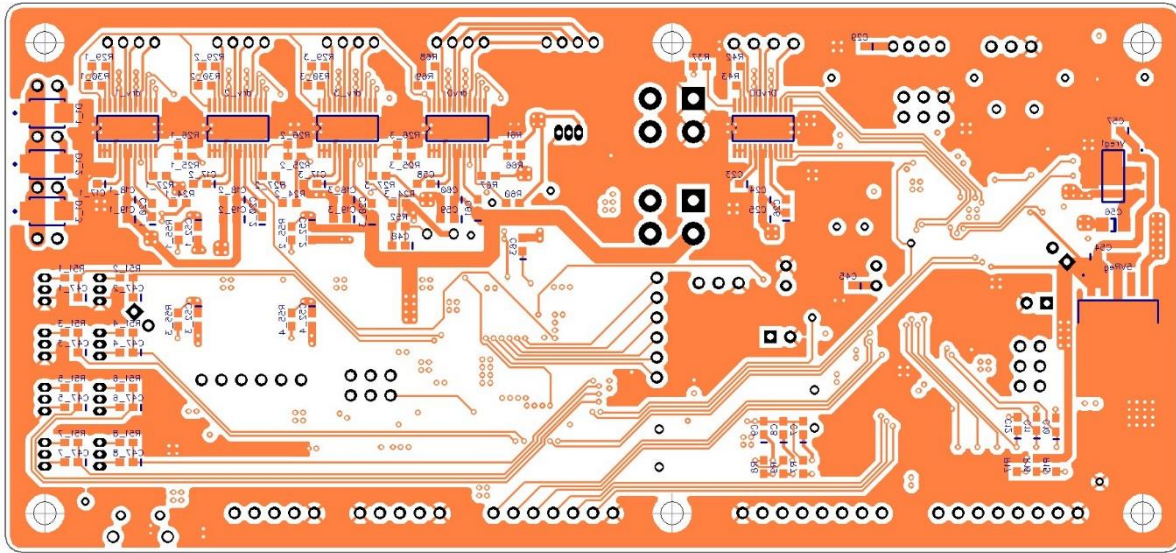


Figure 19: Bottom layer of PCB art.



## Table of Components

The table below summarizes the function and lists all components required for proper assembly of the board.

Reference	Type	Value	Description
3V3, 5V, ENBL_n, ENBL1, MNIM, RX, TX, SOL_D	LED	LED 0805	Indicator LEDs
5VReg	V Reg	LT1529CQ-5	Main regulator (5V)
ACC	ACC	ADXL337	3-Axis Analog Accelerometer
ATMEGA1	MCU	ATMEGA2560 TQFP	Main Microcontroller
ATMEGA_NIM, ATMEGA_UI	MCU	ATMEGA328P TQFP	Support Microcontrollers
C1-C4, C13-C16, C30-C34, C36	CAP 0603	100 nF	MCU Decoupling Capacitors
C5, C6, C21, C22, C38, C39	CAP 0603	20 pF	Crystal Load Capacitors
C7-C12	CAP 0603	10 nF	Encoder Decoupling Capacitors
C17_n, C23, C58	CAP 0603	2.2 uF	Internal Decoupler Cap for Stepper Driver (VINT)
C18_n, C24, C59	CAP 0603	100 nF	Decoupler for Stepper Driver (VM)
C19_n, C25, C60	CAP 0603	10 uF	Decoupler for Stepper Driver (VM)
C20_n, C26, C61	CAP 0603	10 nF	Decoupler for Stepper Driver (VCP)
C27, C29	CAP 0603	100 nF	Decoupler for Force Sensor Circuit
C28	CAP 0603	20 pF	Force Sensor Low Pass Filter
C35, C37	CAP 0603	1 uF	Decoupler for ATMEGA1 Analog Supply
C40, C41, C42	CAP 0603	100 nF	Part of FTDI Circuit (Decoupler, Debouncer)
C43, C45	CAP 0603	100 nF	Decoupler for Pressure Sensor Circuit
C44	CAP 0603	20 pF	Pressure Sensor Low Pass Filter
C46	CAP 0603	100 nF	Decoupler for IMU
C47	CAP 0603	10 nF	Debouncer for End Stop
C48	CAP 0603	10 nF	Low Pass Filter for LDR
C49	CAP 0603	10 nF	Low Pass Filter for Temperature Sensor
C50	CAP 0603	100 nF	Decoupler for Temperature Sensor
C51_n	CAP 0603	100 nF	Delay Adjust Capacitor for Solenoid Driver
C52_n	CAP 0603	10 uF	Decoupler for Solenoid Driver
C53, C55, C65, C66	CAP E	100uF 20V	Main (Large) Decoupling Capacitors
C54	CAP 0603	100 nF	Main (Small) Decoupling Capacitor
C56	CAP T 1206	33uF 0.5 OHM	3V3 Decoupling Capacitor
C57	CAP 0603	1 uF	3V3 Regulator Input Decoupler
C62-C64	CAP 0603	100 nF	Low Pass Filter for IMU Outputs
CHARGER	CON	6x2.54mm Header	Connects to Charging Circuit Board
D1_n	Diode	S1GB-13-F	Diode for Solenoid Quenching
DCOUT	CON	640456-4	Connector for DC Motors
DRV, DRVD, DRVDC	Driver	DRV8834	Stepper Motor Driver
ENC1, ENC2	CON	640456-8	8 Pin Header for Connection to Encoders

END	CON	B3B-ZR(LF)(SN)	1.5mm JST Connector for End Stops
FORCE	CON	640456-4	4 Pin Header for Connection to Force
FTDI	FTDI	FT232RL	UART to USB Converter
ICSP, ICSP_NIM, ICSP_UI	CON	2X3 POS 2.54mm	Headers for Programming of Board
IRRIG, LCD_P	CON	640456-5	5 Pin Header for Connect to IRRig and LCD Power
LCD_D	CON	640456-7	7 Pin Header for Connection to LCD Data
LDR	SENSE	PDV-P8103	Light Dependent Resistor
MAXONJ5	CON	DF3DZ-6P-2V(50)	Connector for Maxon Digital Pins
MAXONJ6	CON	DF3DZ-7P-2V(20)	Connector for Maxon Analog Pins
MAXONP	CON	3X2.54mm Header	Connector for Maxon Power
MOT,MOTD1,MOTD2	CON	B4B-PH-K-S	Connector for Stepper Motors
POT	CON	640456-3	Connector for External Potentiometer (Ex: Firgelli)
PP1-PP13	PP	--	Probe Points
PRE1	SENSE	TBPDANS015PGUCV	Pressure Sensor
PWR_IN,PWR_SW	CON	39-28-1043	Power Input and Output to Switch
R1-R3,R10-R12	RES 0603	150 OHM	Current Limiter to Encoder LEDs
R4-R6,R13,R14,R19	RES 0603	150 OHM	Part of Debouncing Circuit for Encoders
R7-R9,R15-R17	RES 0603	10 KOHM	Pullers of Encoder Outputs
R18	RES	P3V103CT-ND	10 KOHM Trimmer for LCD Contrast
R20	RES 0603	10 OHM	Current Limiter for LCD Backlight
R21,R31,R40	RES 0603	10K OHM	Pull Up for MCU Reset
R22_n,R23_n,R28,R57, R35,R36	RES 1206	620m OHM 1/2W 1%	Current Setting for Stepper Drivers
R24,R60	RES 0603	47 KOHM	Pull up for Stepper Driver (CONFIG)
R25_n,R26_n,R27_n, R61,R66,R67	RES 0603	SEE TABLE	Microstepping Size Selector for Stepper Driver
R29,R30,R42,R43, R68,R69	RES 0603	49K9 OHM	Decay Rate Selector for Stepper Driver
R33,R34,R38,R39, R55,R58,R71	RES 0603	150 OHM	Current Limiter for Indicator LEDs
R37	RES 0603	47K OHM	Pull Up for Double DC Driver (nSLEEP)
R41,R48	RES 0603	100 OHM	Part of Pressure Sensor Gain Circuitry
R44,R45	RES 0603	1 KOHM	Part of Force Sensor Gain Circuitry
R46	RES 0603	100 KOHM	Part of Force Sensor Gain Circuitry
R47	RES 0603	100 KOHM	Part of Force Sensor Gain Circuitry
R49	RES 0603	100 KOHM	Part of Pressure Sensor Gain Circuitry
R50	RES 0603	100 KOHM	Part of Pressure Sensor Gain Circuitry
R51	RES 0603	150 OHM	Part of End Stop Debouncing Circuit
R52	RES 0603	10K OHM	Voltage Divider with LDR
R53	RES 0603	150 OHM	Part of Low Pass Filter for Temperature Sensor
R54	RES 0603	47K OHM	Duty Cycle Selector for Solenoid Driver
R56	RES 0603	100 KOHM	Frequency Selector for Solenoid Driver
R59	RES 0603	100 OHM	Current Limiting Resistor for 3V3 Indicator LED

R62-R65	RES 0603	10K OHM	Part of Logic Level Shifter
RASPI	CON	640456-6	6 Pin Connector to Raspberry Pi
RSTMAIN	Switch	FSMJSMA	Tactile Switch for MCU RST
SLND	CON	640456-2	Connectors for Solenoids
SOL	Driver	DRV103	Solenoid Drivers
Temp	SENSE	TMP37	Temperature Sensor
U1,U2	OP AMP	LMV321	Operation Amplifier for Pressure and Force Sensor
U4	MOSFET	BSS138DW-7-F	Part of Level Shifter for UART to Rasp Pi
USB	CON	609-4618-1-ND	Micro USB Connector from FTDI
Vreg1	V REG	LM3940	5V to 3V3 Regulator
Y1-Y3	XTAL	16 MHz 20 pF	Crystal for MCU

<sup>1</sup> Unless indicated otherwise all capacitors are ceramic

## Errata

<b>Error</b>	<b>Description</b>	<b>Date</b>
Encoder Con Flipped	One of the encoder connectors are flipped. Aesthetically unpleasing.	11/4/14
Solenoid Drivers Unconnected	The solenoid drivers are not connected to the microcontroller. Can be soldered with wires to the charger pins temporarily.	12/13/14

Last Edited: January 15, 2015

# Appendix F

## Low-Level Communication Protocol



# INTERFACE DOCUMENT

## Low Level Communication Protocols V2

### Summary

This document contains a full description of the low level protocols used for communication within the Main Board V2.

## Table of Contents

Table of Tables .....	2
Overview .....	3
Packets .....	4
Overview .....	4
Frame ID and Messages .....	4
Summary .....	7
Errata .....	8

## Table of Tables

Table 1: Overview of outgoing packets.....	4
Table 2: Description of frame IDs and messages for outgoing transmission. ....	4



## Overview

This manual contains all information necessary for implementing the communication protocol within and between the MainBoardV2 of the Phlebot MQP and a computer. The packet is optimized for bandwidth and is ubiquitous among all communicable devices.

# Packets

## Overview

Table 1: Overview of outgoing packets.

Name	Start Delimiter	Length <sup>1</sup>	Frame ID	Message	Checksum
Size (Bytes)	1 (0xFD)	1	1	NA	1

<sup>1</sup>Number of bytes between the length and checksum fields. Does not include length, checksum or start delimiter.

<sup>2</sup>0xFF minus 8-bit sum of bytes between the start delimiter and checksum fields.

The above protocol version is meant for high speed low latency transmission of data. The message length is allowed to vary for optimization purposes and a checksum insures data integrity. A hand-shake is used for guaranteeing message reception.

## Frame ID and Messages

Table 2: Description of frame IDs and messages for outgoing transmission.

Frame ID	Description	Size
0x10	Requests the receiving device to report the state of the stepper driver nFAULT and ENABLE lines.	0
0x1[1-4]	Sets the desired stepper motor position for the corresponding stepper. Ex: 0x11 0x00 0xFF; sets stepper motor 1 to position 255.	2
0x15	Sets the speed of the stepper drivers. More precisely determines the minimum time between steps in microseconds.	8
0x16	Returns the state of the ENABLE lines appended with nFAULT lines as a single byte. Usually in response to 0x10 header. Ex: 0x16 0b11011001; means that ENABLE lines for motors 1,2 and 4 are HIGH while nFAULT lines for motors 1 and 4 are HIGH.	1
0x17	Requests the prototype to return the current position of all stepper motors.	0
0x18	Sets motors to home. Message byte corresponds to the motors that should home. Ex: 0x18 0b10010000; means that motors 1 and 4 should home.	1
0x19	Gets motors to home. Returns which motors are currently set to home. Ex: 0x19 0b10000000; indicates that motor 1 is set to home.	1
0x1A	Reports the position of all stepper motors.	8
0x1B	Reports the desired position of all stepper motors.	8
0x1C	Requests the desired position of all stepper motors.	0
0x1D	Requests the motors that have homed.	0
0x1E	Reports which motors have homed as a single byte. Ex: 0x1E 0b11000000; indicates that the first two motors have homed.	1
0x1F	Reports the current speed of the stepper motors as unsigned integers.	8
0x20	Sets the state of each solenoid as a single byte appended with zeros. Ex: 0x20 0b11010000; turns ON solenoids 1, 2, 4 and powers off solenoid 3.	1
0x21	Returns the state of each solenoid as a single byte appended with zeros. Ex: 0x21 0b11010000; Means solenoids 1, 2, 4 are ON while solenoid 3 is OFF.	1
0x22	Requests that the state of the solenoids be sent as a single byte.	0

0x30	Request for update on values of all sensors.	0
0x31	Sends the raw IMU readings for the three axis in the order X, Y, Z. Ex: 0x31 0x00 0x00 0x00 0x01 0x00 0x02; means that the X, Y, Z analog reads are 0, 1 and 2 respectively.	6
0x32	Sends the raw temperature reading. Ex: 0x32 0x01 0x00; means the temperature reading is of 256.	2
0x33	Sends the raw LDR reading. Ex: 0x33 0x00 0xFF; means the ADC reading from the LDR is 255.	2
0x34	Sends the raw reading from the force sensor. Ex: 0x34 0x00 0x01; means the force sensor has a reading of 1.	2
0x35	Sends the raw reading from the pressure sensor. Ex: 0x35 0x00 0x01; means the pressure sensor has a reading of 1.	1
0x36	Sends the raw ADC reading from the potentiometer. Applicable to NIM MCU. Ex: 0x36 0x00 0x00; means the potentiometer is returning a value of 0.	2
0x37	Sends the raw ADC reading from the 3V3 bus voltage rail. Ex: 0x37 0x00 0x10; means that the current voltage reading is 16 ADC ticks.	2
0x40	Returns the value of all end stops of the prototype as a single byte. Ex: 0x40 0b11111110; indicates that all end stops except end-stop 8 are triggered.	1
0x41	Returns the mode as either input (end-stop) or output (servo, GPO) of each end-stop connector. Ex: 0x41 0b11110000; indicates that the first 4 connectors are configured as end-stop while the last four (5-8) are servos.	1
0x42	Requests the status of all end stops. Does not contain a message.	0
0x43	Requests the type (input or output) of each end-stop. Does not contain a message.	0
0x50	Requests that the UI be locked to user input.	0
0x51	Requests that the UI query user with a specific message: <ul style="list-style-type: none"> <li>• 0x00: EXAMPLE TEXT: Y/n</li> <li>• 0x01: EXAMPLE TEXT: Y/NA/n</li> </ul> Ex: 0x51 0x00; Requests that the UI query the user with the message provided after the colon and options after second colon.	1
0x52	Returns the result of a query to the user. First byte is the query value and second byte is the query result. Ex: 0x52 0x00 0x03; means that the result of query of value 0 is 3.	2
0x53	Requests the UI to display specific messages: <ul style="list-style-type: none"> <li>• 0x00: EXAMPLE TEXT</li> </ul> Ex: 0x52 0x00; Requests that text 0 be displayed on UI.	1
0x54	Recedes previous request that the UI be blocked by the user.	0
0x60	Requests that the IRRig be set to the following PWM values. Ex: 0x60 0x00 0x05 0xFA; means that the IRRig PWM will be set to 0, 5 and 250 for each of its independent wavelengths.	3
0x61	Requests the value of the IRRig PWMs. The UI controller will usually issue this command to the ATMEGA2560.	0
0x62	Returns the value of the IRRig PWMs as three bytes. Ex: 0x62 0x00 0x05 0xFA; means that the IRRig PWM is set to 0, 5 and 250 for each of its independent wavelengths.	3
0x70	RESERVED FOR NIM: Requests that the controller start an insertion	0
0x71	RESERVED FOR NIM: Requests that the controller end an insertion. Remove needle.	

0x72	RESERVED FOR NIM: Informs that a failure has occurred. Is followed by a byte with an identifier that related to the type of failure including: <ul style="list-style-type: none"> <li>• 0x01: Controller Related Failure</li> <li>• 0x02: Motor Related Failure</li> <li>• 0x03: Force Sensor Failure</li> </ul> Ex: 0x72 0x01; when received by the main MCU implies that the NIM microcontroller has had a motor controller failure.	1
0x73	RESERVED FOR NIM: Informs the failure mode. Byte containing different failure modes. Possible failure modes include: <ul style="list-style-type: none"> <li>• 0x01: Ignore failure.</li> <li>• 0x02: Emergency stop.</li> </ul> Ex: 0x76 0x01; when received after an error has been sent indicates that NIM controller should continue with insertion ignoring the current error.	1
0x75	SET and GET header. Can be used both for setting the desired speed of the NIM or to report (by the NIM MCU) the current desired speed. Is followed by two bytes of data. Ex: 0x75 0x00 0x01; when sent by the Main MCU to the NIM MCU, sets the desired speed to 1 unit.	2
0x76	SET and GET header. Can be used both for setting the desired force of the NIM or to report (by the NIM MCU) the current desired force. Is followed by two bytes of data.	2
0x77	SET and GET header. Can be used both for setting the desired position of the NIM or to report (by the NIM MCU) the current desired position. Is followed by two bytes of data.	2
0x7a	Requests all NIM sensors to be reported. Can be sent by the computer UI to request from the Main MCU the status of all NIM sensors or from the Main MCU to directly poll from the NIM.	0
0x7b	Returns the current reading from the NIM MCU. Ex: 0x7b 0x00 0x01; implies that the current is at 1 unit.	2
0x7c	Returns the speed reading from the NIM MCU.	2
0x7d	Returns the force reading from the NIM MCU.	2
0x7e	Returns the position reading from the NIM MCU.	2
0x78	RESERVED FOR NIM: Motor status update. TBA	TBA
0x80	Requests the return of the last checksum. May or not be successful.	1
0x81	Returns the last checksum on the receiving side.	1
0x82	Requests the cumulative count of start delimiter fail.	0
0x83	Returns the cumulative count of start delimiter fail as an unsigned integer. 0x83 0x00 0xFF; implies that 255 start delimiters have failed.	2
0x84	Requests the cumulative count of all checksum fails.	0
0x85	Returns the number of checksum fails as an unsigned integer. 0x85 0x00 0xFF; implies that 255 checksums have failed checking.	2
0x86	Requests the number of checksum passes. Usually correlates with number of successful packages unless there were header errors.	0
0x87	Returns the number of checksum passes as an unsigned integer. 0x86 0x00 0xFF; implies that 255 checksums have passed checking.	2
0x88	Requests the number of header fails.	0
0x89	Returns the number of header fails as an unsigned integer. 0x83 0x00 0xFF; implies that 255 headers have failed to parse.	2
0x90	Requests the loop time of the receiving device. Usually used to determine the loop time of the ATMEGA2560 which affects several	0

	parameters such as minimum step time and response time.	
0x91	Returns the loop time of the device as an unsigned integer.	2
0xA0	Requests the return of all motors that are currently set to home.	0
0xA1	Requests the current speed setting of all stepper motors.	0
0xE0	Requests the status of the reset lines to the support microcontrollers.	0
0xE[1-2]	Requests a RESET of the microcontroller. Ex: 0xE1 resets the support microcontroller 1. Microcontroller will be restored to normal state after reset.	0
0xE3	Returns the RESET line status of the support microcontrollers as a single byte. Ex: 0xE3 0b10000000; means that support MCU 1 has reset line HIGH while support MCU 2 has reset line low.	1
0xF0	Acknowledge proper receipt of package. Followed by the one byte checksum of the package whose receipt is being acked. Ex: 0xF0 0xF3 indicates that a package of checksum 0xF3 was received properly.	1
0xF1	Acknowledge completion of all pending commands.	0
0xF2	Indicates microcontroller is ready to receive new command/data/etc.	0
0xF3	Debugging header. Is followed by 20 characters of human readable error message.	20
0xFC	Reports the emergency stop condition of the microcontroller. Followed by a byte where 0xFF indicates activated and 0x00 is inactive. Ex: 0xFC 0xFF indicates microcontroller is in emergency stop.	1
0xFE	Removes emergency stop condition.	0
0xFF	Emergency Stop.	0

### Summary

Header	Description	Pi	NIM MCU	UI MCU
0x1X	Motor driver related headers. Serve both the stepper drivers as well as the DC motor driver.	Y	Y	Y
0x2X	Solenoid related commands	Y	N	Y
0x3X	Sensor data requests and sensing.	Y	Y	Y
0x4X	End-Stop/Servo related requests.	Y	N	Y
0x5X	UI Related commands.	Y	N	Y
0x6X	IRrig related commands	Y	N	Y
0x7X	NIM Controller related commands.	Y	Y	Y
0x8X	Communication related commands. Most for debugging.	Y	Y	Y
0x90	General debugging commands	Y	?	Y
0AX	Miscellaneous headers. Used for headers that did not have space in allotted series.	Y	Y	Y
0EX	Reset related commands	Y	N	N
0FX	High level commands and E-Stop.	Y	Y	Y

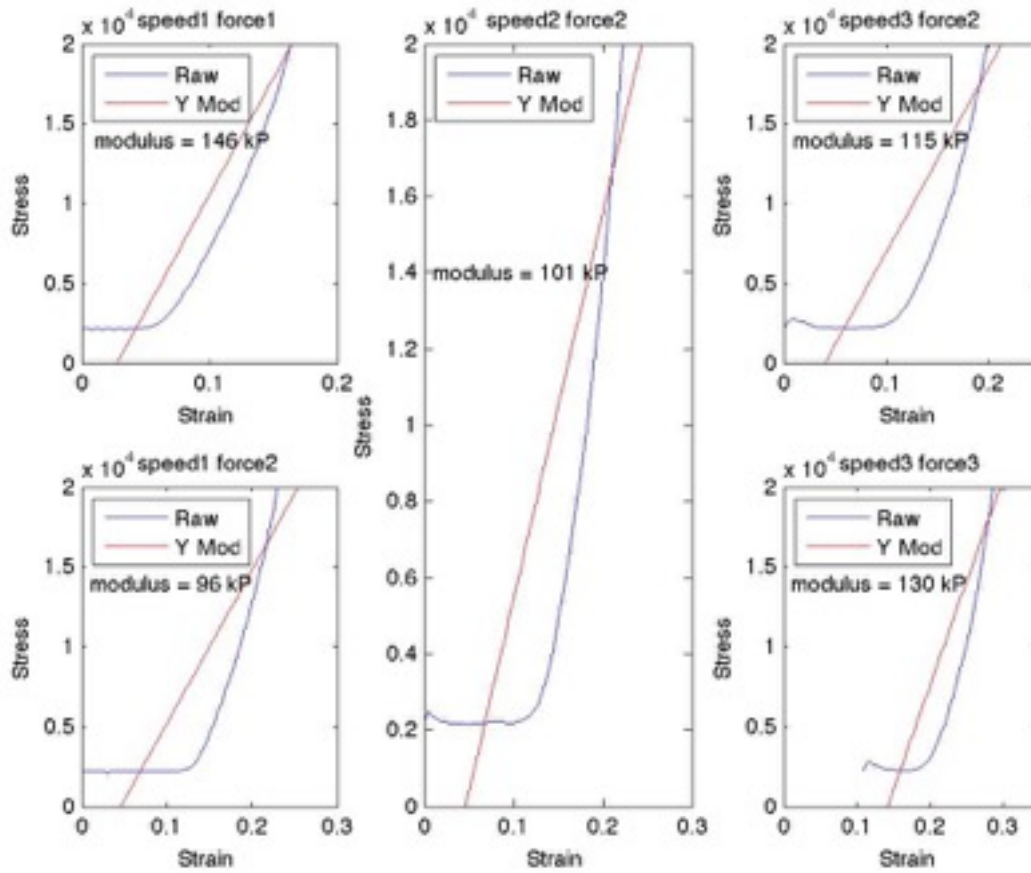
## Errata

Last Edited: November 7, 2014

# Appendix G

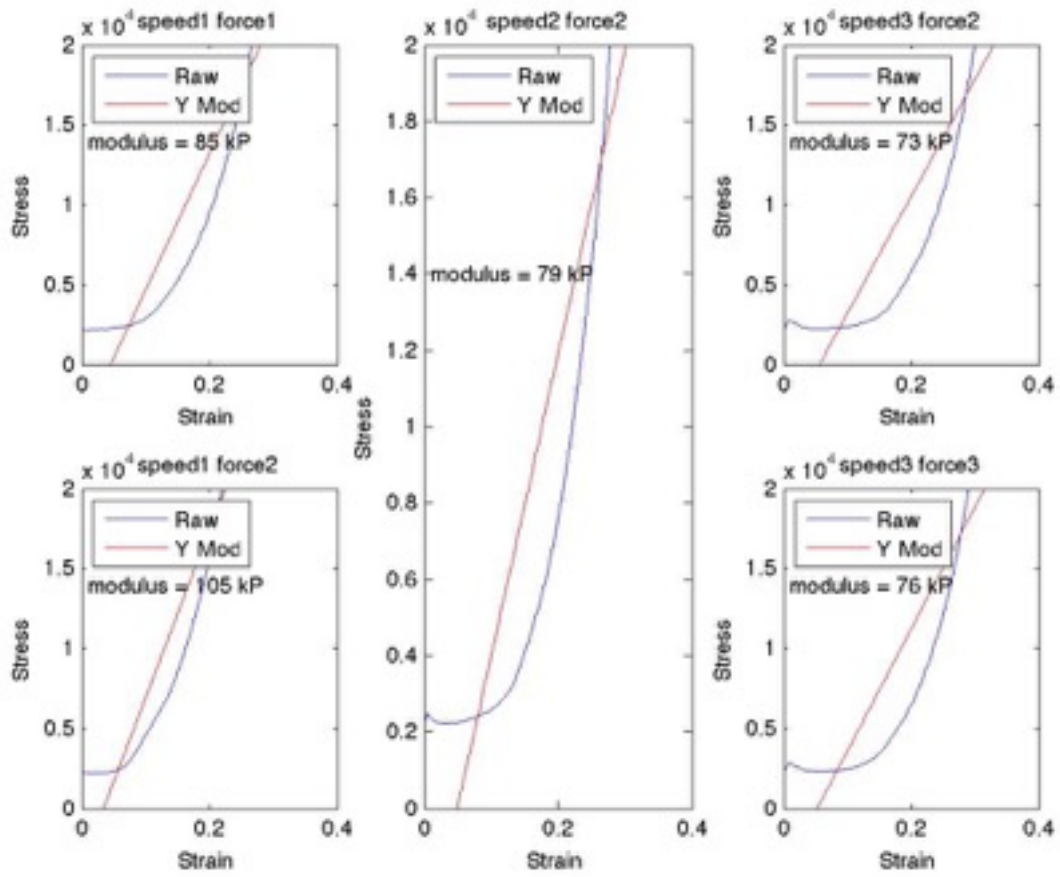
## Phantom Testing on Instron

# Appendix G

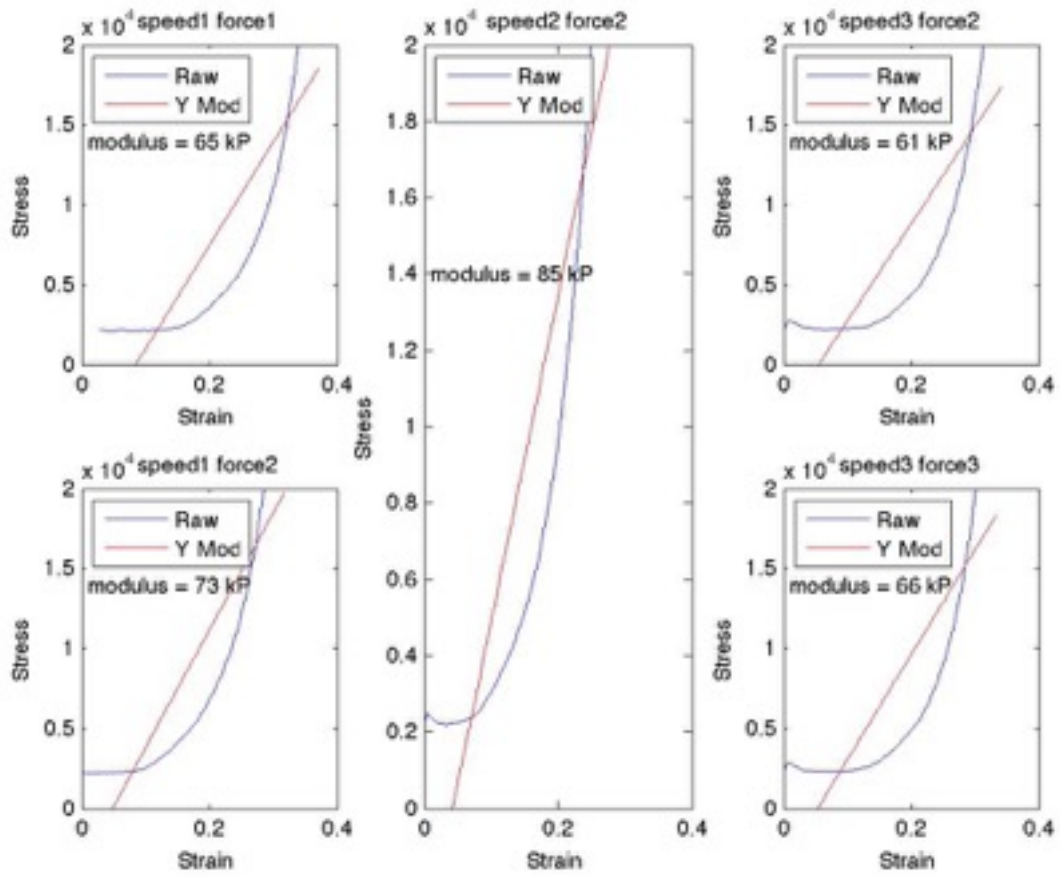


SAMPLE 1

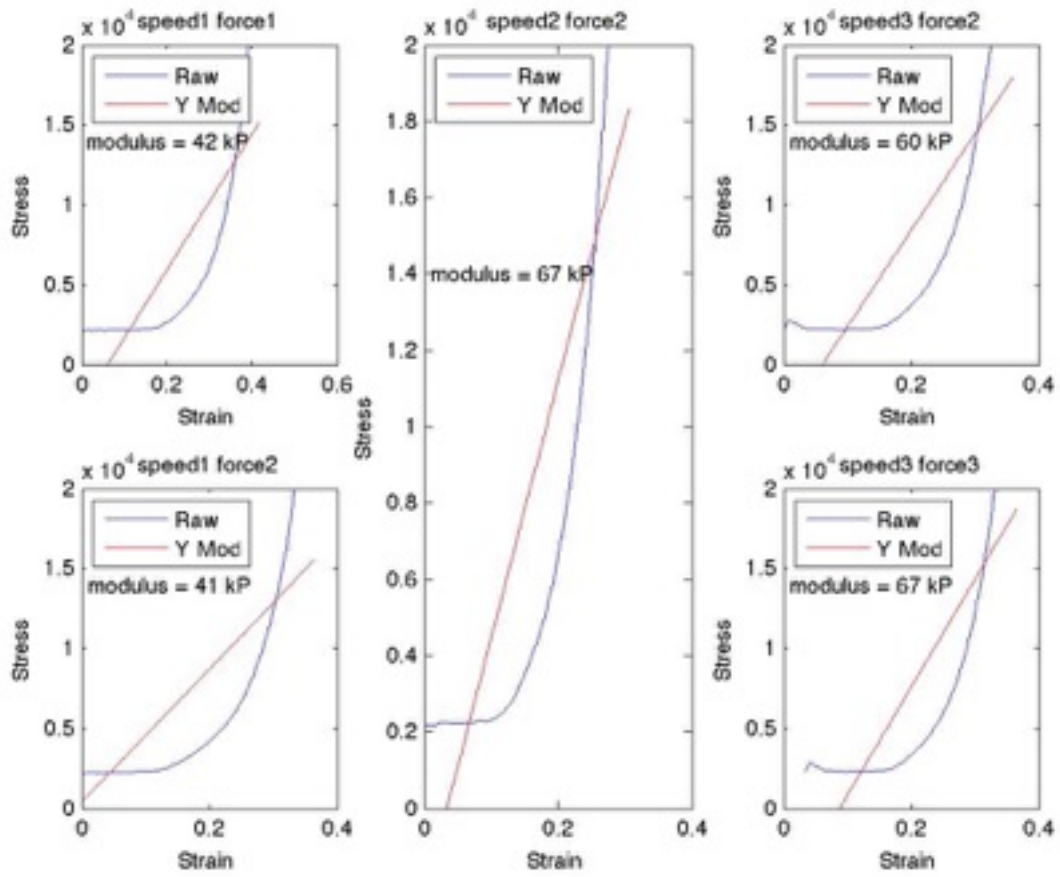




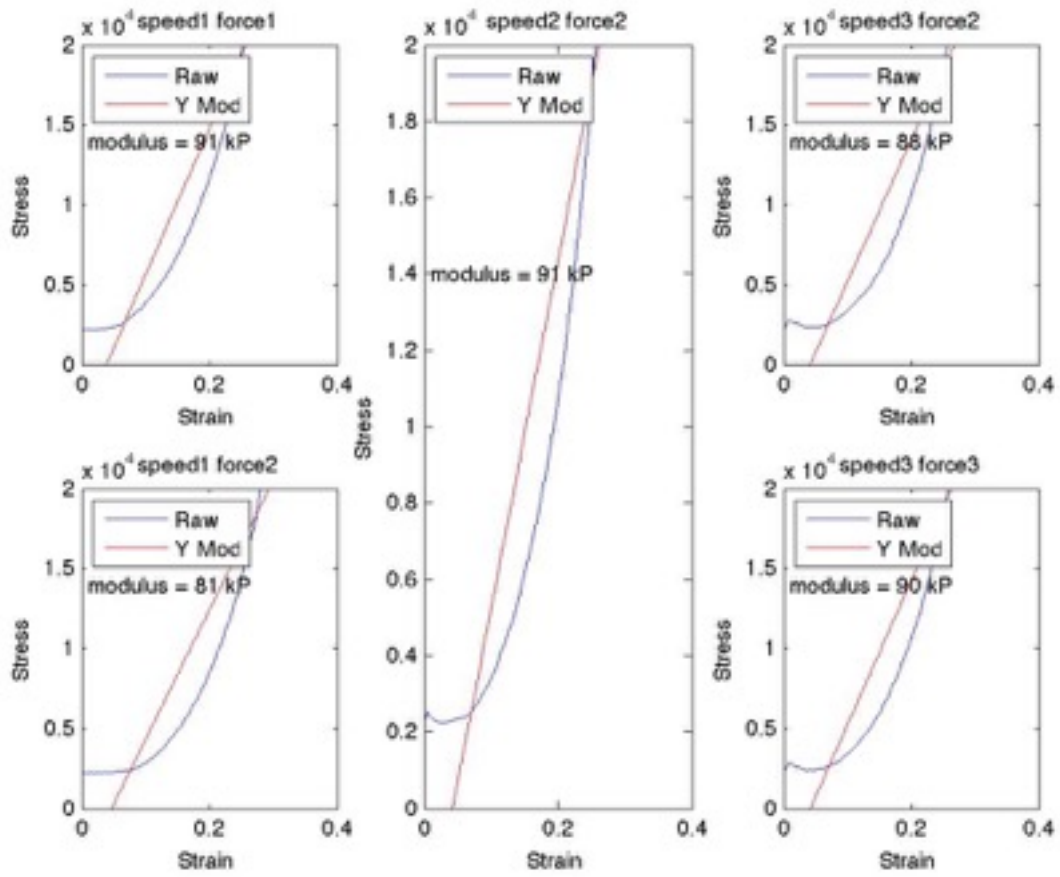
**SAMPLE 2**



**SAMPLE 3**



**SAMPLE 4**



**SAMPLE 5**

# Appendix H

## Notes on Failure Conditions

## **Phlebot MQP: Preliminary Notes on Possible Failure Conditions**

This paper will consider several possible failure scenarios for the robotic phlebotomist. These possible scenarios will be used in order to design the product in such a way that these conditions are less likely therefore making the robot safer. This paper will be organized by different levels of severity.

### SEVERE

- 1. Moving while Inserted:** A significant danger of the robotic assistant is that of non-insertion related motion once the needle has penetrated the skin. This can cause dilacerations and induce severe bleeding by rupturing the vessel. Possible safety mechanisms to prevent this problem include:
  - 1. Mechanical locking during insertion:** Once the insertion procedure is started a mechanical lock impedes motion of the motors not related to the mechanism that moves the needle towards the venipuncture point.
  - 2. Use of stepper motor:** By using a stepper motor it becomes unlikely that a hardware issue would cause the mechanism to move continuously. It would likely limit any hardware related malfunction to moving the carriage a maximum of one step in either direction.
  - 3. Software locking:** Once the procedure is started some software routine would lead to a “decoupling” of the mechanisms that control the motors involved in moving the carriage.
- 2. Inserting needle through vein:** Another major danger is puncturing the second wall of the vein during the insertion procedure. Several conditions can lead to this scenario including: Patient movement; over-insertion due to inaccuracies in the sensors; and, mis-calibration. Some mechanisms can be placed in order to reduce the likelihood of deep insertion including:
  - 1. Mechanical end stop:** A mechanical insertion limiter would impede that the needle be inserted too deep. This solution may be impractical as no a-priori knowledge towards the required depth of insertion is known during the setup of the device. This mechanical end stop could be automatically adjusting which would cause it to be more applicable. The adjusting would occur during the tactile feedback.
  - 2. Redundant vein penetration sensing:** As of the publication of this document the team appears to have settled on force sensing for detecting when the needle has penetrated

the vessel. Secondary mechanisms may could be implemented to ensure proper detection including:

1. IR Background Illumination
  2. Ultrasonic
  3. Flashback
3. **Dropping of blood:** Although unlikely, it is possible that when changing the vial that is being filled with blood the hose is left leaking blood. Assuming that the vial changing mechanism gets locked blood may be left leaking and lead the patient to shock and even death. This is a very severe condition but the inherent properties of the phlebotomy devices do not make this likely. This condition can be avoided by:
1. **Pressure based valve on hose:** Blood is only capable of going through the hose when connected to the vacuum cylinder.
  2. **Solenoid valve:** An electronically controlled valve only opens when the hose has been properly connected to vial.

#### MODERATE

1. **Wrong Insertion Location:** Under the condition that the mechanisms that limit insertion depth are operating well, this issue should only be an inconvenience. Nonetheless, this condition should be avoided as the whole premise of the robotic phlebotomist is to make a REALIABLE phlebotomy assistant. Chances of this occurring can be reduced by:
  1. **Redundant sensing:** Using more than once sensor for detecting veins would reduce significantly the chances of this occurring. Currently the team is proposing to use infrared imaging together with tactile feedback for detaching and confirming the vein.
  2. **Significant testing:** By trying the phlebotomist on a significant candidate pool it may be ensured that the mechanism will operate properly when placed into use.
2. **Sterilization:** Standard sterilization techniques must be applied to the device. Extreme conditions may occur in cases where the device is used over open wounds and significant contamination may occur. The device has to be designed in such a way that this can condition can be reversed.

#### MINOR ISSUES

1. **Cut off Circulation:** If the device is allowed to compress the arm with a high tension for extended periods of time it may lead to a reduction in the circulation and its natural side

effects. As this can only occur over very long periods of time (which is not the operating regime of the robot) this is not considered a significant issue.

**2. Deterioration of UI:** It is possible that over repeated use the buttons (or touchscreen) becomes unresponsive which may be vexing to the operators.



# Appendix I

## JIRA Log



## WPI JIRA

Issue Type	Key	Status	Priority	Summary
Task	<a href="#">PHLEBOT-143</a>	Open	Major	Design Conclusions from Small Scale Study
Task	<a href="#">PHLEBOT-124</a>	Closed	Major	Confirm IRB Approval
Task	<a href="#">PHLEBOT-123</a>	Closed	Major	Small Scale Study Proposal
Task	<a href="#">PHLEBOT-122</a>	Closed	Major	Submit IRB Application
Task	<a href="#">PHLEBOT-109</a>	Closed	Major	Review of the DOE and IRB approval form
Task	<a href="#">PHLEBOT-103</a>	Closed	Major	Review of the DOE and IRB approval form
Task	<a href="#">PHLEBOT-93</a>	Closed	Major	Order Nuts for the 1.6mm Screws
Task	<a href="#">PHLEBOT-92</a>	Closed	Critical	Procure Power Supplies for the Lab
New Feature	<a href="#">PHLEBOT-22</a>	Closed	Minor	Purchase IR-pass milky acrylic
Task	<a href="#">PHLEBOT-7</a>	Closed	Trivial	Update Expense Report
Task	<a href="#">PHLEBOT-6</a>	Closed	Trivial	Update Expense Report
Task	<a href="#">PHLEBOT-3</a>	Closed	Minor	Clone phlebot git repo and test commit
New Feature	<a href="#">PHLEBOT-1</a>	Closed	Minor	Needle Insertion Force Sensor
Task	<a href="#">PHLEBOT-121</a>	Reopened	Major	Needle Insertion Mechanism V4
-> Sub-task	<a href="#">PHLEBOT-158</a>	Closed	Major	-> Redo the whole NIM with pinched butterfly and yaw axis
-> Sub-task	<a href="#">PHLEBOT-144</a>	Closed	Major	-> Characterize the Honeywell Force Sensor
-> Sub-task	<a href="#">PHLEBOT-164</a>	Closed	Major	-> Assemble NIM V4
-> Sub-task	<a href="#">PHLEBOT-156</a>	Closed	Major	-> 3D print (low res)
-> Sub-task	<a href="#">PHLEBOT-151</a>	Closed	Major	-> Model all the interconnecting parts for 3D printing
-> Sub-task	<a href="#">PHLEBOT-150</a>	Closed	Major	-> Model the force sensor and other stock parts
Task	<a href="#">PHLEBOT-117</a>	Closed	Major	Mechanics V4 - Stage
-> Sub-task	<a href="#">PHLEBOT-118</a>	Closed	Major	-> Design Stage - Trial 1
-> Sub-task	<a href="#">PHLEBOT-153</a>	Closed	Major	-> Assemble - Trial 1
-> Sub-task	<a href="#">PHLEBOT-152</a>	Closed	Major	-> Laser Cutting - Trial 1
-> Sub-task	<a href="#">PHLEBOT-149</a>	Closed	Major	-> Review and Export to DWG - Trial 1
Task	<a href="#">PHLEBOT-89</a>	Closed	Critical	Mechanics V3
-> Sub-task	<a href="#">PHLEBOT-94</a>	Closed	Major	-> Integrate NIM and Stage
-> Sub-task	<a href="#">PHLEBOT-90</a>	Closed	Critical	-> Design and Model Needle Insertion Mechanism V3
-> Sub-task	<a href="#">PHLEBOT-91</a>	Closed	Critical	-> Design and Model Cartesian Stage as Sub Assemblies
-> Sub-task	<a href="#">PHLEBOT-106</a>	Closed	Major	-> Make Corrections and Laser Cut New Parts (1)
-> Sub-task	<a href="#">PHLEBOT-102</a>	Closed	Major	-> Export Assembly to DWG for Laser Cutting
-> Sub-task	<a href="#">PHLEBOT-104</a>	Closed	Major	-> Laser Cut Mechanics V3 (First Session)
-> Sub-task	<a href="#">PHLEBOT-108</a>	Closed	Major	-> Make Corrections and Laser Cut New Parts (2)
-> Sub-task	<a href="#">PHLEBOT-105</a>	Closed	Major	-> Assemble Mechanics V3
Task	<a href="#">PHLEBOT-51</a>	Closed	Minor	Software Architecture Design
Task	<a href="#">PHLEBOT-159</a>	In Progress	Major	Patent Application
-> Sub-task	<a href="#">PHLEBOT-160</a>	Open	Major	-> Invention Disclosure Form - Trial 1
Task	<a href="#">PHLEBOT-20</a>	Closed	Major	Test Fixture for Small Scale Experiment Completed

-> Sub-task	<a href="#">PHLEBOT-135</a>	Closed	Major	-> Machine, Assemble, and Test
-> Sub-task	<a href="#">PHLEBOT-133</a>	Closed	Major	-> Order Materials for the Tester
-> Sub-task	<a href="#">PHLEBOT-132</a>	Closed	Major	-> Horizontal Carriage
-> Sub-task	<a href="#">PHLEBOT-131</a>	Closed	Major	-> Camera Module
-> Sub-task	<a href="#">PHLEBOT-130</a>	Closed	Major	-> Vertical Carriage
-> Sub-task	<a href="#">PHLEBOT-127</a>	Closed	Major	-> Arm Fixture
-> Sub-task	<a href="#">PHLEBOT-126</a>	Closed	Major	-> Platform
-> Sub-task	<a href="#">PHLEBOT-125</a>	Closed	Major	-> CAD Design of Tester
-> Sub-task	<a href="#">PHLEBOT-157</a>	Closed	Major	-> Develop Protocol for Tester to Raspberry Pi Communication
-> Sub-task	<a href="#">PHLEBOT-136</a>	Closed	Major	-> Program and Test
Task	<a href="#">PHLEBOT-21</a>	Open	Major	Small Scale Experiment Completed
-> Sub-task	<a href="#">PHLEBOT-142</a>	Open	Major	-> Results of Phase 4
-> Sub-task	<a href="#">PHLEBOT-141</a>	Open	Major	-> Results of Phase 3
-> Sub-task	<a href="#">PHLEBOT-140</a>	Open	Major	-> Results of Phase 2
-> Sub-task	<a href="#">PHLEBOT-139</a>	Open	Major	-> Results of Phase 1
-> Sub-task	<a href="#">PHLEBOT-138</a>	Open	Major	-> Program for analyzing the results of the experiment.
-> Sub-task	<a href="#">PHLEBOT-137</a>	Closed	Major	-> Recruit Subjects for Experiment
New Feature	<a href="#">PHLEBOT-165</a>	In Progress	Major	Create a Cross-Platform Front-End Application for Phlebot
-> Sub-task	<a href="#">PHLEBOT-182</a>	Resolved	Major	-> Implement Serial Communication with an Arduino Due
Task	<a href="#">PHLEBOT-179</a>	Open	Major	Design On-Device UI
Task	<a href="#">PHLEBOT-162</a>	Open	Major	Attachment Mechanism V1
-> Sub-task	<a href="#">PHLEBOT-171</a>	Closed	Major	-> Select a Pressure Sensor for the Cuff
-> Sub-task	<a href="#">PHLEBOT-185</a>	Resolved	Major	-> Determine Best Material/Sealant Combination
-> Sub-task	<a href="#">PHLEBOT-163</a>	In Progress	Major	-> Design Attachment Mechanism - Trial 1
Task	<a href="#">PHLEBOT-155</a>	Open	Minor	Video Presentation of Project
Task	<a href="#">PHLEBOT-52</a>	Closed	Critical	Manufacture Velcro Based Cartesian Stage V2
-> Sub-task	<a href="#">PHLEBOT-53</a>	Closed	Major	-> Laser Cutting of Velcro Based Cartesian Stage V2
-> Sub-task	<a href="#">PHLEBOT-66</a>	Closed	Blocker	-> Fix Errors that are Impeding Assembly and Export (1)
-> Sub-task	<a href="#">PHLEBOT-67</a>	Closed	Blocker	-> Laser Cut Corrected/Missing Components (1)
-> Sub-task	<a href="#">PHLEBOT-57</a>	Closed	Major	-> Assemble Velcro Based Cartesian Stage V2
Task	<a href="#">PHLEBOT-166</a>	Resolved	Major	Electronics V2
-> Sub-task	<a href="#">PHLEBOT-180</a>	In Progress	Major	-> Write Documentation
-> Sub-task	<a href="#">PHLEBOT-178</a>	Resolved	Major	-> Route PCB
-> Sub-task	<a href="#">PHLEBOT-181</a>	Resolved	Major	-> Order Components
-> Sub-task	<a href="#">PHLEBOT-184</a>	In Progress	Major	-> Debug PCB
-> Sub-task	<a href="#">PHLEBOT-174</a>	Resolved	Major	-> Layout of PCB
Task	<a href="#">PHLEBOT-70</a>	Closed	Minor	Assemble and Test IRRigV2
-> Sub-task	<a href="#">PHLEBOT-72</a>	Closed	Major	-> Test IRRigV2
-> Sub-task	<a href="#">PHLEBOT-86</a>	Closed	Major	-> Order Missing Components
-> Sub-task	<a href="#">PHLEBOT-96</a>	Closed	Minor	-> Assemble Remaining IRRigV2 Boards After Testing
-> Sub-task	<a href="#">PHLEBOT-71</a>	Closed	Minor	-> Assemble IRRigV2

Task	<a href="#">PHLEBOT-168</a>	Closed	Critical	Create Presentation for Gennert
Task	<a href="#">PHLEBOT-11</a>	Closed	Major	Electronic V1
-> Sub-task	<a href="#">PHLEBOT-84</a>	Closed	Major	-> Write Documentation
-> Sub-task	<a href="#">PHLEBOT-81</a>	Closed	Critical	-> Review and Perform DRC Check
-> Sub-task	<a href="#">PHLEBOT-80</a>	Closed	Major	-> Review and Comment
-> Sub-task	<a href="#">PHLEBOT-77</a>	Closed	Major	-> Component Placement
-> Sub-task	<a href="#">PHLEBOT-63</a>	Closed	Major	-> Determine Rasp Pi FPC Cable Pin Out
-> Sub-task	<a href="#">PHLEBOT-83</a>	Closed	Major	-> Contact 4PCB to Ensure Manufacturability
-> Sub-task	<a href="#">PHLEBOT-85</a>	Closed	Major	-> Order Components
-> Sub-task	<a href="#">PHLEBOT-82</a>	Closed	Critical	-> Send Board to Manufacturing
-> Sub-task	<a href="#">PHLEBOT-74</a>	Closed	Major	-> Determine Pins to be Used on Pi Header
-> Sub-task	<a href="#">PHLEBOT-60</a>	Closed	Major	-> Check SODIMM Compatibility and Pattern Correctness.
-> Sub-task	<a href="#">PHLEBOT-79</a>	Closed	Major	-> Route PCB
-> Sub-task	<a href="#">PHLEBOT-75</a>	Closed	Major	-> Determine Ethernet Jack Used in Rasp Pi
-> Sub-task	<a href="#">PHLEBOT-64</a>	Closed	Major	-> Ethernet Transceiver Selection
-> Sub-task	<a href="#">PHLEBOT-61</a>	Closed	Blocker	-> Check SODIMM Schematic
-> Sub-task	<a href="#">PHLEBOT-49</a>	Closed	Major	-> Create Block Diagram for Board
-> Sub-task	<a href="#">PHLEBOT-46</a>	Closed	Major	-> Create Schematic
Task	<a href="#">PHLEBOT-173</a>	Resolved	Major	Needle Insertion Mechanism V5 + V6
-> Sub-task	<a href="#">PHLEBOT-177</a>	Resolved	Major	-> Assemble NIM V6
-> Sub-task	<a href="#">PHLEBOT-176</a>	Resolved	Major	-> Send to Manufacture
Task	<a href="#">PHLEBOT-134</a>	Closed	Major	Debugging Software V1
Task	<a href="#">PHLEBOT-183</a>	In Progress	Major	Write Communication Protocol V2
Task	<a href="#">PHLEBOT-148</a>	In Progress	Minor	Set Up RasPis
Task	<a href="#">PHLEBOT-24</a>	Closed	Major	Inform Professors of Study Direction
Task	<a href="#">PHLEBOT-120</a>	Closed	Major	Test White Ebay Linear Stepper Motor
New Feature	<a href="#">PHLEBOT-38</a>	Closed	Major	Integrate Needle Insertion Mechanism and Cartesian Stage
-> Sub-task	<a href="#">PHLEBOT-43</a>	Closed	Major	-> Convert to laser-cuttable AutoCAD .dwg and lay out.
-> Sub-task	<a href="#">PHLEBOT-50</a>	Closed	Minor	-> Add End-Stop Holders
-> Sub-task	<a href="#">PHLEBOT-44</a>	Closed	Major	-> Choose End-Stop Sensors
-> Sub-task	<a href="#">PHLEBOT-42</a>	Closed	Major	-> Create Missing Components
-> Sub-task	<a href="#">PHLEBOT-41</a>	Closed	Major	-> Fix Bugs with Mating in Cartesian Stage
-> Sub-task	<a href="#">PHLEBOT-40</a>	Closed	Major	-> Prepare Needle Insertion Mechanism
Task	<a href="#">PHLEBOT-18</a>	Closed	Minor	Determination of Wavelengths for Small Scale Study
Task	<a href="#">PHLEBOT-110</a>	Closed	Major	Assemble Main Board V1
-> Sub-task	<a href="#">PHLEBOT-111</a>	Closed	Major	-> Order Missing Components (1)
Task	<a href="#">PHLEBOT-172</a>	Open	Major	Select Solenoid Valve
Task	<a href="#">PHLEBOT-169</a>	Resolved	Major	Mechanics V5 - Stage
-> Sub-task	<a href="#">PHLEBOT-175</a>	Closed	Major	-> Export Parts For Laser Cutting
-> Sub-task	<a href="#">PHLEBOT-170</a>	Closed	Major	-> Design of Stage - Trial 1
Task	<a href="#">PHLEBOT-167</a>	In Progress	Major	Make Decisions Regarding DMD Conference
Task	<a href="#">PHLEBOT-161</a>	Closed	Minor	Update Expense Report

Task	<a href="#">PHLEBOT-112</a>	Closed	Major	Test Main Board
-> Sub-task	<a href="#">PHLEBOT-115</a>	Closed	Major	-> Measure Power Up Sequencing of the RaspBerry Pi IO Board
-> Sub-task	<a href="#">PHLEBOT-113</a>	Closed	Major	-> Power Rail Voltage Levels and Sequencing Verification
Task	<a href="#">PHLEBOT-101</a>	Closed	Critical	Order the Honeywell force sensor
Bug	<a href="#">PHLEBOT-47</a>	Closed	Major	Add ON/OFF ability for each LED wavelength through CLI args to script.
-> Sub-task	<a href="#">PHLEBOT-48</a>	Closed	Minor	-> Prevent image dumps to stash
Task	<a href="#">PHLEBOT-4</a>	Closed	Major	Write scripts on Raspi and Mac to automate image capture
-> Sub-task	<a href="#">PHLEBOT-37</a>	Closed	Minor	-> Bug fix to enable argument passage to python script
-> Sub-task	<a href="#">PHLEBOT-36</a>	Closed	Major	-> File management for image capture system
-> Sub-task	<a href="#">PHLEBOT-35</a>	Closed	Major	-> Work out the RasPi GPIO configs
Task	<a href="#">PHLEBOT-30</a>	Closed	Minor	Write Documentation for IRRigV2
Task	<a href="#">PHLEBOT-114</a>	Closed	Major	Create Communication Protocol Between Boards
Task	<a href="#">PHLEBOT-107</a>	Closed	Major	Order Acrylic Glue and M2 Hardware
Improvement	<a href="#">PHLEBOT-13</a>	Closed	Major	Design new multi-wavelength IR blaster
-> Sub-task	<a href="#">PHLEBOT-29</a>	Closed	Major	-> Send PCB to Fabrication
-> Sub-task	<a href="#">PHLEBOT-28</a>	Closed	Minor	-> Review Board
-> Sub-task	<a href="#">PHLEBOT-27</a>	Closed	Major	-> Routing of Board
-> Sub-task	<a href="#">PHLEBOT-26</a>	Closed	Major	-> Create Board Layout (Component Placement)
-> Sub-task	<a href="#">PHLEBOT-25</a>	Closed	Major	-> Create Schematic
Task	<a href="#">PHLEBOT-95</a>	Closed	Major	Order more 6mm acrylic
Task	<a href="#">PHLEBOT-62</a>	Closed	Major	Reflash a RasPi board with an expanded file system.
Task	<a href="#">PHLEBOT-39</a>	Closed	Major	Setup git repositories on RasPi for code testing and development
Task	<a href="#">PHLEBOT-17</a>	Closed	Minor	Order Raspberry Pi Compute Module Development Kit
Task	<a href="#">PHLEBOT-56</a>	Closed	Minor	Follow up on Nanotec Orders with Tracey
Task	<a href="#">PHLEBOT-12</a>	Closed	Minor	Order Longer FPC Cables for NOiR Camera
Task	<a href="#">PHLEBOT-55</a>	Closed	Minor	Email Toby Regarding Laser Cutter Access
Task	<a href="#">PHLEBOT-69</a>	Closed	Minor	Order Voltage Regulators for Main Board V1
Task	<a href="#">PHLEBOT-45</a>	Closed	Major	Order Components for IRRigV2
Task	<a href="#">PHLEBOT-31</a>	Closed	Trivial	Send Pictures of Lab to Professors
Task	<a href="#">PHLEBOT-87</a>	Closed	Trivial	Set Up Camera for Recording / Snapshotting
-> Sub-task	<a href="#">PHLEBOT-88</a>	Closed	Minor	-> Order SD Card
Bug	<a href="#">PHLEBOT-54</a>	Closed	Minor	Make Corrections to IRRigV2 Interface Document
Task	<a href="#">PHLEBOT-154</a>	Closed	Major	Meeting Minutes for Sep 09
Task	<a href="#">PHLEBOT-147</a>	Closed	Minor	Set Up GrabCAD
Task	<a href="#">PHLEBOT-146</a>	Closed	Minor	Develop Force Sensor Data Collection Software
Improvement	<a href="#">PHLEBOT-145</a>	Closed	Minor	Modify Stash Repository
Task	<a href="#">PHLEBOT-119</a>	Closed	Major	Test GrabCad
Bug	<a href="#">PHLEBOT-116</a>	Closed	Minor	Fix Problematic LEDs in IRRigV2 Boards
Task	<a href="#">PHLEBOT-99</a>	Closed	Critical	Create a Working Demo of a Vein Viewer System

Bug	<a href="#">PHLEBOT-78</a>	Closed	Minor	Follow up with the supplier on new display and camera adapters
Task	<a href="#">PHLEBOT-76</a>	Closed	Critical	Get the RasPi compute module up and running
Task	<a href="#">PHLEBOT-73</a>	Closed	Minor	Update Expense Report
Task	<a href="#">PHLEBOT-68</a>	Closed	Minor	Make Myrtle Into NVR for IP Camera
Task	<a href="#">PHLEBOT-59</a>	Closed	Major	Take Human Subjects Research Training
Task	<a href="#">PHLEBOT-58</a>	Closed	Major	Take Human Subjects Research Training
Task	<a href="#">PHLEBOT-33</a>	Closed	Trivial	Make presentation for July 27th
-> Sub-task	<a href="#">PHLEBOT-34</a>	Closed	Trivial	-> Help Doctor prepare the presentation
-> Sub-task	<a href="#">PHLEBOT-65</a>	Closed	Minor	-> Create a Jira project activity tracker on the lab TV
Task	<a href="#">PHLEBOT-32</a>	Closed	Trivial	Label Remaining Drawers
Improvement	<a href="#">PHLEBOT-23</a>	Closed	Major	Improve Needle Insertion Mechanism (see description)
Task	<a href="#">PHLEBOT-19</a>	Closed	Major	IRB Application Small Scale Study
-> Sub-task	<a href="#">PHLEBOT-98</a>	Closed	Blocker	-> Review IRB application and Experimental procedure
-> Sub-task	<a href="#">PHLEBOT-97</a>	Closed	Blocker	-> Review IRB application and Experimental procedure
Task	<a href="#">PHLEBOT-16</a>	Closed	Major	Design Velcro Based Cartesian Stage V2
Task	<a href="#">PHLEBOT-15</a>	Closed	Major	Request Free Sample for Force Sensor
Task	<a href="#">PHLEBOT-14</a>	Closed	Critical	Design Needle Insertion Mechanism V1
Task	<a href="#">PHLEBOT-10</a>	Closed	Major	Design Needle Insertion Mechanism V1
Task	<a href="#">PHLEBOT-9</a>	Closed	Major	Order Phlebotomy Supplies
Task	<a href="#">PHLEBOT-8</a>	Closed	Trivial	Update Expense Report
Task	<a href="#">PHLEBOT-5</a>	Closed	Major	Build scikit-image on development machines and install OpenCV
Improvement	<a href="#">PHLEBOT-2</a>	Closed	Trivial	Update Foscam IP Camera firmware
			<b>Total</b>	



120		90		30	
		0		660	
1200	1200	1200	1200		
2400	2880	1185	1185	1215	1695
480		0		480	
720	720	720	720		
480	840	480	710		490
240		230		10	
		0		240	
120		0		240	
600	600	600	600		
360	780	360	492		468
180		75		105	
60		30		30	
60		27		33	
120		0		300	
1200	2460	240	480	960	2040
360		120		240	
480		90		390	
60		30		30	
		0		60	
360		0		360	
240	750	240	295		575
60		30		30	
30		25		5	
240		0		240	
180		0		300	



300	300	282	282	18	18
	1680	0	242	90	1942
240		30		210	
120		30		90	
30		30			
180		30		150	
30		30			
30		24		6	
30		20		10	
30		18		12	
30		15		15	
30		15		15	
360		0		540	
30		0		90	
30		0		30	
30		0		30	
120		0		120	
360		0		534	
960	1560	0	240	1200	1560
480		180		300	
120		60		60	
360	360	210	210	150	150
240	240	176	176	64	64
180	180	140	140	40	40
180	180	120	120	60	60
120	120	100	100	20	20
	375		93		417
180		93		87	
60		0		90	
45		0		60	
30		0		60	
60		0		60	
		0		60	
90	90	90	90		
360	390	60	70	300	320
30		10		20	
60	60	60	60		
300	660	0	60	360	1020
120		60		60	
240		0		600	
60	60	60	60		
60	60	60	60		

	120		0	60	60	120
60			30		30	
60			30		30	
60	60		60	60		
120	180		0	60	180	180
60			60			
	180			60		300
180			60		120	
			0		60	
			0		120	
180	180		54	54	126	126
180	180		50	50	130	130
60	60		50	50	10	10
	420		0	48	240	672
30			24		6	
30			24		6	
120			0		120	
60			0		120	
180			0		180	
60	60		30	30	30	30
120	120		30	30	90	90
60	60		30	30	30	30
30	30		30	30		
30	30		24	24	6	6
24	24		24	24		
30	30		18	18	12	12
30	30		15	15	15	15
60	60		15	15	45	45
30	30		15	15	15	15
120	132		0	11	204	205
12			11		1	
12	12		6	6	6	6
			0	0	15	15
120	120		0	0	180	180
			0	0	60	60
			0	0	60	60
			0	0	60	60
60	60		0	0	100	100
			0	0	300	300

		0	0	1	1
150	150	0	0	330	330
30	30	0	0	30	30
120	120	0	0	180	180
		0	0	15	15
		0	0	60	60
	60		0		90
60		0		90	
60	60	0	0	60	60
		0	0	240	240
900	960	0	0	2662	2782
30		0		90	
30		0		30	
1800	1800	0	0	1200	1200
		0	0	36	36
		0	0	960	960
		0	0	120	120
		0	0	120	120
		0	0	30	30
0	0	0	0	540	540
		0	0	30	30
42183	42183	24212	24212	26991	26991





0		0	0
		0	0
0	0	0	0
0		0	0
		0	0
	-360	0	-42
0		0	0
-120		-100	-100
		0	0
	-180	0	-23
0		0	0
0		0	0
0		0	0
-180		-150	-150
0	-60	0	-2
0		0	0
0		0	0
0		0	0
0		0	0
	-120	0	-16
0		0	0
0		0	0
0		0	0
-120		-66	-66

0	0	0	0
	-504		-30
0		0	0
0		0	0
		0	0
0		0	0
		0	0
0		0	0
0		0	0
0		0	0
0		0	0
0		0	0
-180		-50	-50
-60		-200	-200
0		0	0
0		0	0
0		0	0
-174		-48	-48
-240	-240	-25	-15
0		0	0
0		0	0
0	0	0	0
0	0	0	0
0	0	0	0
0	0	0	0
0	0	0	0
	-135		
0		0	0
-30		-50	-50
-15		-33	-33
-30		-100	-100
0		0	0
		0	0
0	0	0	0
0		0	0
		0	0
-60	-420	-20	-63
0		0	0
-360		-150	-150
		0	0
		0	0

	-60		-50
0		0	0
0		0	0
		0	0
-60	-60	-50	-33
		0	0
	-180		
0		0	0
0	0	0	0
0	0	0	0
0	0	0	0
	-300		-71
0		0	0
0		0	0
0		0	0
-60		-100	-100
0		0	0
0	0	0	0
0	0	0	0
0	0	0	0
		0	0
0	0	0	0
		0	0
0	0	0	0
0	0	0	0
0	0	0	0
0	0	0	0
0	0	0	0
-84	-84	-70	-63
0		0	0
0	0	0	0
-60	-60	-50	-50
-40	-40	-66	-66

-180	-180	-120	-120
0	0	0	0
-60	-60	-50	-50
	-30		
-30		-50	-50
0	0	0	0
-1762	-1822	-195	-189
-60		-200	-200
0		0	0
600	600	33	33
-540	-540		
-9020	-9020	-21	-21

